Goethe University • Institute of Pharmaceutical Technology
Prof. Dr. Jennifer B. Dressman

Yang Fei

Mechanistic Understanding of Enhanced Human Oral Bioavailability of Fenofibric Acid from Novel Lipid Carriers Using Semi-Physiologically Based Pharmacokinetic Model and Various Analytical Approaches Including Biorelevant Dissolution Testing

Cuvillier Verlag Göttingen
Internationaler wissenschaftlicher Fachverlag

Mechanistic Understanding of Enhanced Human Oral Bioavailability of Fenofibric Acid from Novel Lipid Carriers Using Semi- Physiologically Based Pharmacokinetic Model and Various Analytical Approaches Including Biorelevant Dissolution Testing

Mechanistic Understanding of Enhanced Human Oral Bioavailability of Fenofibric Acid from Novel Lipid Carriers Using Semi- Physiologically Based Pharmacokinetic Model and Various Analytical Approaches Including Biorelevant Dissolution Testing

Dissertation
for attaining the PhD degree
of Natural Sciences

Submitted to Faculty 14
Biochemistry, Chemistry and Pharmacy
of the Johann Wolfgang Goethe University
in Frankfurt am Main

by

Yang Fei
from Hohhot, China

Frankfurt am Main, 2018
(D 30)

Bibliografische Information der Deutschen Nationalbibliothek
Die Deutsche Nationalbibliothek verzeichnet diese Publikation in der Deutschen Nationalbibliografie; detaillierte bibliografische Daten sind im Internet über http://dnb.d-nb.de abrufbar.
1. Aufl. - Göttingen: Cuvillier, 2018
Zugl.: Frankfurt, Univ., Diss., 2018

Accepted by the Faculty 14 Biochemistry, Chemistry and Pharmacy of the Johann Wolfgang Goethe University as a dissertation.

Dean: Prof. Dr. Clemens Glaubitz
1. Expert assessor: Prof. Dr. Jennifer B. Dressman
2. Expert assessor: Dr. Brendan T. Griffin (University College Cork, Ireland)

Date of the disputation: 22.06.2018

Nonnenstieg 8, 37075 Göttingen
Telefon: 0551-54724-0
Telefax: 0551-54724-21
www.cuvillier.de

1. Auflage, 2018
Gedruckt auf umweltfreundlichem, säurefreiem Papier aus nachhaltiger Forstwirtschaft.

ISBN 978-3-7369-9768-4
eISBN 978-3-7369-8768-5

For my family

Acknowledgements

This work was performed in the Institute of Pharmaceutical Technology of the Johann Wolfgang Goethe University Frankfurt am Main (08.2010 – 03.2014).

I would like to thank my Ph.D. supervisor, Prof. Dr. J.B. Dressman, one of the most famous dissolution and biopharmaceutical scientists in the world. I am grateful for Jenny's effort planning my research theme based on well-established platform; for her precise guidance throughout my experiments; for her profound academic knowledge; and for her persistent care when I was studying in Germany. Jenny's personality left me a deep impression.

I would like to thank my second Ph.D. supervisor, Dr. E.S. Kostewicz. He has spent huge amount of time supervising my experiments, revising my papers as well as thesis. Ed is very nice and always ready to help whenever there are difficulties. His creative ideas benefit me along the journey.

I would like to acknowledge the colleagues in institute during my residence: Prof. Dr. J. Kreuter, Dr. M. Wacker, E. Herbert, B. Johann, S. Niederdorf, H. Kaufmann, M. Weisser, H. Berger, Dr. Y. Shono, Dr. M. Kilic, Dr. D. Jünemann, Dr. A.C. Pertereit, Dr. S. Strauch, Dr. T. Taupitz, Dr. M. Arndt, Dr. C. Wagner, Dr. A. Nair, Dr. M. Berlin, Dr. K. Otsuka, Dr. A. Kambayashi, A. Fuchs, A. Ruff, G.F. Born, J. Thinnes, C. Andreas, S. Hansmann, L. Gusseck, Dr. Y.C. Chen, Dr. S. Wohlfart, Dr. S. Gaca, Dr. K. Sempf, Dr. A. Mühlstein, Dr. M. Dadparvar, Dr. W. Watcharin, Dr. I. Rosenberger, Dr. S. Beyer, and C. Janas. Many thanks to all these colleagues. It was a pleasure to work with them.

Thanks to Prof. Dr. M.T. Sheu of Taipei Medical University for providing PK data.

I owe a lot to my parents Zhong and Yan, my wife Shaoying, as well as my children Simei and Kaiwen. This achievement belongs to them.

Oh, the depth of the riches of the wisdom and knowledge of God! To him be the glory forever! Amen.

Frankfurt am Main, 2018

Yang Fei

Table of contents

List of Figures

List of Tables

Abbreviations

A	surface area of the Caco-2 mono layer in the *in vitro* permeability tests
ACAT	advanced compartmental absorption and transit
ADAM	advanced dissolution absorption and metabolism
ADME	absorption, distribution, metabolism and excretion
ANOVA	analysis of variance
API	active pharmaceutical ingredient
AUC	area under the plasma concentration curve
$AUC_{0\text{-inf}}$	area under the plasma concentration curve from time zero to infinity
BHA	butylatedhydroxyanisole
BHT	butylatedhydroxytoluene
B/P	blood to plasma partition ratio
BS	bile salts
C_0	initial concentration in the donor chamber in the permeability tests
CAT	compartmental absorption and transit
Cl	clearance
cm	centimeter(s)
C_{max}	maximum plasma concentration
Conc.	concentrated/concentration
CR	controlled release
C_s	drug solubility in the dissolution medium
$C_{s,intestine}$	solubility in the intestinal fluid
$C_{s,stomach}$	solubility in the gastric fluid
C_t	concentration of dissolved drug at time *t*
CYP	cytochrome P450
D	diffusion coefficient
DDT	dichloro-diphenyl-trichloroethane

D/P	dissolution/permeation
dpm	dips per minute
dQ/*dt*	permeation rate with the amount of drug represented as a fraction
EDTA	ethylenediamine tetraacetic acid
et al.	et alii, et aliae or et alia
etc.	et cetera
F	factor applied to reference input value used in the sensitivity analysis
f_2	similarity factor
FA	fatty acids
fa	fraction of dose absorbed
FaSSGF	fasted state simulated gastric fluid
FaSSIF	fasted state simulated intestinal fluid
FaSSIF-V2	fasted state simulated intestinal fluid - version 2
FaSSIF-V2(PO_4)	fasted state simulated intestinal fluid - version 2 (phosphate buffer)
FeSSGEm	fed state simulated gastric emulsion
FeSSGF	fed state simulated gastric fluid
FeSSIF	fed state simulated intestinal fluid
FFB (occasionally)	fenofibrate
fu	fraction unbound in plasma
g	gram(s)
GI	gastrointestinal
GRAS	generally recognized as safe
h	hour
HDL	high-density lipoprotein
h_{eff}	effective diffusion layer thickness
HLB	hydrophilic-lipophilic balance
HPLC	high-performance liquid chromatography
HPMC	hypromellose (hydroxypropyl methylcellulose)
HPMCAS	hydroxypropyl methylcellulose acetate succinate

Inc.	Incorporated
IR	immediate release
IUPAC	International Union of Pure and Applied Chemistry
i.v.	intravenous
IVISIV(C/R)	*in vitro-in silico-in vivo* (correlation/relationship)
$J_{DI}(t)$	dissolution rate for the formulated drug content in the small intestine
$J_{DS}(t)$	dissolution rate for the formulated drug content in the stomach
k_0	zero order rate constant of the precipitation process
k_{10}	elimination rate constant
k_{12}	rate constant from central to peripheral compartment
k_{21}	rate constant from peripheral to central compartment
ka	absorption rate constant
kcal	kilocalorie
k_{GE}	first order kinetic rate constant for gastric emptying
K_m	substrate concentration at which the reaction rate is half of V_{max}
LBF	lipid-based formulation
LC(T)	long chain (triglyceride)
LFCS	lipid formulation classification system
LDL	low-density lipoprotein
logP	partition coefficient
LOQ	limit of quantification
Ltd.	Limited
M	mol per liter
MC(T)	medium chain (triglyceride)
MDS	micronized dispersion system
mg	milligram(s)
min	minute(s)
mL	milliliter(s)
mM	millimoles per liter (millimolar)
mmol	millimol

mOsm	milliosmolar
MR	modified release
M_t	amount of drug permeated from gut into the blood circulation at time *t*
MW	molecular weight
n	number of tests
n/a	not available
NMR	Nuclear Magnetic Resonance
ODE	ordinary differential equation
o/w	oil in water
PBPK	physiologically based pharmacokinetic(s)
$P_{Caco\text{-}2}$	apparent Caco-2 permeability coefficient
P_{eff}	effective permeability coefficient
PEG	polyethylene glycol
P-gp	P-glycoprotein
Ph. Eur.	European Pharmacopoeia
PK	pharmacokinetic(s)
PK/PD	Pharmacokinetic/pharmacodynamic
PL	phospholipids
p.o.	per oral
PSG	porous silica gel
PSP	porous silica powder(s)
P_t	amount of drug precipitated at time *t*
PTFE	polytetrafluoroethylene
P_{UWL}	permeation rate through the unstirred water layer
PVDF	polyvinylidene fluoride
QC	quality control
rpm	revolutions per minute
RT	room temperature
S	available intestinal surface area for absorption
s	second(s)

SD	standard deviation
SEDDS	self-emulsifying drug delivery system
si	small intestine
SIF	simulated intestinal fluid
SMEDDS	self-microemulsifying drug delivery system
stom	stomach
t	time
T_{max}	time of maximum plasma concentration
TPGS	D-α-tocopheryl polyethylene glycol 1000 succinate
UGT	UDP glucuronyl transferase
USP	United States Pharmacopoeia
UWL	unstirred water layer
V	volume
vcf	volume of distribution including factor for bioavailability
V/F	volume of distribution corrected for the fraction absorbed
vfge	time factor (f) of gastric emptying (ge) of the fluid volume (v)
vfluid	volume of coadministered fluid
$V_F(t)$	time evolution of the coadministered water volume in the stomach
V_{max}	maximum rate achieved at maximum substrate concentrations
vs.	versus
V_{ss}	volume of distribution at steady state
W	mass of drug remaining to be dissolved
W_t	amount of drug dissolved at time t
$X_{DO}(t)$	time evolution of orally administered formulated drug dose in stomach
$X_{DS}(t)$	time evolution of the dissolved drug mass in the stomach
$X_{FI}(t)$	time evolution of the formulated drug mass in the small intestine
$X_{IL}(t)$	time evolution of the dissolved drug mass in the intestinal lumen
$X_{PE}(t)$	time evolution of the absorbed drug mass in the periphery tissue
$X_{PL}(t)$	time evolution of the absorbed drug mass in the plasma

X_s	amount of drug that saturates the dissolution medium
z	an apparent parameter for describing the initial drug dissolution rate
$z_{intestine}$	dissolution rate in the small intestine
$z_{stomach}$	dissolution rate in the stomach
µg	microgram(s)
µL	microliter(s)
µm	micrometer(s)

Chapter 1. Introduction

1.1 Lipid-based formulation – an overview

Lipid-based formulations (LBFs) are not a recent invention (Hauss, 2007), their history dates back to more than 50 years ago (Feeney et al., 2016). However, LBFs do not occupy a large segment of the market for the oral delivery of poorly soluble drugs (Hauss, 2007). The majority of formulation endeavors remains solid state, e.g. blending, complex formation, and/or solid dispersion of active pharmaceutical ingredient (API) with solid excipients. API modifications such as salt formation, modification of particle size and/or morphology etc. are also applied often. Sometimes, a solid formulation can prove to be very difficult, especially for drugs with extremely high lipophilicity or a pronounced food effect. In such cases, lipid-based formulations may be an appropriate alternative (e.g. Lin et al., 2011; Wei et al., 2010). In addition, lipid formulations have some advantages over traditional, solid formulations in product development. Nowadays, several types of lipid-based drug delivery systems, such as emulsions, suspensions, oil solutions, and self-microemulsifying drug delivery systems (SMEDDSs) are available (Han et al., 2009). The mechanisms by which lipid formulations can improve bioavailability of poorly soluble drugs include: by direct presentation of the drug in solubilized form in the gastrointestinal (GI) tract, thus avoiding slow dissolution from solid state (Mohsin et al., 2009) and, utilization of alternative uptake pathways through the lymph circulation. If physical stability issues can be solved, the perspective of LBFs will be even more promising in the future.

1.2 Oral Lipid-based formulation with examples

There are numerous examples showing significantly enhanced absorption of poorly soluble drugs using LBFs under fasted condition (e.g. Humberstone and Charman, 1997; Porter et al., 2008). Among them, the application of oral solutions and lipid suspensions include: acetyl sulfisoxazole, dicumarol, griseofulvin, antimalarial amine, cinnarizine, cyclosporin, DDT, halofantrine, probucol, seocalcitol, vitamin D_3, progesterone and dexamethasone. Examples of studies investigating drugs from

oil-in-water emulsions include: danazol, griseofulvin, penclomedine, phenytoin, vitamin E, ibuprofen and acyclovir. In addition, examples of studies of SEDDSs and SMEDDSs include: cyclosporin, halofantrine, ontazolast, vitamin E, coenzyme Q_{10}, simvastatin, biphenyl dimethyl dicarboxylate, indomethacin, progesterone, tocotrienols, danazol, carvedilol, solvent green 3, silymarin, atorvastatin, itroconazole, atovaquone, seocalcitol, disopyramide, ibuprofen, ketoprofen and tolbutamide (e.g. as summarized by Porter et al., 2008).

An extensive review of commercially available oral LBFs was published by Hauss (Hauss, 2007). According to his analysis, oral lipid-based products began entering the marketplace around 1981. As of 2005, at least 31 drugs in 41 lipid-based formulations intended for oral delivery were commercially available in the United States, the United Kingdom, and Japan. By 2007, they accounted for approximately 3% of commercially available oral formulations. Most of these LBFs were housed in soft gelatin capsules with the unit dose ranging from 0.25μg to 500mg. Most of them comprised both lipid excipients/surfactants and nonlipid excipients. Table 1-1 contains a summary of selected LBF products (Hauss, 2007).

Table 1-1

List of selected commercially available LBFs for oral administration in the United States in 2005 (table taken from Hauss, 2007).

Molecule	Trade name	Company	Date of initial marketing
Amprenavir	Agenerase®	GlaxoSmithKline	2000 in the U.K.
Bexarotene	Targretin®	Ligand	2001 in the U.K.
Calcitriol	Rocaltrol®	Roche	1996 in the U.K. (capsules only)
Ciprofloxacin	Cipro®	Bayer	
Cyclosporin A	I. Neoral®	Novartis	1995 in the U.K.
CyclosporinA	II. Sandimmune®	Novartis	

Table 1-1 (*Continued*)

CyclosporinA	III Gengraf®	Abbott	
Cyclosporin A	IV Cyclosporin capsules	Sidmak	
Doxercalciferol	Hectorol®	Bone care	
Dronabinol	Marinol®	Roxane and Unimed	
Dutasteride	Avodart™	GlaxoSmith Kline	2003 in the U.K. (capsules only)
Isotretinoin	Accutane®	Roche	1983 in the U.K.
Lopinavir and ritonavir	Kaletra®	Abbott	2001 in the U.K.
Progesterone	Prometrium®	Solvay	
Ritonavir	Norvir®	Abbott	1999 in the U.K.
Saquinavir	Fortovase™	Roche	1998 in the U.K. Discontinued in 2006
Sirolimus	Rapamune®	Wyeth-Ayerst	2001 in the U.K.
Tipranavir	Aptivus®	Boehringer Ingelheim	
Tolterodine tartrate	Detrol® LA	Pharmacia & UpJohn	2001 in the U.K.
Tretinoin	Vesanoid®	Roche	2001 in the U.K.
Valproic acid	Depakene®	Abbott	

1.3 The Lipid Formulation Classification System and its application

The Lipid Formulation Classification System (LFCS) was first described by Pouton (Pouton, 2000). LFCS briefly classifies lipid-based formulations into four types according to their composition and the possible effect of dilution and digestion on their ability to prevent drug precipitation (Porter et al., 2008). As summarized in Table 1-2, type I LBFs consists of excipients that comprise of API in triglycerides or an oil-in-water emulsion which can be stabilized by a small amount of emulsifier(s). This category exhibits poor initial aqueous dispersion. Thus it requires digestion to generate more amphiphilic products in order to promote drug transfer into the colloidal aqueous phase. Type II LBFs are isotropic mixtures of lipids and lipophilic surfactants,

Table 1-2

The Lipid Formulation Classification System (LFCS) showing typical compositions and properties of lipid-based formulations (table taken from Porter et al., 2008; Pouton, 2006).

Increasing hydrophilic content →					
	Type I	Type II	Type IIIA	Type IIIB	Type IV
	Typical composition (%)				
Triglycerides or mixed glycerides	100	40-80	40-80	<20	-
Water-insoluble surfactants (HLB<12)	-	20-60	-	-	0-20
Water-soluble surfactants (HLB>12)	-	-	20-40	20-50	30-80
Hydrophilic co-solvents	-	-	0-40	20-50	0-50
Characte-ristics	Non-dispersing; requires digestion	SEDDS without water-soluble components	SEDDS/SMEDDS with water-soluble components	SMEDDS with water-soluble components and low oil content	Oil-free formulation based on surfactants and cosolvents
Particle size of dispersion (nm)	Coarse	100-250	100-250	50-100	<50
Significance of aqueous dilution	Limited importance	Solvent capacity unaffected	Some loss of solvent capacity	Significant phase changes and potential loss of solvent capacity	Significant phase changes and potential loss of solvent capacity
Significance of digestibility	Crucial requirement	Not crucial but likely to occur	Not crucial but may be inhibited	Not required	Not required

Table 1-2 (*Continued*)

Solvent capacity advantage	GRAS status; simple; excellent capsule compatibility	Unlikely to lose solvent capacity on dispersion	Clear or almost clear dispersion; drug absorption without digestion	Clear dispersion; drug absorption without digestion	Good solvent capacity for many drugs; disperses to micellar solution
Solvent capacity disadvantage	Formulation has poor solvent capacity unless drug is highly lipophilic	Turbid o/w dispersion (particle size 0.25–2μm)	Possible loss of solvent capacity on dispersion; less easily digested	Likely loss of solvent capacity on dispersion	Loss of solvent capacity on dispersion; may not be digestible

which can self-emulsify to form fine oil-in-water emulsions when introduced in an aqueous solution. They can generate a large interfacial area, which in turn allows efficient partitioning of the API between the oil droplets and the aqueous phase, and facilitate effective absorption. Type III LBFs, usually referred to as Self-MicroEmulsifying Drug Delivery Systems (SMEDDS), are formed by inclusion of co-solvents with hydrophilic surfactants. Type IIIA formulations typically achieve a somewhat slower dispersion rate than the Type IIIB counterpart, although the risk of API precipitation on dilution is lower, given the higher lipid content. Type IV LBFs contain predominantly hydrophilic surfactants and cosolvents without natural lipids, thus represent the most hydrophilic category. They usually offer enhanced API loading and can produce extremely fine dispersions when introduced to aqueous media (see Table 1-2).

Many studies regarding development of LBFs within the LFCS framework, including some with fenofibrate (e.g. Hu et al., 2011; Mohsin et al., 2009; Ratanabanangkoon et al., 2008), have been published. Their major focus has been composition optimization by varying type and amount of lipid-based excipients with the help of phase diagram and dispersion experiments (Anby et al., 2012; Hu et al., 2011; Mohsin et al., 2009; Ratanabanangkoon et al., 2008; Williams et al., 2012). Prior

to the present work (Fei et al., 2013c), however, few if any attempts have been made to simulate plasma concentration profiles following treatment with LBFs. In chapter 5, a novel *in vitro-in silico-in vivo* (*IVISIV*C) approach using *in vitro* biorelevant dissolution data and mechanistic *in silico* pharmacokinetic (PK) modeling will be discussed in detail.

1.4 Potential advantages / disadvantages of lipid formulations

LBFs share the feature that they are able to present the API as a stabilized solution over a period of time (ideally the GI transit time). In fact, the term "lipid-based formulation" means a variety of formulations that share many similarities (Table 1-3).

Table 1-3

Options for lipid formulation of poorly water-soluble drugs (table taken from Pouton, 2006).

Technology	Potential advantage	Potential disadvantage
Lipid solutions (LFCS Type I lipid systems)	Freedom to operate, safe and effective for lipophilic actives, drug is presented in solution avoiding the dissolution step	Limited to highly lipophilic or very potent drugs, requires encapsulation
Self-emulsifying drug delivery systems (SEDDS) and SMEDDS (LCFS Type II or Type III lipid systems)	Prior art available, dispersion leads to rapid absorption and reduced variability, absorption not dependent on digestion	Surfactant may be poorly tolerated in chronic use, soft gel or hard gel capsule can be used in principle but seal must be effective
Solid or semi-solid SEDDS	Could be prepared as a free flowing powder or compressed into tablet form	Surfactant may be poorly tolerated in chronic use, reduced problem of capsule leakage, physical stability of product questionable—drug or polymer may crystallize
Surfactant-cosolvent systems (LFCS Type IV 'lipid' systems)	Relatively high solvent capacity for typical APIs	Surfactant may be poorly tolerated in chronic use, significant threat of drug precipitation on dilution

The disadvantages of LBFs are listed in the right column of Table 1-3. In short, the potential formulation difficulty, tolerance and stability issues should be noted.

1.5 Evaluation of oral lipid-based formulations

The design of LBFs can be challenging, particularly for appropriate selection of lipid excipients to ensure reliable *in vivo* performance (Griffin et al., 2014). Considerations should be taken not only for achieving maximum drug load in LBF, but also for maintaining the API in a solubilized state throughout the gastrointestinal exposure. For the past decade, although a variety of *in vitro* approaches was available, the influence of dilution, dispersion, precipitation and digestion on *in vivo* performance of LBFs is still unclear. In addition to the present *IVISIV*C approach (Fei et al., 2013c), updated and predictive *in vitro* tools for LBF characterization are still needed.

1.5.1 Dispersion

The dispersion test is a typical and useful approach to characterize dispersion property of LBFs. In earlier times, Mohsin et al. (2009) studied the dispersion behaviour of fenofibrate LBFs in 100mL water at 30°C. The amount and rate of API precipitated during dispersion were measured. However, the testing did not reflect *in vivo* conditions in the human GI tract well. Since the volume of fasted stomach is around 50mL and patients are taking a dose with 240mL of water, the average available volume for dispersion could be as high as 290mL. Considering the continuous emptying pattern of water from the stomach, the actual volume for dispersion could also be considerably less. In the small intestine, poorly soluble drugs will follow the colloid phases during dispersion/digestion and will finally end up in mixed micelles. When they dissociate in the unstirred water layer (UWL), the released drug will be absorbed as a free molecule. However, many of the mechanisms involved in the absorption processes are not completely understood (Müllertz et al., 2010). In order to address the *in vivo* conditions better, modified dispersion and dynamic dispersion testing methods (using USP dissolution apparatus) were evolved, as described by Griffin et al. (2014). Among these, microscopic and macroscopic

evaluation of diluted fenofibrate LBF in biorelevant media was part of the work in Frankfurt, and will be described in detail in Chapter 4.

1.5.2 Digestion

One important aspect to consider when developing LBFs is the environment that the delivery system will meet upon ingestion. This includes both the gastrointestinal juices and the digestion processes. In the fasted intestine, the dispersed lipid formulation encounters a relatively small concentration of bile salt and presumably a low level of enzymes. Food intake induces secretion of gastric lipase in the stomach, where a minor proportion of lipid digestion (about 20-30%) takes place. The major part of digestion occurs in the small intestine and is catalyzed by pancreatic lipases.

The *in vitro* lipid digestion (lipolysis) model is recognized as an effective tool to facilitate improved evaluation of LBFs (e.g. Sek et al., 2002; Griffin et al., 2014). While the experimental detail of the model differs slightly between laboratories (Devraj et al., 2013a,b; Lee et al., 2013; Mu et al., 2013; Williams et al., 2013a,b), the basic principles are the same (see Fig. 1-1).

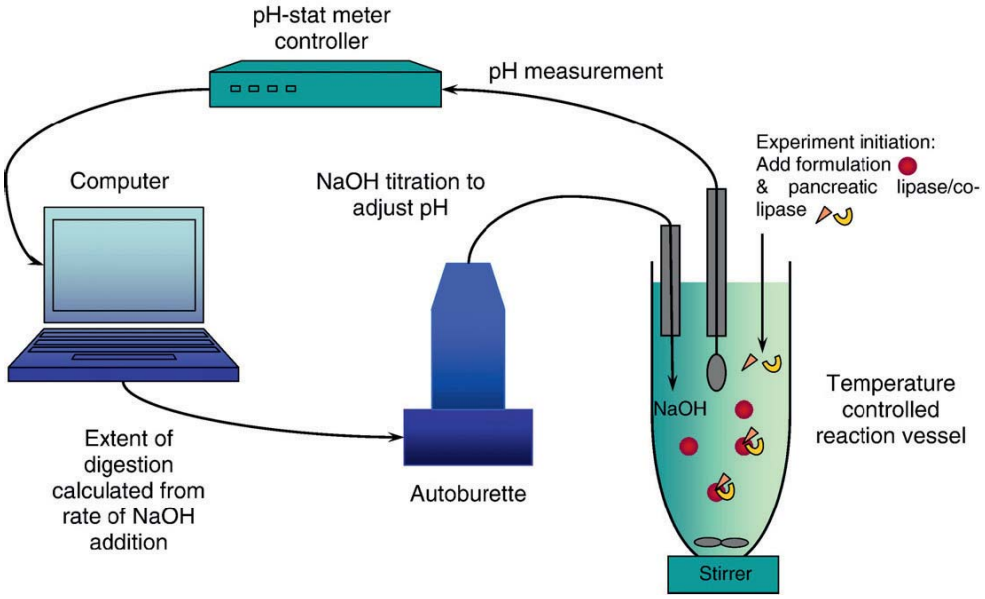

Fig. 1-1. Lipid digestion model for *in vitro* assessment of lipid formulations (figure taken from Porter et al., 2008).

The model is built around a temperature controlled (37°C) vessel containing digestion buffer, bile salts (BS) and phospholipids (PL), into which the LBF is introduced. Digestion is initiated by addition of pancreatic lipase/co-lipase. The onset of lipid digestion results in liberation of fatty acids (FA), which in turn causes a transient drop in pH. This is quantified by a pH electrode, which is coupled with a pH-stat controller and autoburette. The liberated FA is automatically titrated via addition of an equimolar quantity of NaOH. Thus, the pH is maintained, and quantification of the digested lipid content is possible. Throughout the process, samples are taken and separated into a poorly dispersed oil phase, a highly dispersed aqueous phase and a precipitated pellet phase (see Fig. 1-2). Quantification of drug in solubilized form provides an indication of relative likelihood of the LBF regarding *in vivo* precipitation, and therefore provides a mechanism to rank-order potential *in vivo* performance for a series of lipid formulations (Porter et al., 2008).

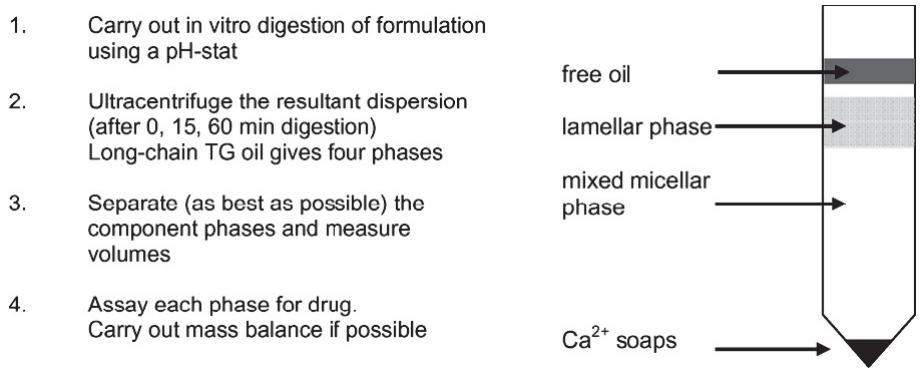

Fig. 1-2. *In vitro* simulation of the fate of LBF in the intestinal lumen (figure taken from Pouton, 2006).

It should be noted that however, this *in vitro* lipolysis method is not always *in vivo* predictive. For instance, Griffin et al. (2014) investigated the digestion behavior of three fenofibrate lipid formulations using above-mentioned *in vitro* model. While extensive precipitation was observed with the Type IIIB/IV formulation relative to the Type IIIA during *in vitro* digestion, no significant difference in *in vivo* bioavailability could be found in Landrace pigs following oral administration of these formulations.

1.5.3 Dissolution

In vitro dissolution testing is widely used for quality control (QC) of drug release from formulations, including LBFs. However, *in vivo* relevance is not always ensured.

As an example of comparing performance of different lipid dosage forms, Shah et al. (1994) investigated *in vitro* release of Ro 15-0778 from an oral solution, a SEDDS, a spray-dried powder, and a micronized formulation. Samples were determined in USP2 and 900mL dissolution medium with 5% of surfactant (Alkamuls EL-719). Superior *in vitro* drug release was observed for the PEG400 solution and SEDDS (Fig. 1-3), indicating its usefulness in comparing LBF-enhanced release of poorly soluble drug against their solid dosage forms. However, this trend was not reflected well in *in vivo* results (data not shown). A potential reason for the lack of concurrence is that the presence of the solubilizing surfactant in the dissolution medium led to an underprediction of drug precipitation *in vivo* (Hauss, 2007).

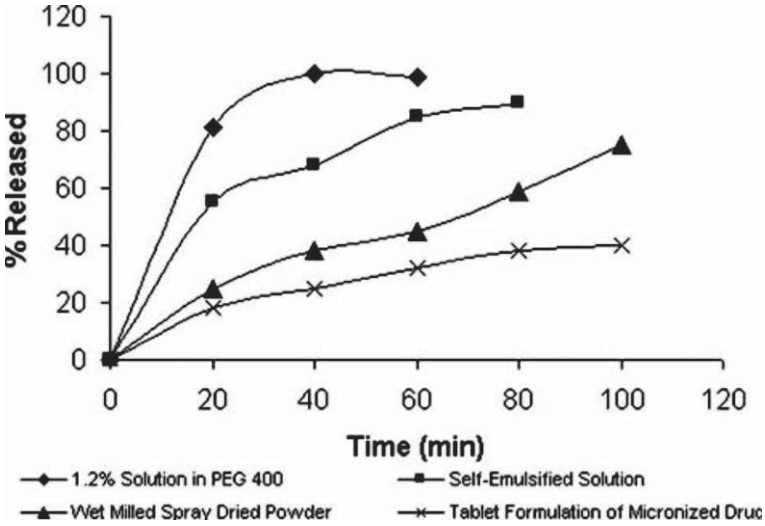

Fig. 1-3. *In vitro* release profiles of Ro 15-0778 from different formulations (Shah et al., 1994).

As another example, the effect of chain length, HLB and saturation of fatty acid present in the glyceride on Ro 15-0778 release from lipid-based solutions was evaluated using the paddle apparatus at 50rpm in 900mL of 5% Cremophor EL solution (Hauss, 2007; Shah et al., 1994). Drug release was optimal from a SEDDS

formulation prepared with surfactant Labrafac CM10 BM 287 (HLB approximately 10), while drug release declined as the surfactant HLB either increased (e.g. Labrasol®, HLB = 14) or decreased (e.g. Labrafil M 10 / NA 10, HLB < 10) from the optimal value of 10 (Labrafac CM10 BM 287).

Similarly, Serajuddin et al. (1988) examined *in vitro* dissolution of REV5901 from capsules that were filled with molten lipid-based solid dispersions of various PEGs and Gelucire 44/14, a self-emulsifying waxy semi-solid at room temperature. The results indicated incomplete dissolution from all of the PEG-based solid dispersions, whereas complete dissolution was obtained with Gelucire 44/14. This study also demonstrated the potential value of dissolution testing to discriminate drug release from LBFs.

Recently, Griffin et al. (2014) performed a kinetic assessment of dispersion and potential precipitation behaviors of fenofibrate LBFs using a mini-paddle dissolution apparatus (Erweka modified DT6 dissolution system). For all three LBFs studied, dispersion was complete in 10min with greater than 90% of the dose solubilized. The extent of drug precipitation was minimal (i.e. less than 5%) for over 2h. This *in vitro* finding was in line with the observed *in vivo* PK study in pigs, which also gave similar plasma profiles for different LBFs.

Based on an overview of these previous publications, in order to address the *in vivo* conditions in the human GI tract, biorelevant dissolution testing need to be carried out for prototype LBFs. This is one of the major research objectives of this dissertation.

1.6 Introduction of PBPK software applied in this research

1.6.1 Overview of STELLA® software, including establishment of the PBPK model

The STELLA® software, developed by Cognitus Ltd., North Yorkshire, UK, is a mechanistic *in silico* platform to run systematic dynamic modeling. In the last two decades, in the cases where post-absorptive pharmacokinetics are available, the STELLA® software has been successfully applied to simulate the plasma profile for

solid dosage formulations of various drugs (e.g. Dressman et al., 2008; Juenemann and Dressman, 2012; Juenemann et al., 2011; Muria et al., 2010; Nicolaides et al., 2001; Shono et al., 2011; Wagner et al., 2012). Different from commercial available whole-body PBPK software, STELLA® enables the user to build the *in silico* model. It allows a simple-but not simplified-semi-PBPK model to be built, usually comprising several interconnected compartments. Behind the graphic model map interface, input of ordinary differential equations (ODEs) and initial values are necessary in order to quantify the flows and compartments. In addition, the relevant human physiology in the GI tract and the prandial state need to be represented. Permeability, which is a molecule-specific parameter, is essential for the simulation. Post-absorptive PK parameters such as peripheral partition and drug elimination should be known as well. These parameters can be derived from fitting respective *in vivo* intravenous data using commercially available PK software. By incorporation of translated characteristic parameters of biorelevant *in vitro* dissolution data, the targeted plasma profile can be generated by the software by numerically solving the differential equation set.

As STELLA® software is a straightforward approach, it is favored when only limited knowledge is available for a certain case. Recent studies indicate the software's flexibility can also allow model adaption to facilitate incorporation of data from the transfer model[1] (Berlin et al., 2014; Fei et al., 2013a,b,c; Kostewicz et al., 2014a; Ruff et al., 2017).

Regarding the drawbacks of STELLA®, setting up a model for MR dosage forms, including their release and absorption in the colon, would be impractical. Further, barriers exist if first-pass metabolism, P-gp effect and regional differences in

[1] The transfer model is an *in vitro* dissolution model for predicting *in vivo* performance of oral dosage forms (Kostewicz et al., 2014b). It was originally described by Kostewicz et al. (2004), in which the predissolved drug in gastric vessels is pumped into the intestinal vessels (n = 1 or 3). Samples are withdrawn and analysed from the intestinal vessels. Transfer model experiments for the fenofibrate LBFs will be addressed as well in the present dissertation (Chapter 4).

absorption have to be considered. In such cases, commercially available whole-body PBPK software seems to be more appropriate (Kostewicz et al., 2014a).

1.6.2 Introduction of the Simcyp simulator and its application to evaluating LBFs

Simcyp was originally developed in the UK by Professor G. Tucker and is now part of the Certara company. The Simcyp simulator is a whole-body PBPK software built on a multi-compartmental GI transit platform, with the Advanced Dissolution Absorption and Metabolism (ADAM) algorithm. Population, species and pharmacodynamic features are addressed in Simcyp, too (Jamei et al., 2009a,b). The lengths/diameters of the GI segments for a virtual individual can be adjusted, while a variety of CYP enzymes are distributed in the intestinal tract (Kostewicz et al., 2014a).

In the present dissertation, in addition to STELLA®, Simcyp is used to simulate plasma profiles following administration of fenofibrate LBFs. With Simcyp, quite a few default parameters can be used without modification, thanks to the optimized human ADAM package. In addition, a prediction toolbox is available for calculation of some essential model parameters, which makes the software more user-friendly. To run a simulation, input of dissolution data is not mandatory, as an independent supersaturation value and/or precipitation rate can be included. The model captures a detailed description of the elimination pathways and drug-drug interactions that cannot be achieved by STELLA®.

1.7 Introduction of the LBFs and methodology used for the present dissertation

Two of the LBFs described in Chapter 5 were SMEDDSs (Type IIIA-MC, medium-chain lipids) administered as an oral solution on one occasion and as a capsule formulation on another occasion. A third SMEDDS formulation, with Tween 20 substituting for Tween 80, was also filled into capsules. The fourth formulation was a suspension of fenofibrate in a lipid-based excipient mixture. In addition, several trial lipid-based formulations are described in Chapter 4. In both Chapter 4 and 5, the LBFs are examined in biorelevant media with different *in vitro* approaches. Then, their plasma profiles are simulated using e.g. STELLA®, to combine the *in vitro* dissolution

with gastrointestinal parameters appropriate to the given prandial state (Nicolaides et al., 2001; Schiller et al., 2005; Yu, 1999), as well as the essential post-absorptive PK parameters that were obtained through deconvolution of the observed *in vivo* data.

Chapter 2. Aims of the thesis

2.1 Overall aim of the thesis

In order to provide a thorough performance evaluation of lipid formulations of fenofibrate, a variety of biorelevant analytical approaches and modeling demonstrations are needed in both fasted and fed state. Ability to predict the enhancement in oral bioavailability was used as the yardstick.

2.2 Aims of Chapter 4

This chapter discusses several prototype LBFs of fenofibrate that were developed at the Goethe University, Frankfurt. The major focus was on the biorelevant *in vitro* dilution, dispersion and dissolution testing, in increasing order of complexity. The risk of drug precipitation, as well as insight into *in vivo* findings is highlighted. Additionally, the STELLA® and Simcyp software were utilized to predict the plasma profiles.

2.3 Aims of Chapter 5

Thanks to the *in vivo* data of several proposed SMEDDSs/MDS of fenofibrate from Taipei Medical University, an *in vitro-in silico-in vivo* approach to predicting enhanced oral bioavailability of the drug was possible. The role of solubilization, dissolution and other potential key determinants of the absorption of fenofibrate (e.g. permeability, precipitation, food effect etc.) were identified and examined using the STELLA® based semi-PBPK model. This, in turn, should point the way to optimizing strategies for LBFs that consist mostly of surfactant excipients (Fei et al., 2013c).

Chapter 3. Materials and equipment

3.1 Materials

3.1.1 Chemicals

Table 3-1 lists the chemicals used in the experiments of this thesis.

Table 3-1

Chemicals used in the experiments

Chemical	Registered Trade Name/ Specification	Manufacturer	Lot
Acetonitrile	Analytical grade	Merck KGaA, Darmstadt, Germany	I525330007
C_8/C_{10} triglycerides	Myritol 318	Cognis GmbH, Düsseldorf, Germany	CE71900007
Conc. HCl	37% hydrochloric acid	VWR International GmbH, Darmstadt, Germany	10L060526
Copovidon	PVPVA	BASF, Ludwigshaven, Germany	not available
D-α-tocopheryl polyethylene glycol 1000 succinate	TPGS	Sigma-Aldrich Chiemie GmbH, Steinheim, Germany	BCBG6651V
Deionized water	Milli-Q, freshly prepared	Merck KGaA, Darmstadt, Germany	F9PN62936
Dichloromethane	Analytical grade	Merck KGaA, Darmstadt, Germany	DX0834-6
Egg phosphatidylcholine	Lipoid E PC®, 99.1% pure	Lipoid GmbH, Ludwigshafen, Germany	108015-1/42
Ethanol	Analytical grade	Merck KGaA, Darmstadt, Germany	K41470027
Fenofibrate	Ph. Eur.	Sigma-Aldrich Chiemie GmbH, Steinheim, Germany	BCBB4253

Table 3-1 (*Continued*)

Glacial acetic acid	Analytical grade	VWR International GmbH, Darmstadt, Germany	12B220508
Glycerylmonololeate	99.5% monoglyceride	Danisco Specialities, Brabrand, Denmark	173403-2202/107
H_3PO_4	85% ortho-phosphoric acid	Fluka Chemie AG, Buchs, Switzerland	12K210017
Hydrochloric acid solution	0.1N HCl	VWR International GmbH, Darmstadt, Germany	10H100500
Hydroxypropyl Methylcellulose Acetate Succinate	HPMCAS	Shin-Etsu, Tokio, Japan	not available
Hypromellose	HPMC	Colorcon GmbH, Idstein, Germany	not available
Long-life milk	3.5% fat	Milfina, Germany	not available
Maleic acid	99% pure	Sigma-Aldrich Chiemie GmbH, Steinheim, Germany	056K5473
Medium chain mono and diglycerides	Imwitor 988	Sasol GmbH Werk Witten, Germany	003041
Medium chain triglycerides	Labrafac™	Gattefosse, Lyon, France	not available
Medium chain triglycerides, C8-C10	Miglyol 812	Sasol GmbH Werk Witten, Germany	126822
Microsized fenofibrate tablets	Lipidil-Ter® 160mg	Solvay Arzneimittel GmbH, Hannover, Germany	15873
Nanosized fenofibrate tablets	Tricor® 145mg	Abbott Laboratories, North Chicago, USA	132452E
Pepsin	Ph. Eur., 0.51 U/mg	Fluka Chemie AG, Buchs, Switzerland	1241256

Table 3-1 (*Continued*)

Polysorbates	Tween 20	Wilton Site Redcar, Cleveland, UK	0000340418
Polysorbates	Tween 80	Sigma-Aldrich Chiemie GmbH, Steinheim, Germany	MKBD3974
Polyvinylpyrrolidone	PVP	BASF, Ludwigshaven, Germany	not available
Porous silica gel	PSG A and B	Merck KGaA, Darmstadt, Germany	not available
Sodium dihydrogen phosphate monohydrate	Analytical grade	Merck KGaA, Darmstadt, Germany	A0214049112
Sodium chloride	Analytical grade	VWR International GmbH, Darmstadt, Germany	08F160026
Sodium hydroxide pellets	Analytical grade	VWR International GmbH, Darmstadt, Germany	09G300017
Sodium hydroxide solution	0.1N NaOH	VWR International GmbH, Darmstadt, Germany	12C130503
Sodium oleate	82.7% pure	Riedel-de Haen, Seelze, Germany	51110
Sodium taurocholate	NaTC, > 97% pure	Prodotti Chimici Alimentari SpA, Basaluzzo, Italy	2011040152
Taurocholate and lecithin	SIF® Powder	Biorelevant.com, UK	01-1210-05

3.1.2 Overview of fenofibrate drug substance

The pure drug of fenofibrate is a near white fine powder in crystalline state, with the IUPAC name: propan-2-yl-2-(4-(4-chlorobenzoyl)phenoxy)-2-methylpropanoate (Mutschler, 2001). Its melting point is 80°C. Fenofibrate is a lipophilic neutral compound, and is poorly soluble in water (see value in Table 3-2). The water

solubility is not significantly influenced by pH. Fenofibrate is categorized as BCS class II, since its permeability is good (see value in Table 3-2), but its solubility is low. Its active metabolite, fenofibric acid, is a lipid-lowering agent for treatment of hypertriglyceridemia and hypercholesterolemia. The pharmacological effects lead to a reduction in total cholesterol, LDL-C, apo B, total triglycerides and triglyceride-rich lipoproteins. These effects are related to the activation of the peroxisome proliferator activated receptor α (PPAR α), resulting in increased lipolysis, and clearance of triglyceride-rich particles from plasma, as well as synthesis of HDL particles via synthesis of AI and AII (Buch et al., 2009b; Hanafy et al., 2007; Juenemann, 2012).

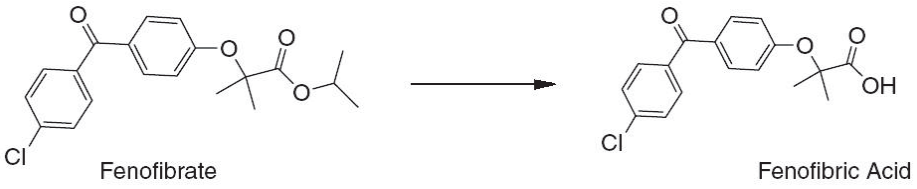

Fig. 3-1. Structure of fenofibrate and its metabolite fenofibric acid.

Table 3-2

Physicochemical properties of fenofibrate.

Property	Value
Molecular weight	360.83g/mol
Intestinal permeability	$2.66x10^{-5}$cm/s (Buch, 2010; Fei et al., 2013c) Experimentally measured, calculation details see Chapter 5
Melting point	80.5°C
logP	5.28
pKa	-4.9
water solubility	0.25µg/mL at 25°C, practically insoluble

Fenofibrate was chosen as the model drug because it is a poorly soluble compound that has shown an enhancement in absorption utilizing the lipid formulation approach, and the *in vivo* behavior of the LBFs in healthy volunteers is available in the open literature (Lin et al., 2011; Wei et al., 2010). Thus, it is possible to evaluate oral absorption of these LBFs through a novel *in vitro-in silico-in vivo* approach.

3.2 Equipment

The equipment, software and accessories used for this thesis are listed in Table 3-3.

Table 3-3

Equipment, software and accessories used in the experiments.

Name of equipment	Type	Manufacturer
Air dry oven	B12	Heraeus Instruments, Hanau, Germany
Balance	PA4102	Ohaus Corp. Pine Brook, NJ, USA
Cannula filter	Polyethylene, Erweka compatible	not available
Cannula for dissolution sampling	Stainless steel bent cannula device, Erweka compatible	not available
Centrifuge machine	Centrifuge 5417	Gerätebau Eppendorf GmbH, Germany
Digital photo camera	DMC-FS30 Lumix DC Vario	Panasonic AVC Networks Xiamen Co., Ltd., China
Filter	GF/D wGMF, 2.7µm pore	Whatman GmbH, Dassel, Germany
Filter	PTFE, 0.45µm pore	Whatman GmbH, Dassel, Germany
Filter	RC Anotop 25, 0.2µm pore	Whatman GmbH, Dassel, Germany
Filter	RC Spartan 30, 0.45µm pore	Whatman GmbH, Dassel, Germany
Glass syringes	5mL	Poulten & Graf GmbH, Wertheim, Germany
HPLC autosampler	LaChrom® L-7200	Merck Hitachi, Darmstadt, Germany

Table 3-3 (*Continued*)

HPLC column	LiChroCART® Purospher RP-18e 5µm, 125×4mm	Merck, Darmstadt, Germany
HPLC data integration software	EZ-Chrom Elite™ Version 2.8 Data System	Biochrom Ltd., Cambridge, UK
HPLC detector	LaChrom® L-7400 UV-Vis	Merck Hitachi, Darmstadt, Germany
HPLC pump	LaChrom® L-7110 pump	Merck Hitachi, Darmstadt, Germany
Magnetic stirring apparatus	VMS-C7 Advanced	VWR International GmbH, Darmstadt, Germany
Microscope	Leica DMI 4000B	Leica GmbH, Germany
Milli-Q water generator	Direct-Q® 3 UV	Millipore, Merck KGaA, Darmstadt, Germany
Orbital shaker	polymax 1040	Heidolph, Germany
Origin® software	Version 8.0	OriginLab Corporation, MA, USA
Osmolality tester	OSMOMAT 030	Gonotec GmbH, Berlin, Germany
PC	OPTIPLEX 745	DELL, Germany
Peristaltic pump	ISM915A	IDEX Health & Science GmbH, Wertheim, Germany
pH meter	pH1000H	pH enomenalTM, VWR Int., Leuven, Belgium
Pipette	100µL Reference	Eppendorf GmbH, Germany
Pipette	1000µL Research	Eppendorf GmbH, Germany
Pipette	5000µL Research	Eppendorf GmbH, Germany
Precision balance	AB204-A	Mettler Toledo, Switzerland
Refrigerator	362351	Gorenje, Germany

Table 3-3 (*Continued*)

Rotary evaporator	R114	BÜCHI Labortechnik GmbH, Essen, Germany
Simcyp® software	V12 Simulator/Animal	Simcyp Ltd., Sheffield, UK
Sonication water bath	T790/H	Elma, Germany
STELLA® software	Version 9.1.3	Cognitus Ltd., North Yorkshire, UK
Transfer pipettes	3.5mL REF 86.1171	Sarstedt Aktiengesellschaft & Co., Nümbrecht, Germany
Tubing for the pump	2.5mm diameter, rubber material	not available
Uniprep™ filter	PTFE, 0.45µm pore	Whatman Inc., NJ, USA
USP II Dissolution apparatus plus mini-paddles and mini-vessels	Erweka Dissolution-Tester DT 700, 250mL medium is filled per mini-vessel	ERWEKA GmbH, Heusenstamm, Germany
USP II Dissolution apparatus plus paddles and vessels	Erweka Dissolution-Tester DT 80, 500mL medium is filled per vessel	ERWEKA GmbH, Heusenstamm, Germany
USP III Dissolution apparatus	RRT 8	ERWEKA International Ltd., Baettwil, Switzerland
Vortex mixer	G560E	Scientific Industries, Inc., USA
Water bath	W1	Prüfgeräte-Werk Medingen GmbH, Germany
WinNonlin® software	Version 5.2.1	Pharsight Corporation, Mountain View, CA, USA

Chapter 4. Study of LBF No.1 – No.7 of fenofibrate

4.1 Dispersion and dilution experiments

The fenofibrate LBFs No.1 and No.2 were developed by the LFCS Consortium: the LBF No.1 is a Type IIIA formulation, while LBF No.2 is a Type IIIB. Their compositions are listed in Table 4-1.

4.1.1 LBFs (No.3 – No.4) developed at the Goethe University Frankfurt

4.1.1.1 Choice of lipid-based excipients

Fenofibrate LBFs No.3 and No.4 referred to in this chapter were designed at the Goethe University. The lipid-based excipients were chosen and composed according to the LFCS guidance. These formulations belong to LFCS Type IIIA and IIIB respectively, and contain glycerides, water-soluble surfactants and hydrophilic co-solvents (see Table 4-1 for detailed LBF compositions).

Table 4-1

Composition of the lipid formulations used in Chapter 4.

LFCS	Per capsule	Nominal ratio	Frankfurt	Per dose	Nominal ratio
No.1 Type IIIA	500mg	100%	No.3 Type IIIA	2660mg	100%
Fenofibrate	20mg	4.0%	Fenofibrate	160mg	6.0%
Labrafac	168mg	33.6%	Miglyol 812	833.3mg	31.3%
Tween 80	240mg	48.0%	Tween 80	833.3mg	31.3%
Imwitor 988	72mg	14.4%	Imwitor 988	833.3mg	31.3%
No.2 Type IIIB	500mg	100%	No.4 Type IIIB	2660mg	100%
Fenofibrate	20mg	4.0%	Fenofibrate	160mg	6.0%
Ethanol	168mg	33.6%	Tween 80	1250mg	47.0%
Tween 80	240mg	48.0%	Imwitor 988	1250mg	47.0%
Imwitor 988	72mg	14.4%	-	-	-

Among the excipients used, Labrafac and Miglyol 812 belong to medium chain triglycerides; Tween 80 is a water-soluble surfactant; Imwitor 988 belongs to the medium chain mono- and diglycerides; and ethanol is a hydrophilic co-solvent with medium polarity. According to the LFCS, LBF No.4 is not a typical Type IIIB formulation, since no hydrophilic co-solvent is present in its composition, LBF No.4 can be viewed as an intermediate type between IIIA and IIIB.

Whilst LBF No.1 & No.2 were prepared in soft-gelatin capsules, dose aliquots of the LBF No.3 & No.4 for dissolution in 500mL medium were quantified using a pipette (by direct withdrawal from the drug loaded, homogenous bulk LBF mixture), so that no capsule shells were needed. It can be seen from Table 4-1 that the LBFs No.3 & No.4 had a higher concentration of drug than LBFs No.1 & No.2.

4.1.1.2 Preparation of fenofibrate lipid formulations

To prepare 20g of bulk LBF No.1, 6.72g of Labrafac, 9.6g Tween 80 and 2.88g Imwitor (previously melted at 50°C) was added to a 100mL Schott flask. Using a magnetic stirrer, they were gently mixed for approx. 10min to obtain a homogeneous mixture. Then, 0.8g fenofibrate powder was added to the lipid vehicle and subsequently stirred until completely dissolved (approx. 30min).

To prepare 20g of bulk LBF No.2, 6.72g of ethanol, 9.6g Tween 80, 2.88g Imwitor and 0.8g fenofibrate were formulated according to the above-mentioned protocol.

Capsules containing LBF No.1 or No.2 were prepared for testing in USP 3 apparatus. Using a pair of scissors, a capsule was cut open at the narrow edge (approx. midway), placed on a precision balance and tared. A 2mL plastic syringe fitted with 0.9x40mm cannula was used to fill the capsule with ca. 500mg of above lipid formulation (accurately weighed). Once filled, the capsule was re-sealed with a pair of preheated forceps.

To prepare 21.28g of bulk LBF No.3, 6.67g Miglyol, 6.67g Tween 80 and 6.67g Imwitor and 1.28g fenofibrate were formulated according to the same protocol used for LBF No.1 and 2.

To prepare 21.28g of bulk LBF No.4, 10g Tween 80, 10g Imwitor and 1.28g fenofibrate were formulated according to the above-mentioned protocol.

All above operations were performed at room temperature. The excipients and API were from the same batches. The LBFs were freshly prepared prior to various *in vitro* experiments.

4.1.1.3 Media preparation

To simulate conditions in the fasted and fed stomach in the dilution and dispersion experiments, Fasted State Simulated Gastric Fluid pH 1.6 (FaSSGF) and Fed State Simulated Gastric Fluid pH 5.0 (FeSSGF) were used. To simulate the intestinal conditions, the Simulated Intestinal Fluid pH 6.8 (SIF_{sp}), and an updated version of Fasted State Simulated Intestinal Fluid pH 6.5 (FaSSIF-V2) were used. The media were prepared as previously described (Galia et al., 1998; Jantratid et al., 2008; Vertzoni et al., 2005). In addition, water was used as a reference medium for dissolving the LBFs.

For the *in vitro* transfer model study, FaSSGF was used, but with the pH adjusted to 2 (FaSSGF pH 2). Correspondingly, a modified version of FaSSIF containing phosphate salt and 0.5mM Lecithin was used (FaSSIF-V2(PO_4)). Table 4-2 summarizes composition of these media.

The original intention of using FaSSIF-V2(PO_4) was to examine the potential risk of drug precipitation due to pH elevation with GI transit. For the transfer model, 250mL of FaSSGF pH 2 is pumped over a period of time into 500mL of FaSSIF-V2(PO4). By using the FaSSIF-V2(PO_4) (which shows somewhat higher buffer capacity than the maleate version) together with FaSSGF pH 2, the reduction in pH of the intestinal compartment can be minimized, thus circumventing the need to add NaOH to adjust the pH of the medium.

Table 4-2

Composition of gastric and intestinal media in the fasted state for the transfer model.

	FaSSGF pH 2	FaSSIF-V2(PO_4)
Composition		
Sodium taurocholate (mM)	0.08	3
Lecithin (mM)	0.02	0.5
Pepsin (mg mL^{-1})	0.1	–
Sodium chloride (mM)	34.2	62.6
Hydrochloric acid (mM)	12.6	–
Monobasic sodium phosphate (mM)	–	28.6
Sodium hydroxide (mM)	–	8.7
Characteristic parameter		
pH	2.0	6.5
Osmolality (mOsm kg^{-1})	120 ± 2.5	180 ± 10
Buffer capacity (mmol L^{-1} ΔpH^{-1})	–	12

FaSSIF-V2(PO_4) was developed by modifying a previous version of FaSSIF, which has a buffer capacity of 12mmol L^{-1} ΔpH^{-1} and osmolality of 270±10mOsm kg^{-1} (Vertzoni et al., 2004). As the buffer capacity was determined through the acid-base titration method, the consumed amount of monobasic sodium phosphate can be monitored. Van Slyke equation (Donald and Van Slyke, 1922) was used to calculate the buffer concentration needed to obtain the target buffer capacity.

Fig. 4-1 shows the result of the titration experiment. Consistent profiles can be drawn among all three media ued: 3 – 3.5mL consumption of 0.1N HCl resulted in a pH reduction from 6.5 to 5.5 for all three media. This result shows that the newly developed FaSSIF-V2(PO_4) has the same buffer capacity as the old version FaSSIF.

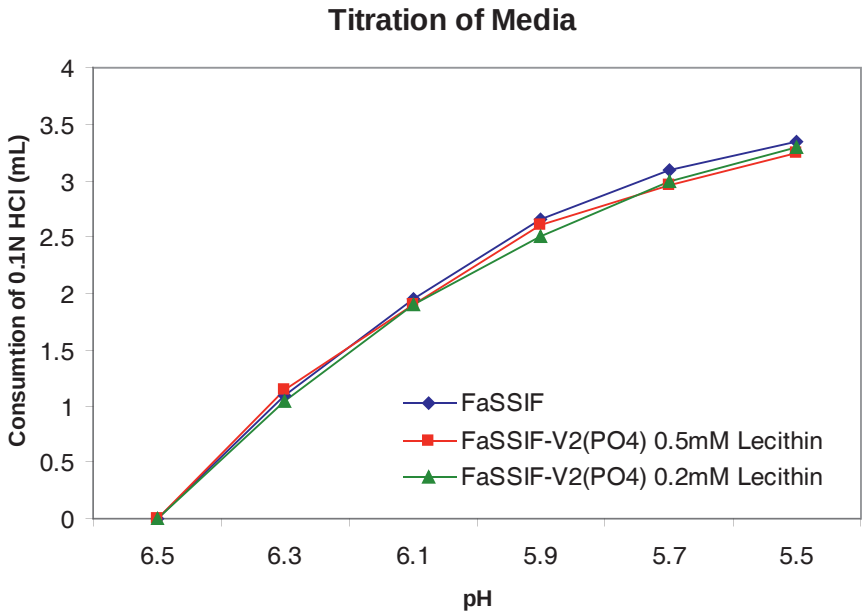

Fig. 4-1. Comparison of buffer capacity among various versions of FaSSIF.

The osmolality of FaSSIF-V2(PO_4) was adjusted by adding NaCl. Calculation of the osmolality was based on the freezing point depression of the solution (Arndt et al., 2013). An osmolality tester was used for these measurements.

In summary, FaSSIF-V2(PO_4) was successfully developed with a buffer capacity of 12mmol L^{-1} ΔpH^{-1} and an osmolality of 180±10mOsm kg^{-1} (Table 4-2). FaSSIF-V2(PO_4) is the most frequently used fasted state intestinal medium for the present dissertation.

4.1.1.4 Dispersion and dilution test set-up of LBF No.2

As the dispersion of the LBF No.1 of fenofibrate was not performed by the author, those results are not provided in this thesis. Rather, the dilution experiments of Section 4.1.1 were conducted solely with LBF No.2 (Type IIIB).

Water, 0.1N HCl, FaSSGF, FaSSIF and FeSSGF were used as the dilution media. In order to achieve the target dilutions, different ratios of medium and LBF No.2 were studied, as summarized in Table 4-3.

Table 4-3

Medium dilution and sample weights of LBF No.2:

Formulation-medium-ratio (m:m) & significance	Mass formulation	Mass medium
1:2 (initiation of LBF dilution)	2.00 g	4.00 g
1:5 (laminar phase formed with dilution)	1.00 g	5.00 g
1:200 (fine dispersion formed by e.g. 2x capsules together with a glass of water, of *in vivo* relevance)	0.04 g	8.00 g

For each evaluation, the medium was weighed into glass vials and warmed to 37°C. Then formulation No.2 was added to the medium. The medium/formulation mixture was gently agitated on an orbital shaker located in a 37°C oven, and was examined macroscopically and microscopically. Samples were withdrawn at 10, 30 and 120min, which represent the initial stage of LBF dilution *in vivo* (10min), the middle stage of LBF dispersion *in vivo* (30min), and the late stage of LBF residence *in vivo* (2h). An additional macroscopic picture of the vial was taken after 24 hours. Some of the equipment involved is shown in Fig. 4-2.

Fig. 4-2. Experimental equipment used for dilution studies (water bath, vortex mixer, vials etc.)

4.1.1.5 Discussion of the dilution results of LBF No.2

The dilution results of LBF No.2 are presented in water, 0.1N HCl, FaSSGF, FaSSIF and FeSSGF. For brevity, only a summary of the results and overall trends is given here. Detailed results can be found in Tables A-1 to A-15 in the Appendix.

Microscopically, as is shown from Table A-1 to Table A-15, the outcomes with dilution ratios of 1:2, 1:5 and 1:200 (m:m) of fenofibrate LBF No.2 showed similar trends in the various media tested, i.e. water, 0.1N HCl, FaSSGF, and FaSSIF (Table A-1 to Table A-12): For most of the 1:2 dilutions (i.e. Table A-1, Table A-4, Table A-7 and Table A-10), some precipitate or API crystals were detected at 2h. For the dilution ratio 1:5, precipitation was less pronounced than that of 1:2 (see Table A-2, Table A-5, Table A-8 and Table A-11), while for the dilution ratio 1:200, almost no precipitation was detected microscopically in any of the media (see Table A-3, Table A-6, Table A-9 and Table A-12). These observations can be attributed to the lower degree of supersaturation in the 1:200 dilutions. In all fasted state media, the dispersion behavior of the fenofibrate lipid formulation No.2 was coherent. This indicates that the major contributor to fenofibrate solubilization may arise from the lipid-based excipients, rather than the dissolved bile salts / lecithin etc. in the biorelevant media.

By contrast, microscopic observation of the dilution tests in FeSSGF showed pronounced flocculation of the LBF/medium mixture at dilution ratios of 1:2 and 1:5 (Table A-13 and A-14). This might due to an interaction of the concentrated LBF with the milk protein in FeSSGF. Only the 1:200 dilution of FeSSGF resulted in a homogeneous emulsion with finely dispersed particles/droplets (Table A-15). In addition, for FeSSGF, no precipitation was detected at any dilution ratio. This suggest that the fenofibrate LBF can be successfully solubilized in the fed state stomach.

Macroscopic observation of the dilutions by direct addition of the lipid formulations into water, 0.1N HCl, FaSSGF and FaSSIF showed clear to partially clear appearance of the formulation/media mixture. On the other hand, the dilutions in FeSSGF showed a uniform or separated milky white appearance of the liquids in the vials.

4.1.2 LBFs developed by scientists from Ireland, Switzerland, Greece and Germany (No.5 – No.7)

The fenofibrate LBFs described in Section 4.1.2 were arbitrarily assigned Serial No.5 – No.7 in thesis. They were first described by Griffin et al. (2014) from University College Cork. Other collaborating partners included the University of Applied Sciences and Arts Northwestern Switzerland, the National & Kapodistrian University of Athens, and the Goethe University Frankfurt. The work in Frankfurt focused on dilution testing of the lipid formulations.

An *in vitro* digestion study by the UCC partner suggested different behaviour for different lipid formulations. However, an *in vivo* study in pigs showed a lack of significant difference in bioavailability (Griffin et al., 2014). Thus, a more suitable *in vitro* test needed to be developed to better reflect their behaviour *in vitro*.

4.1.2.1 Dilution test set-up of LBFs No.5 – No.7

The Self Micro-Emulsifying Drug Delivery Systems (SMEDDSs) of LBFs No.5 – No.7 are either Type IIIA LC/MC or Type IIIB/IV formulations. They contain the following components (Table 4-4):

Table 4-4

Composition of fenofibrate LBFs No.5 – No.7

Serial number in thesis	LBF No.5	LBF No.6	LBF No.7
Lipid formulation classification	Type IIIA LC	Type IIIA MC	Type IIIB/IV
Olive Oil – LCT (% blank formulation)	40	-	-
Miglyol 812 – MCT (% blank formulation)	-	40	-
Cremophor RH (% blank formulation)	20	20	33
Tween 85 (% blank formulation)	40	40	67
Fenofibrate (drug load: mg/g blank LBF)	80	80	80

The three SMEDDSs of LBFs No.5 – No.7 were prepared with a lipid (0-40% w/w of LCT or MCT), a surfactant (20-33% w/w of Cremophor RH 40) and a co-surfactant

(40-67% w/w of Tween 85). The exact quantity of each excipient was weighed into a screw-cap flask. Cremophor RH was melted before weighing in. The flask was heated to 50°C and gently stirred for approx. 5min to ensure thorough mixing. Accurately weighed fenofibrate (80mg/g of blank LBF) was then mixed into the lipid blend under gentle agitation to facilitate drug dissolution. After a homogeneous mixture was attained, the loaded SMEDDS was cooled to ambient temperature. Additional visual inspection was also performed.

Although fenofibrate was completely dissolved in the lipid excipients under stirring and heating when preparing the formulation, the API in the LBF No.5 precipitated overnight at room temperature. Thus, before using LBF No.5, it was always heated under stirring to redissolve the API. Meanwhile, LBF No.6 & No.7 showed no evidence of precipitation after overnight storage. Their excipient components (see Table 4-4) are relatively stable at room temperature. Nevertheless, before using LBF No.6 & No.7, they were incubated in a 37°C water bath under stirring.

The dilution experiment of LBF No.5 – No.7 comprised three phases. In Phase I, 1:5 and 1:200 dilutions were carried out using deionized water and SGF at room temperature. Photographs of each formulation were taken at 10, 30, 60, 120min and 24h. In Phase II, the same procedure as Phase I was performed at 37°C. In Phase III, the same procedure as Phase II was performed using FaSSGF and FaSSIF-V2.

First, the diluted samples were vortexed to ensure complete mixing. Then the samples were periodically analyzed macroscopically and microscopically. Photographs were taken using a digital camera (Lumix DC Vario, Panasonic) without shaking the samples. Additionally, microscopic photos were taken at 30 and 120min to allow identification of crystal formation. For photography under the microscope, samples were withdrawn after gentle shaking of the vials. Glass slides and cover slips were used to hold the sample droplets. Sample fields were captured at 40x magnification with a Leica DMI 400B microscope.

4.1.2.2 Results and discussion

Owing to the large number of photographs taken, only a few representative pictures of the dilution test (e.g. in biorelevant media) are shown in this section. Outcome of the other tests are summarized in the text.

Water at room temperature (RT) showed development of medium sized crystals from the Type IIIA LC formulation (No.5) at a dilution ratio of 1:5 after 120min. Both Type IIIA LC and IIIA MC (No.5 & No.6) showed slight precipitation under the microscope. As expected, for dilutions of the Type IIIB/IV formulation (No.7), precipitation could be observed from water and SGF at room temperature. For the Phase II experiment at 37°C, fenofibrate did not precipitate from the water dilution of Type IIIA LC formulation (No.5). However, it precipitated slightly from the Type IIIB/IV (No.7) at a dilution ratio of 1:5. For the 1:200 dilutions, no precipitation was observed from the Type IIIB/IV formulation (No.7).

With a temperature elevation from 25°C to 37°C, which reflects the *in vivo* condition better, drug solubility was increased in the 1:200 dilutions. In the Phase III experiment, fenofibrate was better solubilized in biorelevant media. As FaSSGF and FaSSIF-V2 resemble the real conditions in the upper GI tract much better than SGF and water, it was concluded that the lipid formulations would generate more solubilized API available for *in vivo* absorption.

Although precipitation decreased in FaSSGF and FaSSIF-V2, some crystals were observed microscopically in both the 1:5 and 1:200 dilutions, as exhibited in Fig. 4-3. Occasionally, fine crystals could be detected macroscopically as well. As can be seen from Fig. 4-3, the three LBFs (No.5 – No.7) formed isotropic fine emulsions with 1:200 dilutions in both FaSSGF and FaSSIF-V2. The Type IIIB/IV formulation (No.7) formed a pale white colloidal dispersion, suggesting formation of an ultra-fine dispersion. In the 1:5 dilutions, turbidity was increased and the samples were less transparent. Microscopically, the Type IIIA LC and IIIA MC formulations (No.5 & No.6) exhibited minimal precipitation. For the Type IIIB/IV (No.7), crystals of fenofibrate were observed in the 1:5 dilutions. While precipitation was greater in the

1:5 dilutions, this represented the worst case scenario *in vivo*, in which the LBF would undergo a low level of dilution in the GI tract. At a dilution level of 1:200, precipitation was minimal for all three LBFs. This reflected the best case scenario i.e. when ca. 200mL of water was co-administered with the formulation.

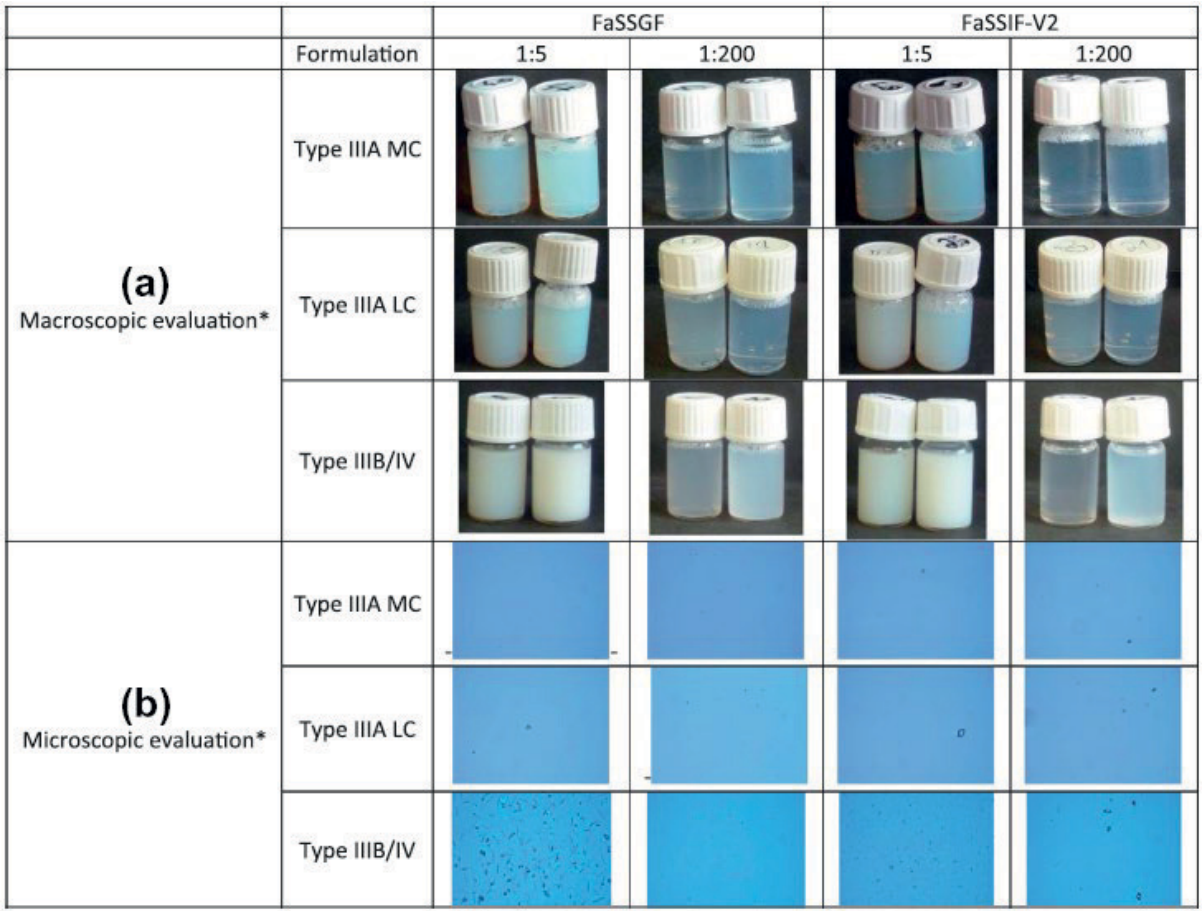

Fig. 4-3. Macroscopic and microscopic observations following dilution of the LBFs in biorelevant media. The Type III A LC (No.5), Type IIIA MC (No.6) and Type IIIB/IV (No.7) formulations were diluted 1:5 and 1:200 using FaSSGF and FaSSIF-V2. (a) Macroscopic observations of glass vials containing drug-free (left) and fenofibrate-loaded formulations (right) under various dilution conditions. (b) Micrographs showing images of fenofibrate precipitates observed to varying degrees in the media, *120min after dilution.

Summarizing the Phase III experiments using FaSSGF and FaSSIF-V2 at 37°C, the same trend can be found with each formulation. Some precipitation was observed

from the Type IIIB/IV formation (No.7) at a low dilution level, while at a higher dilution level the degree of precipitation was minimized across all three LBFs investigated, as is depicted in Fig. 4-3 (Griffin et al., 2014).

Summarizing all the Phase I – III experiments of LBF No.5 – No.7, the Type IIIB/IV formulation (No.7) showed observable precipitation at all media temperature combinations. Type IIIA MC (No.6) exhibited the least amount of precipitation (full data not shown), while the Type IIIA LC (No.5) formulation showed a medium level of precipitation in the media tested (full data not shown). However, no significant difference in precipitation behavior among the formulations was found in these dilution tests. Thus, this *in vitro* approach is in line with the *in vivo* data in pigs.

4.2 Solubility experiments

The solubility of fenofibrate drug substance in several dissolution media is given in Table 4-5 and 4-6. Solubility enhancement of fenofibrate in the presence of lipid-based excipients was also measured. Through these studies, a better understanding of the following points was achieved: (a) Solubilization effect of the micelle components from biorelevant media; (b) Contribution of lipid formulation to the overall solubilization of fenofibrate from the diluent mixture.

4.2.1 Literature Data

The solubility of fenofibrate drug substance was previously determined by Vogt et al. (2008) in water, FaSSIF and FeSSIF. Using a standardized shake flask method, the samples were incubated at 37°C for 48h, filtered through a 0.22µm membrane filter, and assayed by using HPLC. The Vogt data shown in Table 4-5 were used as a reference for comparison to the values measured in updated biorelevant media, in the lipid formulations and their dilutions.

Table 4-5

Solubility study of fenofibrate in various media at 37°C, unit in μg/mL (mean ± SD) (Vogt et al., 2008)

Water	Blank FaSSIF	FaSSIF	Blank FeSSIF	FeSSIF
0.3 ± 0.0	0.2 ± 0.0	13.7 ± 0.5	0.2 ± 0.0	35.6 ± 1.0

Another solubility experiment was performed by Arndt et al. (2010) using the Fed State Simulated Gastric Emulsion (FeSSGEm) together with Whatman Uniprep™ filters (0.45μm pore size) at 37°C. Moreover, solubility in FeSSGF was performed using 2.7μm GF/D filters using the shake flask method. In these cases, approx. 20mg of fenofibrate was weighed into each unit and 3mL of medium was added. After 24h incubation, the samples were filtered, diluted and analyzed (result see Table 4-6). The implication of these values will be discussed in Section 4.2.4.

Table 4-6

FFB solubility in FeSSGF & Fed State Simulated Gastric Emulsion (FeSSGEm) at 37°C, unit in μg/mL (mean ± SD) (Arndt et al., 2010)

	FeSSGF	Middle FeSSGEm
Solubility of Fenofibrate	219.7 ± 39.7	1454.5 ± 203.3

FeSSGEm, representing the Fed State Simulated Gastric Emulsion, was developed by Kilic et al. (2010). Representative middle stage FeSSGEm contains 181.7mM sodium chloride, 18.31mM acetic acid, 32.98mM sodium acetate and 8.75% of Lipofundin®. The middle stage FeSSGEm has a fat content of 1.75%. It has a pH of 5.0, an osmolality of 400±10mOsm kg^{-1}, and a buffer capacity of 25mmol L^{-1} ΔpH^{-1}. Among the ingredients, Lipofundin® MCT 20 is a commercially available parenteral emulsion, which contains 10% of soybean oil, 10% of MCT, 1.2% of egg phosphatidylcholine, 2.5% of glycerol, 0.02% of α-tocopherol, and 0.03% of sodium oleate.

4.2.2 Solubility test set-up and sample preparation

In this study, solubility data of fenofibrate were generated in (a) FaSSGF, FaSSIF-V2, and FeSSIF-V2 using 0.45µm Uniprep™ filters. The results were compared with literature data generated from the old versions of FaSSIF and FeSSIF (Table 4-5). (b) The solubility in FeSSGEm was tested by shake flask method. (c) In addition, the solubility enhancement in presence of LBF was examined using Uniprep™ filters in media simulating the conditions achieved when the gastric content is completely transferred into the proximal intestine (i.e. a mixture of 250mL gastric medium and 500mL intestinal medium).

(a) Solubility of fenofibrate drug substance in Blank FaSSIF-V2, FaSSIF-V2, Blank FeSSIF-V2, FeSSIF-V2 and FaSSGF media was performed using 0.45µm Uniprep™ filters on an orbital shaker that was incubated at 37°C for 24h.

FeSSIF-V2 showed slight phase separation/precipitation when mixed with organic solvent (i.e. with the mobile phase at 1:1 volume ratio). Thus, the diluted solubility samples of FeSSIF-V2 were centrifuged at 14000rpm for 5min before HPLC injection.

(b) Solubility of fenofibrate in middle FeSSGEm was assessed at 37°C for 24h on an orbital shaker using the shake flask method. Filters with 2.7µm (Whatman GF/D w/GMF), 0.45µm (Whatman PVDF w/GMF) and 0.20µm (Sartorius RC Membrane) pore were tested. This was done to determine the effect of pore size and filter material and their possible ramifications for the accuracy of the solubility results.

Within each above-mentioned unit (i.e. Uniprep™ filters or glass vials), 3mL of medium and approx. 10mg of fenofibrate were added. Three units were used to generate a mean solubility value for each condition (n = 3).

To get rid of the excipient molecules that were introduced form the FeSSGEm medium (e.g. soybean oil, medium chain triglycerides, glycerol etc.), 1.2mL of acetonitrile was added into 0.3mL of sample with FeSSGEm in a 2mL centrifuge tube. The tube was vortexed for a few seconds to ensure effective mixing. Then, the sample

tube was centrifuged at 14000rpm for 5min. The supernatant was withdrawn and an aliquot was subsequently transferred into the HPLC vial.

(c) Solubility of LBF No.1 – No.4 loaded fenofibrate was assessed in the combined media of FaSSGF pH2 + FaSSIF-V2(PO_4) 0.2mM Lecithin, FaSSGF pH2 + FaSSIF-V2(PO_4) 0.5mM Lecithin, and SGF pH2 + SIF pH6.8. To maintain sufficient supersaturation, the highest strengths were used for the solubility test (i.e. 100mg for No.1 & No.2, and 150mg for No.3 & No.4). A dilution ratio of 1:300 was used to match the dilution of the highest dose in the volume used for the dissolution test, i.e. 2.5mL of API loaded lipid vehicles added to 750mL of the combined gastric (250mL) and intestinal (500mL) media. In practice, the volumes were scaled down so that ca. 10mg of each fenofibrate lipid formulation (accurately weighed) was added to 3mL of prewarmed media combination in a Uniprep™ filter (n = 3). Deviations from 10mg in the weighing procedure were corrected by normalizing the recovery. After 24h incubation at 37°C, the samples were filtered and immediately diluted 1:1 with the mobile phase.

4.2.3 Solution preparation and HPLC method (common to the entire thesis)

A calibration curve was prepared by appropriate dilution of the stock solution with mobile phase. The standard curve typically comprised 5 – 6 concentrations. The stock solution was prepared using the mobile phase at an API concentration of 1000µg/mL. The mobile phase was a mixture of acetonitrile and Milli-Q water (v/v, 80/20) and its pH was adjusted to 2.5 with ortho-phosphoric acid. The reference solutions were diluted 1:1 using the respective medium or media combination (exception: for FeSSGEm, it was 4:1). The reference and test solutions for HPLC analysis were prepared in the same manner. For the calibration curve, to show linearity should be no less than $r^2 = 0.999$ over the range 25 – 120% of the nominal concentration of a single dose. Reference solutions were freshly prepared on the day of sample analysis. The LOQ was set as 10-fold of the residual standard deviation of y-intercept of the regression line divided by its slope. The LOQ should be no greater than the lower limit of the specified range of the calibration curve.

As an example, a typical chromatogram and calibration curve for dissolution of fenofibrate are shown by Fig. A-1 and Fig. A-2 in the Appendix. Using ANOVA regression, the LOQ was calculated to be 23.6µg/mL, which equaled 11.8% of the nominal concentration (Note: the nominal concentration was 200µg/mL, single 50mg dose strength was dissolved in 250mL medium, see Fig. 5-2). Since 11.8% is smaller than the range lower limit of 25%, the specified concentration range of 25 – 120% can be well quantified.

The HPLC hardware components used are listed in Table 3-3. The wavelength of UV detector of the HPLC system was set at 254nm. The injection volume was 20µL. The flow rate of mobile phase was 0.85mL/min. The analysis was performed at ambient temperature. Using these conditions, fenofibrate was typically eluted at 4.5 – 4.6min.

The above conditions are common for all the quantification of fenofibrate concentration using HPLC, across the thesis.

4.2.4 Results and discussion of the solubility tests

Fenofibrate solubility in FaSSIF-V2 and FeSSIF-V2 is listed in Table 4-7. The values are somewhat different from the old version FaSSIF/FeSSIF (Table 4-5)

Table 4-7

Solubility of fenofibrate in updated biorelevant media

	Blank FaSSIF-V2	FaSSIF-V2	Blank FeSSIF-V2	FeSSIF-V2	FaSSGF
Solubility (µg/mL)	0.79 ± 0.04	2.63 ± 0.08	0.98 ± 0.05	50.07 ± 1.70	0.68 ± 0.02

For the intestinal media, the measured solubility of fenofibrate is 13.7µg/mL in FaSSIF, and 2.63µg/mL in FaSSIF-V2. In the fed state, the solubility values are 35.6µg/mL in FeSSIF, and 50.1µg/mL in FeSSIF-V2. Thus, a pronounced positive food effect is predicted for fenofibrate drug substance. The difference in solubility

using different version of media can be attributed to their difference in composition and buffer capacity. The solubilization of fenofibrate mostly comes from the fat content of food, micelles and bile salts from the biorelevant media, since their respective blank buffer dissolved the drug only slightly (less than 1µg/mL).

For the gastric media, solubility of fenofibrate is 0.68µg/mL in FaSSGF (Table 4-7), and more than 200µg/mL in FeSSGF (Table 4-6). This indicates a meal can remarkably enhance the solubility of fenofibrate in the stomach. For the intestinal media, the same trend can be observed comparing the solubility in FaSSIF-V2 and FeSSIF-V2 (see Table 4-7).

In the case of FeSSGEm, phase separation occurred when filtering the samples using 0.20µm RC and 0.45µm PVDF filters (Table 4-8). Using these filters, the initial portion of filtrate was transparent, whilst the later portion of filtrate had a milky white appearance. This might explain why a larger standard deviation was observed for these filters than for the 2.7µm GF/D filter. While the 0.45µm PVDF filters work well, using the 0.20µm RC filter also appears possible, since the resistance of the syringe attached to the RC filter dropped significantly after initial saturation.

Table 4-8

Solubility of fenofibrate in middle FeSSGEm

Filter type	FeSSGEm 2.7µm Whatman GF/D w/GMF	FeSSGEm 0.45µm Whatman PVDF w/GMF	FeSSGEm 0.20µm Sartorius RC Membrane
Solubility (µg/mL)	797.67 ± 32.88	301.60 ± 207.91	1160.83 ± 289.57
Observation of the filtrate	Milky	Initially clear, later milky	Initially clear, later milky

From another point of view, the 0.20µm RC filter has the smallest pore size, but it gives the greatest solubility value (more than 1000µg/mL). This could also be due to a defective filter. Comparing the 0.45µm PVDF and the 2.7µm GF/D filters, the value generated by the 0.45µm PVDF filter (301.6µg/mL) appears more reasonable, because it is more in line with the results with the 2.7µm filter.

In the literature results shown in Table 4-6 (Arndt et al., 2010), the fenofibrate solubility assessed in FeSSGEm using Uniprep™ filters was more than 1400µg/mL. This enormously high value indicates that Uniprep™ filters are not suitable for filtration of FeSSGEm. In contrast, fenofibrate solubility assessed in FeSSGF using 2.7µm GF/D filters was found to be 219.7µg/mL. This combination seems to be more reasonable, as the solubility value generated is comparable to that obtained from the FeSSGEm medium using 0.45µm PVDF filters (301.6µg/mL).

Pure fenofibrate dissolved poorly in compendial media of SGF + SIF (0.09µg/mL). Same improvement was observed when biorelevant media were utilized (1.31 – 4.31µg/mL). However, the solubilization effect induced from bile salts and/or lecithin was minimized once the lipid formulation was involved.

As exhibited in Table 4-9, in the presence of lipid-based excipients, the solubility of fenofibrate increased significantly (57.2 – 86.3µg/mL) in comparison to the pure drug substance alone (≤ 4.3µg/mL). Independant to the media used, all of the lipid blends (No.1 – No.4) showed potent solubilization of fenofibrate.

Table 4-9

24h solubility of fenofibrate at 37°C in presence of lipid-based excipients in different media combinations (unit in µg/mL, fixed drug load with 1:300 dilution ratio, n = 3)

Formulation	FaSSGF pH2 + FaSSIF-V2(PO_4) 0.2mM Lecithin	FaSSGF pH2 + FaSSIF-V2(PO_4) 0.5mM Lecithin	SGF pH2 + SIF pH6.8
LBF No.1	86.34 ± 1.61	78.75 ± 6.46	77.04 ± 10.40
LBF No.2	65.61 ± 2.19	76.36 ± 2.21	75.75 ± 2.47
LBF No.3	58.15 ± 3.56	62.92 ± 10.19	59.63 ± 5.69
LBF No.4	65.89 ± 8.80	57.20 ± 6.93	61.89 ± 3.59
Pure drug	1.31 ± 0.12	4.31 ± 0.23	0.09 ± 0.04

Summarizing above solubility tests, for fenofibrate drug substance, the fed state media showed much greater solubility values than the fasted state (Table 4-7 and

Table 4-8). Further, solubility of fenofibrate in presence of the lipid-based excipients was much greater than for the unformulated drug (Table 4-9). These findings support the LBF approach in order to overcome the poor dispersion of fenofibrate in the fasted state.

4.3 Dissolution experiments

4.3.1 Dissolution testing using USP III apparatus

4.3.1.1 Dissolution test set-up

In order to better reflect the GI motility *in vivo*, the USP III apparatus (BioDis) was used to test the dissolution of LBF No.1 and No.2. A mild dip rate was applied to the reciprocating cylinders, i.e. 10 dips per minute (dpm). Sieves with 800μm mesh were used. The media volume was 200mL and the temperature was kept at 37 ± 0.5°C.

Samples were taken at 10, 30, 60 and 120min for dissolution in water, SIF, FaSSGF, and FaSSIF-V2; while samples were taken up to 240min when FeSSGF was used.

At each time point, an aliquot of 5mL sample was withdrawn. Using a 0.45μm PTFE filter (Whatman), the initial 2mL of filtrate was discarded, and the rest of filtrate was collected in a test tube. A sample of FeSSGF was then filtered through a 2.7μm glass microfiber filter. As contrast, a sample was also collected in parallel without filtration. The withdrawn volume was replaced with prewarmed fresh medium. Samples were appropriately diluted using mobile phase (as described in Section 4.2.3). Particularly, the diluted samples of FeSSGF were centrifuged at 7500rpm for 3min prior to HPLC analysis. All dissolution experiments were performed with three units (n = 3).

4.3.1.2 Results and discussion

Fig. 4-4 shows the dissolution outcome of LBF No.2 in water using USP III with and without filter. The filtered sample profile represents the dissolved amount, while

the unfiltered sample profile represents the dispersed amount. As can be seen from Fig. 4-4, the maximum values were achieved at approx. 30min. Plateaus were maintained between 30 and 60min. The released fenofibrate declined after 60min, probably due to subsequent precipitation. Concentrations in the dispersed (unfiltered) samples were somewhat higher than the dissolved (filtered) samples in 37°C water. This indicated that undissolved API was suspended in the dissolution media by the reciprocating cylinders (USP III).

As API precipitation took place in water, LBF No.2 was not as resistant to dilution (exhibited less solvent capacity) as LBF No.1. This was possibly due to the cosolvent ethanol, which was used in place of the triglycerides in the LBF No.1 (see Table 4-1).

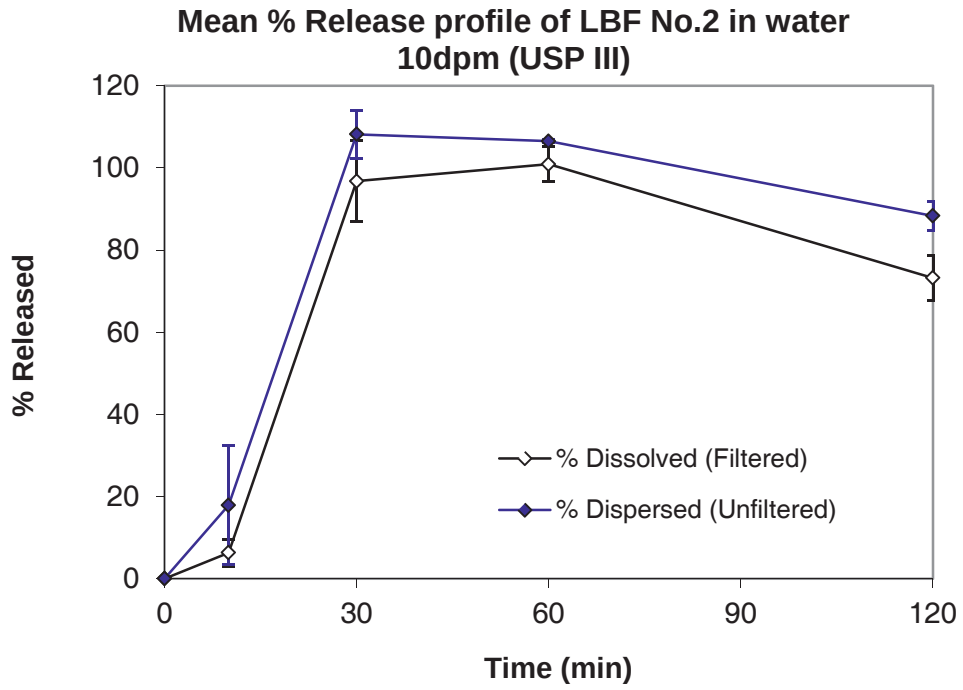

Fig. 4-4. Dispersion/dissolution of LBF No.2 in water using USP III.

The dissolution results obtained in SIFsp pH 6.8 are shown in Fig. 4-5. As can be seen, the percent dissolved (filtered) and the percent dispersed (unfiltered) are very close. Dissolution max was achieved at 30min. Precipitation occurred thereafter.

Visual observation suggested that the blue colour of capsule shells began to dissolve at about 6min of dissolution. At ca. 8min, one or two of the capsules began to

float when the cylinders were dipping, while the other capsules still moved up and down together with the cylinders. At ca. 12min, the capsules began to break gradually. At ca. 30min, substantial foaming occurred on surface of the media, and the media became increasingly blue. At 60min, no apparent change could be observed compared with 30min.

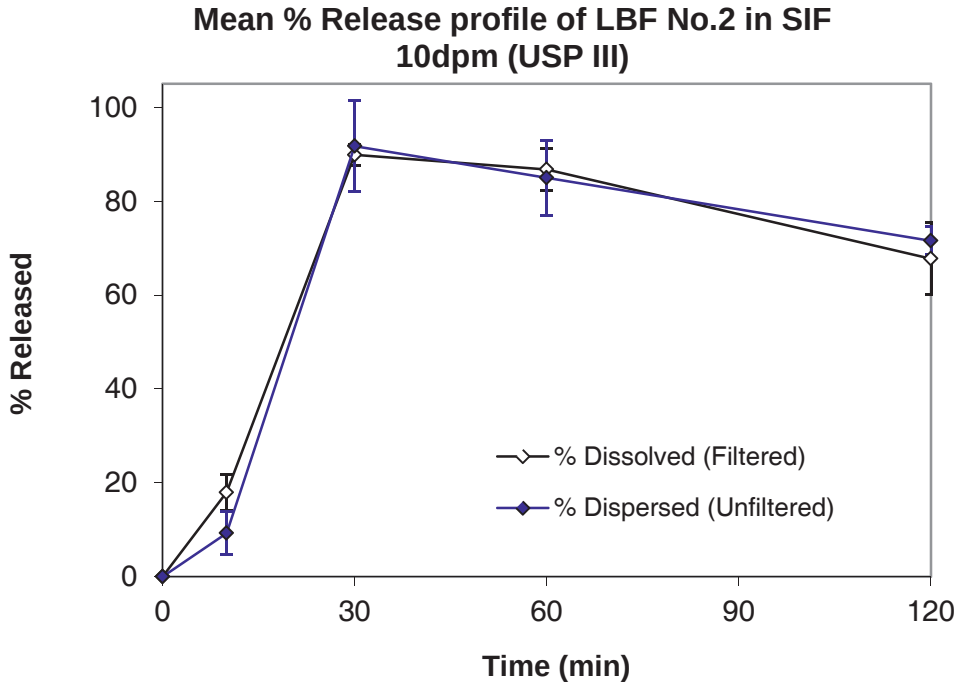

Fig. 4-5. Dispersion/dissolution of LBF No.2 in SIFsp pH 6.8 using USP III.

Fig. 4-6 shows the dispersion and dissolution profiles of the LBF No.2 in FaSSGF pH 1.6. On the whole, the maximum percent release in both the filtered and unfiltered samples was achieved between 10 and 30min. The profiles declined gradually after 30min. Concentrations in the unfiltered samples were somewhat higher than the filtered samples, as the latter represent only the dissolved part of fenofibrate.

In FaSSGF, the onset of drug release was very quick due to rapid dissolution of the soft gelatine capsule at the acidic pH (most capsule shells dissolved fully at ca. 9min). At 120min, the media showed transparent light green colour, without foaming on top of the liquid surface. Some fine precipitates were found at the bottom of each vessel.

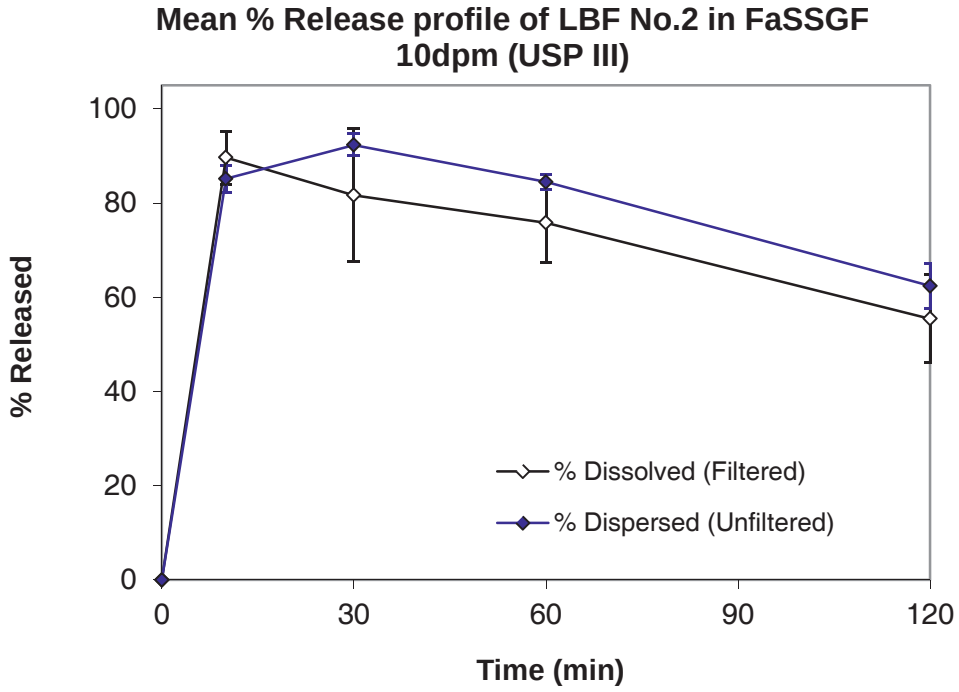

Fig. 4-6. Dispersion/dissolution of LBF No.2 in FaSSGF pH 1.6 using USP III.

Fig. 4-7 showes the results of USP III dissolution in FaSSIF-V2. The overall trend was similar to findings in other media: the maximum percent dissolved was achieved at 30min, followed by a reduction in concentration. However, concentrations in the filtered samples were distinctly lower than in the unfiltered samples. This indicated fenofibrate was only partially dissolved in FaSSIF-V2.

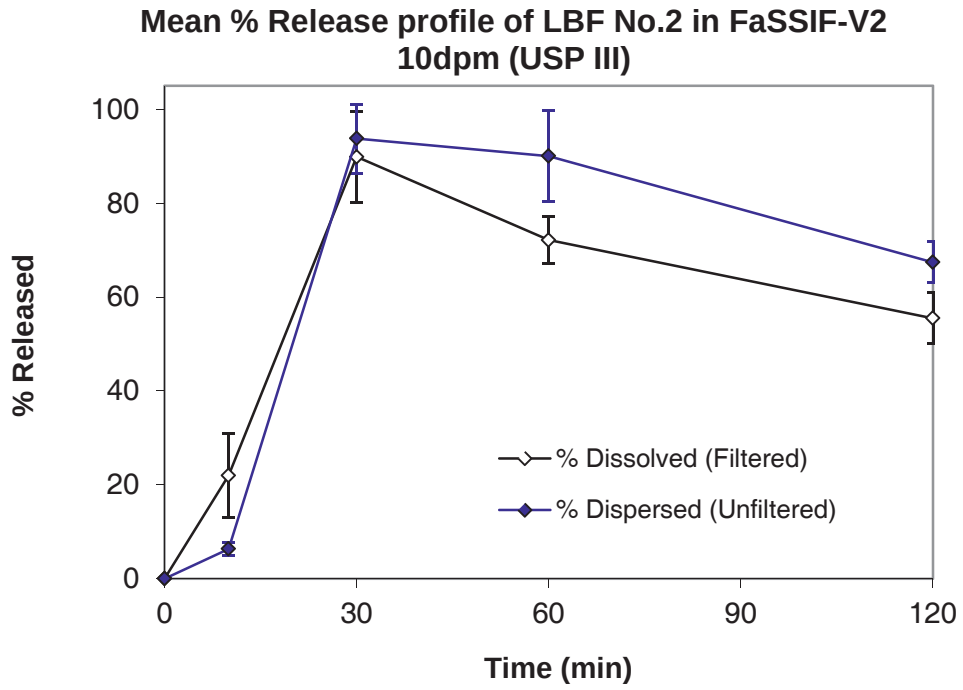

Fig. 4-7. Dispersion/dissolution of LBF No.2 in FaSSIF-V2 using USP III.

Fig. 4-8 showed the USP III dissolution that was performed in FeSSGF. Owing to the solubilization effect of food content, the concentration of fenofibrate was maintained throughout 4h of the dissolution test (without precipitation). Similar to the other media, the dispersed fenofibrate concentration was somewhat higher than the dissolved. Notably, the filtered samples gave a greater standard deviation than the unfiltered ones.

For FeSSGF at 7min, one or two capsules floated to the media surface as the cylinders were dipping. Other capsules moved up and down together with the cylinders, and foaming was observed on the media surface. The blue colour of capsule shells dissolved at ca. 9min. By 30min, the light blue colour overlaid with the milky white from FeSSGF. Little foaming could be found. At 4h, no further apparent change was observed.

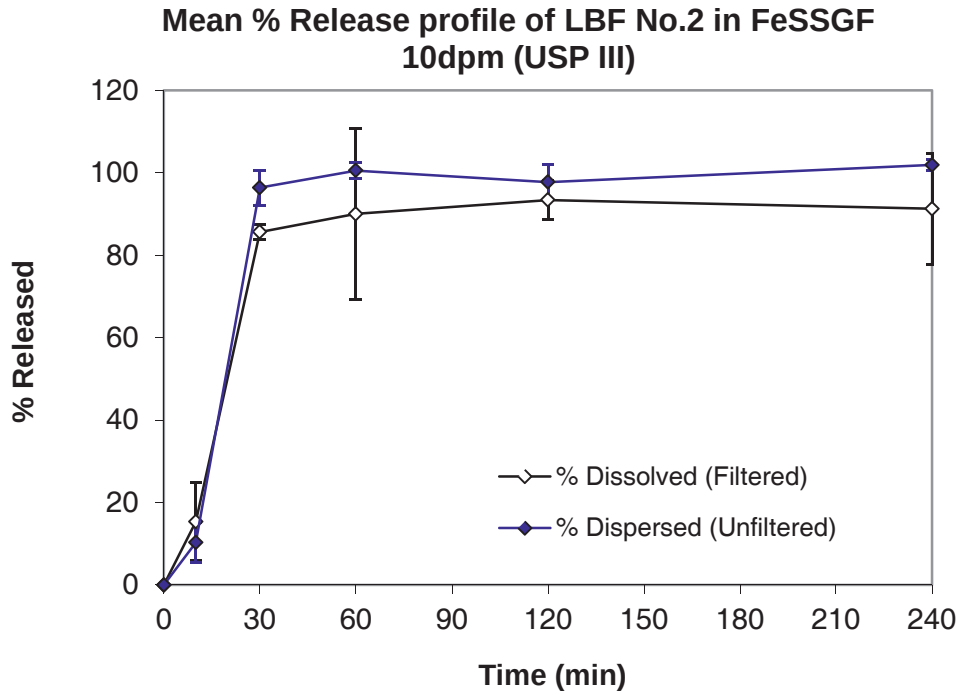

Fig. 4-8. Dispersion/dissolution of LBF No.2 in FeSSGF using USP III.

Summarizing, for the fasted state, LBF No.2 behaved similarly in compendial media (water & SIFsp pH 6.8) and biorelevant media (FaSSGF & FaSSIF-V2): some precipitation occurred after 30min (Fig. 4-4 to Fig. 4-7). However, precipitation was not observed in FeSSGF owing to the solubilization effect of food (Fig. 4-8). As expected, the profile dispersed was in most cases 0–20% higher than the profile dissolved.

4.3.2 Dissolution testing using USP II apparatus

4.3.2.1 Dissolution test set-up

In order to compare the agitation modes in various dissolution apparatus, the USP II paddle was also used to measure the dissolution of LBF No.1 – No.4 (see Table 4-1 for composition), a drug substance (as contrast), as well as a drug product (Lipidil-Ter®, micronized tablet) of fenofibrate. The dissolution media used were SGF pH 2, SIF pH 6.8, FaSSGF pH 2 and FaSSIF-V2(PO_4).

For the gastric media (i.e. SGF pH 2 & FaSSGF pH 2), dissolution experiments were performed using the USP II mini-paddle assembly with 250mL of dissolution medium. For the intestinal media [i.e. SIF pH 6.8 & FaSSIF-V2(PO_4)], dissolution studies were performed using the USP II paddle assembly with 500mL of dissolution medium. The temperature was maintained at 37°C and the paddle rotation speed was 75rpm. Samples were periodically withdrawn from either the gastric (2.5mL) or the intestinal (5mL) media, immediately filtered through 0.45µm PTFE filters (Whatman), and diluted 1:1 (volume ratio) with mobile phase (composition of the mobile phase see Section 4.2.3). The withdrawn volume was replaced with the respective blank medium, prewarmed to 37°C.

4.3.2.2 Results and discussion

As shown in Fig. 4-9 (SGF pH 2), Fig. 4-10 (SIF pH 6.8), Fig. 4-11 (FaSSGF pH 2) and Fig. 4-12 [FaSSIF-V2(PO_4)], three of the four lipid formulations (i.e. LBF No.1, No.3 & No.4) demonstrated a rapid (within 15min) and relatively complete (greater than 80%) dissolution in each respective compendial/biorelevant media. Although LBF No.2 showed a tendency to precipitate after the initial “spring”, for all the media tested, at least 60% of fenofibrate remained dissolved throughout the 4h period. Precipitation of fenofibrate from LBF No.2 was probably due to the 33.6% of cosolvent ethanol in the formulation, which upon dispersion of the LBF would lead to a loss of solubilization capacity.

As an example, Fig. 4-9 shows the dissolution profile in SGF pH 2. It can be seen that LBF No.1 had the most complete dissolution after 2 h (>90%), followed by LBF No.3 (>80%) and LBF No.4 (<80%). The dissolution profile of LBF No.2 gradually declined to ca. 60% at 4h. By contrast, dissolution of the fenofibrate drug substance and drug product (Lipidil-Ter®, micronized tablet) in SGF pH 2 was very slow (<0.1%). This can be explained by the high lipophilicity of fenofibrate: due to its logP of 5.28, this API is very poorly soluble in aqueous media without surfactant. The solubilization of fenofibrate was highly enhanced by the presence of lipid-based excipients.

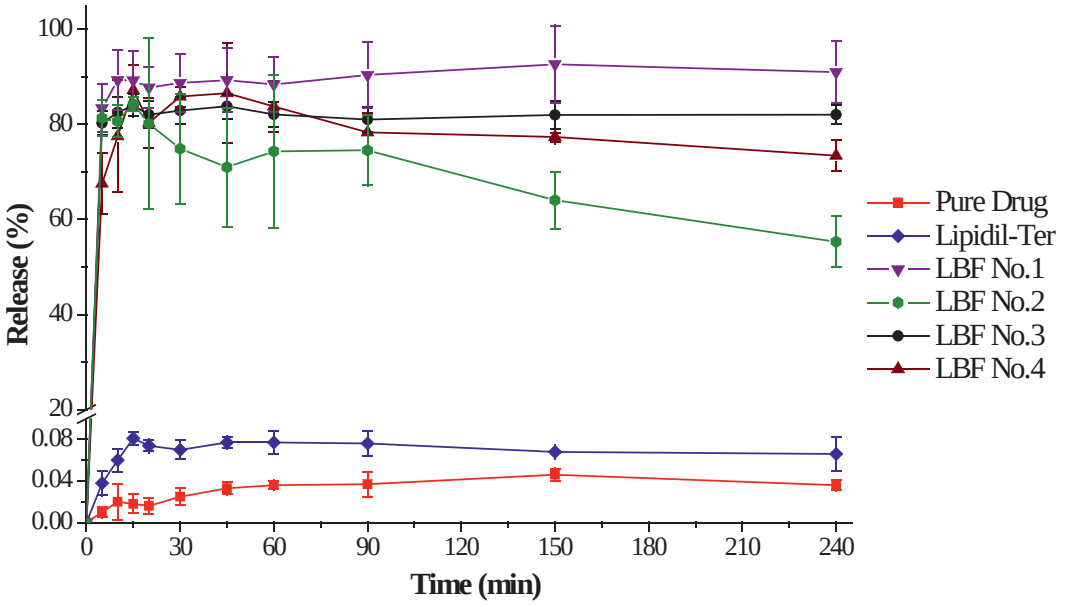

Fig. 4-9. USP II (mini paddle) dissolution profiles of various fenofibrate formulations in SGF pH 2 (n = 3).

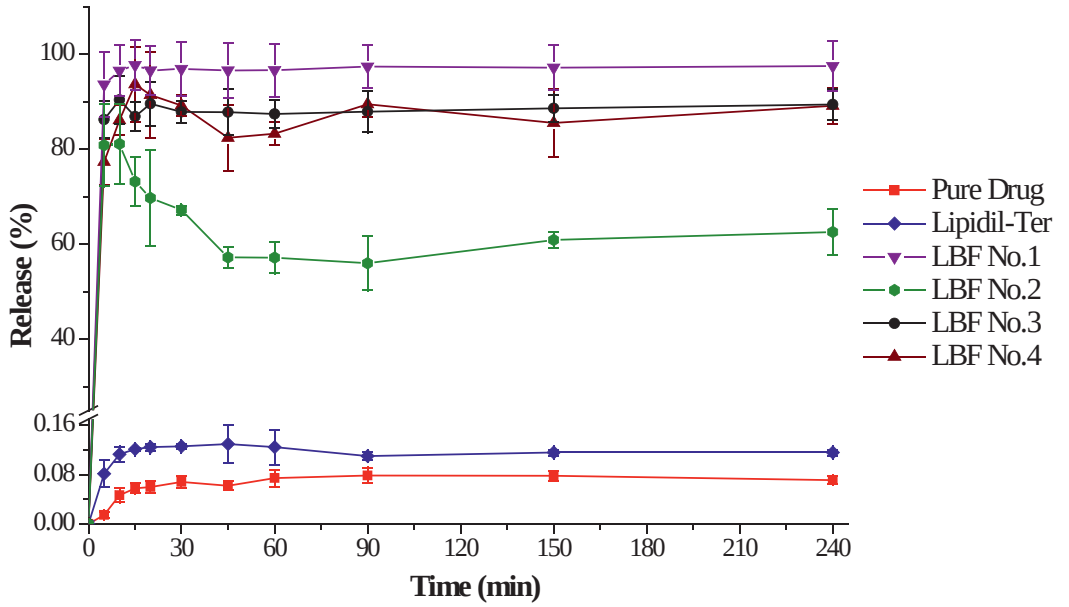

Fig. 4-10. USP II dissolution profiles of various fenofibrate formulations in SIF pH 6.8 (n = 3).

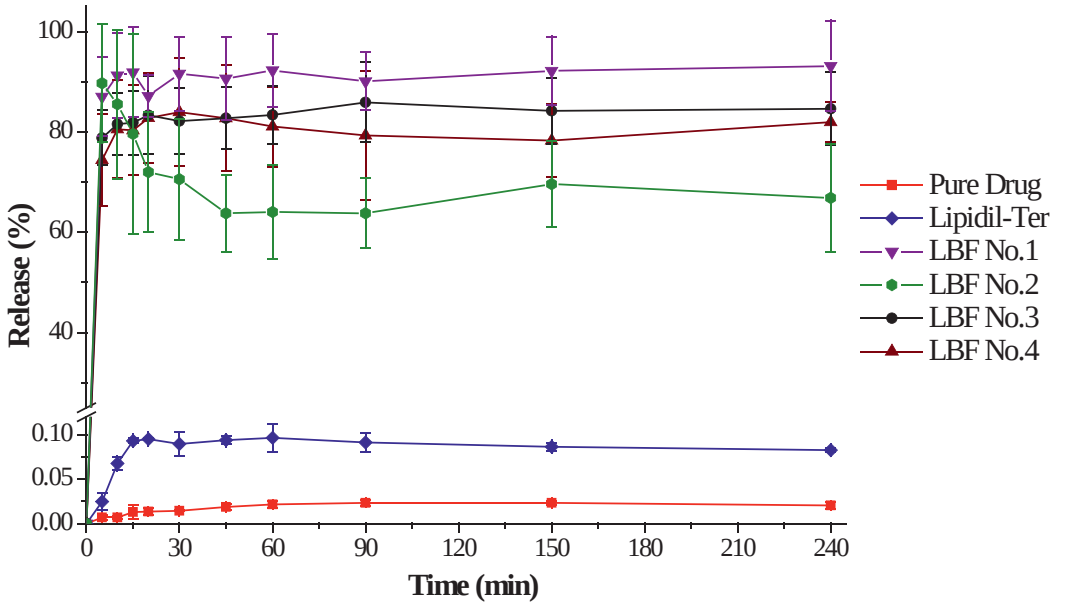

Fig. 4-11. USP II (mini paddle) dissolution profiles of various fenofibrate formulations in FaSSGF pH 2 (n = 3).

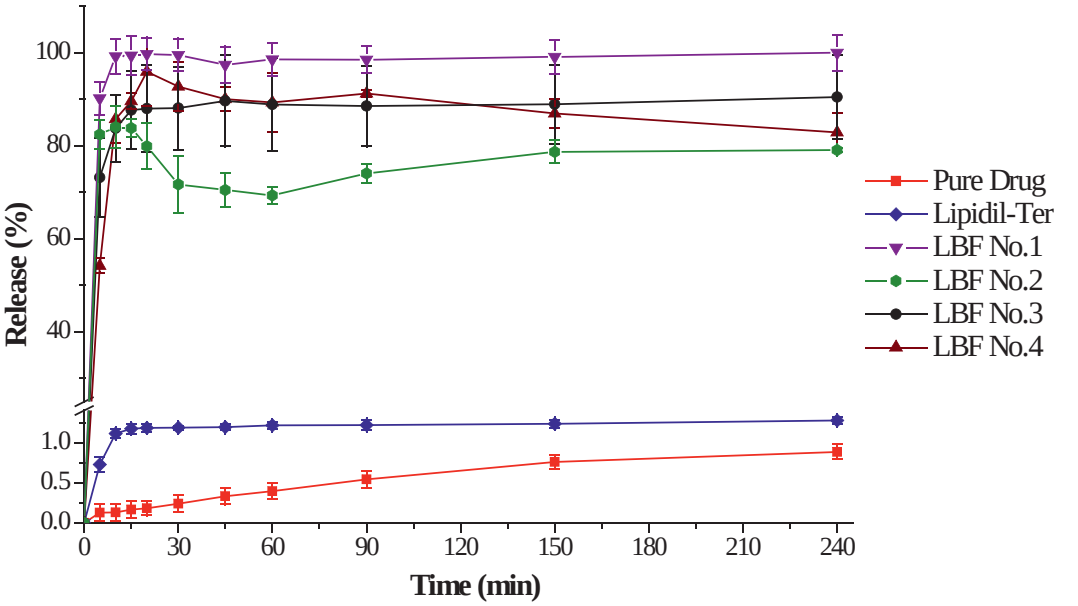

Fig. 4-12. USP II dissolution profiles of various fenofibrate formulations in FaSSIF-V2(PO_4) (n = 3).

Comparing Fig. 4-10, Fig. 4-11 and Fig. 4-12 with Fig. 4-9 regarding the LBF No.1 – No.4, no significant media effect (variation in media composition, bile salt, pH etc.) can be found in the dissolution profile for any of the lipid formulations. Any slight differences were probably due to analytical variability. In contrast, Fig. 4-9, Fig.

4-10, Fig. 4-11 and Fig. 4-12 all show that dissolution of the fenofibrate drug substance and Lipidil-Ter® was very slow. A maximum dissolution of only 0.9% (Fig. 4-12) was achieved for the drug substance and only 1.3% (Fig. 4-12) was achieved for Lipidil-Ter® after 240min. This slightly enhanced release of fenofibrate in FaSSIF-V2(PO_4) was due to the presence of bile components.

Comparing dissolution of the LBFs with the non-LBFs for each medium, an overall conclusion can be drawn: the lipid formulation technique is an effective approach to greatly improve the dissolution performance of fenofibrate.

4.3.3 Dissolution experiment using the transfer model

4.3.3.1 Dissolution testing set-up of the transfer model

In order to confirm the slight "precipitation" observed in the dissolution experiments for LBF No.3 (see Section 4.3.2.2), the transfer model (Kostewicz et al., 2004; Wagner et al., 2012) was used. As illustrated in Fig. 4-13, the model set-up consisted of a donor phase representing the stomach, and an acceptor phase representing the small intestine. A drug dose was predissolved in the donor phase, which was subsequently transferred into the acceptor phase through a pump.

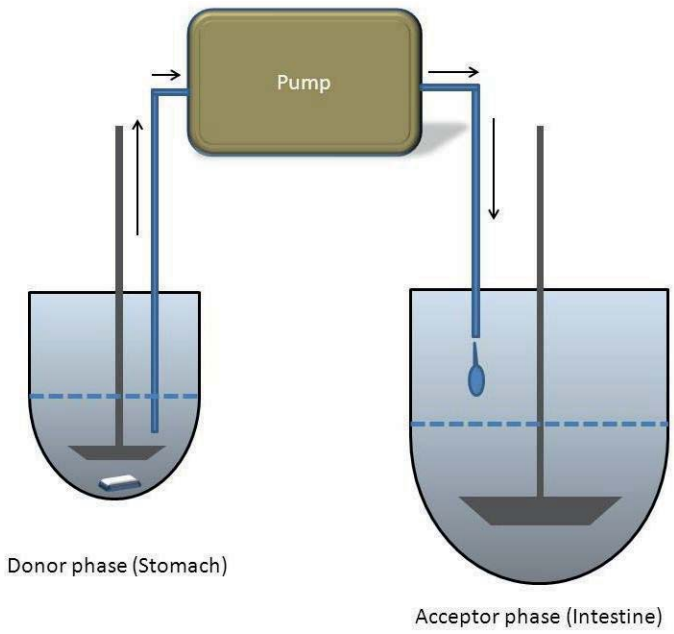

Fig. 4-13. Transfer model for prediction of intestinal precipitation (figure taken from Kostewicz et al., 2004).

To simulate *in vivo* conditions in the fasted state, the highest usual single dose of fenofibrate in LBF No.3 (2660mg lipid formulation containing 160mg API) was added into 250mL of FaSSGF pH 2 in a mini-vessel at time zero. Simultaneous dispersion and transfer took place into a standard dissolution vessel containing 500mL of FaSSIF-V2(PO_4). A linear transfer rate of 2.0mL/min was used to mimic mild gastric emptying conditions *in vivo*. The transfer model dissolution experiments were performed in triplicate. The paddle rotation speed was 75rpm, and the operating temperature was 37°C.

Samples from the acceptor compartment were collected at 5, 10, 15, 20, 25, 30, 40, 50, 60, 75, 90, 105, 120, 135, 150, 180, 210, and 240min. As the media volume of the intestinal vessels was increased by gastric transfer, the withdrawn sample volume was not replaced. The difference in calculating the corrected cumulative profile was taken into account. The other experimental conditions (e.g. filtration, dilution and HPLC, etc.) were the same as previously described in Section 4.3.2.1.

4.3.3.2 Results and discussion

For the transfer model dissolution test, LBF No.3 was chosen as a representative formulation from LBF No.1 – No.4. This is because LBF No.3 dissolved neither the fastest nor the slowest among these formulations in single medium dissolution testing (e.g. see Fig. 4-11 and Fig. 4-12). Also, as no significant precipitation from LBF No.3 was observed in Fig. 4-11 and Fig. 4-12, it would be easier to identify whether any precipitation using the transfer model arises from mixing of the gastric and intestinal media.

Results of the transfer model for LBF No.3 are shown in Fig. 4-14. The value for the % release corresponding to the solubility (27.26%) was taken from Table 4-9 (58.15µg/mL).

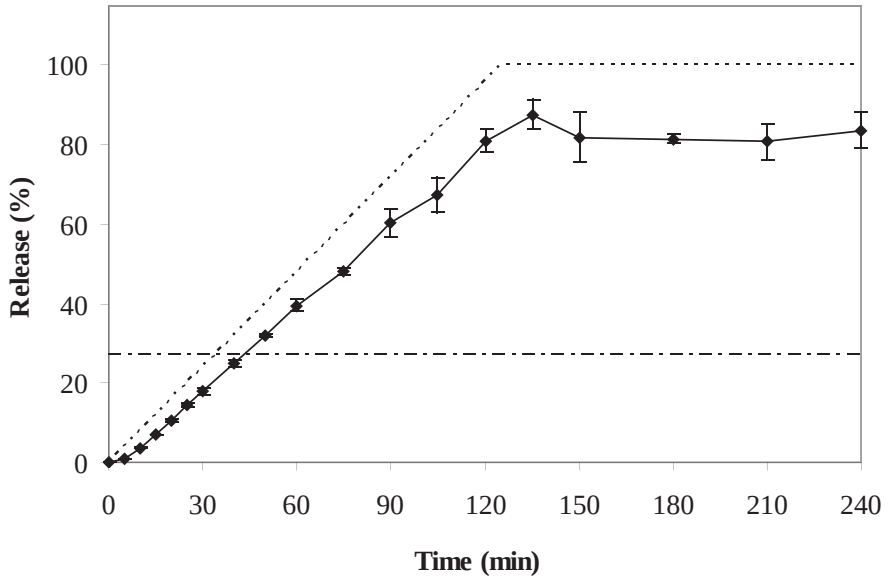

Fig. 4-14. Dissolution result using transfer model for predicting intestinal precipitation of LBF No.3 in the mixed fasted state biorelevant media (The dashed line depicts the theoretical cumulative 100% release with the designated transfer rate; while the horizontal dash and dots line represents the equilibrium solubility value at 24h).

As is shown in Fig. 4-14, no significant precipitation was detected in the intestinal compartment. Most of the dissolved drug remained solubilized for an additional 2h after completion of the media transfer. These results for LBF No.3 are consistent with the dissolution curves in the single gastric or small intestinal media (Fig. 4-11 and Fig. 4-12): fenofibrate LBF No.3 was able to solubilize 80-90% for 4h in either FaSSGF pH 2 or FaSSIF-V2(PO_4) alone.

On the other hand, the transfer model of LBF No.3 gave a slightly lower initial dissolution curve than the theoretical curve. This was probably owing to the lag time required for formulation dispersion in the donor phase: the transfer experiment was initiated as soon as the LBF No.3 formulation was placed into the gastric compartment. This configuration aimed at reflecting oral dosing of an LBF drug product.

It was presumed that the LBF No.3 results were representative. Transfer model dissolutions were not performed on the other LBFs.

4.4 *In silico* simulation of plasma profiles following oral administration of LBFs

4.4.1 STELLA® software approach

Proposed mechanisms of drug dissolution and modeling case examples incorporating *in vitro* experiments are given here in Section 4.4.1, while a detailed description of the STELLA®-based semi-PBPK model is given in Chapter 5.

4.4.1.1 Mathematical description of dissolution mechanisms

Different mechanisms can be used to describe the dissolution processes of fenofibrate LBFs in the STELLA® model. Commonly used approaches include the Weibull distribution function and the Noyes-Whitney theory. The Weibull distribution can be written as the following equations:

$$W = 1 - \exp[-(\frac{t - T_{lag}}{a})^b] \tag{4-1}$$

$$\frac{dW(t)}{dt} = \frac{b}{a} \cdot (\frac{t - T_{lag}}{a})^{b-1} \cdot \exp[-(\frac{t - T_{lag}}{a})^b] \tag{4-2}$$

Eq. (4-1) is a cumulative Weibull function, which can be used to fit the *in vitro* dissolution data, and to extract characteristic parameters. To quantify the drug fluxes of gastric and intestinal dissolution in STELLA®, Eq. (4-2) can be used. Eq. (4-2) was derived from differentiation of Eq. (4-1) against time. Using this approach, the simulated plasma profiles can be steered by the *in vitro* dissolution input. The parameter W represents the cumulative amount of drug dissolved; a is a time parameter that defines the scale of the process; b is a shape parameter; and T_{lag} is the lag time until the dissolution process starts (e.g. Wagner et al., 2013). As the Weibull function is time explicit, the upper and lower limits of time need to be defined in the STELLA® model.

Another widely used approach to describe drug dissolution is the Noyes-Whitney theory, as expressed in Eq. (4-3). It was first described about a century ago. The model was originally intended to describe dissolution of solid particles. *dw/dt* is the dissolution rate of the drug; D is the diffusion coefficient; h is the diffusion layer

thickness; *A* is the available surface area of the drug remain to be dissolved; *Cs* is the saturated drug concentration representing full solubility in the dissolution medium; and *Ct* is the current drug concentration in the medium at time *t*. From the Noyes-Whitney equation, it can be seen the dissolution rate is proportional to the diffusion coefficient *D*, the effective surface area *A*, and the concentration driving force / difference between solubility and bulk solution.

$$\frac{dw}{dt} = \frac{D}{h} \cdot A \cdot (Cs - Ct) \tag{4-3}$$

$$\frac{dX(t)}{dt} = \frac{D}{\delta} \cdot \Gamma N (\frac{W}{N\rho})^{2/3} \cdot [\frac{X_s}{V} - \frac{X(t)}{V}] \tag{4-4}$$

To expand Eq. (4-3) in detail, Eq. (4-4) is developed. This equation assumes all the undissolved drug particles are mono-distributed spheres. Thus, $\Gamma N (\frac{W}{N\rho})^{2/3}$ equals *A*, $\frac{X}{V}$ equals *C*, and δ equals *h*. Γ is a shape factor which equals 1 for spheres and is greater than 1 for non-spherical particles. *N* is the number of particles; *V* is the volume of dissolution medium; δ is the diffusion layer thickness; and ρ is the density of drug. The term $\frac{D\Gamma N^{1/3}}{\delta \rho^{2/3}}$ can be pooled into a constant, *z*. The *z*-value can be derived by fitting *in vitro* dissolution data. $X(t)$ is the cumulative amount of drug that is already dissolved at time *t*; *W* is the amount of drug remain to be dissolved; and X_s is the mass of drug which saturates the dissolution medium (e.g. Juenemann et al., 2011). Thus, Eq. (4-4) can be rearranged as Eq. (4-5). X_0 in Eq. (4-5) represents the dose strength of drug that is placed into each dissolution vessel.

$$\frac{dX(t)}{dt} = \frac{z}{V} \cdot [X_0 - X(t)]^{2/3} \cdot [X_s - X(t)] = z \cdot [X_0 - X(t)]^{2/3} \cdot [C_s - C(t)] \tag{4-5}$$

Eq. (4-5) can be rewritten as Eq. (4-6) to calculate the *z*-value, where $dX(t)/dt$ represents slope of the dissolution curve at time *t*:

$$z = \frac{V \cdot [dX(t)/dt]}{[X_0 - X(t)]^{2/3} \cdot [X_s - X(t)]} \tag{4-6}$$

Integration of above differential equation gives Eq. (4-7), in which X_1 and X_2 are the cumulative dissolved amount of drug at time t_1 and t_2, respectively. Thus, the *z*-value can be calculated using available raw dissolution data and Eq. (4-7).

$$z = \frac{V}{t_2 - t_1} \cdot \int_{X_1}^{X_2} \frac{dX(t)}{[X_0 - X(t)]^{2/3}[X_s - X(t)]} \tag{4-7}$$

As the upper and lower limits in Eq. (4-7) are the amount of drug *X* rather than time *t*, calculation of the *z*-value is sometimes not straightforward. In order to change the upper and lower limits to time *t*, a mathematical transformation can be applied to Eq. (4-7) to arrive at Eq. (4-8):

$$\begin{aligned} z = \frac{V}{t} \cdot \int_0^t d\{\{ & \ln \frac{(X_S - X_0)^{2/3} - (X_S - X_0)^{1/3}[X_0 - X(t)]^{1/3} + [X_0 - X(t)]^{2/3}}{(X_S - X_0)^{2/3} - (X_S - X_0)^{1/3} \cdot X_0^{1/3} + X_0^{2/3}} \\ & - 2\ln \frac{(X_S - X_0)^{1/3} + [X_0 - X(t)]^{1/3}}{(X_S - X_0)^{1/3} + X_0^{1/3}} - 2\sqrt{3} \arctan \frac{2[X_0 - X(t)]^{1/3} - (X_S - X_0)^{1/3}}{\sqrt{3}(X_S - X_0)^{1/3}} \\ & + 2\sqrt{3} \arctan \frac{2X_0^{1/3} - (X_S - X_0)^{1/3}}{\sqrt{3}(X_S - X_0)^{1/3}} \} / [2(X_S - X_0)^{2/3}] \} \end{aligned} \tag{4-8}$$

The *z*-value can be drawn by solving Eq. (4-8), which involves both the current state of the system [e.g. $X(t)$] and the later one [e.g. $X(t+\Delta t)$]. According to its definition, this is a time-implicit algorithm.

The disadvantage of Eq. (4-8) is its length and complexity. In order to keep it easy to use, a Microsoft® Excel spreadsheet (Fig. 4-15) based upon Eq. (4-8) was developed to calculate the experimental z-values. In the spreadsheet, input values include the dissolution data points, the equilibrium solubility of drug (X_s), and the dose strength of API in each dissolution vessel (X_0). Applying linear regression to the initial slopes, an output of the mean *z*-value can be calculated from the individual dissolution data of three experiments.

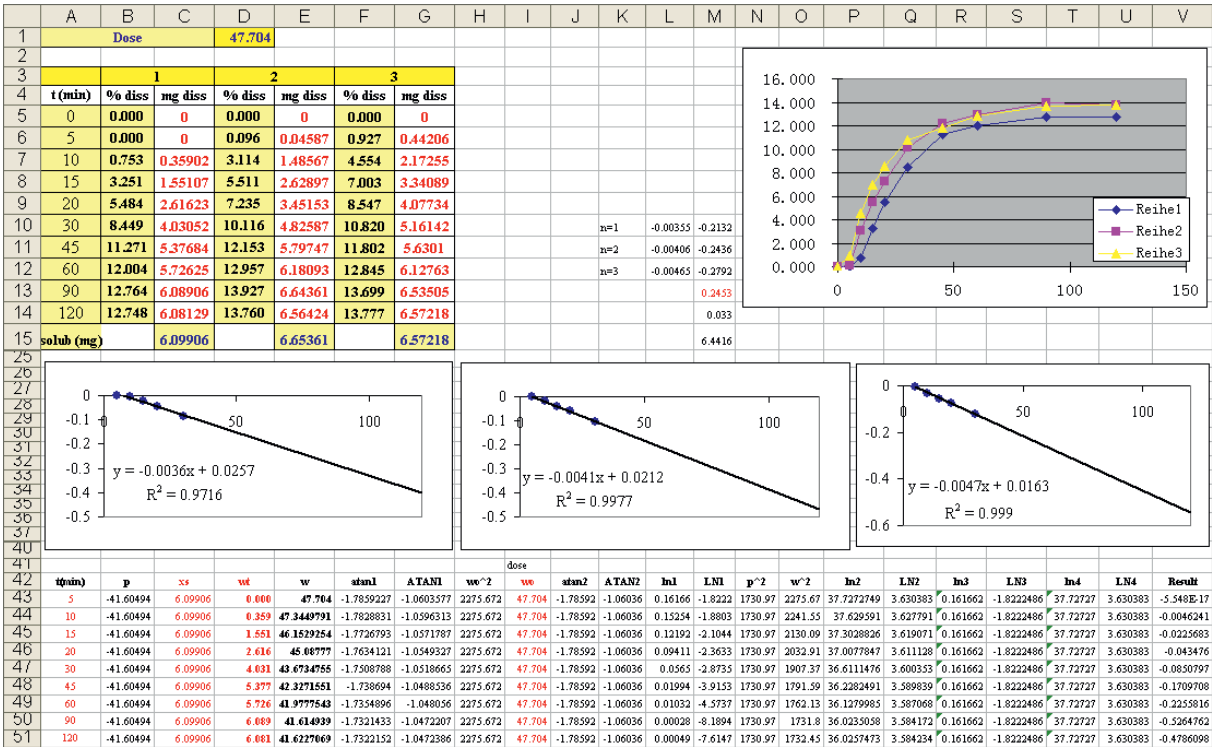

	A	B	C	D	E	F	G
1	Dose			47.704			
2							
3		1		2		3	
4	t (min)	% diss	mg diss	% diss	mg diss	% diss	mg diss
5	0	0.000	0	0.000	0	0.000	0
6	5	0.000	0	0.096	0.04587	0.927	0.44206
7	10	0.753	0.35902	3.114	1.48567	4.554	2.17255
8	15	3.251	1.55107	5.511	2.62897	7.003	3.34089
9	20	5.484	2.61623	7.235	3.45153	8.547	4.07734
10	30	8.449	4.03052	10.116	4.82587	10.820	5.16142
11	45	11.271	5.37684	12.153	5.79747	11.802	5.6301
12	60	12.004	5.72625	12.957	6.18093	12.845	6.12763
13	90	12.764	6.08906	13.927	6.64361	13.699	6.53505
14	120	12.748	6.08129	13.760	6.56424	13.777	6.57218
15	solub (mg)		6.09906		6.65361		6.57218

	J	K	L	M
10		n=1	-0.00355	-0.2132
11		n=2	-0.00406	-0.2436
12		n=3	-0.00465	-0.2792
13				0.2453
14				0.033
15				6.4416

	dose																				
42	t(min)	p	xs	wt	w	atan1	ATAN1	we^2	we	atan2	ATAN2	ln1	LN1	p^2	w^2	ln2	LN2	ln3	LN3	ln4	LN4	Result
43	5	-41.60494	6.09906	0.000	47.704	-1.7859227	-1.0603577	2275.672	47.704	-1.78592	-1.06036	0.16166	-1.8222	1730.97	2275.67	37.7272749	3.630383	0.161662	-1.8222486	37.72727	3.630383	-5.548E-17
44	10	-41.60494	6.09906	0.359	47.3449791	-1.7828831	-1.0596313	2275.672	47.704	-1.78592	-1.06036	0.15254	-1.8803	1730.97	2241.55	37.629591	3.627791	0.161662	-1.8222486	37.72727	3.630383	-0.0046241
45	15	-41.60494	6.09906	1.551	46.1529254	-1.7726793	-1.0571787	2275.672	47.704	-1.78592	-1.06036	0.12192	-2.1044	1730.97	2130.09	37.3028826	3.619071	0.161662	-1.8222486	37.72727	3.630383	-0.0225683
46	20	-41.60494	6.09906	2.616	45.08777	-1.7634121	-1.0549327	2275.672	47.704	-1.78592	-1.06036	0.09411	-2.3633	1730.97	2032.91	37.0077847	3.611128	0.161662	-1.8222486	37.72727	3.630383	-0.043476
47	30	-41.60494	6.09906	4.031	43.6734755	-1.7508788	-1.0518665	2275.672	47.704	-1.78592	-1.06036	0.0565	-2.8735	1730.97	1907.37	36.6111476	3.600353	0.161662	-1.8222486	37.72727	3.630383	-0.0850797
48	45	-41.60494	6.09906	5.377	42.3271551	-1.738694	-1.0488536	2275.672	47.704	-1.78592	-1.06036	0.01994	-3.9153	1730.97	1791.59	36.2282491	3.589839	0.161662	-1.8222486	37.72727	3.630383	-0.1709708
49	60	-41.60494	6.09906	5.726	41.9777543	-1.7354896	-1.048056	2275.672	47.704	-1.78592	-1.06036	0.01032	-4.5737	1730.97	1762.13	36.1279985	3.587068	0.161662	-1.8222486	37.72727	3.630383	-0.2255816
50	90	-41.60494	6.09906	6.089	41.614939	-1.7321433	-1.0472207	2275.672	47.704	-1.78592	-1.06036	0.00028	-8.1894	1730.97	1731.8	36.0235058	3.584172	0.161662	-1.8222486	37.72727	3.630383	-0.5264762
51	120	-41.60494	6.09906	6.081	41.6227069	-1.7322152	-1.0472386	2275.672	47.704	-1.78592	-1.06036	0.00049	-7.6147	1730.97	1732.45	36.0257473	3.584234	0.161662	-1.8222486	37.72727	3.630383	-0.4786098

Fig. 4-15. Excel spreadsheet for calculating *z*-value.

The flows of both gastric and small intestinal dissolution of the mechanistic model can be quantified using the rearranged Noyes-Whitney equations, as shown in Eq. (4-9) and Eq. (4-10).

$$J_{DS}(t) = \frac{z_{sto}}{V_{sto}} \cdot W_{DO}^{2/3}(t) \cdot [X_{s,sto} - W_{DS}(t)] = z_{sto} \cdot W_{DO}^{2/3}(t) \cdot [C_{s,sto} - C_{DS}(t)] \tag{4-9}$$

$$J_{DI}(t) = \frac{z_{si}}{V_{si}} \cdot W_{FS}^{2/3}(t) \cdot [X_{s,si} - W_{IL}(t)] = z_{si} \cdot W_{FS}^{2/3}(t) \cdot [C_{s,si} - C_{IL}(t)] \tag{4-10}$$

In fact, Eq. (4-9) and Eq. (4-10) are not restricted to dissolution of solid particles, but should be applicable to a variety of formulations including lipid-based formulations. This is because the *z*-value is an apparent parameter that is derived from fitting *in vitro* dissolution data: although the *z*-value equals $\frac{DIN^{1/3}}{\delta \rho^{2/3}}$, these combined parameters do not need to be individually identified.

In summary, both of the Weibull function and the Noyes-Whitney theory can be used to derive dissolution parameters for the STELLA®-based semi PBPK model. The

Weibull function is time explicit, while the customized Noyes-Whitney algorithm is not. For the Noyes-Whitney approach, fitting of *z*-value is not only applicable to solid-state drug product, but also to lipid-based formulations.

4.4.1.2 Results and discussion

The following simulations were conducted using *in vitro* dissolution profiles of LBF No.4 in biorelevant media (Fig. 4-11 and Fig. 4-12). For these, the differential Weibull function of Eq. (4-12) was used to describe the gastric and intestinal dissolution flows of the mechanistic model.

The Weibull parameters were derived by fitting above mentioned dissolution data for LBF No.4 in FaSSGF pH 2 and FaSSIF-V2(PO_4). As proposed by the Origin 8.0 software, the cumulative Weibull function of Eq. (4-11) was used to extract corresponding characteristic parameters.

$$Wt = W_{max} * (1\text{-}e^{-kt}) \tag{4-11}$$

$$dWt / dt = W_{max} * k * e^{-kt} \tag{4-12}$$

The optimized dissolution curve fitting suggested the following parameters: for dissolution in the stomach, W_{max} = 114.9 and k = 29.54; for dissolution in the small intestine, W_{max} = 127.9 and k = 13.01. The STELLA® model is described in Chapter 5.

The corresponding clinical PK study was initially reported by Sauron et al. (2006). Using a 3-way crossover design, 45 subjects took fenofibrate tablets under different prandial conditions. Plasma profiles were measured up to 120h post-dose. For the nanosized tablet, T_{max} = 2.922h and C_{max} = 7.329µg/mL; for the micronized tablet, T_{max} = 5.845h and C_{max} = 2.629µg/mL. These observations are shown as open triangles and circles, respectively, in Fig. 4-16. Using WinNonlin® 5.2.1 software, the deconvoluted post-absorptive PK parameters from *in vivo* data were k_{10} = 0.145h^{-1}, k_{12} = 0.290h^{-1}, k_{21} = 0.194h^{-1} and V/F = 7802mL.

For LBF No.4, the simulated plasma profile exhibited a T_{max} of 2.0h and a C_{max} of 8.08µg/mL, as is shown in the boldface curve of Fig. 4-16. For comparative purposes,

previous PK modeling following administration of FFB tablets by Juenemann et al. (2011) is also shown, as the thin dashed and solid curves of Fig. 4-16.

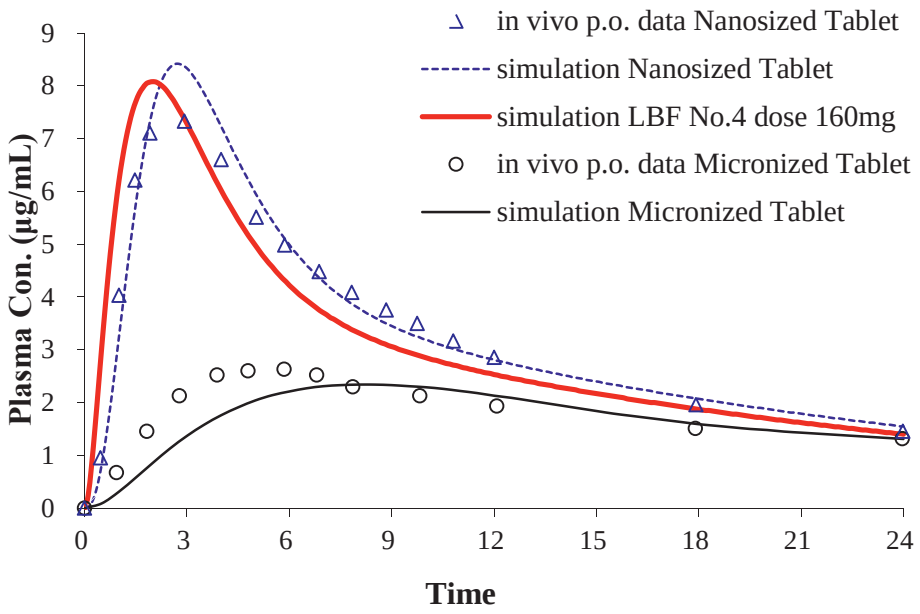

Fig. 4-16. Modelling case study using FFB LBF No.4 and Weibull function plus an overlay of literature data (Juenemann et al., 2011; Sauron et al., 2006).

Simulation outcome of FFB LBF No.4 at a dose of 160mg yielded comparable C_{max} and AUC levels as the nanosized FFB tablet in the fasted state. This indicates the effectiveness and promise of the lipid formulation technique. By omitting the dissolution step from the solid state, FFB from the lipid-based excipients can be absorbed faster. Indeed, as most of the LBF No.1 – No.4 almost reached 85% dissolved at 15min (Fig. 4-11 and Fig. 4-12), they can be viewed as immediate release (IR) formulations, in which the API essentially behaves as a Class I drug.

For comparison purposes, the simulated plasma profiles of LBF No.4 using respective *in vitro* dissolution data in compendial and biorelevant media (Fig. 4-9, Fig. 4-10, Fig. 4-11 and Fig. 4-12) are displayed in overlay in Fig. 4-17.

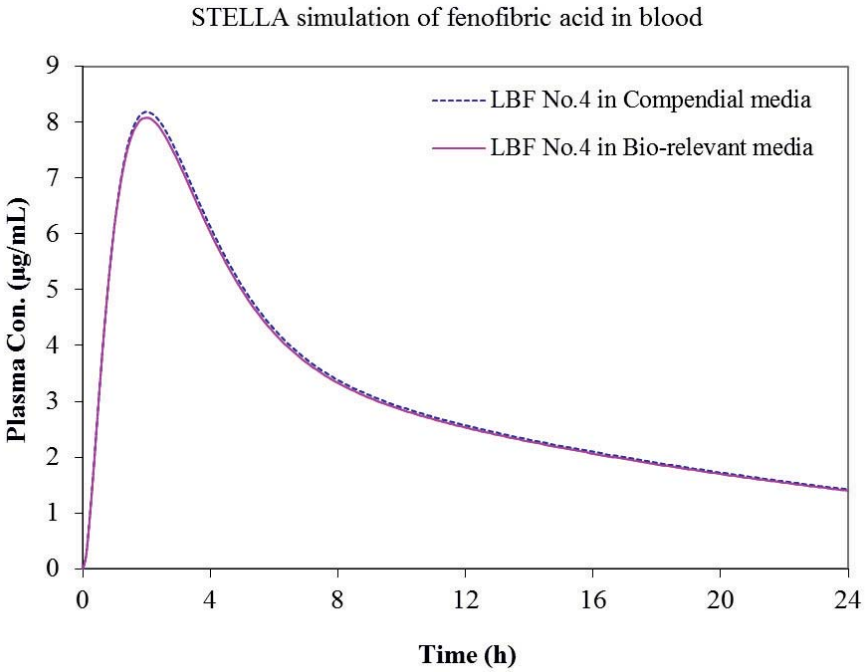

Fig. 4-17. Simulated human plasma concentration profiles following administration of LBF No.4 using *in vitro* data from compendial and biorelevant dissolution.

As can be seen from Fig. 4-17, the simulation outcome of LBF No.4 was almost identical for plasma profiles obtained using dissolution input from either compendial or biorelevant media. Being a Type IIIB formulation, LBF No.4 can disperse well and solubilize in dilutions of either SGF/SIF or FaSSGF/FaSSIF-V2(PO_4). This finding is in line with the solubility results (Table 4-9), which show that the delivery of fenofibrate is dominated by the lipid-based excipients rather than the bile salts from the biorelevant media.

4.4.2 Simcyp® software approach

4.4.2.1 Description of the Simcyp® model parameters

Still focusing on LBF No.4, the commercially available full PBPK software of Simcyp® was used in parallel with the above mentioned STELLA® platform. In doing so, the modelling work can be enriched, as each of the softwares can complement and verify the results from the other.

For the Simcyp® model, the following input parameters were obtained from the literature. PK parameters of ka (h^{-1}): 0.73 – 1.00; $P_{eff,man}$ (10^{-4}cm s^{-1}): 0.266; V_{ss} (L

kg^{-1}): 0.095; Cl_{po} (L h^{-1}): 0.707 (Fei et al., 2013c). In addition, the diffusion coefficient of fenofibrate was estimated to be $4.32x10^{-4}cm^2$ min^{-1} (Granero et al., 2005). The related enzymes were P450 CYP3A4 and CYP2C9 (Miller and Spence, 1998). V_{max} and K_m were set as 10.6pmol min^{-1} mg^{-1} and 2.6µM, respectively (Goosen et al., 2007).

As the human organ distribution data of fenofibric acid has been rarely reported, the essential model parameters were inputted as rat clinical data (Chapman, 1987), assuming human and rat are similar in organ drug partitioning. Taking the drug concentration in blood as the reference point, the suggested distribution abundances in different organs were: Liver 2.77, Kidney 1.94, Gut 1.23, Blood 1, Lung 0.57, Heart 0.23, Skin 8, and Testis 8. Further, the elimination pathway was 81% urine and 19% faces.

The following default PBPK values from the Simcyp® simulator were implemented: Blood to Plasma partition ratio (B/P) 1.318, Fraction unbound in Plasma (fu) 0.01, Fraction absorbed (fa) 0.95, Main Plasma Binding Protein was albumin, Effective diffusion layer thickness (µm) 0.1.

In vitro experiments with LBF No.4 were conducted to determine the biorelevant solubility (µg mL^{-1}): 123.4 (as tested in combined media of FaSSGF and FaSSIF-V2, volume ratio 1:2) for input into Simcyp®. The experimental dissolution profile was not a mandatory input, since the LBF No.4 categorized as an IR dosage form. By incorporation of all the above parameters, the plasma profiles were simulated. As there was no available *in vivo* data for this formulation, the simulated outcome cannot be directly verified. Rather, the obtained fasted state *in silico* plasma profile was compared to the outcome using the STELLA® model.

4.4.2.2 Results and discussion

Fig. 4-18 and Fig. 4-19 show the simulated plasma profiles following administration of LBF No.4 in fasted and fed state using the Simcyp® human population based simulator (n.b. STELLA® does not have the population feature). The

simulation virtual trial comprised 5 groups of 5 individuals, in total 25 human subjects. Each subject was randomly chosen from a population database containing all individuals' information.

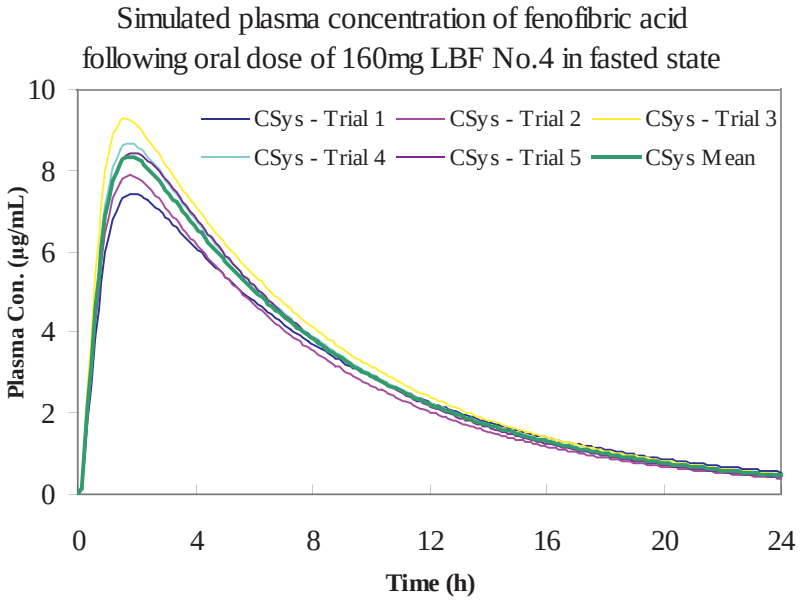

Fig. 4-18. Simulated fasted state human plasma profiles following administration of LBF No.4 using Simcyp® human population based simulator.

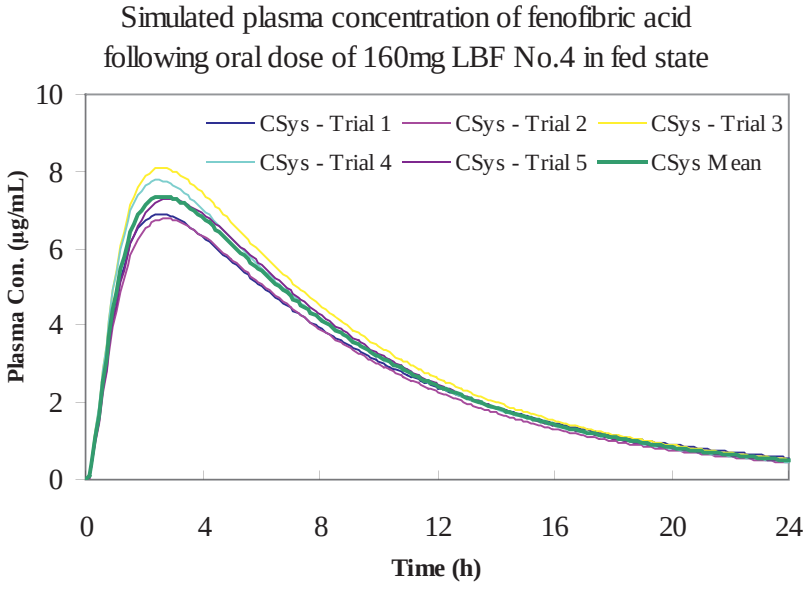

Fig. 4-19. Simulated fed state human plasma profiles following administration of LBF No.4 using Simcyp® human population based simulator.

As shown in Fig. 4-18, the mean plasma profile obtained in the fasted state with Simcyp® exhibited a C_{max} value of 8.43µg/mL, and a T_{max} of 1.78h. The AUC was 72.23µg mL^{-1} h. The simulated profile is very similar to the result obtained using the STELLA®-based simulation, which exhibited a C_{max} value of 8.08µg/mL, a T_{max} of 2.0h, and an AUC of 76.79µg mL^{-1} h (see Fig. 4-16).

As shown in Fig. 4-19, the mean plasma profile obtained in the fed state exhibited a C_{max} value of 7.48µg/mL, and a T_{max} of 2.73h. The AUC was 71.92µg mL^{-1} h. The later absorption peak in the fed state was probably due to prolonged gastric emptying when food was ingested. Unlike fenofibrate tablets, which showed a 2-3 fold positive food effect (Juenemann et al., 2011), the simulated AUC of LBF No.4 remained the same regardless of food intake, according to the Simcyp simulation. This finding suggests the lipid formulation technique would be advantageous over the micronized tablet formulation in the fasted state, assuming that the model is predictive.

Fig. 4-20 showes the oral clearance results for 5 groups of 5 individuals, i.e. total population of 25, in the fasted state. Theoretically, trials following i.v. dose should be used to calculate the clearance. However, as i.v. data was not available, the p.o. clearance was used as a compromise. Fig. 4-21 showes the trial results for 5 groups of 5 individuals with respect to AUC in the fasted state.

As can be seen, the Group No.3 had a slower clearance rate than the overall median value (Fig. 4-20). Hence, the corresponding AUC level of Group No.3 was higher than the overall median AUC of the 25 subjects (Fig. 4-21). Although there was variance among the trial groups, the individual extremes fell within the 5^{th} - 95^{th} percentile range of the total population in most cases.

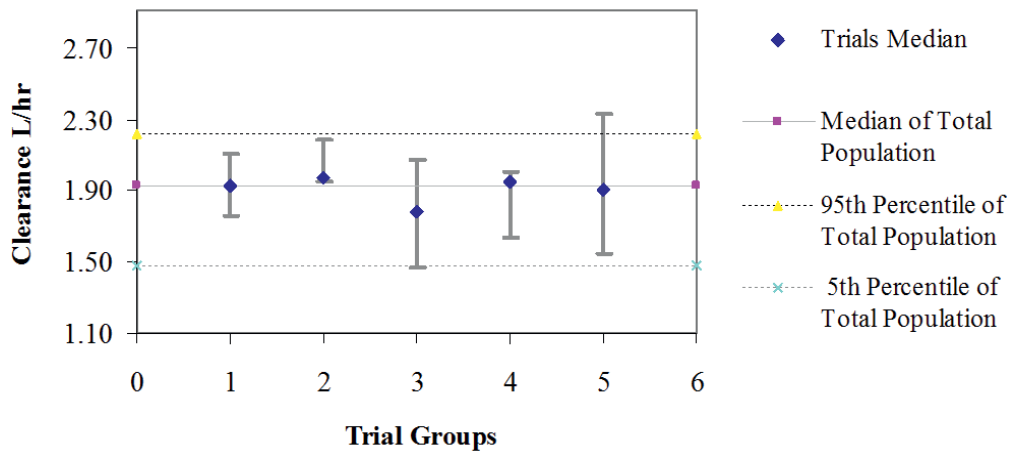

Fig. 4-20. Oral clearance trials for 5 groups of 5 individuals (total population of 25) in the fasted state.

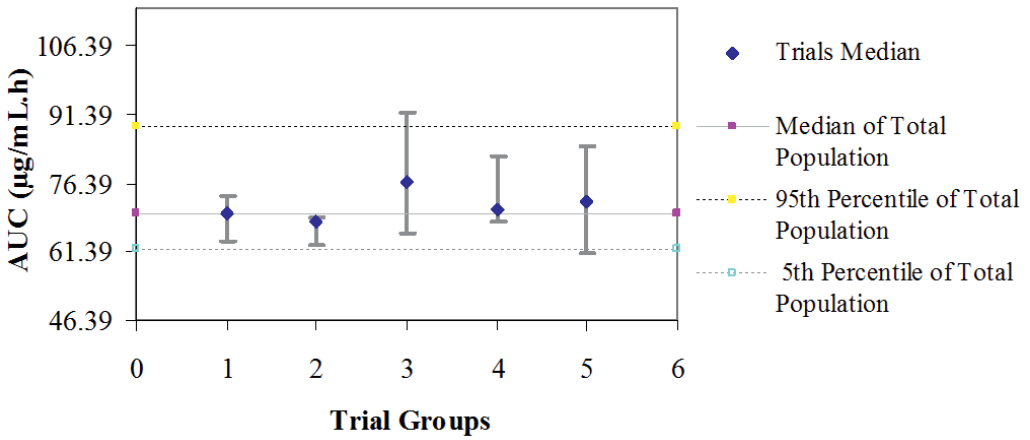

Fig. 4-21. Trial results for 5 groups of 5 individuals (total population of 25) for a PK profile simulation in the fasted state.

Fig. 4-22 depicts the calculated regional distribution of the fraction of dose absorbed along the GI tract in the fasted state. This feature of Simcyp® cannot be achieved by the semi-PBPK model of STELLA®. As shown by Fig. 4-22, Jejunum-I was one of the major segments of drug absorption (with a fraction of 0.45), followed by Duodenum and Jejunum-II (with absorbed fractions of 0.28 and 0.16, respectively). From Ileum-II to Colon, absorption of fenofibrate was minimal.

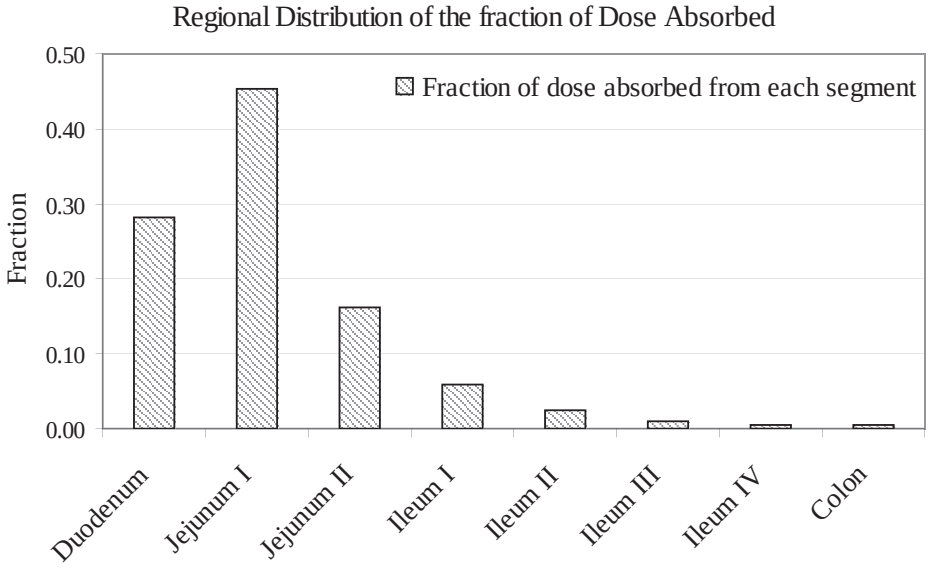

Fig. 4-22. Calculated regional distribution of the fraction of dose absorbed along GI tract in the fasted state.

In summary, both STELLA® and Simcyp® provided useful models for simulating the behavior of LBF. After verifying the STELLA® model using previous data (Juenemann et al., 2011), the fasted state behavior of LBF No.4 was simulated. It behaved similarly to the nanosized tablet formulation. Simcyp® results were similar in the fasted state to these obtained for LBF No.4 in the STELLA® model. On this basis, the fed state behavior of LBF No.4 was then modeled with Simcyp®, revealing that LBF No.4 would not be expected to show a food effect. An advantage of Simcyp® over STELLA® is that population effects can be explored: in this case it was found that variation in AUC is attributable to changes in clearance. Further, it was shown that fenofibrate is mainly absorbed in the upper small intestine from the LBF No.4 formulation.

Chapter 5. Study of LBF No.8 – No.11 of fenofibrate

5.1 Preparation of LBF No.8 – No.11

The compositions of LBF No.8 – No.11 (3 SMEDDSs and 1 micronized dispersion system (MDS)) used for dissolution and solubility tests have been described previously (Wei et al., 2010) and are summarized in Table 5-1. The SMEDDSs (E5(80) and E5(20) formulations) comprised 25% medium-chain triglyceride oil (Myritol 318), 60% surfactant mixture consisting of TPGS (D-α-tocopheryl polyethylene glycol 1000 succinate) and polysorbates (Tween 80 or Tween 20) at ratios of 1:4, and 5% MilliQ-water.

Table 5-1

Composition of the lipid formulations used in Chapter 5[a].

Dose 50 mg	LBF No.8	LBF No.9	LBF No.10	LBF No.11
Another name	E5(80) solution	E5(80) capsule	E5(20) capsule	MDS capsule
Fenofibrate (%)	10	10	10	20 (micronised)[b]
Myritol 318 (%)	25	25	25	27.5
TPGS (%)	12	12	12	9.5
Tween 20 (%)	–	–	48	38
Tween 80 (%)	48	48	–	–
H_2O (%)	5	5	5	5

[a] This table was summarized from literature (Wei et al., 2010).

[b] The fenofibrate was pre-sieved through a 40μm analytical sieve.

As Lin et al. (2011) and Wei et al. (2010) have reported a clinical study of fenofibrate LBF No.8 – No.11 in healthy human volunteers, *in vivo* data was available for conducting the STELLA®-based plasma profile simulations.

To prepare the different formulations, each of the excipients (see Table 5-1) was directly weighed into a glass flask and heated to 80°C under stirring for approximately 10min to obtain a homogeneous melt. 10% of fenofibrate was then dissolved in the melt. Once fully dissolved, the SMEDDS was allowed to cool down to ambient temperature and 500mg aliquots were then manually transferred to size 1 transparent hard gelatin capsules. The MDS formulation comprised 20% fenofibrate, which had been pre-sieved through a 40μm analytical sieve (likely resulting in a similar, but slightly different particle size distribution than what was administered in the *in vivo* study, in which a particle size "smaller than 37μm" was used), dispersed in a mixture of 27.5% Myritol 318, 9.5% TPGS, 38% Tween 20 and 5% MilliQ-water. Owing to the high percentage of API in the MDS formulation, fenofibrate was mostly suspended in this formulation. To keep the dose strength the same as the SMEDDSs (equivalent to 50mg in each capsule), 250mg of the MDS suspension was manually transferred to size 3 transparent hard gelatin capsules. As the dose of fenofibrate in the formulation administered to humans was 54mg, the slight dose difference between the *in vitro* and *in vivo* tests was taken into account when performing the simulations.

5.2 Fasted state *IVISIV*C of LBF No.8 – No.11

A fasted state *IVISIV*C of LBF No.8 – No.11 was attempted. The fasting *in vivo* data were available and the *in vitro* biorelevant solubility and dissolution experiments under fasted conditions were conducted to provide input for the STELLA® model. A brief outline of the work is as follows. 1) Solubility and dissolution testing of LBF No.8 – No.11 (3 SMEDDSs and 1 MDS) in FaSSGF pH 2 and FaSSIF-V2(PO_4). 2) Dissolution rate calculations; 3) *In silico* PBPK model set-up including estimation of precipitation and permeability; 4) Comparison of the simulated and observed plasma profiles; and 5) Parameter sensitivity analysis of the model.

5.2.1 Solubility of fenofibrate in biorelevant dissolution media in the presence of lipid-based excipients

5.2.1.1 Solubility test set-up

The change in solubility of fenofibrate due to the presence of the lipid-based excipients was examined in FaSSGF pH 2 and FaSSIF-V2(PO_4) using the shake-flask method (n = 3). To replicate the ratio of volume of excipients to volume of medium used in the dissolution studies (in which 50mg of API in 0.5mL of lipid vehicle was introduced as a solution in a capsule or as a dispersion in a capsule to 250mL of FaSSGF pH 2 or to 500mL of FaSSIF-V2(PO_4)), the volumes for the solubility study were scaled down proportionally. Using a pipette, ca. 10mg of each freshly prepared fenofibrate lipid formulation was accurately weighed into a vial containing either 5mL pre-warmed FaSSGF pH 2 or 10mL pre-warmed FaSSIF-V2(PO_4). The weighing error (i.e. deviation from the target 10mg) was corrected by normalizing recovery. The sample vials were closed using screw caps and vortexed for 5 seconds to ensure a fine dispersion. Subsequently, the samples were gently shaken on an orbital shaker which was incubated in a 37°C oven for 24 hours. Thereafter, the dispersions were filtered (0.45µm PTFE membrane filters, Whatman, Germany) and the concentration of fenofibrate in the resulting filtrate was analyzed by HPLC (see Section 4.2.3 for the HPLC method). The concentration of dissolved fenofibrate after 24h was defined as the equilibrium solubility of the LBF. As this value was less than the concentration initially generated by adding the formulation to the medium, we assume the level of supersaturation is gradually reduced in the experiment. As a check, the experiment was repeated on a larger scale and, after 24h, a further amount of fenofibrate powder was added to the medium. There was no change in the concentration of dissolved fenofibrate after the further addition of fenofibrate, confirming that equilibration had been reached after 24h. As a control experiment to allow comparison between LBF and API, the solubility of fenofibrate drug powder in the absence of the lipid excipients was evaluated according to the same protocol in the two media.

5.2.1.2 Results and discussion

The measured solubility of fenofibrate in FaSSGF pH 2 and FaSSIF-V2(PO_4) from the lipid-based formulations is shown in Fig. 5-1. The influence of the lipid formulation components on solubilization is illustrated by comparison with the solubility of unformulated fenofibrate powder in the fasted state media (0.22 ± 0.01µg/mL in FaSSGF (Juenemann et al., 2011) and 4.31 ± 0.23µg/mL in FaSSIF-V2(PO_4)). As can be seen from the figure, the solubility of fenofibrate in physiologically relevant dilutions of the formulations is significantly greater than that of the pure drug in both media (horizontal dashed lines, Fig. 5-1). By using a lipid-based formulation, the solubility of fenofibrate has been increased by about 15-fold in FaSSIF-V2(PO_4) and up to 650-fold in FaSSGF pH 2.

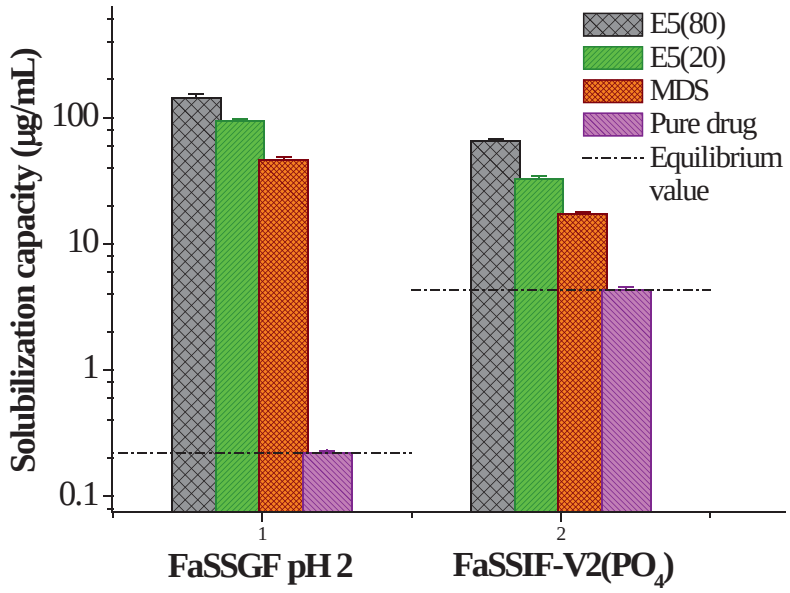

Fig. 5-1. Solubility data (n = 3) of fenofibrate in diluted lipid-based formulations (E5(80), E5(20) and MDS) and the unformulated drug substance in FaSSGF pH 2 and FaSSIF-V2(PO_4).

As shown in Fig. 5-1, the measured solubility of fenofibrate in gastric media was as follows: 142.01 ± 10.65µg/mL from the E5(80) formulation, 93.25 ± 3.33µg/mL from E5(20) and 46.01 ± 2.30µg/mL for MDS. In intestinal media, the respective values were as follows: E5(80) 65.44 ± 2.61µg/mL, E5(20) 32.74 ± 1.50µg/mL and MDS 17.22 ± 0.57µg/mL. The rank order of solubility was the same in both media:

E5(80) > E5(20) > MDS. This trend can be explained by the lipid formulation classification system (Pouton, 2006). The SMEDDS of E5(80) is expected to be more resistant to dilution and thus more likely to maintain the solubilization capacity of fenofibrate than the E5(20) lipid formulation: Tween 80 [HLB = 15 (Lin et al., 2011)], which is used in E5(80), is more lipophilic than Tween 20 [HLB = 16.7 (Lin et al., 2011)], which is used in the E5(20) formulation.

The data also show that the solubility of fenofibrate under gastric conditions is slightly higher than under intestinal conditions when applying the various formulations, despite the fact that fenofibrate is a neutral compound. This trend is due to the different ratios of formulation vs. medium applied for the solubility tests in FaSSGF pH 2 and FaSSIF-V2(PO_4). Since the dilution of excipients by the medium in the solubility tests in FaSSIF-V2(PO_4) is double that with FaSSGF pH 2, they will exert less influence on fenofibrate solubility.

5.2.2 Dissolution studies

5.2.2.1 Dissolution test set-up

The dissolution characteristics of each lipid formulation was also examined in FaSSGF pH 2 and FaSSIF-V2(PO_4). In gastric media, the dissolution studies were performed using 250mL of media in a USP II mini-paddle apparatus, whilst in intestinal media, the studies were performed in a USP II apparatus in 500mL of media. The mini-paddle apparatus is based on a USP paddle set-up but scaled down geometrically with respect to dimensions (Klein, 2006). An Erweka Dissolution-Tester DT 600 (Erweka, Heusenstamm, Germany) was used. The experiments were carried out at 37°C using a paddle speed of 75rpm. Introduction of lipid formulation into the dissolution medium was as follows: the E5(80) solution formulation (500 mg lipid blend) was placed into the dissolution media under stirring using a 1000μL pipette. For the capsule formulations, the required amount of the E5(80), E5(20) and MDS lipid blends were filled into hard gelatin capsules and sealed one day before the dissolution tests (see details in Section 5.1). Before manual

placement into the dissolution vessels, a helix wire sinker was slipped over to the capsule shell to prevent floating of the capsule. Samples were periodically (5, 10, 15, 20, 30, 45, 60, 90, 120, 180 and 240min) withdrawn from the gastric (2.5mL) and intestinal (5mL) media. After each sample withdrawal, the volume was replaced with an equivalent volume of blank fresh dissolution media pre-warmed to 37°C. Once withdrawn, the samples were immediately filtered (0.45µm PTFE membrane). The first 1mL from samples of gastric media and the first 2mL from samples of intestinal media were discarded, and the rest of the filtrate was collected into 10mL glass tubes and immediately diluted with 80% acetonitrile, and subsequently assayed by HPLC (see Section 4.2.3 for the HPLC method). All dissolutions were carried out in triplicate. Dissolution profiles were generated and the initial dissolution rate of fenofibrate was calculated using data points from the first hour of the profiles (see Section 5.2.2.2 and Section 5.2.2.3). Where it occurred [e.g. E5(20)], the impact of observed precipitation *in vitro* was also considered: a precipitation rate constant was calculated from fitting the descending slope of respective dissolution curve (see the green curves of Fig. 5-2), and was incorporated to the adapted STELLA® model (Fig. 5-4) to give a prediction of the obtained plasma profile.

5.2.2.2 Results and discussion

The dissolution profiles of the different fenofibrate formulations and pure drug in the simulated gastric and intestinal media are shown in Fig. 5-2A and Fig. 5-2B.

The dissolution experiments were carried out over 4h, a time which reflects the transit time through the small intestine (Shono et al., 2011; Sunesen et al., 2005). For comparison purpose, samples were also collected from the gastric media out to 4h, even though the residence time would typically not be this long in the fasted stomach. For comparison purpose, the solubility values (for fenofibrate in the respective formulation) are also shown in these profiles as horizontal lines. However, it should be noted that the horizontal line representing “Solubility pure drug” in Fig. 5-2A is too low to be clearly seen, as it almost overlapped on the X-axis.

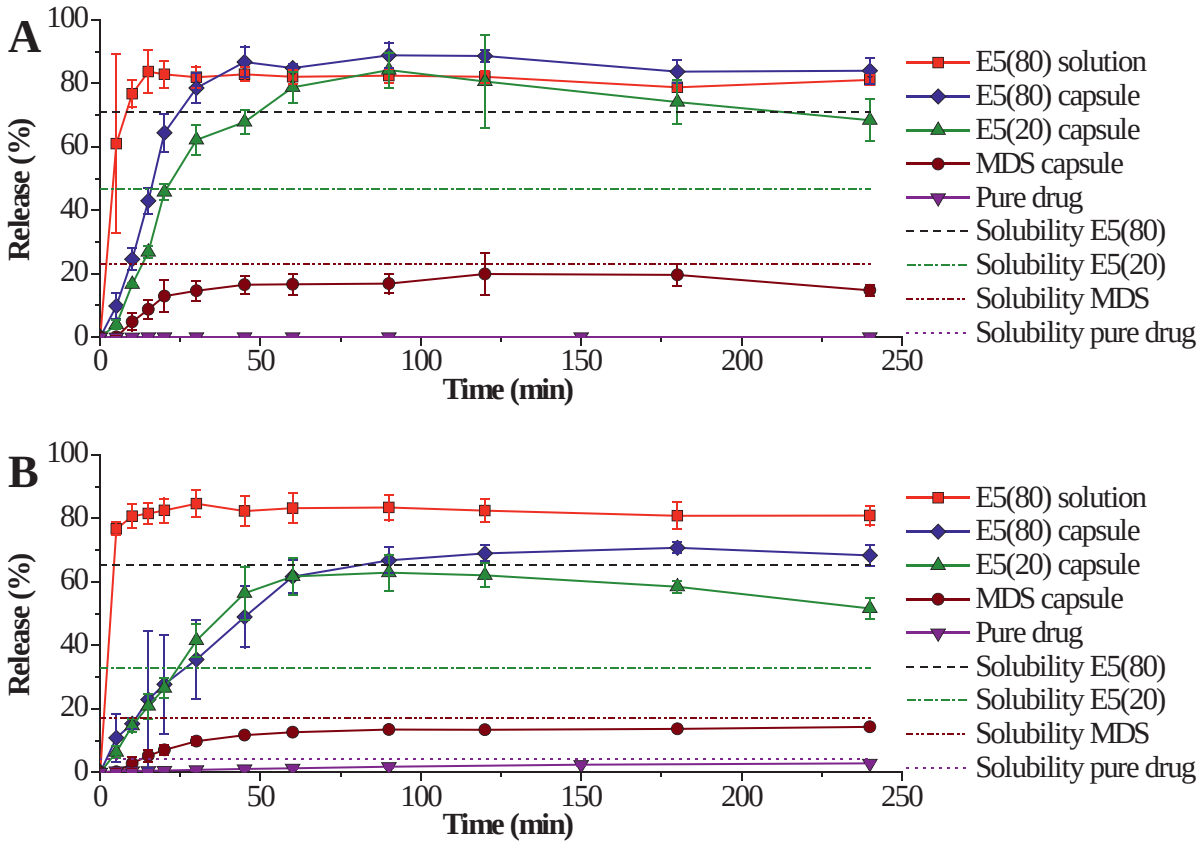

Fig. 5-2. Dissolution profiles (n = 3) of four fenofibrate lipid formulations: E5(80) solution, E5(80) capsule, E5(20) capsule and MDS capsule of 50 mg dose in 250mL of FaSSGF pH 2 (A) and in 500mL of FaSSIF-V2(PO4) (B). The horizontal lines depict the mean equilibrium solubility (n = 3) of fenofibrate in the diluted E5(80), E5(20) and MDS formulations in each respective media.

As expected, the E5(80) solution showed very rapid dissolution in both media (see the red curves of Fig. 5-2A and Fig. 5-2B), with the maximum dissolution of just over 80% occurring after approximately 10min. After 500mg of E5(80) was added using a pipette, the formulation mixed well with the dissolution media and formed a turbid emulsion. Although the dissolution profiles suggested the E5(80) solution was able to maintain the dispersion and dissolution following dilution in the media over 4h, some drug particles were found at the bottom of the vessels after the dissolution test. This could account for the incomplete dissolution observed. In contrast, the unformulated drug powder dissolved only very slowly in each of the media, with only 0.07% released after 60min in FaSSGF pH 2 (see the purple curve of Fig. 5-2A) and 1.7% after 90min in FaSSIF-V2(PO_4) (see the purple curve of Fig. 5-2B).

The E5(80) and E5(20) capsule formulations reached their maximum percent dissolved (60-80%) somewhat more slowly, after approximately 1h (see the blue and green curves of Fig. 5-2A and Fig. 5-2B). These differences between the oral solution and capsule formulations are also reflected by the significantly greater *z* value for the solution compared to the lipid filled capsules (see Table 5-2). On the other hand, although the MDS formulation showed a faster rate of dissolution in the FaSSGF pH 2 media than in FaSSIF-V2(PO_4) (see the brown curves of Fig. 5-2A and Fig. 5-2B), the maximum percent released in both media was just under 20%. These values correspond closely to the solubility of fenofibrate (from the MDS formulation) in the two media.

As expected from the solubilities, the percent dissolution was much higher from the E5(20) and E5(80) capsule formulations compared to unformulated fenofibrate. Both achieved a supersaturation in FaSSGF pH 2 as well as in FaSSIF-V2(PO_4) even compared to the fenofibrate solubility in the presence of the excipients. The E5(20) capsules achieved concentrations almost doubling the solubility in the presence of excipients, but then began to precipitate after approximately 90min. For the E5(80) capsules, the supersaturation was less extensive, but the concentrations were maintained over the four hour period.

It is clear from the results that the composition of the lipid excipients, the ratio of drug to lipid excipients, and the dosage form presentation all have a direct influence on the dissolution profile of fenofibrate. First, the E5(80) capsule, in which Tween 80 is used, and the E5(20) capsule, in which Tween 20 is incorporated, differ in their ability to create and maintain drug supersaturation in the simulated GI fluids. Second, comparing the dissolution of MDS capsule with E5(20) capsule, a drug load in excess of the fenofibrate solubility in these excipients leads to reduced drug release and third, it is clear that the oral solution dissolves much faster than the release of fenofibrate from the E5(80) capsule formulation.

Wei et al. (2010) performed dissolution of the above LBFs of fenofibrate in media consisting 0.0125 and 0.025 M SLS solutions, while Lin et al. (2011) studied

dissolution of the same LBFs of fenofibrate in SGF pH 1.2. Owing to surfactant or pH induced enhancement of drug solubility, the dissolution rates in their experiments were more rapid than these in biorelevant media (see Fig. 5-2A and Fig. 5-2B). Through use of the biorelevant media, it was possible to better discriminate among the different LBFs. This plays an important role in the success of the *IVISIV*C approach using STELLA®.

5.2.2.3 *z* value estimation

The initial dissolution rate (*z* value) was calculated from the initial data points (up to 60min) of the *in vitro* dissolution curves, according to the Noyes-Whitney theory Eq. (5-8). The values are summarized in Table 5-2. As anticipated, the *z* value for the E5(80) solution was greater than for the capsule formulations, reflecting the faster initial dissolution rate from this formulation. Compared to the other formulations, the unformulated drug powder had the slowest dissolution rate (lowest *z* value).

Table 5-2

Summary of *z* values of fenofibrate LBFs in fasted state biorelevant media.

	z/V-Value[a] ($mg^{-2/3}\ h^{-1}$)	
Formulation	FaSSGF pH 2	FaSSIF-V2(PO_4)
E5(80) solution	9.4565 ± 4.2330	7.5276 ± 1.1784
E5(80) capsule	0.5248 ± 0.1361	0.2595 ± 0.0815
E5(20) capsule	0.2724 ± 0.0398	0.2036 ± 0.0463
MDS capsule	0.3835 ± 0.0892	0.2453 ± 0.0330
Pure drug	0.0741 ± 0.0114	0.0232 ± 0.0039

[a] Value corrected for *in vivo* dose (54mg), and calculated from the *in vitro* dissolution data (n = 3).

5.2.3 STELLA® model set-up

5.2.3.1 Overall description of the model map and assumptions

Using STELLA® 9.1.3 (Cognitus Ltd., North Yorkshire, UK), the fenofibric acid plasma concentration vs. time profiles were simulated by incorporating the experimental solubility and dissolution results for the different lipid formulations.

Fig. 5-3 shows the model map for the STELLA®-based simulations. It comprises seven compartments and nine first-order flows. Each compartment is governed by a specific ODE (see Eq. (5-1) to Eq. (5-7)). The upper-left compartment accommodates the undissolved amount of dose in the stomach at time zero. It will spontaneously undergo a stomach dissolution step and a gastric emptying step. The compartment corresponding to the intestinal lumen takes the dissolution flux in the intestine, as well as the gastric emptying flux of dissolved drug in the stomach into account. Concomitantly, a standby compartment representing the co-administered fluid volume is depicted, providing real-time input to quantify the other related flows (see the respective pointed pink arrows). The dissolved amount of drug in the small intestine goes through the absorption step to become available in the central plasma compartment. Being double-connected, the peripheral compartment functions like a reservoir, which allows equilibration of the distributed fenofibric acid in the systematic circulation. Finally, elimination takes place from the central plasma compartment. The time evolution of the drug presented into the central compartment is monitored so that the *in silico* human plasma curve can be numerically solved.

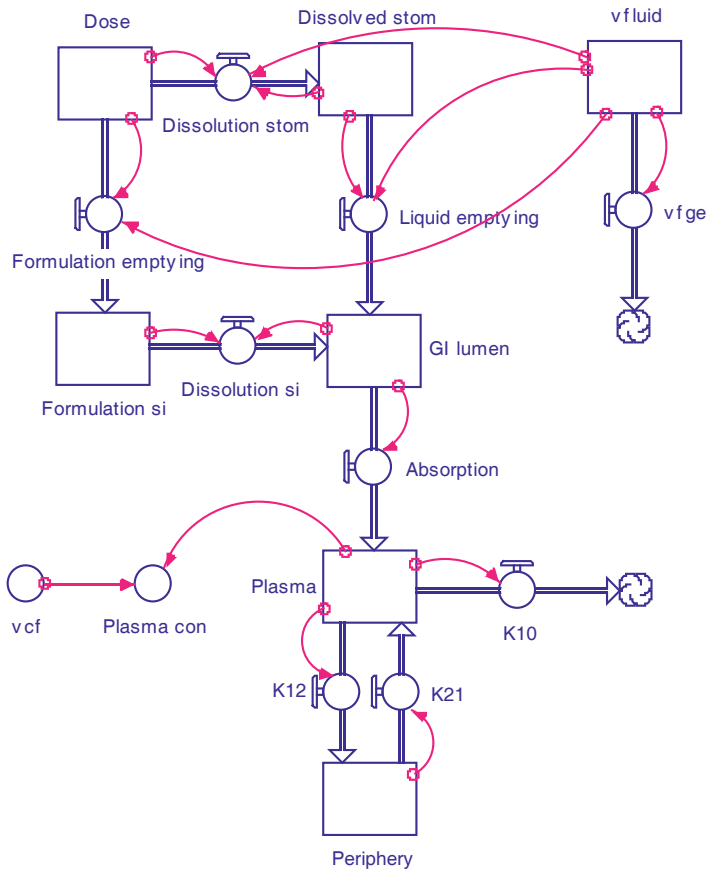

Fig. 5-3. Stella® model map used to simulate the plasma profiles of the fenofibrate lipid-based formulations (shown without precipitation and re-dissolution elements). stom, stomach; si, small intestine; vfluid, volume of coadministered fluid; vfge, time factor of gastric emptying of the fluid volume; GI lumen, intestinal lumen; plasma con, plasma concentration; vcf, volume of distribution including factor for bioavailability.

Part of the present model map was based on the research of an elder Ph.D. student in institute (Juenemann, 2012; Juenemann et al., 2011). The assumptions in this model include: (a) there is no absorption of drug from the stomach; (b) gastric emptying into the small intestine of the dispersed drug formulation and coadministered water can occur simultaneously; (c) the average first order gastric emptying rate constant (k_{GE}) is 2.8h^{-1} (Nicolaides et al., 2001; Vertzoni et al., 2005); (d) limitations to the drug permeation processes can be simulated by incorporating a compartment to reflect the unstirred water layer and/or penetration into the mucosa. Further assumptions, specific to this case, were that (e) the volume of coadministered water is 240mL (Wei et al.,

2010) and (f) although fenofibrate was used in the dissolution and solubility tests, fenofibric acid was used in describing all the plasma concentration profiles post-absorption, since *in vivo* fenofibrate is rapidly and completely hydrolysed within the gut wall and liver by esterases, which convert it to its active metabolite fenofibric acid (Hanafy et al., 2007; Hu et al., 2011; Juenemann et al., 2011; Najib, 2002).

5.2.3.2 Description of the ODEs involved

Eq. (5-1) to Eq. (5-7) describe drug flux within each compartment of the STELLA® model (Fig. 5-5). Eq. (5-1) and (5-2) represent conditions of the gastric lumen; Eq. (5-3) and (5-4) represent conditions of the intestinal lumen; Eq. (5-5) represents the pathway for the co-administered water volume; and Eq. (5-6) and (5-7) represent the plasma and periphery tissue compartments, respectively.

$$\frac{dX_{DO}(t)}{dt} = -J_{DS}(t) - k_{GE}X_{DO}(t) \tag{5-1}$$

$$\frac{dX_{DS}(t)}{dt} = J_{DS}(t) - k_{GE}X_{DS}(t) \tag{5-2}$$

$$\frac{dX_{FI}(t)}{dt} = k_{GE}X_{DO}(t) - J_{DI}(t) \tag{5-3}$$

$$\frac{dX_{IL}(t)}{dt} = J_{DI}(t) + k_{GE}X_{DS}(t) - k_{a}X_{IL}(t) \tag{5-4}$$

$$\frac{dV_{F}(t)}{dt} = -k_{GE}V_{F}(t) \tag{5-5}$$

$$\frac{dX_{PL}(t)}{dt} = k_{a}X_{IL}(t) + k_{21}X_{PE}(t) - (k_{12} + k_{10})X_{PL}(t) \tag{5-6}$$

$$\frac{dX_{PE}(t)}{dt} = k_{12}X_{PL}(t) - k_{21}X_{PE}(t) \tag{5-7}$$

In the above equations, $X_{DO}(t)$ describes the time evolution for the orally administered formulated drug dose in the stomach, mg; $X_{DS}(t)$ describes the time evolution for the dissolved drug mass in the stomach, mg; $X_{FI}(t)$ describes the time evolution for the formulated drug mass in the small intestine, mg; $X_{IL}(t)$ describes the

time evolution for the dissolved drug mass in the intestinal lumen, mg; $X_{PL}(t)$ describes the time evolution for the absorbed drug mass in the plasma, mg; $X_{PE}(t)$ describes the time evolution for the absorbed drug mass in the periphery tissue, mg; $J_{DS}(t)$ represents the dissolution rate for the formulated drug content in the stomach, mg h^{-1}; $J_{DI}(t)$ represents the dissolution rate for the formulated drug content in the small intestine, mg h^{-1}; k_{GE} is a first order kinetic rate constant for gastric emptying, h^{-1}; k_a is the absorption rate constant from the small intestinal lumen to plasma compartment, h^{-1}; and $V_F(t)$ describes the time evolution of the coadministered water volume in the stomach, mL. The code for the STELLA® model is shown in the appendix (Table A-60).

To describe the dissolution behavior of the different lipid formulations in the PBPK model, the Noyes-Whitney theory was utilized, as shown in the following equation (Nicolaides et al., 2001):

$$\frac{dW_t}{dt} = \frac{z}{V} W^{2/3}(X_s - W_t) = zW^{2/3}(C_s - C_t) \tag{5-8}$$

In this case, the amount of drug (W_t) dissolved at time t is described by the following parameters: z value, an apparent parameter for describing the initial drug dissolution rate from the lipid formulation which can be calculated using the *in vitro* dissolution data, mL $mg^{-2/3}$ h^{-1}; V, the dissolution medium volume, mL; W, the mass of drug remaining to be dissolved, mg; X_s, the amount of drug that saturates the dissolution medium, mg; C_s, the drug solubility in the dissolution medium, mg mL^{-1} and C_t, the concentration of dissolved drug at time t (h), mg mL^{-1}.

5.2.3.3 Modeling of precipitation process

It has been hypothesized that lipid formulations that consist mainly of surfactants may lose their solvent capacity when diluted by GI-fluids and exposed to physical agitation in the GI-tract, leading the metastable phase system to undergo phase separation and cause precipitation of the API (Mohsin et al., 2009). For the lipid formulations in this study, the solubilization capacity of fenofibrate in gastric and

intestinal media was significantly enhanced by the excipients, leading to a high degree of supersaturation in comparison with the solubility of pure fenofibrate in the same media. For the E5(80) solution and E5(80) capsule formulation, although incomplete drug release was observed from their respective dissolution profiles (see Fig. 5-2), they showed little tendency to precipitate after dissolving. By contrast, for the E5(20) formulation, some precipitation in the gastric and small intestinal media was detected analytically (see Fig. 5-2), so precipitation and re-dissolution were taken into consideration in the STELLA® model for this formulation (see Fig. 5-4). A zero order precipitation rate constant (k_0) was calculated from fitting the descending slope of respective *in vitro* dissolution curve of E5(20) using data points taken after 90min (see the green curves of Fig. 5-2). The respective fitted value of the *in vitro* precipitation rate was 3.426mg h^{-1} in stomach and 0.777mg h^{-1} in small intestine. As r^2 of both regressions were greater than 0.95, the zero-order kinetic was considered to be optimal for data fitting. Eq. (5-9) provides input of the precipitation flows in STELLA®.

$$\frac{dP_t}{dt} = -k_0 \tag{5-9}$$

Hereby, dP_t / dt is the rate of drug precipitation at time t (mg h^{-1}); and k_0 is the zero order rate constant of the precipitation process (mg h^{-1}).

Additionally, to account for any re-dissolution of the precipitate, which could then be absorbed, the re-dissolution rate was assumed to be identical to the initial dissolution rate of the pure drug substance in each of the respective media. The z values were therefore taken from Table 5-2 (unformulated drug).

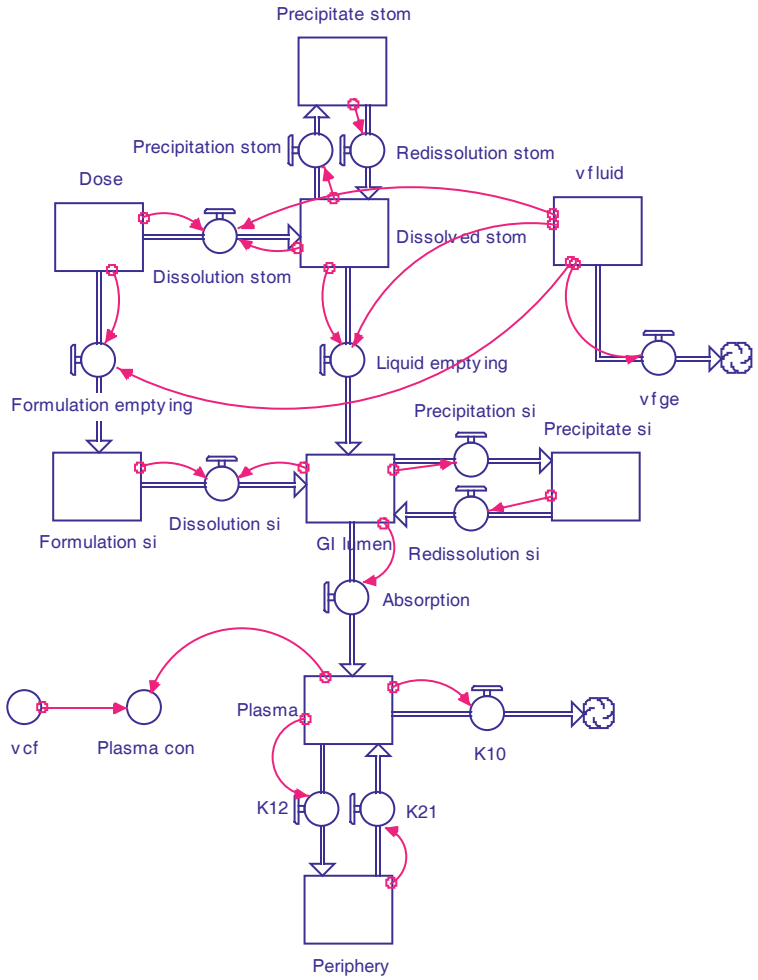

Fig. 5-4. Stella® model map used to simulate the plasma profiles of the fenofibrate lipid-based formulations (shown with precipitation and re-dissolution elements). stom, stomach; si, small intestine; vfluid, volume of coadministered fluid; vfge, time factor of gastric emptying of the fluid volume; I lumen, intestinal lumen; plasma con, plasma concentration; vcf, volume of distribution including factor for bioavailability.

5.2.3.4 Fenofibrate permeability estimation and STELLA® intestinal absorption model

Although fenofibrate is often assumed to be a BCS Class II drug, it has been discussed in the literature that for nanosized formulations of fenofibrate membrane uptake may also partially play a limiting role (Juenemann et al., 2011). From a mechanistic viewpoint, this may also be the case for lipid formulations from which dispersion/dissolution is rapid. Therefore, a permeability restriction was incorporated in the STELLA® model for the PK simulations. Up until 2013, few if any publications had a directly listed permeability coefficient or absorption rate constant of fenofibrate

based on *in vitro* human intestinal permeability tests. Thus, a Caco-2 permeability coefficient for fenofibrate was estimated using data obtained from the literature (Buch et al., 2009a,b; Kataoka et al., 2003). In these experiments, a U-shaped chamber divided into two compartments was used to fix the Caco-2 monolayer in between (see Fig. 5-5). Following addition of drug to the donor chamber under stirring, samples were periodically taken from both chambers, which contained buffer solutions simulating conditions on both the apical and basal sides of the intestinal membrane (apical side: pH = 6.5, volume = 8mL; basal side: pH = 7.4, volume = 5.5mL). For this set-up, the apparent Caco-2 permeability ($P_{Caco\text{-}2}$, cm s^{-1}) was calculated according to the following equation (Artursson and Karlsson, 1991):

$$P_{Caco-2} = \frac{dQ}{dt} \times \frac{1}{A \cdot C_0} \tag{5-10}$$

where dQ/dt is the permeation rate with the amount of drug represented in fraction (%), s^{-1}; C_0 is the initial concentration in the donor chamber with the amount of drug represented in fraction (%), mL^{-1}; and A is the surface area of the monolayer, cm^2.

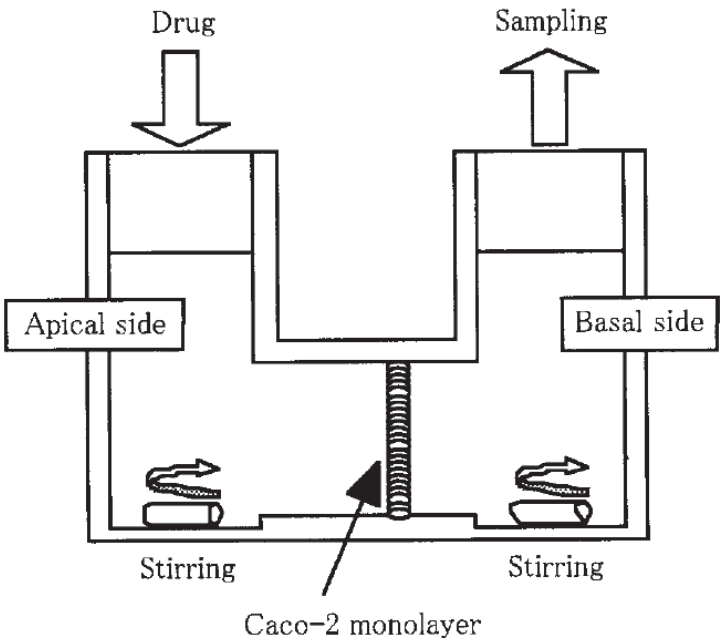

Fig. 5-5. Schematic illustration of the dissolution/permeation system (D/P system). Caco-2 monolayer was mounted between the apical and basal chambers (figure taken from Kataoka et al., 2003).

Since drug diffusion through the Unstirred Water Layer (UWL) adjacent to the intestinal epithelial membrane might also limit the intestinal permeation of highly permeable drugs (Takano et al., 2006), the permeation rate through the UWL (P_{UWL}) and the permeation rate through Caco-2 cells ($P_{Caco\text{-}2}$) was compared. Eq. (5-11) was used to calculate the permeation coefficient through the UWL (Takano et al., 2006):

$$(P_{UWL})_{MW} = 10 \times 10^{-4} \times \left(\frac{180}{MW}\right)^{1/3} \tag{5-11}$$

where $(P_{UWL})_{MW}$ is the UWL permeability calculated using the molecular weight (MW) of the drug, cm s^{-1}. In Eq. (5-11), glucose is used as the reference compound under the assumption that glucose permeation across the human intestine is completely limited by diffusion through the UWL. The values $10x10^{-4}$ and 180 represent the human UWL permeability value (cm s^{-1}) and the molecular weight of glucose, respectively (Takano et al., 2006).

The effective permeability coefficient (P_{eff}, cm s^{-1}) accounts for contributions of both the Caco-2 cell permeability and the UWL, as given in Eq. (5-12):

$$\frac{1}{P_{eff}} = \frac{1}{P_{Caco-2}} + \frac{1}{P_{UWL}} \tag{5-12}$$

The flux of drug from the intestinal tract into the blood circulation was calculated using Eq. (5-13):

$$\frac{dM_t}{dt} = k_a \cdot M_t = 3600 \cdot P_{eff} \cdot S \cdot \frac{M_t}{V} \tag{5-13}$$

As shown by Eq. (5-13) (Grass, 1997), the amount of drug (M_t, mg) permeated from the intestinal tract into the blood circulation at time t (h) was calculated using the P_{eff} value calculated from Eq. (5-12); the available intestinal surface area for absorption (S), which was assumed to be 800cm^2 (Yu, 1999); and the intestinal fluid volume (V), which was assumed to be 105 ± 72mL in the fasted state (Schiller et al., 2005). This equation was then used to calculate the absorption rate constant and the value was compared with the one used in previous simulations of fenofibrate plasma profiles (Juenemann et al., 2011).

Since the simulated plasma profile of micronized fenofibrate tablets had been successfully predicted without considering permeability restrictions (Juenemann et al., 2011), the rate limiting step for oral administration of the micronized solid dosage forms was assumed to be dissolution rather than uptake rate through the intestinal mucosa. However, since fenofibrate dissolves much faster from lipid formulations than from tablets, the initial dissolution rate might be comparable to its permeation rate in this case. As a result, we assumed for the modeling that permeability restrictions should be accounted for when simulating plasma profiles for the fenofibrate lipid formulations.

Eq. (5-14) can be derived from Eq. (5-10). This of course is only an approximation, since it is a mean value calculated from the *in vitro* data of different fenofibrate formulations (Fig. 5-6, n = 5) from Ussing chamber experiments (Buch, 2010; Buch et al., 2009a,b). Those formulations were immediate release (IR) fenofibrate dosage forms based either upon solid dispersion techniques using hydrophilic polymer (MeltDose®), or upon nanoparticulate tablet technology (Tricor®) (Buch, 2010). As they were all IR dosage forms, we assume the maximum dissolved concentration in the donor chamber *in vitro* was very quickly reached and maintained throughout the permeation test for 120min. Therefore, the C_0 in Eq. (5-10) was approximated to be constant, allowing integration of Eq. (5-10), yielding Eq. (5-14). Hereby, A was the effective area of Caco-2 monolayer, and was reported to be 1.77cm^2 (Kataoka et al., 2003).

$$P_{Caco-2}(cm/s) = \frac{\text{permeated amount at 2 h - permeated amount at 1.5 h}}{\text{apical (dissolved) concentration at 2 h} \cdot \text{A} \cdot 1800} \qquad (5\text{-}14)$$

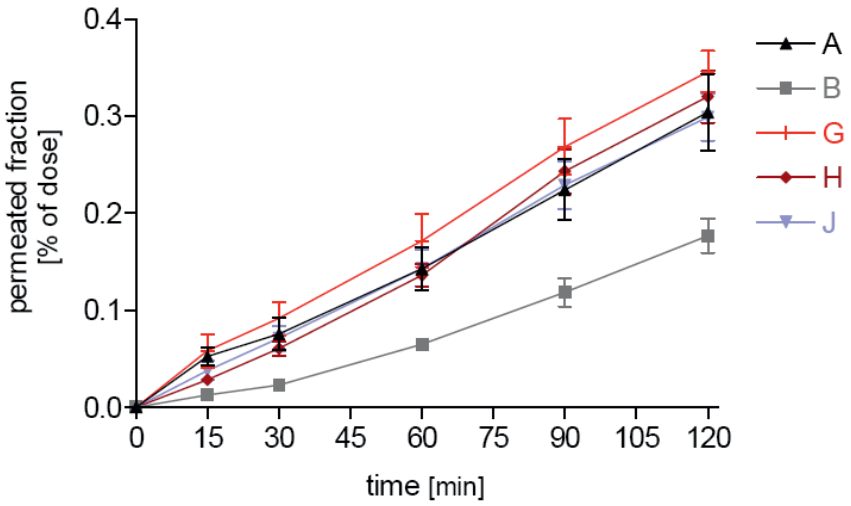

Fig. 5-6. Effect of different formulations on permeation of fenofibrate in the D/P system. Each data point is the mean ± SEM of three to six independent experiments (figure taken from Buch, 2010).

Table 5-3

Summary of the Caco-2 permeability calculation using fenofibrate IR dosage forms.

Formulation	%D(P1.5h) [a]	%D(P2h) [b]	%D(D2h) [c]	Con(D2h) [d]	P_{app} [e]	Ka [f]
A	0.223	0.304	7.49	0.936	2.73	0.748
B	0.117	0.177	7.67	0.959	1.97	0.541
G	0.269	0.346	5.71	0.714	3.38	0.927
H	0.244	0.320	6.35	0.794	2.99	0.821
J	0.230	0.299	6.37	0.796	2.71	0.743
Mean ± SD	–	–	–	–	2.76 ± 0.51	0.76 ± 0.14

[a] Permeated fraction (%) of dose at 1.5h, value taken from literature (Buch, 2010).

[b] Permeated fraction (%) of dose at 2h, value taken from literature (Buch, 2010).

[c] Dissolved fraction (%) of dose at 2h, value taken from literature (Buch, 2010).

[d] Dissolved concentration fraction (mL^{-1}) at 2h, calculated value.

[e] Apparent permeability coefficient ($x10^{-5}cm/s$), calculated value using Eq. (5-14).

[f] Absorption rate constant (h^{-1}), calculated value using Eq. (5-11) – Eq. (5-13).

As shown in Table 5-3, using the *in vitro* Caco-2 data for fenofibrate from the literature (Buch, 2010; Buch et al., 2009a,b) and Eq. (5-14), the average human permeability coefficient of fenofibrate was calculated to be 2.76×10^{-5}cm/sec ($P_{app} = P_{Caco\text{-}2}$). Using Eq. (5-11) and the molecular weight of fenofibrate, the permeability coefficient of fenofibrate through the unstirred water layer (P_{UWL}) was calculated to be 7.93×10^{-4}cm/sec. The P_{UWL} is thus approximately 30 times higher than the $P_{Caco\text{-}2}$. This suggests that fenofibrate permeation through the unstirred water layer of the gut wall is much faster than permeation through the enterocytes. Consequently, the permeation through the enterocytes should be the primary rate limiting step to uptake once fenofibrate is in solution. In fact, both steps were accounted for using Eq. (5-12), resulting in an overall effective permeability (P_{eff}) of 2.66×10^{-5}cm/sec.

Applying the calculated P_{eff} [$(2.66 \pm 0.48) \times 10^{-5}$cm/sec, n = 5], S [800cm^2 (Yu, 1999)] and V [105 ± 72mL (Schiller et al., 2005)] parameters in Eq. (5-13), one arrives at an absorption rate constant, k_a value of 0.730h^{-1}, which is a little lower than the overall k_a used for the simulations [1.00h^{-1}, the best fitted empirical value used by Juenemann et al. (2011)]. As these values are also in good agreement with the k_a value (0.830 ± 0.241h^{-1}, n = 4) obtained using WinNonlin® software to deconvolute the *in vivo* plasma profiles, this calculation of the absorption rate constant from the effective permeability data seems like a promising approach to bridge the gap between the *in vitro* and *in vivo* permeation behavior of drugs for use in the *in silico* modeling.

In summary, Caco-2 permeability of fenofibrate was calculated and compared to the one from unstirred water layer. Caco-2 permeability, representing uptake into the enterocytes, is found to be the major limiting factor to intestinal permeation. However, the overall absorption rate constant used for *in silico* simulation fit the *in vivo* data best when k_a was a little larger (ca. 25%). This difference could arise from parallel lymph transport of lipid-based vehicles ingested (Trevaskis et al., 2008), although lymphatic uptake of fenofibrate has not been demonstrated in the literature.

5.2.4 *In vivo* clinical study and calculation of PK parameters

The plasma concentration profiles of fenofibric acid after oral administration of 54mg fenofibrate lipid formulations (1 oral solution, 2 SMEDDS capsules and 1 MDS capsule) were obtained from the literature (Wei et al., 2010). Briefly, twelve healthy male Taiwanese volunteers aged between 24-29 years participated in the clinical study after signing an informed consent agreement of ethics. A partial crossover design was used, where each formulation was administered to a group of four subjects. After an overnight fast of at least 10h, each subject was administered either the respective capsule formulation together with 240mL of water, or the oral solution formulation of 0.5mL lipid vehicle, which was pre-dissolved in 240mL of water. After administration of the dosage forms, subjects remained fasted for 4h. For the hour prior to administration and 2h after, no water was permitted. Thereafter, subjects were given free access to water. Lunch and dinner was served by Taipei Medical University Hospital at 4 and 10h after dose administration, respectively.

The post-absorptive PK parameters of fenofibric acid required for the STELLA® based model were calculated from the *in vivo* plasma concentration profiles. Since there are no published i.v. data for fenofibrate, the disposition parameters were calculated according to plasma concentration for the oral solution E5(80), assuming its clearance was very similar to an ideal i.v. condition. Using WinNonlin® Professional Edition 5.2.1 software (Pharsight Corporation, Mountain View, CA, USA) and the *in vivo* data of four individuals (subject A, B, C and D, see Figure 9-1 and Figure 9-3), their plasma concentrations were fitted to a two compartment model with first order micro rate constants without lag time (model 11). The resulting constants of E5(80) solution which included k_{10} (elimination rate constant), k_{12} (rate constant from central to periphery compartment) and k_{21} (rate constant from periphery to central compartment) were kept fixed and then used to simulate the plasma profiles for the rest of fenofibrate LBF (i.e. E5(80) capsule, E5(20) capsule and MDS capsule). The *V/F* value (volume of distribution corrected for the fraction absorbed) from the oral solution was also given (see Table 5-4).

Table 5-4

Summary of calculated mean values of human post-absorptive parameters of fenofibric acid using individual *in vivo* plasma concentration profiles following oral administration of the E5(80) solution in fasted state using WinNonlin® software.

Subject	A	B	C	D	Mean[a] ± S.D.
k_{12} (h^{-1})	0.705	0.512	0.392	0.312	0.480 ± 0.171
k_{21} (h^{-1})	0.284	0.330	0.231	0.171	0.254 ± 0.069
k_{10} (h^{-1})	0.078	0.223	0.093	0.103	0.124 ± 0.066
V/F (mL)	4817.0	5516.7	6551.8	5978.4	5716.0 ± 733.8
Cl/F (mL h^{-1})	377.9	1228.0	606.6	616.5	707.2 ± 364.3

[a] The arithmetic mean values of the four individuals (subject A, B, C and D) are incorporated to the STELLA® model to simulate the mean plasma profiles following treatment of various fenofibrate lipid formulations.

As a commonly used approach suggested by e.g. Cardot and Davit (2012), the arithmetic mean values of the individual parameters were derived, and these data were incorporated into STELLA® as input human PK parameters to simulate the mean plasma profiles for the lipid formulations. This approximation is based upon the assumption that the mean disposition parameters for subject A, B, C and D are very close to the mean drug disposition parameters of all twelve subjects who participated in the study (see Fig. A-5, Fig. A-7, Fig. A-9 and Fig. A-11 for the individual *in vivo* plasma profiles).

5.2.5 *f*2 approach and simulation outcome using STELLA® software

In order to compare similarity of the observed and simulated plasma concentration profiles under fasting conditions, a model-independent approach using the similarity factor (f_2) was applied (Moore and Flanner, 1996). The following equation was used to calculate the f_2 value.

$$f_2 = 50\log\left[1\Big/\sqrt{0.0001+\frac{1}{n}\sum_{t=1}^{n}(R_t - T_t)^2}\right] \qquad (5\text{-}15)$$

where T (test) is the relative fraction of *in silico* plasma drug concentration compared to the C_{max} value of R (reference) at time t, R is the relative fraction of observed plasma drug concentration compared to the C_{max} value of R at time t, and n is the number of sampling time points. The f_2-value can range between 0 to 100, a value above 50 indicates that the difference between the two dissolution (plasma) profiles is less than 10% and they are therefore assumed to be similar to each other (Dressman and Kraemer, 2005; O'Hara et al., 1998). Although the f_2 tool was originally aimed at comparing dissolution profiles, it can also be used to compare similarity of plasma concentrations. To ensure a valid comparison of test and reference, the *in silico* (T) and *in vivo* (R) plasma profiles were normalized before comparison.

Fig. 5-7A shows the simulated and observed fenofibric acid plasma concentration profiles for the E5(80) solution at a dose strength of 54mg in the fasted state. Since precipitation of dissolved material was minimal for the E5(80) solution during the 4h tests in both the gastric and intestinal media, the model omitting precipitation and re-dissolution was used to simulate the E5(80) solution (see Fig. 5-3). As shown in Fig. 5-7A, the simulated plasma profile (solid line) of the E5(80) solution fits the mean observed data (symbols with error bars) very well, although the T_{max} value was slightly overestimated compared to the *in vivo* profile. With respect to the *in vivo* data, it should be noted that all four individual plasma profiles of E5(80) solution (dash lines and symbols) showed high consistency in T_{max}, but the C_{max} values were variable (see Table A-59 for the observed PK parameters derived from individual curve fitting, as well as the calculated mean PK parameters used for *in silico* simulation). Larger

variability in the data was observed after 5h, reflecting differences among the individual subjects with respect to elimination of fenofibrate (see Table 5-4).

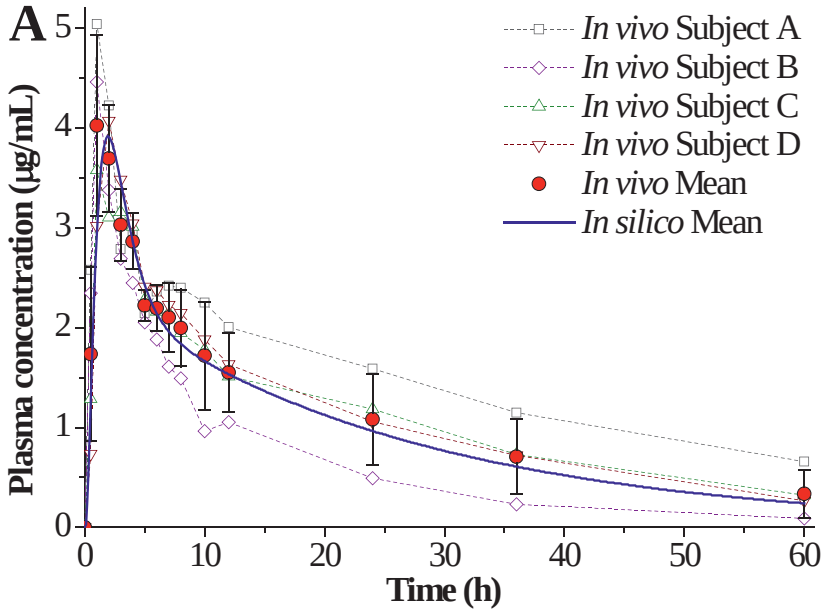

Fig. 5-7A. Fasting simulated and observed (both individual and mean, n = 4) fenofibric acid plasma concentration profiles for the E5(80) solution at a dose strength of 54mg in the fasted state. *In silico* data is shown with solid lines, *in vivo* mean data is shown by symbols with error bars, and *in vivo* individual data is depicted as dashed lines and symbols.

In Fig. 5-7B, the simulated and observed fenofibric acid plasma concentration profiles of the E5(80) capsule at a dose strength of 54mg are shown. The model used to simulate the plasma concentrations was identical to that used for the E5(80) solution. The simulated plasma profile (solid line in Fig. 5-7B) of the E5(80) capsule is in good agreement but slightly lower than the mean observed data out to 12h. Although the simulated profile slightly overestimates the observed data after 12h, the overall difference between the *in silico* and *in vivo* profiles is minimal, and this is also evident by the corresponding f_2 value (66.28) and ratio of the PK parameters (between 0.9 and 1.2, see Table 5-5). Since the *in vivo* study was carried out in parallel rather than as a full crossover study design, the plasma profiles are not directly comparable among different lipid formulations. Even so, from the plasma profile comparison

between E5(80) solution and E5(80) capsule, it seems that there is a delay in plasma peak (from comparison of the T_{max} value) and less complete absorption (from comparison of the AUC) of fenofibric acid from the E5(80) capsule. Thus, the differences observed in the dissolution tests (Fig. 5-2) are quantitatively expressed in the simulated plasma profiles (Fig. 5-7). Comparing Fig. 5-7A and Fig. 5-7B, it is clear that the presentation of the formulation (pre-diluted in a glass of water *vs*. administration as a capsule with a glass of water) has a strong influence on behavior in the GI-tract and hence on the plasma profile.

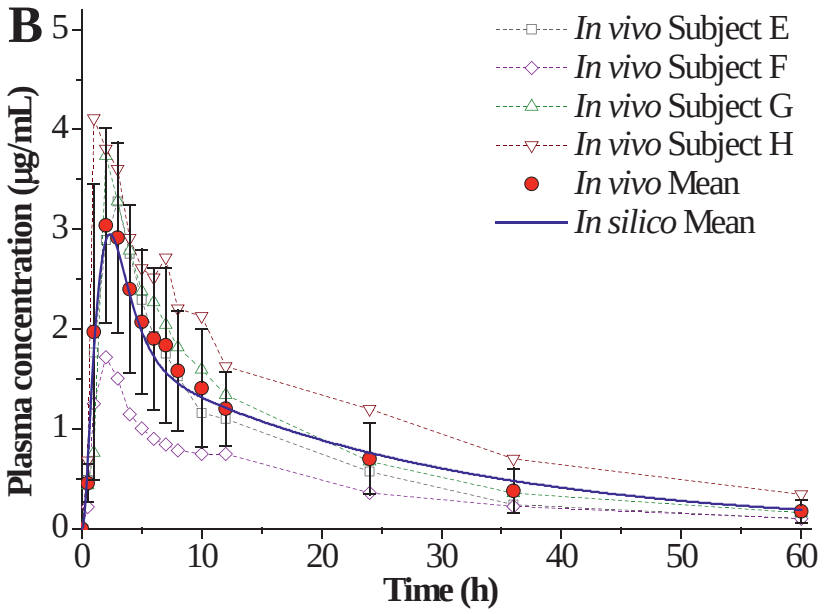

Fig. 5-7B. Fasting simulated and observed (both individual and mean, n = 4) fenofibric acid plasma concentration profiles for the E5(80) capsule at a dose strength of 54mg in the fasted state. *In silico* data is shown with solid lines, *in vivo* mean data is shown by symbols with error bars, and *in vivo* individual data is depicted as dashed lines and symbols.

Fig. 5-7C shows the simulated and observed fenofibric acid plasma concentration profiles for the E5(20) capsule. Since fenofibrate was observed to precipitate in the *in vitro* dissolution profiles, additional compartments to accommodate the precipitation and re-dissolution kinetics in both the stomach and small intestine were included in the original STELLA® model map (see Fig. 5-3 for the original and Fig. 5-4 for modified model map). The precipitation rate was calculated from the dissolution profiles in either FaSSGF pH 2 or FaSSIF-V2(PO_4) using time points after 90min and fitting the data to zero order kinetics (see Section 5.2.3.3). The *in vitro* precipitation rate constants were calculated to be 3.426mg h^{-1} in stomach and 0.777mg h^{-1} in small intestine, respectively. The re-dissolution rate of the precipitate was assumed to be the same as the initial dissolution rate of the pure drug substance in each of the media. Apart from the addition of the precipitation and re-dissolution steps, the STELLA® model used for the simulation of the E5(20) plasma profile was identical to that used for E5(80) formulation.

As shown in Fig. 5-7C, the simulated plasma profile (solid line) for E5(20) capsule correlated well with the mean observed data (symbols with error bars) over the initial 12 hours. Calculation of the overall f_2 value between the *in silico* and *in vivo* profiles (f_2 = 74.40, see Table 5-5) also suggests a very high degree of similarity (e.g. < 10% difference). Removing the precipitation and re-dissolution processes from the STELLA® model still resulted a similar profile, with an f_2 value of 59.29 (indicating less than a 10% difference in the profiles) but was not as close to the observed profile as when these processes were taken into account. Still, this result indicates that precipitation does not pose an important limitation to fenofibrate absorption for the SMEDDS studied. For the E5(20) capsule, less than 10% of dose was precipitated in the intestinal media (see green curve of Fig. 5-2B).

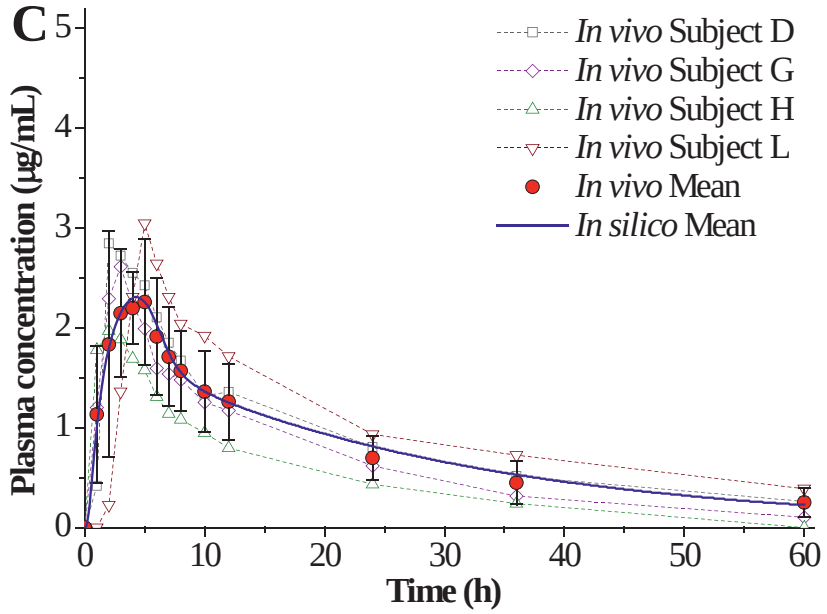

Fig. 5-7C. Fasting simulated (GI-precipitation was taken into account) and observed (both individual and mean, n = 4) fenofibric acid plasma concentration profiles for the E5(20) capsule at a dose strength of 54mg in the fasted state. *In silico* data is shown with solid lines, *in vivo* mean data is shown by symbols with error bars, and *in vivo* individual data is depicted as dashed lines and symbols.

In Fig. 5-7C, it can be seen that the *in vivo* T_{max} values of the individual subjects were highly variable. Compared with the E5(80) formulation, E5(20) dissolved and absorbed slower, which may account for the higher variation of T_{max} values in the E5(20) formulation. The differences in the PK behavior between the E5(80) and E5(20) formulations is most likely a net result from differences in drug dissolution (see Table 5-2), solubilization capacity (see Fig. 5-1), and precipitation properties (see Fig. 5-2).

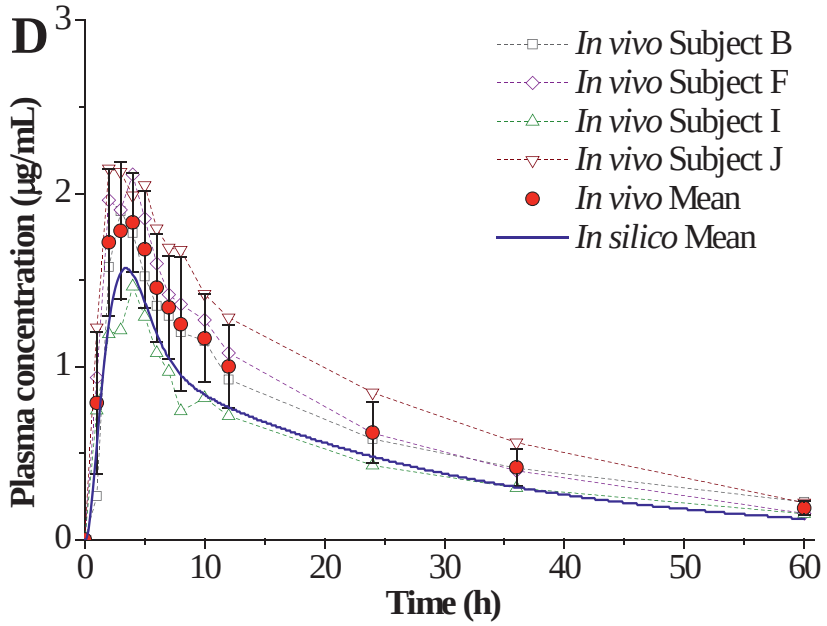

Fig. 5-7D. Fasting simulated and observed (both individual and mean, n = 4) fenofibric acid plasma concentration profiles for the MDS capsule at a dose strength of 54mg in the fasted state. *In silico* data is shown with solid lines, *in vivo* mean data is shown by symbols with error bars, and *in vivo* individual data is depicted as dashed lines and symbols.

Fig. 5-7D shows the simulated and observed fenofibric acid plasma concentration profiles for the MDS capsule. The model setup was identical to that used for the E5(80) solution, in which drug precipitation was not taken into account. As shown in Fig. 5-7D, the model underestimated the *in vivo* plasma profile. This most likely arises from the fact that the particle size of fenofibrate in the MDS formulation used for the *in vitro* dissolution and solubility tests (< 40µm) was slightly larger than that used for the *in vivo* human PK studies (< 37µm). (In fact, since the particle sizes used in the *in vitro* and *in vivo* studies are outside the limit of 1-10µm, neither can really be considered micronized.) Since in the MDS formulation fenofibrate is mostly present as solid drug particles suspended in the lipid blends, it is not surprising that both the observed and simulated AUC and C_{max} values of plasma profiles for the MDS capsule are much lower than those for the other lipid formulations examined (see Fig. 5-8), and suggest incomplete absorption of fenofibric acid. Despite the low absorption, the

individual plasma profiles for MDS capsule showed similar AUC and T_{max} values (see Fig. 5-7D, Fig. A-11 and Table A-65), indicating that the absorption was rather consistent.

An overview of the simulated and observed plasma fenofibric acid concentration for each of the lipid formulations (3 SMEDDSs and 1 MDS) is shown in Fig. 5-8. As can be clearly seen, each lipid formulation behaves differently, with the highest plasma levels observed for the E5(80) solution and the lowest for the MDS capsule. The simulated plasma profiles of each of the formulations were in accordance with the *in vitro* data, suggesting that the *in vitro-in silico-in vivo* (*IVISIV*) approach is useful for the prediction of plasma fenofibric acid concentration from lipid-based formulations.

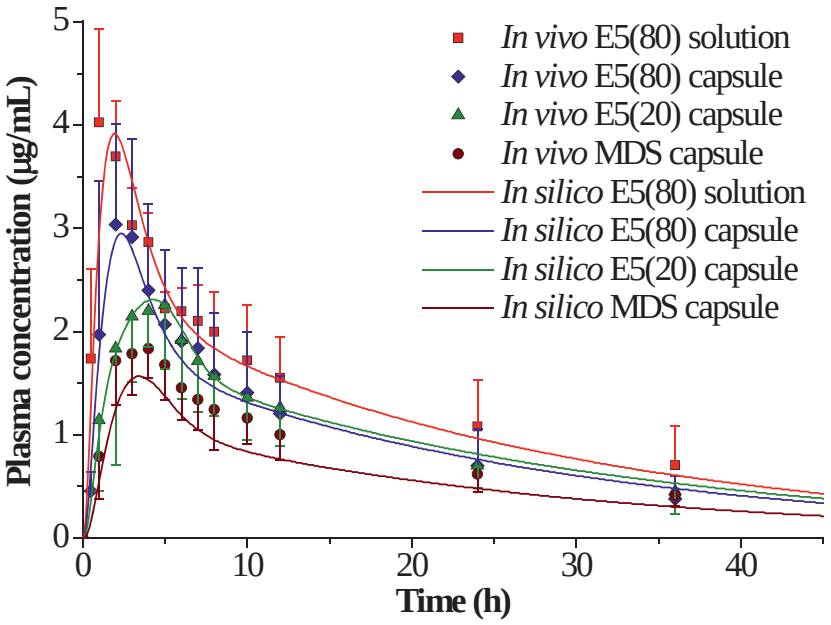

Fig. 5-8. Fasting simulated and observed plasma fenofibric acid concentration profiles for the lipid formulations (three SMEDDSs and one MDS, n = 4). *In silico* data is shown by solid lines, and *in vivo* mean data are depicted by symbols with error bars.

5.2.6 Comparison of simulated and reported plasma concentration profiles

The simulated and observed fenofibric acid PK parameters for each of the lipid formulations are summarized in Table 5-5. The f_2 values were greater than 50 for all of the formulations except the MDS capsule (41.37). This low result was probably due to the API particle size difference from the *in vitro* and *in vivo* experiments.

Table 5-5

Comparison of fasted state *in silico* and *in vivo* pharmacokinetic parameters after treatment of different fenofibrate lipid formulations at a 54mg dose strength.

Pharmacokinetic parameters		E5(80) solution	E5(80) capsule	E5(20) capsule	MDS capsule
$AUC_{0\text{-}inf}$ ($\mu g\ mL^{-1}\ h$)	*In silico*	70.51	53.66	56.75	33.31
	In vivo	78.31[a]	51.66[b]	52.66[b]	44.52[b]
	Ratio[c]	0.90	1.04	1.08	0.75
C_{max} ($\mu g\ mL^{-1}$)	*In silico*	3.92	2.95	2.31	1.57
	In vivo	4.29[a]	3.21[b]	2.62[b]	1.90[b]
	Ratio[c]	0.91	0.92	0.88	0.83
T_{max} (h)	*In silico*	1.90	2.35	4.25	3.40
	In vivo	1.25[a]	2.00[b]	3.00[b]	3.25[b]
	Ratio[c]	1.52	1.18	1.42	1.05
	f_2	52.78	66.28	74.40	41.37

[a] Mean values for *in vivo* data (n = 4), from literature (Lin et al., 2011).

[b] Mean values for *in vivo* data (n = 4), from literature (Wei et al., 2010).

[c] Ratio: PK parameter (*in silico*) / PK parameter (*in vivo*).

The simulated profiles for the lipid formulations were also compared to the *in vivo* data using the point estimate ratios for both $AUC_{0\text{-inf}}$ and C_{max}. The *in silico* and *in vivo* profiles can be considered "equivalent" when the 90% confidence intervals around the point estimate ratios for the simulated plasma profile fall in the 0.8-1.25 range of the *in vivo* profile (EMEA, 2010). Applying this criterion, simulated profiles for all of the lipid formulations except the MDS capsule (which showed an $AUC_{0\text{-inf}}$ ratio of 0.75) can be considered equivalent to their observed profiles.

5.2.7 Sensitivity analysis of the model parameters for simulation of the fenofibric acid plasma profiles in fasted state

In order to better understand which factors drive the pharmacokinetics from these formulations of fenofibrate, sensitivity analyses of the STELLA® model were conducted by varying selected physiological or measured parameters from one-fifth to five times of the nominal reference value. These parameters include dissolution rate in the stomach ($z_{stomach}$), dissolution rate in the small intestine ($z_{intestine}$), solubility in the gastric fluid ($C_{s,stomach}$), solubility in the intestinal fluid ($C_{s,intestine}$), absorption rate (k_a) and gastric emptying rate (k_{GE}). Their impact on the simulated plasma profiles are highlighted in Table 5-6. Detailed simulation results of the plasma concentration profiles of sensitivity analysis are shown in the appendix (Fig. A-17 to Fig. A-20).

Table 5-6

Summary of the fasted state sensitivity analysis for the variable parameters used in the STELLA® model.

Parameter	Range of value tested [a]	Impact of a change in the listed parameters [b]			
		E5(80) solution	E5(80) capsule	E5(20) capsule	MDS capsule
Dissolution rate in stomach	0.2-5	Negligible	Negligible	Negligible	Negligible
Dissolution rate in small intestine	0.2-5	Negligible	Moderate	Significant	Significant
Solubility in gastric fluid	0.5-2	Negligible	Negligible	Negligible	Negligible
Solubility in intestinal fluid	0.5-2	Negligible	Marginal	Moderate	Moderate
Absorption rate	0.2-5	Significant	Significant	Significant	Significant
Gastric emptying rate	0.5-3	Negligible	Negligible	Negligible	Negligible

[a] Factor applied to the reference input value used in the simulations.

[b] The impact of a change in the listed parameter was defined according to the index of C_{max} ratio between the simulated and the reference profiles as follows: Negligible: within 0.9-1.1, Marginal: within 0.8-1.2, Moderate: within 0.7-1.3, Significant: outside 0.7-1.3.

Based on the sensitivity analysis, the oral pharmacokinetics of the lipid formulation is controlled not only by both dissolution and permeability in the small intestine, but also by the solubilization capacity of the lipid formulation for fenofibrate after dilution in the intestinal fluids. Across the formulations, the effects of dissolution rate and solubility in small intestine on the plasma profile are increasingly important in the following rank order: E5(80) solution < E5(80) capsule < E5(20) capsule < MDS capsule. The slower *in vitro* release properties of the E5(80) capsule, E5(20)

capsule and MDS capsule relative to the E5(80) solution appear to be the major driving force for this trend.

Additionally, the hypothesis that fenofibrate lipid formulation performance might be influenced by permeation as well as dissolution (Section 5.2.3.4) was confirmed by the sensitivity of the plasma profile to both parameters. Changing the absorption rate had a noticeable effect on the simulation for each of the formulations, suggesting that whilst fenofibrate has been classified as a BCS class II compound, the plasma profile of its lipid-based formulations is more sensitive to the permeation process than to changes in dissolution and solubility in the intestine. To illustrate how the relative importance of these two parameters varies with formulation, we refer to Fig. 5-9, which shows the sensitivity of the plasma profile for the E5(80) solution to absorption rate, and Fig. 5-10, which shows the sensitivity of the plasma profile of the MDS capsule to dissolution rate in the small intestine. For the E5(80) solution, a change of absorption rate (k_a value) by a factor of 0.2 to 5 times of the reference value resulted in a 2.7-fold variation in C_{max} value in the *in silico* plasma profiles (Fig. 5-9), while a change in the intestinal dissolution rate ($z_{intestine}$) by a factor of 0.2 to 5 resulted in no variation in the *in silico* plasma profiles (Fig. 5-9 insert). For the MDS capsule, by contrast, variations in C_{max} value in the *in silico* plasma profiles resulted when either the dissolution rate in the small intestine (result in a 2.2-fold change in C_{max}, see Fig. 5-10) or the absorption rate (result in a 1.8-fold change in C_{max}, see Fig. 5-10 insert) was varied over a range of 0.2 to 5 times the reference value. This difference between formulations arises because the dissolution and solubility limitations have, to a large extent, been removed by the E5(80) formulation but not for the MDS formulation.

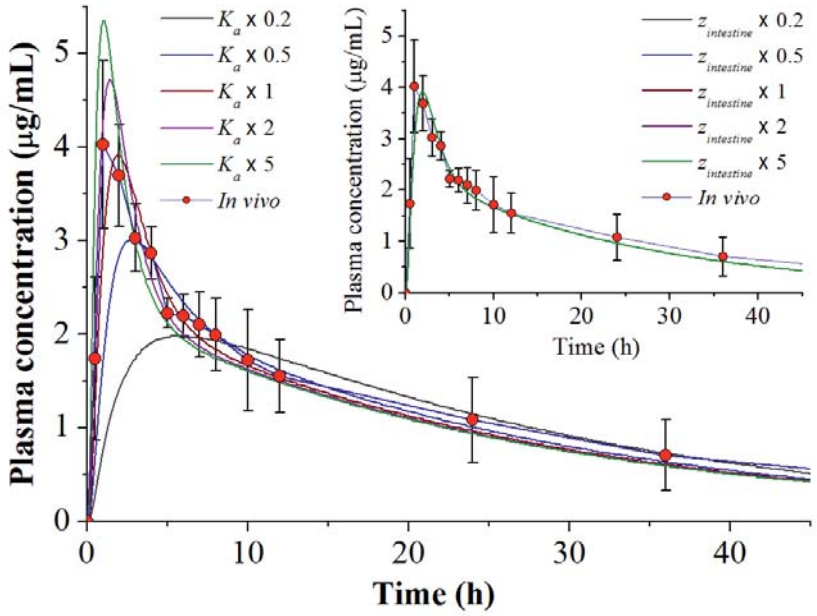

Fig. 5-9. Effect of absorption rate (k_a value) on simulated plasma profiles of E5(80) solution in fasted state. k_a was varied from one-fifth to five times of the reference value. *In silico* data is shown by solid lines, while *in vivo* mean data are depicted by symbols with error bars [insert map: effect of dissolution rate in small intestine ($z_{intestine}$) on simulated plasma profiles of E5(80) solution].

Further, sensitivity analysis revealed that the plasma profiles for these lipid formulations are not likely to be affected by differences in the dissolution rate in stomach, the solubility in gastric fluid, or changes in the gastric emptying rate.

A full sensitivity analysis for the respective parameters on the *in silico* plasma profiles for each formulation was conducted, and all results are summarized in Table 5-6. For parameters where the sensitivity analysis revealed that the C_{max} ratio between the simulated and the reference plasma profiles fell within the range 0.9-1.1, the effect of that parameter on the simulated plasma profile is given as “negligible” in Table 5-6.

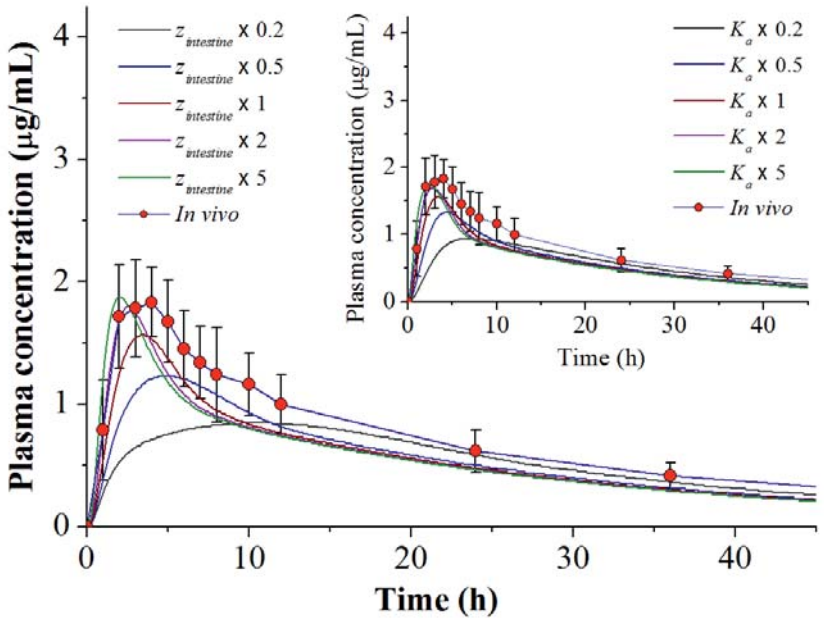

Fig. 5-10. Effect of dissolution rate in small intestine ($z_{intestine}$) on simulated plasma profiles of MDS capsule in fasted state. $z_{intestine}$ was varied from one-fifth to five times of the reference value. *In silico* data is given by solid lines, while *in vivo* mean data are depicted by symbols with error bars [insert map: effect of absorption rate (k_a value) on simulated plasma profiles of MDS capsule].

Interestingly, it was not necessary to consider digestion of the formulation in order to simulate the oral performance of these formulations. This is likely due to their composition: mostly surfactant with a comparatively modest fraction of medium chain glycerides. In addition, as reported by Griffin et al. (2014), no correlation could be found between the *in vitro* digestion and *in vivo* observed plasma profiles in pigs.

5.3 Fed state *IVISIV*C of LBF No.8 – No.11

In Section 5.2, the STELLA® based semi-PBPK model was successfully used to predict plasma profiles for LBF No.8 – No.11 in the fasted state. Although there was no fed state *in vivo* PK data, using the *in silico* model from Section 5.2 with modifications for the fed state and the *in vitro* dissolution in the fed state media, prediction of the *in vivo* human PK after a high fat breakfast was attempted.

5.3.1 Media preparation

To simulate conditions in the fed stomach and small intestine, FeSSGF and FeSSIF-V2 (fed state simulated gastric and intestinal fluids) were used in the *in vitro* dissolution of LBF No.8 – No.11. Table 5-7 summarizes their composition. The media were prepared as previously described (Galia et al., 1998; Jantratid et al., 2008; Vertzoni et al., 2005; Wagner et al., 2012).

Table 5-7

Standard composition of the fed state biorelevant media without further modification

	FeSSGF	FeSSIF-V2
Composition		
Sodium taurocholate (mM)	–	10
Lecithin (mM)	–	2
Ratio milk/buffer	1:1	–
Sodium chloride (mM)	237.0	125.5
Glycerol monooleate (mM)	–	5
Sodium oleate (mM)	–	0.8
Maleic acid (mM)	–	55.0
Sodium acetate (mM)	29.8	–
Acetic acid (mM)	17.1	–
Sodium hydroxide (mM)	–	81.7
Characteristic parameter		
pH	5.0	5.8
Osmolality (mOsm kg^{-1})	400 ± 10	390 ± 10
Buffer capacity (mmol L^{-1} ΔpH^{-1})	25 ± 2	25 ± 2

5.3.2 Solubility testing and results

The solubility samples of fenofibrate in the fed state media were collected from the corresponding dissolution experiments with 500mL media and a single dose of 50mg LBF No.8 – No.11 (Section 5.3.3). The paddles were kept rotating at 75rpm over one day, and the solubility samples were withdrawn at the 24h time point. The water bath remained at 37°C throughout the experiment. The *in vitro* testing was performed in triplicate (n = 3). The solubility samples were analyzed using the same HPLC sequence in which the samples of dissolution were analyzed.

This method for solubility determination is different from the method used for the "fasting" solubility experiment (Section 5.2.1.1). However, this should not impact the results, as in both cases, the LBFs of FFB were kept under mild agitation over a period of 24h.

Table 5-8

Solubility data of FFB (LBFs) in various fed state biorelevant media at 37 °C (n = 3)

Formulation	Media	Solubility (ug/mL)
E5(80) formulation (50mg dose)	FeSSGF (500mL)	99.61 ± 9.36
E5(80) formulation (50mg dose)	FeSSIF-V2 (500mL)	99.26 ± 8.59
E5(20) formulation (50mg dose)	FeSSGF (500mL)	88.08 ± 3.58
E5(20) formulation (50mg dose)	FeSSIF-V2 (500mL)	87.07 ± 2.82
MDS formulation (50mg dose)	FeSSGF (500mL)	41.00 ± 9.49
MDS formulation (50mg dose)	FeSSIF-V2 (500mL)	46.74 ± 2.60
Pure drug (50mg dose)	FeSSGF (500mL)	40.75 (n = 1)
Pure drug (50mg dose)	FeSSIF-V2 (500mL)	62.52 ± 1.81

Note: The upper limit of loaded FFB exposed to ca. 1:1000 dilutions of the lipid excipients with the fed state media is 100μg/mL (100% nominal). Thus, the solubility

data of E5(80) showed there was no solubility limitation at all. In the case of MDS however, less than 50% of FFB was found to be in solution after incubation over 24h.

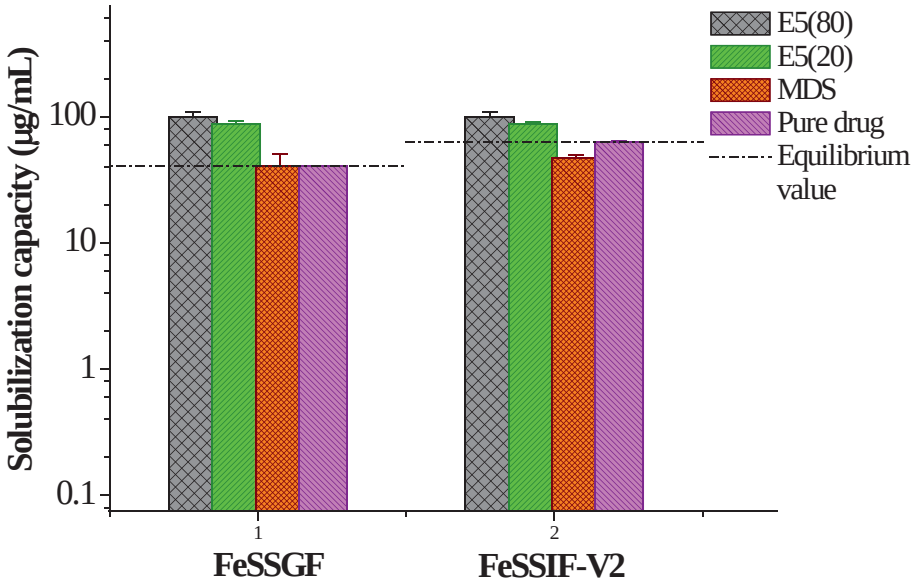

Fig. 5-11. Solubility data (n = 3) of fenofibrate with and without presence of diluted lipid-based excipients [E5(80), E5(20) and MDS] in FeSSGF and FeSSIF-V2.

Table 5-8 shows the solubility measured in fed state media, which is graphically illustrated in Fig. 5-11 as well. For a single oral dose (50mg API strength) in 500mL of fed state media, almost the full dose can be solubilized in the presence of lipid based excipients E5(80) and E5(20).

Comparing the solubility values in Table 5-8 with that displayed in Section 5.2.1.2, the most significant difference between fasted and fed state lies in the pure drug's solubility: it is less than 5µg/mL for the fasted state, and is ca. 50µg/mL for the fed state. Without incorporation into an LBF, solubilization of FFB by the fed state media outweighs that by the fasted state media.

5.3.3 Dissolution testing and results

Previously, it was described that dissolution tests in FeSSGF were difficult to perform owing to filtration problems. In order to circumvent this shortcoming, Fed State Simulated Gastric Emulsion (FeSSGEm) was developed (Kilic et al., 2010). Instead of milk buffer that was used in FeSSGF, Lipofundin® MCT 20 buffer was

incorporated for preparation of FeSSGEm. As Lipofundin® nano-emulsion contains mainly oils and triglycerides without large size proteins, FeSSGEm can be filtered through using 0.45µm filter without significant resistance. Therefore, FeSSGEm seems to be a promising variant, since undissolved drug particles of critical size can be easily excluded from the filtrate. However, as is shown in Table 4-6, FeSSGEm might have overestimated (1454µg/mL) solubility of FFB in the fed stomach, which was found to be 219µg/mL when FeSSGF was used. As milk reflects real composition of the food better than the injectable nano-emulsion (Lipofundin® MCT 20), only FeSSGF results were considered for the simulation work.

An updated preparation procedure of FeSSGF was applied in order to obtain a homogenous medium solution. The key step modified is pH adjustment: Direct addition of concentrated HCl into the buffer/milk mixture should be prevented, as strong acid can lead to phase separation and flocculation/agglomeration/precipitation of milk proteins, which can result in blocked filter pores. However, since the pH of milk is 7, in order to maintain the final pH of FeSSGF mixture (1:1) as 5, the initial pH of blank buffer must be somewhat lower than 5. In other words, the blank buffer must be adjusted with additional 30mM H^+ before mixing with milk. When this is done, filtration is no longer a problem when using the 2.7µm filters (GF/D wGMF).

The dissolution tests were performed in 500mL medium using USP II paddle apparatus at 37°C and 75rpm. Sampling volume was 5mL. Owing to the size of milk proteins in the FeSSGF medium, normal filters could not be used. Rather, 2.7µm filters (GF/D wGMF Whatman) were used for samples containing FeSSGF. For the FeSSIF-V2 medium, normal filters (0.45µm PTFE) were used. Sample volumes were replaced in the dissolution vessels. The filtered samples were immediately diluted 1:4 with acetonitrile. The diluted samples were vortexed and centrifuged at 14000rpm over 5min on an Eppendorf centrifuge device. The supernatants from the precipitates were injected for HPLC analysis. The HPLC condition was same as that used in the fasted state experiments (see Section 4.2.3).

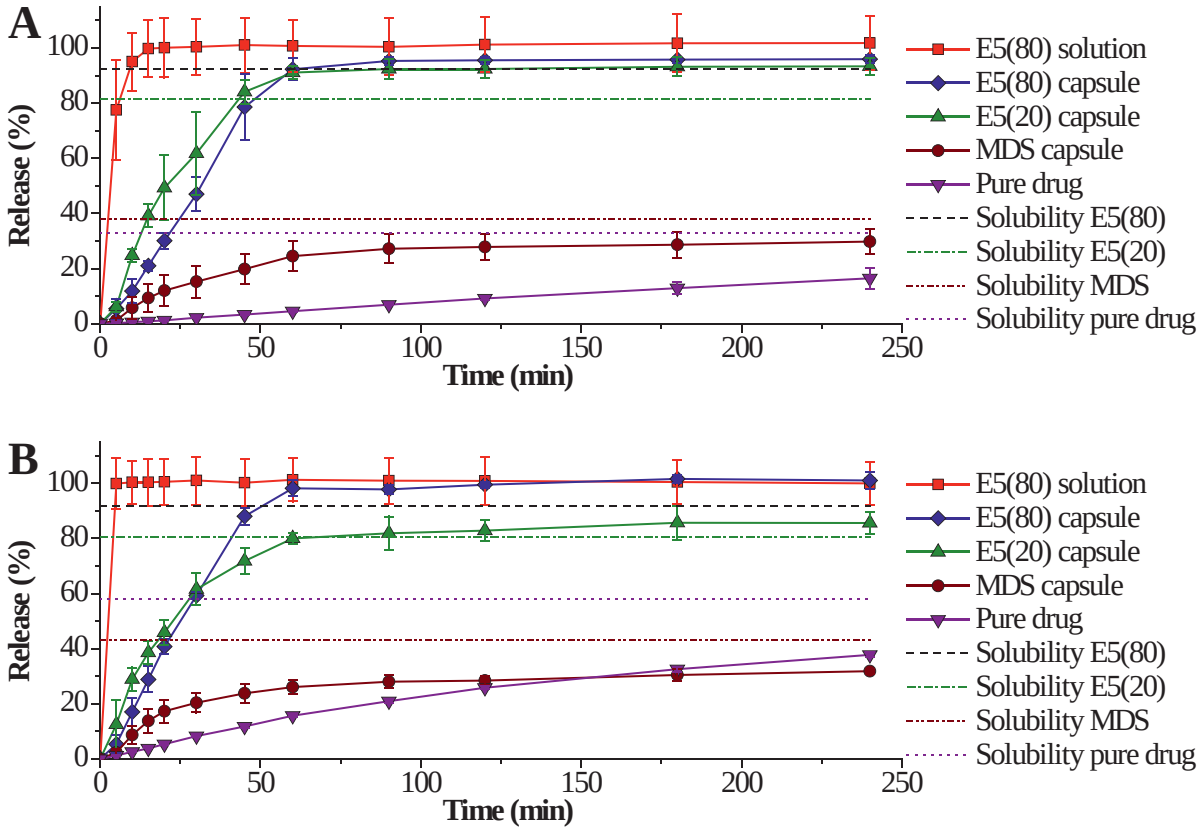

Fig. 5-12. Dissolution profiles (n = 3) of four fenofibrate lipid formulations: E5(80) solution, E5(80) capsule, E5(20) capsule and MDS capsule of 50mg dose in 500mL of FeSSGF (A) and in 500mL of FeSSIF-V2 (B). The horizontal lines depict the mean equilibrium solubility (n = 3) of fenofibrate in the diluted E5(80), E5(20) and MDS formulations in each respective media.

Fig. 5-12 shows the dissolution profiles of LBF No.8 – No.11 in the fed state biorelevant media. Overall, the dissolution behaviour in FeSSGF is similar to FeSSIF-V2: the E5(80) solution dissolved fastest, followed by E5(80) and E5(20) capsules, while the pure drug substance dissolved the slowest. Compared to the profiles in the fasted state media (Fig. 5-2), a major difference is the increased dissolution rate of unformulated drug, which is in accordance with the solubility result (see detailed discussion in Section 5.3.2). With regard to the ascending part of the dissolution curves, the E5(80) solution, E5(80) capsule and E5(20) capsule exhibited similar slopes for both fasting and fed state. For the E5(20) capsule in the fed state media, however, unlike the situation observed in the fasted state media (Fig. 5-2), no

evidence of precipitation was observed. This is most likely due to the media solubilization effect in the fed state. For the MDS capsule formulation, the fed state media also enhanced the dissolution somewhat compared to the fasted state.

5.3.4 *z* value estimation

The initial dissolution rate (*z* value) of the fed state was calculated from the initial data points (up to 60min) of the *in vitro* dissolution curves (Fig. 5-12), according to the Noyes-Whitney theory, and the values are summarized in Table 5-9.

Table 5-9

Summary of *z* values of fenofibrate LBFs in fed state biorelevant media.

	z/V-Value[a] ($mg^{-2/3}$ h^{-1})	
Formulation	FeSSGF	FeSSIF-V2
E5(80)solution	4.0921 ± 2.3193	2.5222 ± 0.1727
E5(80)capsule	0.2107 ± 0.0848	0.2307 ± 0.0142
E5(20)capsule	0.3445 ± 0.1964	0.3214 ± 0.1064
MDS capsule	0.0857 ± 0.0209	0.1094 ± 0.0296
Pure drug	0.0103 ± 0.0006	0.0234 ± 0.0005

[a] Value corrected for *in vivo* dose (54mg), and calculated from the *in vitro* dissolution data (n = 3).

The derived *z* value for the E5(80) solution was greater than that of the capsule formulations. As expected, the *z* values for the LBFs were greater than that of the pure drug substance.

5.3.5 Updated model parameters to predict the fed state plasma profiles

The model map (skeleton of compartments and flows) used in the fed state simulations is same as the set-up for the fasting state. Moreover, post-absorptive parameters (k_{12}, k_{21}, k_{10} and V/F) remained the same as that applied for the fasted state

simulations (see Table 5-4). However, the flow rate of certain arrows and initial value of the compartment representing the administered total volume were adapted to the fed state. In addition to previously defined common model assumptions (Section 5.2.3.1), specific assumptions for the fed state modeling included: (a) Drug, formulation, liquid and food emptying from the stomach occurs simultaneously; (b) A high-fat breakfast containing 1000kcal energy was served to subjects before dosing (Shono et al., 2009); (c) Calorie based zero-order gastric emptying rate was set at 4kcal/min for the fed state (Shono et al., 2009); (d) Volume was set at 740mL for the fed state, as the total volume of co-administered water (240mL) (Fei et al., 2013c) and food content (ca. 500mL) should be taken into account; (e) Applying above assumptions, the calculated coefficient of zero-order gastric emptying is 177.6mL h^{-1}.

5.3.6 Prediction of the fed state plasma profiles of fenofibric acid using STELLA® software

Using the modified fed-state STELLA® model, the fed-state plasma profiles can be predicted. As no fed-state *in vivo* data was available, Fig. 5-13A gives an overlay of the simulated fed state profiles, together with the observed/simulated fasted state fenofibric acid plasma concentrations for the E5(80) solution at a dose strength of 54mg. In Fig. 5-13A, T_{max} (4.7h) of the simulated fed state plasma profile of E5(80) solution is 2-3h delayed in comparison with the mean observed/simulated fasted state data (T_{max} = 1.9h, see Table 5-10), owing to the slower, zero-order gastric emptying observed in the fed state (where gastric emptying time is prolonged to approximately 4h). However, C_{max} and AUC of the simulated plasma profiles remained similar for both prandial states, indicating that fenofibrate could be completely absorbed from the E5(80) solution in both the fasted and fed states.

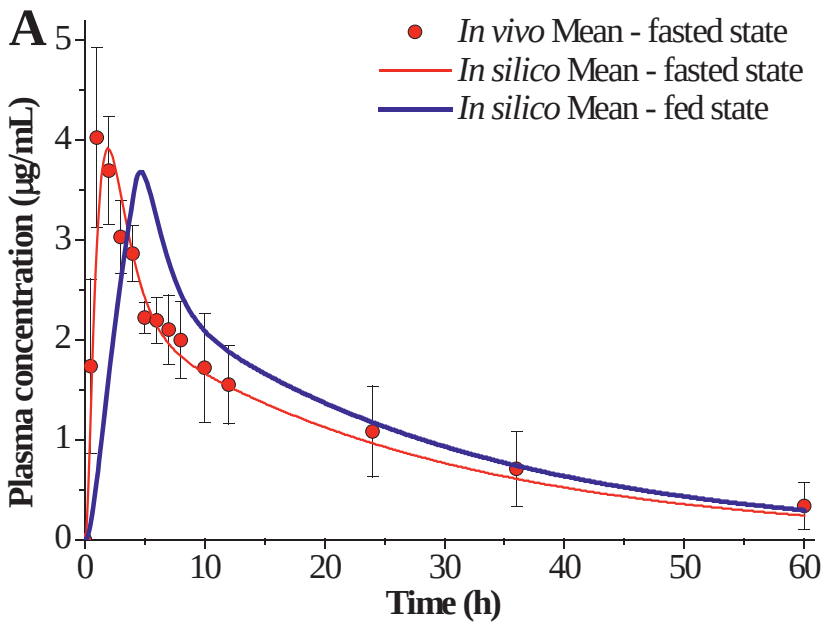

Fig. 5-13A. Simulated fed state mean and observed/simulated fasted state fenofibric acid mean plasma concentration profiles for the E5(80) solution at a dose strength of 54mg. *In silico* mean data is shown with solid lines, while *in vivo* mean data is shown by symbols with error bars.

In Fig. 5-13B, the modeling outcome of E5(80) capsule is shown. Except for respective *z* value of fasted/fed state (see numbers in Table 5-2 and Table 5-9), other model parameter settings remained the same as that used for the E5(80) solution. As indicated in Fig. 5-13B, T_{max} (4.65h) of simulated fed state plasma profile of the E5(80) capsule is also prolonged in comparison with the fasted state (T_{max} = 2.35h, see Table 5-10), probably for the same reason as the oral solution. Comparing the overlaid plasma profiles with E5(80) solution, the E5(80) capsule showed decreased absorption of fenofibrate (see Table 5-10 for AUC values).

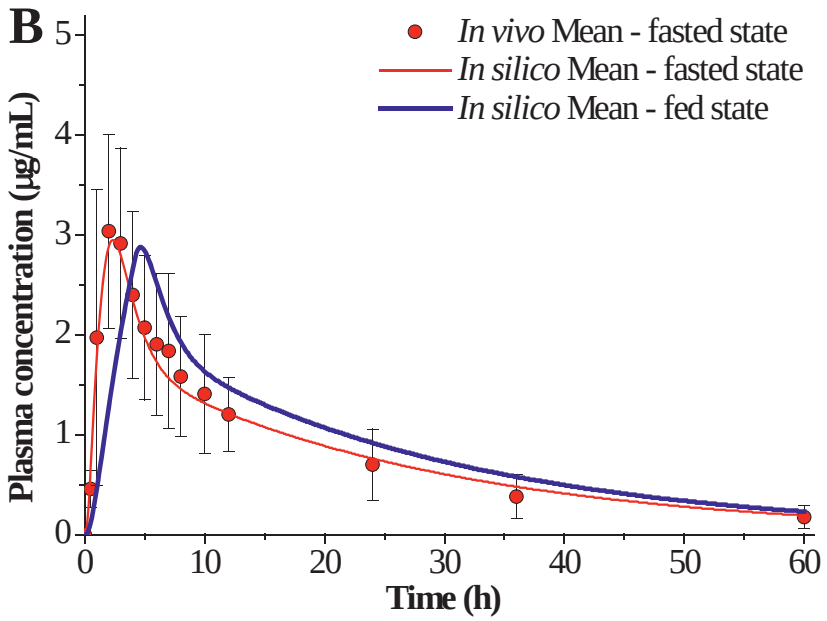

Fig. 5-13B. Simulated fed state mean and observed/simulated fasted state fenofibric acid mean plasma concentration profiles for the E5(80) capsule at a dose strength of 54mg. *In silico* mean data is shown with solid lines, while *in vivo* mean data is shown by symbols with error bars.

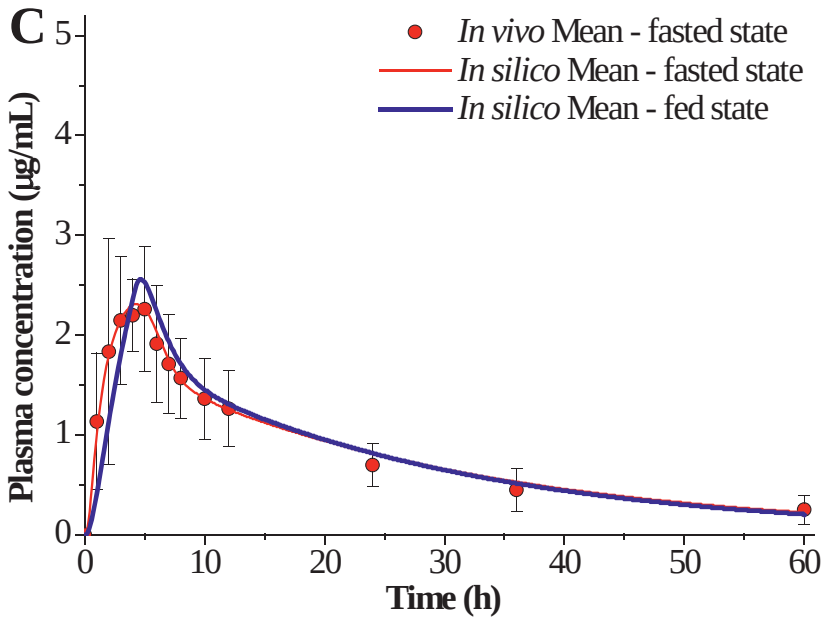

Fig. 5-13C. Simulated fed state mean and observed/simulated fasted state fenofibric acid mean plasma concentration profiles for the E5(20) capsule at a dose strength of 54mg. *In silico* mean data is shown with solid lines, while *in vivo* mean data is shown by symbols with error bars.

Fig. 5-13C shows the simulated result of E5(20) capsule. Different from previous cases, elements considering precipitation and re-dissolution processes were incorporated to the fasted state modeling, but not for the fed state. This setting aimed to mimic previous finding of respective *in vitro* dissolutions (see Fig. 5-2 and Fig. 5-12).

As given in Fig. 5-13C, for the E5(20) capsule formulation, the simulated fed state plasma profile is very similar to that of the fasted state. This is confirmed by the PK parameters in Table 5-10, as minimal differences among respective C_{max}, T_{max} and AUC values can be found between fasted and fed. Since precipitation and redissolution took place in the fasted state, there was some delay in absorption of E5(20) in fasting condition, which could explain the similarity in the profiles.

Fig. 5-13D shows the outcome of MDS capsule, from which a similar trend of food effect can be found: AUC remained similar while T_{max} was delayed by ca. 2h (see values in Table 5-10).

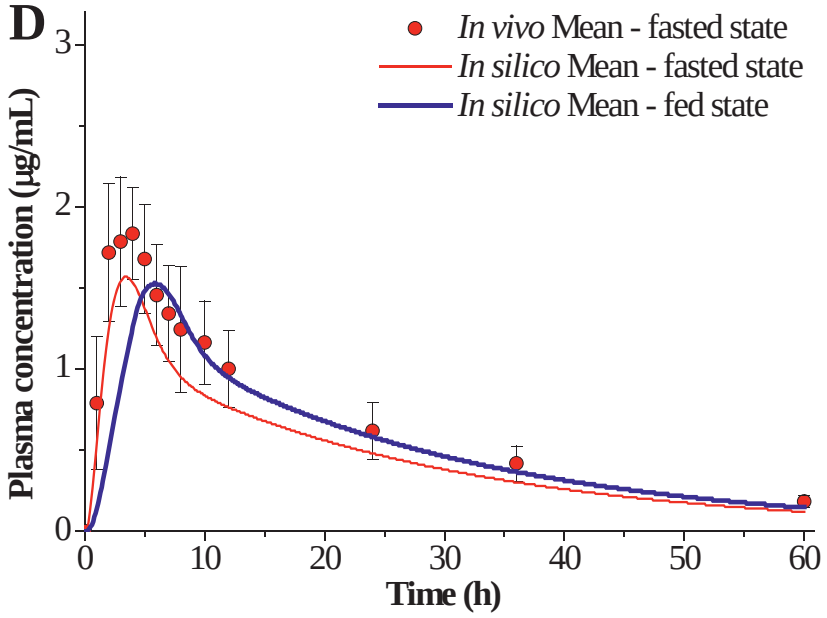

Fig. 5-13D. Simulated fed state mean and observed/simulated fasted state fenofibric acid mean plasma concentration profiles for the MDS capsule at a dose strength of 54mg. *In silico* mean data is shown with solid lines, while *in vivo* mean data is shown by symbols with error bars.

An overview of the simulated fed state and observed fasted state plasma fenofibric acid concentration for each of the lipid formulations (3 SMEDDSs and 1 MDS) is shown in Fig. 5-14, with the highest simulated plasma levels for the E5(80) solution and the lowest for the MDS capsule. As can be seen, all the LBFs in fed state showed similarly delayed T_{max}. Also, C_{max} of most LBFs in fed state was lower than that from fasted state (detailed evidence see Table 5-5 and Table 5-10). In this case, rate-limiting step for absorption in the fed state is probably gastric emptying, which was set at 4kcal/min. This zero-order input rate also explains the straight ascending parts of the simulated plasma curves in the fed state.

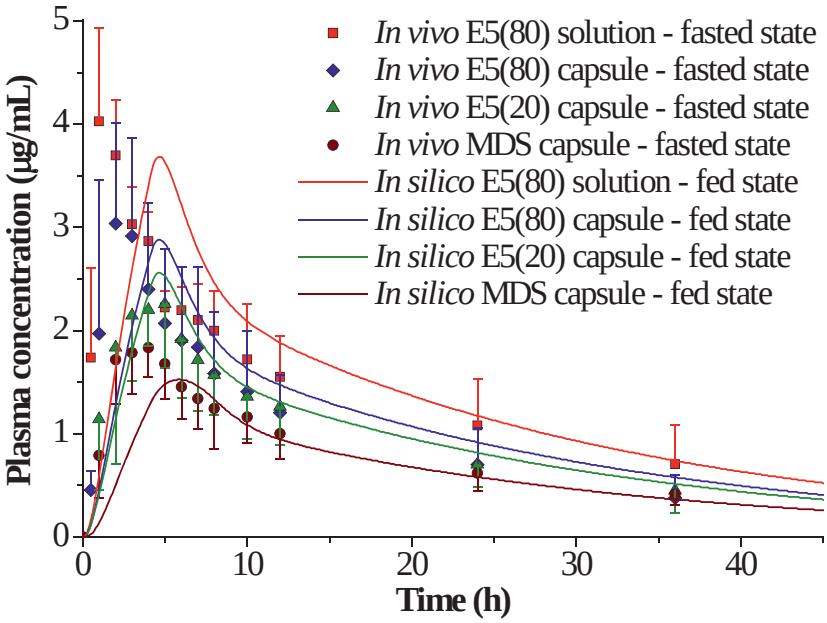

Fig. 5-14. Simulated fed state and observed fasted state plasma fenofibric acid concentration profiles for the lipid formulations (three SMEDDS and one MDS, n = 4). *In silico* data is shown by solid lines, and *in vivo* mean data are depicted by symbols with error bars.

The PK parameters obtained from the plasma profile modeling are given in Table 5-10, in which the $AUC_{0\text{-}inf}$ was calculated using WinNonlin® software.

Table 5-10

Comparison of fed and fasted state *in silico* pharmacokinetic parameters of different fenofibrate lipid formulations at 54mg dose strength.

Pharmacokinetic parameters		E5(80) solution	E5(80) capsule	E5(20) capsule	MDS capsule
$AUC_{0\text{-}inf}$ ($\mu g\ mL^{-1}\ h$)	*In silico* fed	77.74	60.90	54.19	37.67
	In silico fasted	70.51	53.66	56.75	33.31
	Ratio[a]	1.10	1.13	0.95	1.13
C_{max} ($\mu g\ mL^{-1}$)	*In silico* fed	3.68	2.88	2.56	1.53
	In silico fasted	3.92	2.95	2.31	1.57
	Ratio[a]	0.94	0.98	1.11	0.97
T_{max} (h)	*In silico* fed	4.70	4.65	4.65	5.85
	In silico fasted	1.90	2.35	4.25	3.40
	Ratio[a]	2.47	1.98	1.09	1.72

[a] Ratio: PK parameter (*in silico* fed) / PK parameter (*in silico* fasted).

5.3.7 Sensitivity analysis: varying model parameters for response of fenofibric acid plasma profile in the fed state

The fed state sensitivity analyses were conducted on $z_{stomach}$, $z_{intestine}$, $C_{s,stomach}$, $C_{s,intestine}$, k_a and k_{GE}. A result overview of the analysis is summarized as Table 5-10. Detailed simulation outcome of the plasma concentration profiles are shown in appendix (Fig. A-21, Fig. A-22, Fig. A-23 and Fig. A-24).

Table 5-11

Summary of the fed state sensitivity analysis for the variable parameters used in the STELLA® model.

Parameter	Range of value tested [a]	Impact of a change in the listed parameters [b]			
		E5(80) solution	E5(80) capsule	E5(20) capsule	MDS capsule
Dissolution rate in stomach	0.2-5	Negligible	Negligible	Negligible	Negligible
Dissolution rate in small intestine	0.2-5	Negligible	Negligible	Negligible	Significant
Solubility in gastric fluid	0.5-2	Negligible	Negligible	Negligible	Negligible
Solubility in intestinal fluid	0.5-2	Negligible	Negligible	Negligible	Moderate
Absorption rate	0.2-5	Significant	Significant	Significant	Significant
Gastric emptying rate	0.5-3	Significant	Significant	Significant	Moderate

[a] Factor applied to the reference input value used in the simulations.

[b] The impact of a change in the listed parameter was defined according to the index of C_{max} ratio between the simulated and the reference profiles as follows: Negligible: within 0.9-1.1, Marginal: within 0.8-1.2, Moderate: within 0.7-1.3, Significant: outside 0.7-1.3.

Based on sensitivity analyse using the STELLA® model, the fed state plasma profiles of LBF No.8 – No.11 are not governed by GI dissolution processes, nor driven by the solubility sink which is induced from LBFs and diluted GI-fluids (see Table 5-10). However, plasma profiles of LBF No.8 – No.11 can be strongly influenced by intestinal permeability (similar to the fasted state), as well as the gastric emptying rate (different than in the fasted state). It is assumed in the fed state, the

calorie-based zero-order gastric emptying is relatively slow, so that the gastric emptying rate is an important determinant of absorption.

5.3.8 Discussion of food effect and comparison of results in fasted and fed state

Through comparison of the fasted and fed state PK profiles, clear evidence can be seen in terms of food effect on the studied LBFs of fenofibrate: 1) No significant reduction of C_{max}, nor significant difference in AUC were identified, indicating the lipid formulation approach is able to minimize the observed positive food effect of fenofibrate; 2) The major difference in terms of T_{max} between the fasted and fed state originated from the different gastric emptying rates; 3) The permeation step can be rate-limiting for both fasted and fed state, while the importance of the dissolution step depends on the formulation; 4) Although an *in vivo* fed state evaluation was not carried out, using the fed state *in silico* model together with *in vitro* dissolution outcome in fed state media, it was possible to predict the human plasma concentrations after a meal.

Chapter 6. Summary and outlook

6.1 Summary

One of the common themes of the present thesis was to describe various analytical approaches to evaluating improvement of the oral bioavailability of fenofibrate. These included *in vitro* biorelevant solubility, dispersion, and dissolution/precipitation tests on a variety of lipid-based formulations. Subsequently, ordinary differential equation based PBPK models were used to simulate human plasma profiles following administration of the FFB formulations. The established *in vitro-in silico-in vivo* relationship is valid provided the *in silico* predictions are in line with the *in vivo* observations. A mechanistic understanding of the rate-limiting steps involved can then be attained by applying parameter sensitivity analysis.

Lipid-based formulations have established a significant role in the formulation of fenofibrate for oral administration. Chapter 4 describes LBF No.1 – No.7 of FFB, which belong to the Type IIIA and Type IIIB lipid formulations. LBF No.1 – No.4 form a subgroup with a drug load ratio of 4-6%. As a case example, LBF No.2 was chosen for a series of dilution experiments. The dilution ratio ranged from 1:2 to 1:200, and the samples were analyzed macroscopically and microscopically. Although some precipitation was observed in a series of fasted state media with low dilution ratios, no precipitation was found in FeSSGF. LBF No.5 – No.7 formed another subgroup with a drug load ratio of 7.4%. Dilution testing was performed in a similar manner for these three formulations. No significant difference was found regarding their extent of precipitation. This outcome is consistent with respective *in vivo* data obtained in pigs (Griffin et al., 2014).

The solubility of fenofibrate pure drug was measured in buffer solutions with and without bile salts. Thus, the solubilization effect of the micelle components was elucidated. The outcome suggests minimal enhancement of FFB solubility under the fasted state conditions. Similarly, solubility testing of FFB was performed in various biorelevant media under the addition of lipid excipients. This was to check the

potential contribution of LBF on overall solubilization of FFB when ingested with a glass of co-administered water. It was found that solubility of FFB in the presence of some LBF was greatly increased. Moreover, comparing the two prandial states, the fed media demonstrated much better solubilization capability than the fasted state media.

Dispersion testing on FFB lipid formulations is best achieved using the USP 3 apparatus because the GI motility *in vivo* can be better simulated. As a representative formulation, LBF No.2 was chosen for a series of dispersion experiments. It was assumed that unfiltered samples contain some finely dispersed API particles that are not yet dissolved. Comparison of results between filtered and unfiltered samples indicated that finely dispersed, undissolved particles accounted for only 0–20% of the API. With respect to fasted vs. fed state, the lipid formulation studied (LBF No.2) showed some precipitation after 30min in the fasted state media, but none in FeSSGF.

In order to compare the agitation modes in various dissolution apparatus, dissolution testing of LBF No.1 – No.4 of FFB was performed using USP 2. Regardless of compendial or biorelevant media, most of these lipid formulations led to dissolution of a majority of the loaded drug, in contrast to the unformulated fenofibrate, which barely dissolved in fasted state media. Further, the transfer model experiments on the lipid formulations of FFB suggested that intestinal precipitation after gastric dissolution is unlikely.

Dissolution theories based on Weibull function as well as Noyes-Whitney equation were elaborated in detail in Chapter 4. Both *in vitro* fitting tools aim to provide essential input parameters for the STELLA® model. The simplicity of Weibull function makes it easy to understand, while the Noyes-Whitney theory is somewhat more complicated. Mathematical transformation enabled a straightforward Excel toolkit to be applied for the calculation of z-value from *in vitro* dissolution profiles. As a case example, dissolution parameters of LBF No.4 were incorporated in STELLA® to predict the plasma profile following dosing of the formulation in humans. Such *in silico* models pave the way to optimizing the performance of oral lipid-based formulations via an *in vitro-in silico-in vivo* approach.

In parallel with the STELLA® model, a whole-body PBPK approach is available as the Simcyp® software. As long as the required pharmacokinetic parameters are defined, plasma fenofibric acid concentration following oral administration of LBF can be predicted. Moreover, the Simcyp® human population based simulator allows a series of virtual trial experiments to be performed *in silico* to determine the PK variability in different population groups. In addition, the software allows an overview of regional distribution of dose fraction absorbed along the GI tract. To test these features, LBF No.4 was modeled as an oral solution. The simulation outcome from Simcyp® was found to be consistent with that obtained from the STELLA® software.

In Chapter 5, three SMEDDS and one suspension of micronized fenofibrate in lipid excipients were studied (LBF No.8 – No.11). The *in vitro* solubility and dissolution studies were carried out at first in fasted state biorelevant media using the USP 2 apparatus. While unformulated drug exhibited poor solubility (0.22µg/mL in FaSSGF and 4.31µg/mL in FaSSIF-V2) and dissolved less than 2% in dissolution tests, the solubility of fenofibrate in the presence of the lipid excipients increased dramatically (e.g. to 65.44µg/mL in the presence of the Myritol 318 / TPGS / Tween 80 SMEDDS). In addition, there was an attendant increase in dissolution (over 80% from capsules containing the Myritol 318 / TPGS / Tween 80 SMEDDS, and about 20% from the dispersion of fenofibrate in lipid excipients). These results were followed up by *in silico* simulations using STELLA® software, in which the precipitation and re-dissolution of fenofibrate was also taken into account.

In vitro Caco-2 permeation data was used to estimate intestinal permeability and the overall uptake rate through mucosa. The plausibility of the calculation was confirmed by comparing the k_a value derived from deconvolution of *in vivo* PK profile. Thus, the permeation parameter chosen for the STELLA® model appears to be justified.

Combining *in vitro* data in biorelevant media with the PBPK model, human plasma fenofibric acid concentration profiles were accurately predicted for the oral solution and two capsule dosage forms, while the fourth formulation was generally

well predicted (considering that it was not possible to completely reproduce the particle size distribution of the suspension that had been administered in the pharmacokinetic study). The point estimates of C_{max} and AUC ratio calculated from the *in silico* and *in vivo* plasma profiles fell within the 0.8-1.25 range for the SMEDDS solution and capsule formulations, confirming accurate simulation of the *in vivo* profiles. This similarity was supported by calculation of the respective f_2 factors.

Detailed sensitivity analysis in fasted state provided evidence that the absorption of fenofibrate from the lipid-based formulations was highly dependent on the ability of the excipients to enhance fenofibrate solubility and dissolution from the formulation under intestinal conditions, and on the permeation rate of fenofibrate in the small intestine. By contrast, the fasted state plasma profile seems to be dependent neither upon the dissolution performance in the stomach nor on the gastric emptying rate. Furthermore, the modeling revealed that the SMEDDS formulations had virtually removed any dependency of absorption on the dissolution rate in the small intestine, whereas for the dispersion in lipid excipients this barrier remained.

As was indicated from Griffin et al. (2014), for these Type IIIA-MC and Type IIIB-MC lipid-based dosage forms in fasted state, it was not necessary to consider digestion to predict their difference in *in vivo* performance.

Similarly, the fed state *IVISIV*C for LBF No.8 – No.11 was elaborated in Chapter 5.3. For the *in vitro* part, solubility and dissolution testing were performed in FeSSGF and FeSSIF-V2. As expected, there was some enhancement in solubility and percent dissolved, and there was no precipitation observed. The fed state STELLA® model has a total administered volume of 740mL and a constant gastric emptying rate of 177.6mL h^{-1}. Compared to fasted state, the respective fed state plasma profile showed somewhat delayed T_{max}, but their AUC and C_{max} values remained essentially similar. This indicates the lipid formulations are able to virtually eliminate the positive food effect of FFB. As suggested from the fed state sensitivity analysis, in addition to permeability, the gastric emptying rate plays an important role to the simulation

outcome. On the other hand, the fed state dissolution rate seems to be not so important.

Based on these results, it appears that the *in vitro-in silico-in vivo* approach may provide a useful tool for identifying and comparing limitations to oral absorption for lipid-based formulations and for optimizing lipid formulation development of poorly soluble drugs.

6.2 Outlook

Regarding further work, it is likely that more predictive *in silico* tools will be developed. These can be uesd to guide optimization of *in vitro* experiments. Using a mechanistic approach, clinically relevant dissolution methods should be much easier to establish, and corresponding specification limits should be much easier to identify. From both an industrial and a scientific perspective, a verified, discriminative *in vitro* target is much more valuable than a single quality control indicator of the formulation. As long as human physiology and the involved ADME processes can be well reflected in the *in silico* model, the critical material attribute, critical process parameter, and critical quality attribute of a certain drug product can be easily indentified and quantified. On the other hand, in cases where the dissolution process is not rate limiting to absorption, other potential effects such as the impact of excipients on GI motility or transporters could be addressed with a suitable PBPK model. This biopharmaceutical approach could be one of the driving forces for drug development in the future.

Chapter 7. Deutsche Zusammenfassung (German summary)

Gegenstand dieser Dissertation war das Ermitteln der Verbesserung der peroralen Bioverfügbarkeit Fenofibrat (FFB) durch lipid-basierte Formulierung (LBF). Eine weitere Aufgabe bestand darin, verschiedene analytische Methode zur Bewertung der Verbesserung der oralen Bioverfügbarkeit von Fenofibrat einzusetzen. Diese schlossen *in vitro* biorelevante Löslichkeits-, Dispersions-, Auflösungs- und Präzipitationstests ein. Auf Basis der analytischen Ergebnisse wurden dann PBPK-Modelle verwendet, um menschliche Plasmaprofile nach der Verabreichung der FFB-Formulierungen zu simulieren. Die daraus resultierende *in silico*-Vorhersagen stimmten mit den *in vivo*-Beobachtungen überein. Durch Anwendung der Parametersensitivitätsanalyse war es weiterhin möglich, ein mechanistisches Verständnis der beteiligten geschwindigkeitsbegrenzenden Schritte zu erreichen.

Die Löslichkeit von reinem Fenofibrat wurde zuerst in Pufferlösungen mit und ohne Gallenkomponenten gemessen. Somit wurde der Solubilisierungseffekt dieser Mizellenkomponenten unter Magen-Darm-Trakt-Bedingungen aufgeklärt. Das Ergebnis deutet auf eine minimale Erhöhung der FFB-Löslichkeit unter den Bedingungen des nüchternen Zustands hin. In ähnlicher Weise wurde das Testen der Löslichkeit von FFB in verschiedenen biorelevanten Medien unter Zugabe von Lipid-Exzipienten durchgeführt. Es wurde gezeigt, dass die Löslichkeit von FFB in Gegenwart von Lipidkomponenten stark erhöht war. Darüber hinaus Stellen die postprandialen Medien eine viel bessere Solubilisierungsfähigkeit als die Medien im nüchternen Zustand dar.

Formulierungen auf Lipidbasis können nach dem Pouton Klassifizierungssytem eingeteilt werden. Typ I Formulierung bestehen ausschließlich aus Öle während am anderen Ende der Skala die Typ IV Formulierung bestehen weitestgehend aus Tenside. Kapitel 4 beschreibt LBF Nr. 1 - Nr. 7 von FFB, die zu den Lipidformulierungen Typ IIIA und Typ IIIB gehören. LBF Nr. 1 bis Nr. 4 bilden eine Untergruppe mit einem Arzneistoffbeladungsverhältnis von 4 bis 6%. Als ein Fallbeispiel wurde LBF Nr. 2

für eine Reihe von Verdünnungsexperimenten ausgewählt. Das Verdünnungsverhältnis lag im Bereich von 1:2 bis 1:200 und die Proben wurden makroskopisch und mikroskopisch analysiert. Obwohl in einer Reihe von Medien im nüchternen Zustand mit geringen Verdünnungsverhältnissen etwas Niederschlag beobachtet wurde, wurde in FeSSGF kein Ausfall beobachtet. LBF Nr. 5 - Nr. 7 bildete eine weitere Untergruppe mit einem Wirkstoffbeladungsverhältnis von 7,4%. In ähnlicher Weise wurde für diese drei Formulierungen ein Verdünnungstest durchgeführt. Es wurde kein signifikanter Unterschied in Bezug auf ihre Niederschlagsmenge gefunden. Dieses Ergebnis stimmt mit den jeweiligen *in vivo*-Daten überein, die bei Schweinen erhalten wurden (Griffin et al., 2014).

Es wurde gezeigt, dass Dispersionstests an FFB-Lipidformulierungen am besten unter Verwendung der USP 3-Apparatur durchgeführt werden, da in diesem Apparat die GI-Motilität *in vivo* am besten reflektiert werden kann. Als eine repräsentative Formulierung wurde LBF Nr. 2 für eine Reihe von Dispersionsexperimenten ausgewählt. Es wurde angenommen, dass ungefilterte Proben einige fein dispergierte API-Partikel enthalten, die noch nicht gelöst sind. Ein Vergleich der Ergebnisse zwischen gefilterten und ungefilterten Proben zeigte, dass fein dispergierte, ungelöste Partikel nur 0-20% der API ausmachten. In Bezug auf den Fasten- gegenüber dem Fütterungszustand zeigte die untersuchte Lipidformulierung (LBF Nr. 2) eine gewisse Präzipitation nach 30 Minuten in den Medien im nüchternen Zustand, aber keine in FeSSGF.

Um die Hydrodynamik in verschiedenen Auflösungsapparaten zu vergleichen, wurde der Auflösungsversuch von LBF Nr. 1 - Nr. 4 von FFB auch unter Verwendung von USP 2 durchgeführt. Ungeachtet von kompendialen oder biorelevanten Medien führten die meisten dieser Lipidformulierungen zur Auflösung eines Großteils von das beladene Medikament, im Gegensatz zum unformulierten Fenofibrat, das sich in nüchternen Zustand Medien kaum auflöst. Weiter zeigten die Transfermodellexperimente an den Lipidformulierungen von FFB, dass eine intestinale Ausfällung nach einer Magenauflösung unwahrscheinlich ist.

Dissolutionstheorien, die auf der Weibull-Funktion und der Noyes-Whitney-Gleichung basieren, wurden in Kapitel 4 ausführlich beschrieben. Beide *in-vitro*-Fitting-Tools zielen darauf ab, essentielle Eingangsparameter für das *in silico* STELLA®-Modell bereitzustellen. Dabei ist die Beschreibung mit der Weibull-Funktion leichter als mit der Noyes-Whitney-Theorie. Jedoch eine mathematische Transformation der Noyes-Whitney-Gleichung ermöglichte die Verwendung eines einfachen Excel-Toolkits zur Berechnung des *z*-Werts aus *in-vitro*-Auflösungsprofilen. Als ein Fallbeispiel wurden Auflösungsparameter von LBF Nr. 4 in STELLA® verwendet, um das Plasmaprofil nach der Dosierung der Formulierung in Menschen vorherzusagen. Solche *in-silico*-Modelle ebnen den Weg zur Optimierung der Leistung oraler Formulierungen auf Lipidbasis über einen *in vitro-in-silico-in-vivo*-Ansatz.

Parallel zum STELLA®-Modell wurde ein ausführliches, physiologisch-basiertes pharmakokinetisches Modell, Simcyp®, als *in silico*-Modell eingesetzt. Anhand der erforderlichen post-absorptive Parameter kann mithilfe Simcyp® die Plasma-Arzneistoff-Konzentration nach oraler Verabreichung von verschiedenen Formulierungen vorhergesagt werden. Darüber hinaus ermöglicht der Simcyp®-Simulator eine Reihe von virtuellen Versuche die PK-Variabilität vom Wirkstoff in verschiedenen Bevölkerungsgruppen zu bestimmen. Auch einen Überblick über die regionale Verteilung der Dosisfraktion, die im Magen-Darm-Trakt absorbiert wird, ist möglich. Um diese Möglichkeiten am Beispiel Fenofibrat zu testen, wurde LBF Nr. 4 als orale Lösung modelliert. Das Simulationsergebnis von Simcyp® entsprach dem aus der STELLA®-Software.

In Kapitel 5 wurden drei SMEDDS und eine Suspension von mikronisiertem Fenofibrat in Lipid-Hilfsstoffen untersucht (LBF Nr. 8 - Nr. 11). Die *in-vitro*-Löslichkeits- und Auflösungsstudien wurden zunächst in biorelevanten Medien in nüchternem Zustand unter Verwendung der USP-2-Apparatur durchgeführt. Während das nicht formulierte Medikament eine schlechte Löslichkeit aufwies (0,22µg/mL in FaSSGF und 4,31µg/mL in FaSSIF-V2) und in

Auflösungsgeschwindigkeitstests weniger als 2% aufgelöst wurde, erhöhte sich die Löslichkeit von Fenofibrat in Gegenwart der Lipid-Exzipienten dramatisch (z.B. auf 65,44μg/mL in Gegenwart von Myritol 318 / TPGS / Tween 80 SMEDDS). Darüber hinaus gab es eine begleitende Zunahme der Auflösungsausmaß (über 80% von Kapseln, die Myritol 318 / TPGS / Tween 80 SMEDDS enthielten, und etwa 20% von der Dispersion von Fenofibrat in Lipid-Hilfsstoffen). *In-silico*-Simulationen mit STELLA®-Software berücksichtigte nicht nur die Löslichkeit und Auflösungsgeschwindigkeit sondern auch die Präzipitation und Wiederauflösung von Fenofibrat.

In-vitro-Caco-2-Permeationsdaten wurden verwendet, um die intestinale Permeabilität und die Gesamtaufnahmerate durch die Schleimhaut zu bestimmen. Die Plausibilität der Berechnung wurde bestätigt, indem die berechnete Permeabilität mit der k_a-Wert aus der Dekonvolution des *in vivo*-PK-Profils verglichen wurde. Somit scheint der für das STELLA®-Modell gewählte Permeationsparameter gerechtfertigt zu sein.

Unter Verwendung der *in-vitro*-Daten in biorelevanten Medien mit dem PBPK -Modell wurden für die orale Lösung und zwei LBF-Kapsel-Formulierung die Plasmafenofibrinsäure-Konzentrationsprofile genau vorhergesagt. Die Punktschätzwerte für C_{max} und AUC, berechnet aus den *In-silico* und *in vivo* Plasmaprofilen, lagen sogar im Bereich von 0,8-1,25 für die SMEDDS Lösung und Kapselformulierungen. Diese Übereinstimmung in *in vitro-in silico* mit *in vivo* wurde weiterhin durch Berechnung der jeweiligen f_2 Faktoren unterstützt.

Eine detaillierte Sensitivitätsanalyse im nüchternen Zustand ergab, dass die Resorption von Fenofibrat aus den LBF stark von der Fähigkeit der Hilfsstoffe zur Verbesserung der Löslichkeit und Auflösung von Fenofibrat aus der Formulierung unter intestinalen Bedingungen sowie von der Permeationsrate von Fenofibrat ist. Im Gegensatz dazu scheint das Plasmaprofil in nüchternem Zustand weder von der Auflösungsleistung im Magen noch von der Magenentleerungsrate abhängig zu sein. Darüber hinaus zeigte die Parametersensitivitätsanalyse, dass die

SMEDDS-Formulierungen praktisch jede Abhängigkeit der Absorption von der Auflösungsrate im Dünndarm entfernt hatten, während diese Barriere für die Dispersion in Lipid-Exzipienten bestehen blieb.

Wie von Griffin et al. (2014) bestätigt, spielt die Verdauung der Lipide im Magen-Darm-Trakt keine signifikante Rolle für die Bioverfügbarkeit. Offenbar für lipidbasierten Dosierungsformen vom Typ IIIA-MC und Typ IIIB-MC sind einfache Freigabetests adäquat für die Vorhersage der Pharmakokinetik nach peroraler Einnahme in nüchternem Zustand.

In ähnlicher Weise wurde die Verhältnisse *in vitro-in silico-in vivo* für LBF Nr. 8 - Nr. 11 in Kapitel 5.3 ausgearbeitet. Für den *in-vitro*-Teil wurden Löslichkeits- und Auflösungsgeschwindigkeitstests in FeSSGF und FeSSIF-V2 durchgeführt. Wie von den Löslicheitsdaten in den gleichen Medien erwartet, gab es eine gewisse Verbesserung der Löslichkeit und des Prozentsatzes gelöst, und es wurde keine Ausfällung beobachtet. Für das STELLA®-Modell im postprandialen Zustand wurde ein verabreichtes Gesamtvolumen von 740mL und eine konstante Magenentleerungsrate von 177,6mL h^{-1} verwendet. Im Vergleich zum nüchternen Zustand zeigte das jeweilige Plasmaprofil eine etwas verzögerte T_{max}, aber ihre AUC- und C_{max}-Werte blieben im Wesentlichen ähnlich. Dies zeigt, dass die Lipidformulierungen in der Lage sind, den unerwünschten Unterschied in der FFB Pharmakokinetik zwischen nüchternem und postprandialen Zustand praktisch zu eliminieren. Wie aus der Sensitivitätsanalyse des postprandialen Zustands hervorgeht, spielt neben der Permeabilität die Magenentleerungsrate eine wichtige Rolle für das Simulationsergebnis. Auf der anderen Seite scheint die Auflösungsrate weniger wichtig zu sein.

Basierend auf diesen Ergebnissen scheint es, dass der *In-vitro-In-Silico-In-vivo*-Ansatz ein nützliches Werkzeug zum Identifizieren und Vergleichen von Beschränkungen der oralen Absorption für Formulierungen auf Lipidbasis und zum Optimieren der Lipidformulierungsentwicklung von schlecht löslichen Arzneimitteln darstellt.

Appendix

Table A-1

Evaluation of LBF using water as the medium; Dilution 1:2 (m:m):

Time/Method	API + formulation	Blank formulation	Observations
10min Macroscopic observation			Formulation can mix well with water using gentle agitation at 37°C without showing turbid appearance in dilution ratio of 1:2.
10min Microscopic observation (40x)		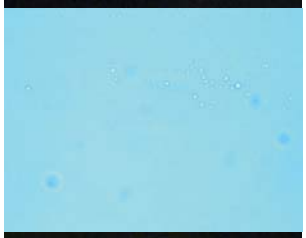	Very tiny amount of precipitates or lipid droplets were detected in 10min on bottom of the liquids.
30min Macroscopic observation			Formulation can mix well with water using gentle agitation at 37°C without showing turbid appearance in dilution ratio of 1:2.
30min Microscopic observation (40x)	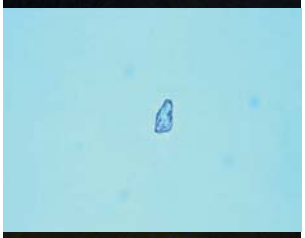	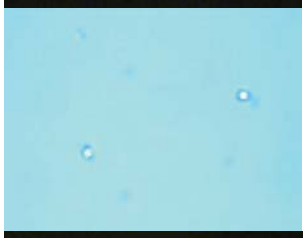	The precipitates or lipid droplets aggregated into larger particles on bottom of the vials.
120min Macroscopic observation			Formulation can mix well with water using gentle agitation at 37°C without showing turbid appearance in dilution ratio of 1:2.
120min Microscopic observation (40x)	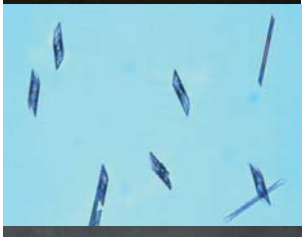		Crystals of API detected in the samples with fenofibrate, but not in the blank formulation.
24h Macroscopic observation			Some crystals can be detected on bottom of the vial in the sample with fenofibrate, but not in the blank formulation.

Table A-2

Evaluation of LBF using water as the medium; Dilution 1:5 (m:m):

Time/Method	API + formulation	Blank formulation	Observations
10min Macroscopic observation			Formulation can mix well with water using gentle agitation at 37°C without showing turbid appearance in dilution ratio of 1:5.
10min Microscopic observation (40x)	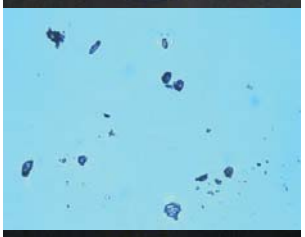	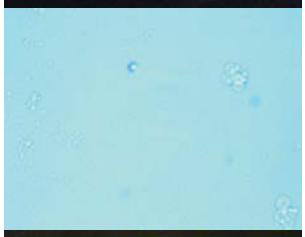	A number of precipitated particles or lipid droplets of medium size were detected. Reduced viscosity compared with 1:2 might accelerate emulsification.
30min Macroscopic observation			Formulation can mix well with water using gentle agitation at 37°C without showing turbid appearance in dilution ratio of 1:5.
30min Microscopic observation (40x)		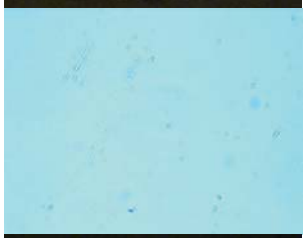	Some of the particles in 10min re-dissolved. Samples might reach maximum solubility, as the dispersion process was more complete.
120min Macroscopic observation			Formulation can mix well with water using gentle agitation at 37°C without showing turbid appearance in dilution ratio of 1:5.
120min Microscopic observation (40x)		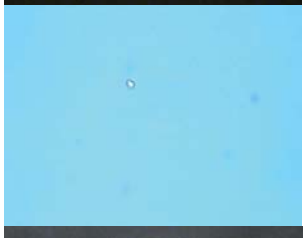	Crystals of API detected in the samples with fenofibrate, but not in the blank formulation.
24h Macroscopic observation			Some crystals can be detected on bottom of the vial in the sample with fenofibrate, but not in the blank formulation.

Table A-3

Evaluation of LBF using water as the medium; Dilution 1:200 (m:m):

Time/Method	API + formulation	Blank formulation	Observations
10min Macroscopic observation			Formulation can mix well with water using gentle agitation at 37°C without showing turbid appearance in dilution ratio of 1:200.
10min Microscopic observation (40x)	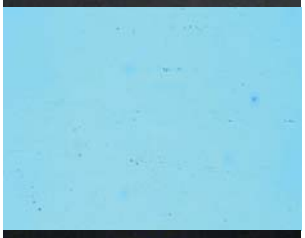		Larger lipid droplets settled on bottom of the vial.
30min Macroscopic observation			Formulation can mix well with water using gentle agitation at 37°C without showing turbid appearance in dilution ratio of 1:200.
30min Microscopic observation (40x)			Ultra fine particles disappeared. The liquids seem to be homogeneous form top to bottom.
120min Macroscopic observation			Formulation can mix well with water using gentle agitation at 37°C without showing turbid appearance in dilution ratio of 1:200.
120min Microscopic observation (40x)	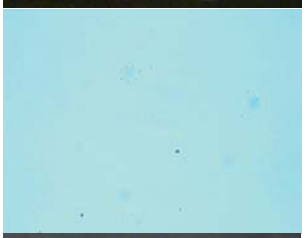	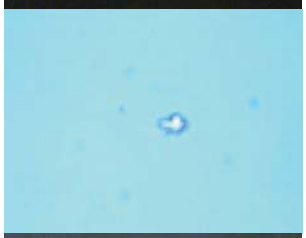	Some aggregation occurred at 120min.
24h Macroscopic observation			No apparent difference in appearance was observed at 24h.

Table A-4

Evaluation of LBF using 0.1N HCl as the medium; Dilution 1:2 (m:m):

Time/Method	API + formulation	Blank formulation	Observations
10min Macroscopic observation			Formulation can mix well with 0.1N HCl using gentle agitation at 37°C without showing turbid appearance in dilution ratio of 1:2.
10min Microscopic observation (40x)			There were a few larger particles on bottom of the liquids in 10min.
30min Macroscopic observation			Formulation can mix well with 0.1N HCl using gentle agitation at 37°C without showing turbid appearance in dilution ratio of 1:2.
30min Microscopic observation (40x)			Small amount of precipitates or lipid droplets were detected in 30min on bottom of the liquids.
120min Macroscopic observation			Formulation can mix well with 0.1N HCl using gentle agitation at 37°C without showing turbid appearance in dilution ratio of 1:2.
120min Microscopic observation (40x)		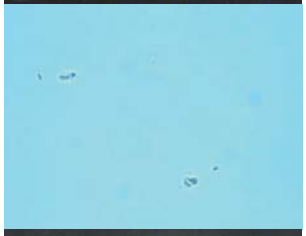	Large particles of API were detected in the samples with fenofibrate, but not in the blank formulation.
24h Macroscopic observation			Tiny amount of precipitates can be detected on bottom of the vial in the sample with fenofibrate, but not in the blank formulation.

Table A-5

Evaluation of LBF using 0.1N HCl as the medium; Dilution 1:5 (m:m):

Time/Method	API + formulation	Blank formulation	Observations
10min Macroscopic observation			Formulation can mix well with 0.1N HCl using gentle agitation at 37°C without showing turbid appearance in dilution ratio of 1:5.
10min Microscopic observation (40x)	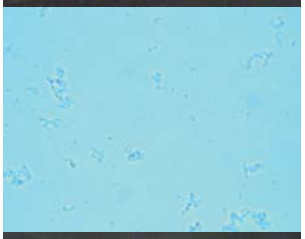		Large amount of irregular shaped lipid flocks were detected. Reduced viscosity compared with 1:2 might accelerate emulsification.
30min Macroscopic observation			Formulation can mix well with 0.1N HCl using gentle agitation at 37°C without showing turbid appearance in dilution ratio of 1:5.
30min Microscopic observation (40x)		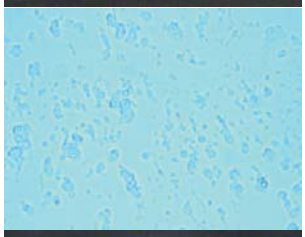	Large amount of irregular shaped lipid flocks were detected. Reduced viscosity compared with 1:2 might accelerate emulsification.
120min Macroscopic observation			Formulation can mix well with 0.1N HCl using gentle agitation at 37°C without showing turbid appearance in dilution ratio of 1:5.
120min Microscopic observation (40x)		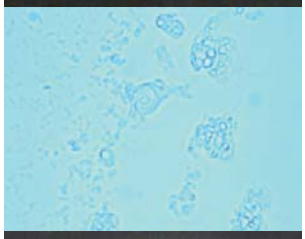	Large particles of API were detected in the samples with fenofibrate, but not in the blank formulation.
24h Macroscopic observation			Tiny amount of precipitates can be detected on bottom of the vial in the sample with fenofibrate, but not in the blank formulation.

Table A-6

Evaluation of LBF using 0.1N HCl as the medium; Dilution 1:200 (m:m):

Time/Method	API + formulation	Blank formulation	Observations
10min Macroscopic observation			Formulation can mix well with 0.1N HCl using gentle agitation at 37°C. Slight turbidity was found in dilution ratio of 1:200.
10min Microscopic observation (40x)			Tiny amount of precipitates or lipid droplets were detected in 10min on bottom of the vial.
30min Macroscopic observation			Formulation can mix well with 0.1N HCl using gentle agitation at 37°C. Slight turbidity was found in dilution ratio of 1:200.
30min Microscopic observation (40x)			Tiny amount of precipitates or lipid droplets were detected in 30min on bottom of the vial.
120min Macroscopic observation			Formulation can mix well with 0.1N HCl using gentle agitation at 37°C. Slight turbidity was found in dilution ratio of 1:200.
120min Microscopic observation (40x)			Small amount of precipitates or lipid droplets were detected in 120min on bottom of the vial.
24h Macroscopic observation			Formulation of 1:200 showed increased turbid appearance, indicating the formulation is not very stable in 1N HCl.

Table A-7

Evaluation of LBF using FaSSGF as the medium; Dilution 1:2 (m:m):

Time/Method	API + formulation	Blank formulation	Observations
10min Macroscopic observation			Formulation can mix well with FaSSGF using gentle agitation at 37°C without showing turbid appearance in dilution ratio of 1:2.
10min Microscopic observation (40x)	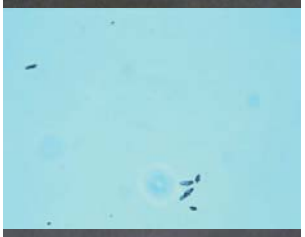	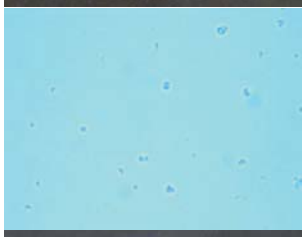	Small amount of precipitates or lipid droplets were detected in 10min on bottom of the vial.
30min Macroscopic observation			Formulation can mix well with FaSSGF using gentle agitation at 37°C without showing turbid appearance in dilution ratio of 1:2.
30min Microscopic observation (40x)			Small amount of precipitates or lipid droplets were detected in 30min on bottom of the vial.
120min Macroscopic observation			Formulation can mix well with FaSSGF using gentle agitation at 37°C without showing turbid appearance in dilution ratio of 1:2.
120min Microscopic observation (40x)	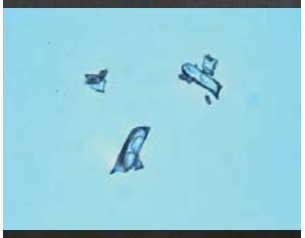		Large particles of API were detected in the samples with fenofibrate, but not in the blank formulation.
24h Macroscopic observation			Tiny amount of precipitates can be detected on bottom of the vial in the sample with fenofibrate, but not in the blank formulation.

Table A-8

Evaluation of LBF using FaSSGF as the medium; Dilution 1:5 (m:m):

Time/Method	API + formulation	Blank formulation	Observations
10min Macroscopic observation			Formulation can mix well with FaSSGF using gentle agitation at 37°C without showing turbid appearance in dilution ratio of 1:5.
10min Microscopic observation (40x)			Large amount of irregular lipid flocks were detected. Reduced viscosity might accelerate emulsification.
30min Macroscopic observation			Formulation can mix well with FaSSGF using gentle agitation at 37°C without showing turbid appearance in dilution ratio of 1:5.
30min Microscopic observation (40x)	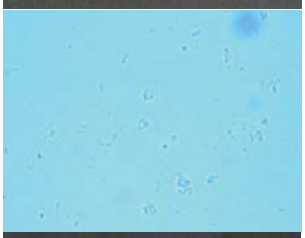		Some irregular lipid flocks were detected. Reduced viscosity might accelerate emulsification.
120min Macroscopic observation			Formulation can mix well with FaSSGF using gentle agitation at 37°C without showing turbid appearance in dilution ratio of 1:5.
120min Microscopic observation (40x)		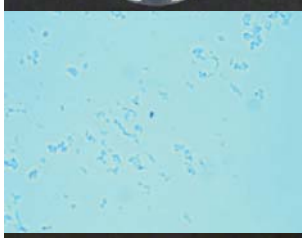	Large particles of API were detected in the samples with fenofibrate, but not in the blank formulation.
24h Macroscopic observation			Small amount of precipitates can be detected on bottom of the vial in the sample with fenofibrate, but not in the blank formulation.

Table A-9

Evaluation of LBF using FaSSGF as the medium; Dilution 1:200 (m:m):

Time/Method	API + formulation	Blank formulation	Observations
10min Macroscopic observation			Formulation can mix well with FaSSGF using gentle agitation at 37°C. Slight turbidity was found in dilution ratio of 1:200.
10min Microscopic observation (40x)			Small amount of precipitates or lipid droplets were detected in 10min on bottom of the vial.
30min Macroscopic observation			Formulation can mix well with FaSSGF using gentle agitation at 37°C. Slight turbidity was found in dilution ratio of 1:200.
30min Microscopic observation (40x)			Tiny amount of precipitates or lipid droplets were detected in 30min on bottom of the vial.
120min Macroscopic observation			Formulation can mix well with FaSSGF using gentle agitation at 37°C. Slight turbidity was found in dilution ratio of 1:200.
120min Microscopic observation (40x)			Small amount of precipitates or lipid droplets were detected in 120min on bottom of the vial.
24h Macroscopic observation			No apparent difference in appearance was observed at 24h.

Table A-10

Evaluation of LBF using FaSSIF as the medium; Dilution 1:2 (m:m):

Time/Method	API + formulation	Blank formulation	Observations
10min Macroscopic observation			Formulation can mix well with FaSSIF using gentle agitation at 37°C without showing turbid appearance in dilution ratio of 1:2.
10min Microscopic observation (40x)			Small amount of precipitates or lipid droplets were detected in 10min on bottom of the vial.
30min Macroscopic observation			Formulation can mix well with FaSSIF using gentle agitation at 37°C without showing turbid appearance in dilution ratio of 1:2.
30min Microscopic observation (40x)			Small amount of precipitates or lipid droplets were detected in 30min on bottom of the vial.
120min Macroscopic observation			Formulation can mix well with FaSSIF using gentle agitation at 37°C without showing turbid appearance in dilution ratio of 1:2.
120min Microscopic observation (40x)			Large particles of API were detected in the samples with fenofibrate, but not in the blank formulation.
24h Macroscopic observation			Tiny amount of precipitates can be detected on bottom of the vial in the sample with fenofibrate, but not in the blank formulation.

Table A-11

Evaluation of LBF using FaSSIF as the medium; Dilution 1:5 (m:m):

Time/Method	API + formulation	Blank formulation	Observations
10min Macroscopic observation			Formulation can mix well with FaSSIF using gentle agitation at 37°C without showing turbid appearance in dilution ratio of 1:5.
10min Microscopic observation (40x)			Small amount of precipitates or lipid droplets were detected in 10min on bottom of the vial.
30min Macroscopic observation			Formulation can mix well with FaSSIF using gentle agitation at 37°C without showing turbid appearance in dilution ratio of 1:5.
30min Microscopic observation (40x)		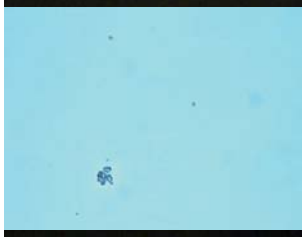	Small amount of precipitates or lipid droplets were detected in 30min on bottom of the vial.
120min Macroscopic observation			Formulation can mix well with FaSSIF using gentle agitation at 37°C without showing turbid appearance in dilution ratio of 1:5.
120min Microscopic observation (40x)			Large particles of API were detected in the samples with fenofibrate, but not in the blank formulation.
24h Macroscopic observation			Compared with1:2, more precipitation was detected on bottom of the vial in the sample with fenofibrate, but not in the blank formulation.

Table A-12

Evaluation of LBF using FaSSIF as the medium; Dilution 1:200 (m:m):

Time/Method	API + formulation	Blank formulation	Observations
10min Macroscopic observation			Formulation can mix well with FaSSIF using gentle agitation at 37°C without showing turbid appearance in dilution ratio of 1:200.
10min Microscopic observation (40x)			Several small particles were detected in 10min on bottom of the vial, but re-dissolved thereafter.
30min Macroscopic observation			Formulation can mix well with FaSSIF using gentle agitation at 37°C without showing turbid appearance in dilution ratio of 1:200.
30min Microscopic observation (40x)			Tiny amount of precipitates or lipid droplets were detected in 30min on bottom of the vial.
120min Macroscopic observation			Formulation can mix well with FaSSIF using gentle agitation at 37°C without showing turbid appearance in dilution ratio of 1:200.
120min Microscopic observation (40x)			Tiny amount of precipitates or lipid droplets were detected in 120min on bottom of the vial.
24h Macroscopic observation			Owing to precipitation of the API, dilution of 1:200 showed turbid appearance after 24h on an orbital shaker at 37°C.

Table A-13

Evaluation of LBF using FeSSGF as the medium; Dilution 1:2 (m:m):

Time/Method	API + formulation	Blank formulation	Observations
10min Macroscopic observation			Phase separation occurred slightly. Milk proteins from FeSSGF precipitated after mixing with LBF.
10min Microscopic observation (40x)	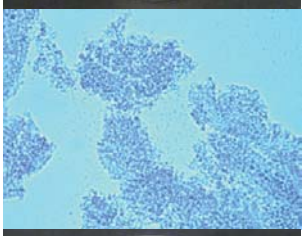	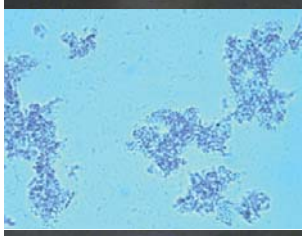	Precipitation of milk proteins was detected.
30min Macroscopic observation			Phase separation occurred slightly. Milk proteins from FeSSGF precipitated after mixing with LBF.
30min Microscopic observation (40x)	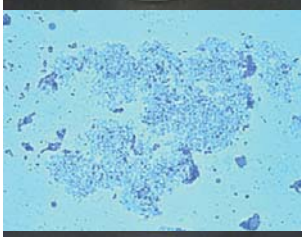	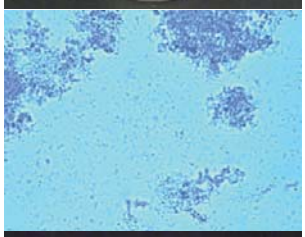	Precipitation of milk proteins was detected.
120min Macroscopic observation			Phase separation was increased. Precipitates migrated to the top and bottom. Liquid in the middle layer was more transparent.
120min Microscopic observation (40x)	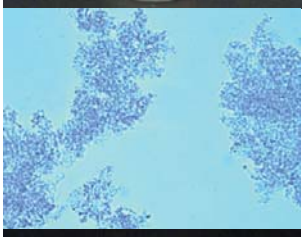	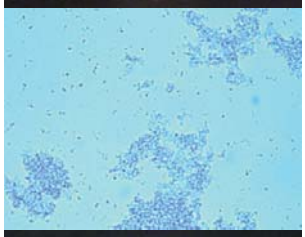	No crystals of API were detected in the dilutions. More lipid droplets were found in the field of blank formulation.
24h Macroscopic observation			Phase separation became more significant. Transparent middle layer of the liquid occupied more place.

Table A-14

Evaluation of LBF using FeSSGF as the medium; Dilution 1:5 (m:m):

Time/Method	API + formulation	Blank formulation	Observations
10min Macroscopic observation			Phase separation occurred slightly. Milk proteins from FeSSGF precipitated after mixing with LBF.
10min Microscopic observation (40x)	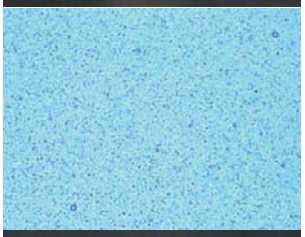	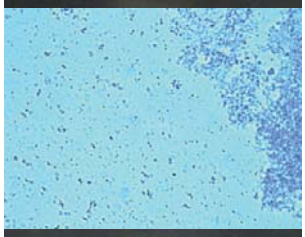	Surprisingly, API loaded formulation dispersed even better than the blank formulation.
30min Macroscopic observation			Phase separation occurred slightly. Milk proteins from FeSSGF precipitated after mixing with LBF.
30min Microscopic observation (40x)	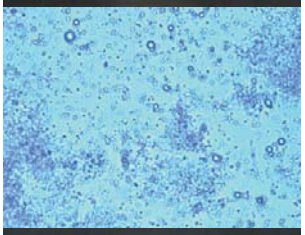	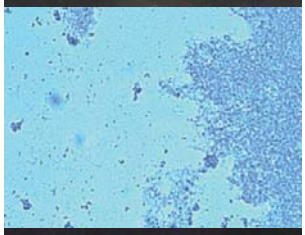	Surprisingly, API loaded formulation dispersed even better than the blank formulation.
120min Macroscopic observation			Significant phase separation occurred in 1:5 dilutions. The precipitation accumulated on bottom of the vial.
120min Microscopic observation (40x)	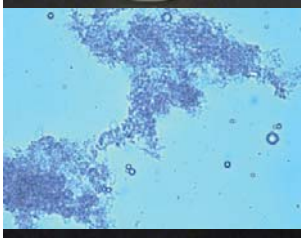	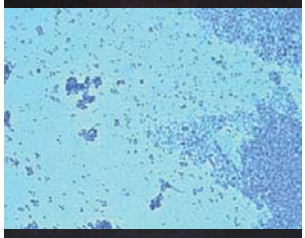	As no API crystals were detected, fenofibrate was assumed to be well solubilized in the dispersed LBF.
24h Macroscopic observation			No apparent difference in appearance was observed at 24h.

Table A-15

Evaluation of LBF using FeSSGF as the medium; Dilution 1:200 (m:m):

Time/Method	API + formulation	Blank formulation	Observations
10min Macroscopic observation			The LBF/FeSSGF mixture showed homogenous appearance without phase separation.
10min Microscopic observation (40x)	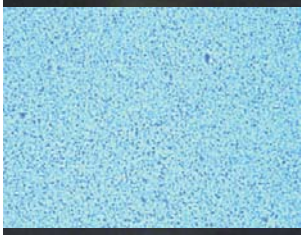	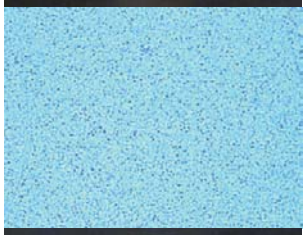	The FeSSGF diluted LBF was homogenous in critical scale. There were only one or two large particles in the field of detection.
30min Macroscopic observation			The LBF/FeSSGF mixture showed homogenous appearance without phase separation.
30min Microscopic observation (40x)	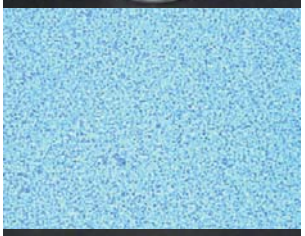	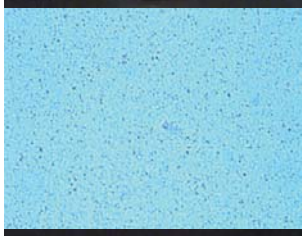	The FeSSGF diluted LBF was homogenous in critical scale. There were only one or two large particles in the field of detection.
120min Macroscopic observation			The LBF/FeSSGF mixture showed homogenous appearance without phase separation.
120min Microscopic observation (40x)		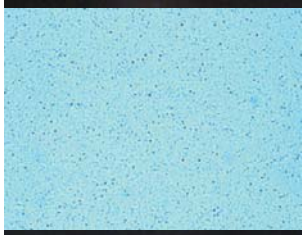	The fine emulsion was homogenous in critical scale. Brownian movement of these tiny particles was detected under microscope.
24h Macroscopic observation			No apparent difference in appearance was observed at 24h.

Data File: D:\EZChrom Elite\Projects\Yang Fei\data\20120216\export\E5(80) cap FaSSGF002
Method: D:\EZChrom Elite\Projects\Yang Fei\method\method fenofibrate.met
Acquired: 16.02.2012 17:33:37
Printed: 06.02.2013 11:27:56

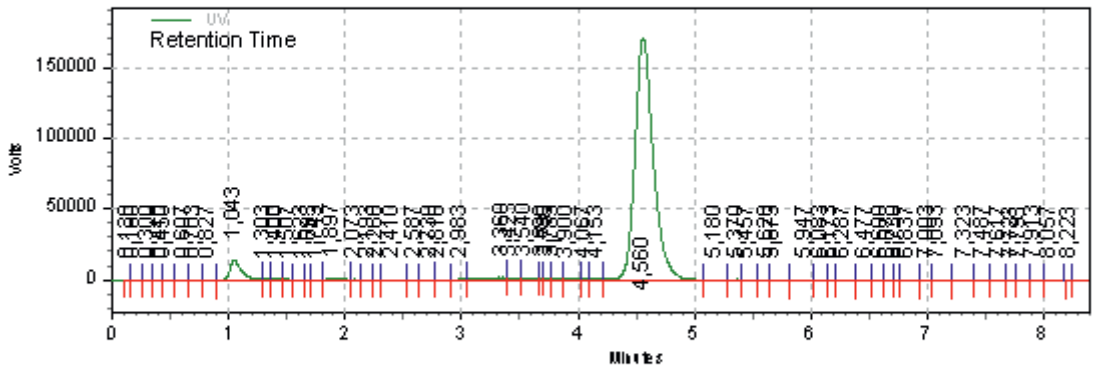

UV Results

Retention Time	Area	Area %	Height	Height %
1,043	115376	4,85	14586	5,98
4,560	1915307	80,44	171864	70,44

Fig. A-1. Typical HPLC chromatogram of a sample from the dissolution test containing fenofibrate lipid-based formulation.

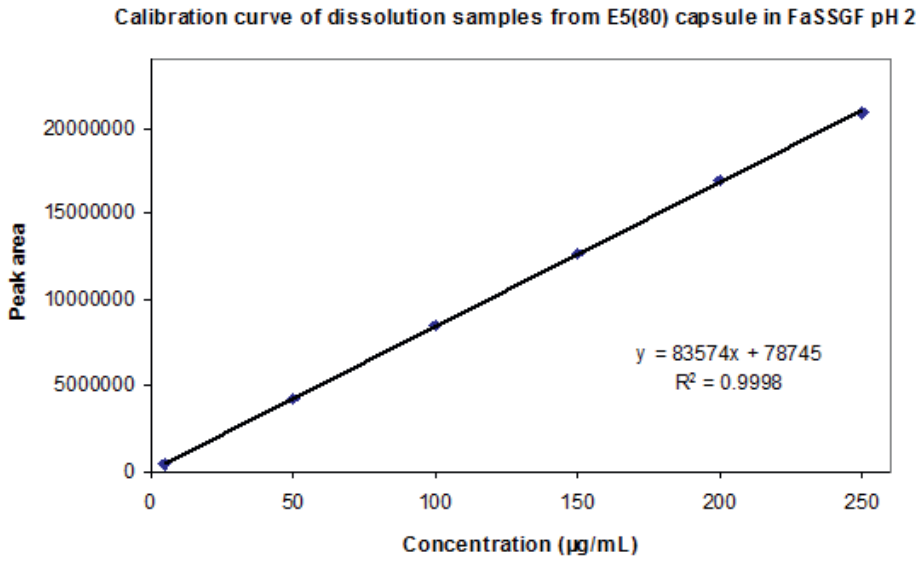

Fig. A-2. Typical calibration curve for testing samples from the dissolution test containing fenofibrate lipid-based formulation.

Table A-16

USP III dissolution data of dissolved samples of LBF No.2 in water.

Time	Vessel Conc. (µg mL^{-1})			Cumulative % Dissoved				
(min)	No. 1	No. 2	No. 3	No. 1	No. 2	No. 3	Mean	SD
0	0.000	0.000	0.000	0.000	0.000	0.000	0.000	0.000
10	10.076	5.075	3.807	10.093	5.078	3.807	6.326	3.323
30	85.408	99.820	104.499	85.804	100.014	104.602	96.807	9.801
60	95.761	95.993	103.098	98.313	98.682	105.814	100.936	4.228
120	62.025	70.824	71.593	66.919	75.897	76.884	73.233	5.491

Table A-17

USP III dissolution data of dispersed samples of LBF No.2 in water.

Time	Vessel Conc. (µg mL^{-1})			Cumulative % Dissoved				
(min)	No. 4	No. 5	No. 6	No. 4	No. 5	No. 6	Mean	SD
0	0.000	0.000	0.000	0.000	0.000	0.000	0.000	0.000
10	9.531	34.779	9.429	9.551	34.705	9.394	17.883	14.568
30	113.577	107.463	102.638	114.052	108.103	102.493	108.216	5.780
60	102.973	103.207	104.454	106.272	106.537	106.859	106.556	0.294
120	80.274	80.562	87.393	86.105	86.514	92.462	88.360	3.558

Table A-18

USP III dissolution data of dissolved samples of LBF No.2 in SIFsp.

Time	Vessel Conc. (µg mL^{-1})			Cumulative % Dissoved				
(min)	No. 1	No. 2	No. 3	No. 1	No. 2	No. 3	Mean	SD
0	0.000	0.000	0.000	0.000	0.000	0.000	0.000	0.000
10	19.736	20.581	13.790	19.484	20.706	13.676	17.956	3.756
30	87.895	90.370	91.302	87.262	91.440	90.890	89.864	2.270
60	85.852	87.681	79.948	87.414	91.008	81.894	86.772	4.591
120	62.706	70.547	56.490	66.682	75.974	60.612	67.756	7.737

Table A-19

USP III dissolution data of dispersed samples of LBF No.2 in SIFsp.

Time	Vessel Conc. (µg mL^{-1})			Cumulative % Dissoved				
(min)	No. 4	No. 5	No. 6	No. 4	No. 5	No. 6	Mean	SD
0	0.000	0.000	0.000	0.000	0.000	0.000	0.000	0.000
10	9.252	4.727	13.999	9.237	4.728	13.848	9.271	4.560
30	97.746	80.344	97.708	97.828	80.469	97.000	91.765	9.792
60	91.754	78.737	77.994	94.285	80.870	79.915	85.023	8.035
120	69.844	67.200	64.709	74.699	71.301	68.701	71.567	3.008

Table A-20

USP III dissolution data of dissolved samples of LBF No.2 in FaSSGF.

Time	Vessel Conc. (µg mL^{-1})			Cumulative % Dissoved				
(min)	No. 1	No. 2	No. 3	No. 1	No. 2	No. 3	Mean	SD
0	0.000	0.000	0.000	0.000	0.000	0.000	0.000	0.000
10	82.019	92.868	91.692	83.189	93.492	92.252	89.644	5.625
30	83.873	89.234	62.946	87.149	92.171	65.636	81.652	14.096
60	63.894	68.014	80.937	69.012	73.054	85.321	75.796	8.493
120	43.939	43.145	59.919	50.392	49.730	66.210	55.444	9.330

Table A-21

USP III dissolution data of dispersed samples of LBF No.2 in FaSSGF.

Time	Vessel Conc. (µg mL^{-1})			Cumulative % Dissoved				
(min)	No. 4	No. 5	No. 6	No. 4	No. 5	No. 6	Mean	SD
0	0.000	0.000	0.000	0.000	0.000	0.000	0.000	0.000
10	87.759	82.772	85.171	88.118	82.433	84.839	85.130	2.854
30	92.224	90.253	88.376	94.804	91.944	90.152	92.300	2.346
60	78.919	79.326	82.330	83.760	83.308	86.330	84.466	1.630
120	61.041	54.793	52.377	67.789	60.851	58.544	62.395	4.812

Table A-22

USP III dissolution data of dissolved samples of LBF No.2 in FaSSIF-V2.

Time	Vessel Conc. (μg mL^{-1})			Cumulative % Dissoved				
(min)	No. 1	No. 2	No. 3	No. 1	No. 2	No. 3	Mean	SD
0	0.000	0.000	0.000	0.000	0.000	0.000	0.000	0.000
10	32.279	15.845	18.144	32.217	15.708	18.052	21.992	8.932
30	80.759	100.904	87.809	81.409	100.424	87.813	89.882	9.675
60	67.163	75.671	66.453	69.854	77.910	68.750	72.171	5.000
120	51.446	56.488	45.768	55.843	60.768	49.823	55.478	5.482

Table A-23

USP III dissolution data of dispersed samples of LBF No.2 in FaSSIF-V2.

Time	Vessel Conc. (μg mL^{-1})			Cumulative % Dissoved				
(min)	No. 4	No. 5	No. 6	No. 4	No. 5	No. 6	Mean	SD
0	0.000	0.000	0.000	0.000	0.000	0.000	0.000	0.000
10	7.842	5.889	5.332	7.796	5.935	5.319	6.350	1.289
30	96.415	84.760	99.900	96.043	85.580	99.802	93.808	7.369
60	77.931	96.540	88.129	80.063	99.590	90.549	90.067	9.772
120	58.467	65.820	63.915	62.651	71.059	68.590	67.433	4.322

Table A-24

USP III dissolution data of dissolved samples of LBF No.2 in FeSSGF.

Time	Vessel Conc. (μg mL^{-1})			Cumulative % Dissoved				
(min)	No. 1	No. 2	No. 3	No. 1	No. 2	No. 3	Mean	SD
0	0.000	0.000	0.000	0.000	0.000	0.000	0.000	0.000
10	26.338	12.105	8.018	26.007	12.070	7.924	15.334	9.473
30	85.089	87.787	85.229	84.669	87.834	84.422	85.642	1.902
60	105.201	94.417	65.270	106.629	96.633	66.804	90.022	20.719
120	94.600	85.950	87.935	98.758	90.544	90.814	93.372	4.666

Table A-25

USP III dissolution data of dispersed samples of LBF No.2 in FeSSGF.

Time	Vessel Conc. (µg mL^{-1})			Cumulative % Dissoved				
(min)	No. 4	No. 5	No. 6	No. 4	No. 5	No. 6	Mean	SD
0	0.000	0.000	0.000	0.000	0.000	0.000	0.000	0.000
10	16.081	6.993	8.026	15.913	6.907	8.017	10.279	4.911
30	93.363	96.355	100.970	92.788	95.335	101.058	96.394	4.236
60	97.980	101.505	96.563	99.666	102.800	99.178	100.548	1.966
120	88.690	96.137	95.277	92.897	100.005	100.305	97.736	4.193

Table A-26

USP II dissolution data of fenofibrate pure drug in SGF pH2.

Time	Vessel Conc. (µg mL^{-1})			Cumulative % Dissoved				
(min)	No. 1	No. 2	No. 3	No. 1	No. 2	No. 3	Mean	SD
0	0.000	0.000	0.000	0.000	0.000	0.000	0.000	0.000
5	0.054	0.037	0.094	0.008	0.006	0.015	0.010	0.005
10	0.056	0.252	0.080	0.009	0.039	0.013	0.020	0.017
15	0.056	0.163	0.126	0.009	0.026	0.020	0.018	0.009
20	0.050	0.152	0.102	0.008	0.025	0.017	0.016	0.008
30	0.096	0.195	0.170	0.015	0.032	0.027	0.025	0.008
45	0.164	0.231	0.226	0.026	0.038	0.036	0.033	0.006
60	0.241	0.183	0.233	0.039	0.031	0.038	0.036	0.004
90	0.145	0.299	0.229	0.024	0.049	0.038	0.037	0.012
150	0.295	0.305	0.231	0.048	0.051	0.038	0.046	0.006
240	0.185	0.244	0.201	0.031	0.042	0.034	0.036	0.005

Table A-27

USP II dissolution data of Lipidil-Ter in SGF pH2.

Time	Vessel Conc. (µg mL^{-1})			Cumulative % Dissoved				
(min)	No. 4	No. 5	No. 6	No. 4	No. 5	No. 6	Mean	SD
0	0.000	0.000	0.000	0.000	0.000	0.000	0.000	0.000
5	0.311	0.165	0.263	0.049	0.026	0.041	0.038	0.012
10	0.396	0.302	0.443	0.063	0.048	0.070	0.060	0.011
15	0.547	0.511	0.472	0.087	0.081	0.075	0.081	0.006
20	0.428	0.464	0.497	0.069	0.074	0.080	0.074	0.005
30	0.408	0.389	0.496	0.067	0.063	0.081	0.070	0.009
45	0.459	0.509	0.441	0.076	0.083	0.073	0.077	0.005
60	0.406	0.442	0.535	0.068	0.073	0.088	0.077	0.011
90	0.364	0.469	0.518	0.062	0.078	0.087	0.076	0.012
150	0.387	0.392	0.396	0.067	0.067	0.069	0.068	0.001
240	0.314	0.329	0.494	0.056	0.058	0.085	0.066	0.016

Table A-28

USP II dissolution data of LBF No.1 in SGF pH2.

Time	Vessel Conc. (µg mL^{-1})			Cumulative % Dissoved				
(min)	No. 1	No. 2	No. 3	No. 1	No. 2	No. 3	Mean	SD
0	0.000	0.000	0.000	0.000	0.000	0.000	0.000	0.000
5	314.396	332.011	354.554	78.599	83.003	88.639	83.413	5.032
10	328.069	353.391	378.482	82.961	89.344	95.684	89.330	6.362
15	322.029	356.883	367.800	82.435	91.277	94.149	89.287	6.105
20	320.616	342.481	352.682	83.047	88.747	91.473	87.756	4.299
30	315.748	337.255	362.038	82.792	88.468	94.870	88.710	6.042
45	308.769	343.141	358.598	81.995	90.951	95.096	89.348	6.696
60	305.214	334.177	347.981	82.032	89.740	93.518	88.430	5.854
90	303.436	350.828	345.166	82.503	94.905	93.858	90.422	6.878
150	303.859	347.687	362.631	83.520	95.172	99.260	92.650	8.167
240	300.268	343.345	338.710	83.533	95.130	94.367	91.010	6.486

Table A-29

USP II dissolution data of LBF No.2 in SGF pH2.

Time	Vessel Conc. (µg mL^{-1})			Cumulative % Dissoved				
(min)	No. 4	No. 5	No. 6	No. 4	No. 5	No. 6	Mean	SD
0	0.000	0.000	0.000	0.000	0.000	0.000	0.000	0.000
5	310.955	341.162	323.878	77.739	85.290	80.969	81.333	3.789
10	305.880	332.950	318.260	77.403	84.261	80.537	80.733	3.433
15	324.732	327.300	336.214	83.034	83.847	85.980	84.287	1.521
20	279.729	256.500	390.876	72.757	67.129	100.654	80.180	17.953
30	233.138	321.171	298.433	61.948	84.067	78.716	74.910	11.540
45	222.774	254.530	318.357	60.057	68.370	84.592	71.006	12.478
60	270.839	214.746	340.884	72.741	59.187	91.179	74.369	16.058
90	244.182	276.333	298.445	66.890	75.228	81.592	74.570	7.373
150	204.017	232.304	246.559	57.581	65.050	69.516	64.049	6.030
240	170.253	192.273	207.442	49.752	55.739	60.476	55.322	5.374

Table A-30

USP II dissolution data of LBF No.3 in SGF pH2.

Time	Vessel Conc. (µg mL^{-1})			Cumulative % Dissoved				
(min)	No. 1	No. 2	No. 3	No. 1	No. 2	No. 3	Mean	SD
0	0.000	0.000	0.000	0.000	0.000	0.000	0.000	0.000
5	496.257	516.517	528.331	77.540	80.706	82.552	80.266	2.535
10	501.733	520.433	543.747	79.326	82.286	85.951	82.521	3.319
15	512.741	521.687	541.079	81.987	83.458	86.554	83.999	2.331
20	490.702	504.270	524.605	79.505	81.715	84.994	82.071	2.762
30	489.684	504.287	523.639	80.266	82.663	85.827	82.919	2.789
45	492.416	501.795	522.973	81.611	83.219	86.705	83.845	2.604
60	475.706	484.084	505.644	79.923	81.392	84.978	82.098	2.600
90	464.004	470.391	493.331	78.987	80.161	84.002	81.050	2.623
150	457.060	480.312	490.959	78.772	82.593	84.556	81.973	2.941
240	463.579	465.973	483.470	80.647	81.253	84.307	82.069	1.961

Table A-31

USP II dissolution data of LBF No.4 in SGF pH2.

Time	Vessel Conc. (μg mL^{-1})			Cumulative % Dissoved				
(min)	No. 4	No. 5	No. 6	No. 4	No. 5	No. 6	Mean	SD
0	0.000	0.000	0.000	0.000	0.000	0.000	0.000	0.000
5	416.209	479.172	401.427	65.033	74.871	62.723	67.542	6.451
10	405.097	522.741	544.875	64.077	82.577	85.889	77.514	11.755
15	534.108	585.550	521.931	84.994	93.371	83.326	87.230	5.383
20	459.862	506.414	522.910	74.395	82.104	84.458	80.319	5.264
30	526.541	538.461	513.137	85.676	88.060	83.911	85.882	2.082
45	448.327	565.115	559.009	74.442	93.235	92.041	86.572	10.522
60	470.687	493.716	535.845	78.776	83.138	89.469	83.795	5.377
90	483.159	465.198	428.998	81.608	79.608	73.779	78.332	4.067
150	452.474	438.174	451.169	77.719	76.258	78.048	77.342	0.953
240	439.453	417.136	394.100	76.533	73.792	69.977	73.434	3.293

Table A-32

USP II dissolution data of fenofibrate pure drug in SIFsp.

Time	Vessel Conc. (μg mL^{-1})			Cumulative % Dissoved				
(min)	No. 1	No. 2	No. 3	No. 1	No. 2	No. 3	Mean	SD
0	0.000	0.000	0.000	0.000	0.000	0.000	0.000	0.000
5	0.038	0.065	0.037	0.012	0.020	0.012	0.015	0.005
10	0.138	0.189	0.117	0.043	0.059	0.037	0.046	0.012
15	0.173	0.211	0.164	0.055	0.067	0.052	0.058	0.008
20	0.171	0.224	0.168	0.054	0.071	0.054	0.060	0.010
30	0.200	0.248	0.191	0.064	0.080	0.061	0.068	0.010
45	0.183	0.216	0.172	0.059	0.071	0.056	0.062	0.008
60	0.185	0.225	0.275	0.061	0.074	0.089	0.074	0.014
90	0.216	0.285	0.219	0.071	0.093	0.072	0.079	0.013
150	0.208	0.244	0.254	0.069	0.081	0.084	0.078	0.008
240	0.194	0.231	0.209	0.065	0.078	0.070	0.071	0.006

Table A-33

USP II dissolution data of Lipidil-Ter in SIFsp.

Time	Vessel Conc. (µg mL^{-1})			Cumulative % Dissoved				
(min)	No. 4	No. 5	No. 6	No. 4	No. 5	No. 6	Mean	SD
0	0.000	0.000	0.000	0.000	0.000	0.000	0.000	0.000
5	0.194	0.255	0.333	0.061	0.080	0.104	0.082	0.022
10	0.387	0.313	0.377	0.121	0.099	0.119	0.113	0.013
15	0.390	0.381	0.374	0.124	0.121	0.119	0.121	0.002
20	0.410	0.372	0.383	0.131	0.119	0.123	0.125	0.006
30	0.406	0.377	0.384	0.131	0.122	0.125	0.126	0.005
45	0.330	0.513	0.349	0.109	0.166	0.115	0.130	0.031
60	0.481	0.340	0.311	0.157	0.113	0.104	0.125	0.028
90	0.353	0.315	0.313	0.118	0.106	0.106	0.110	0.007
150	0.340	0.358	0.328	0.115	0.121	0.111	0.116	0.005
240	0.324	0.355	0.336	0.111	0.121	0.115	0.116	0.005

Table A-34

USP II dissolution data of LBF No.1 in SIFsp.

Time	Vessel Conc. (µg mL^{-1})			Cumulative % Dissoved				
(min)	No. 1	No. 2	No. 3	No. 1	No. 2	No. 3	Mean	SD
0	0.000	0.000	0.000	0.000	0.000	0.000	0.000	0.000
5	171.573	194.560	195.968	85.786	97.280	97.984	93.683	6.848
10	179.448	199.704	194.755	90.582	100.825	98.358	96.588	5.346
15	179.822	198.950	196.307	91.666	101.446	100.107	97.740	5.302
20	175.904	193.650	193.168	90.606	99.791	99.519	96.639	5.226
30	173.680	193.320	191.797	90.374	100.594	99.800	96.923	5.685
45	171.146	190.288	189.909	89.975	100.045	99.815	96.612	5.749
60	170.041	188.714	187.470	90.278	100.209	99.544	96.677	5.552
90	172.113	186.222	186.884	92.164	99.907	100.189	97.420	4.554
150	169.733	186.120	182.782	91.835	100.787	99.072	97.232	4.751
240	167.284	183.617	184.217	91.460	100.466	100.704	97.543	5.270

Table A-35

USP II dissolution data of LBF No.2 in SIFsp.

Time	Vessel Conc. (μg mL^{-1})			Cumulative % Dissoved				
(min)	No. 4	No. 5	No. 6	No. 4	No. 5	No. 6	Mean	SD
0	0.000	0.000	0.000	0.000	0.000	0.000	0.000	0.000
5	167.917	142.112	175.290	83.959	71.056	87.645	80.886	8.711
10	165.344	174.770	142.017	83.512	88.096	71.885	81.164	8.356
15	145.637	152.156	131.996	74.485	77.663	67.584	73.244	5.152
20	149.499	143.066	112.136	77.144	73.878	58.315	69.779	10.062
30	130.300	126.972	127.949	68.292	66.546	66.782	67.207	0.947
45	106.929	111.462	103.175	57.258	59.426	55.034	57.239	2.196
60	98.371	107.689	111.939	53.514	58.097	59.932	57.181	3.306
90	98.041	93.912	115.882	53.841	51.747	62.463	56.017	5.680
150	107.916	111.237	115.182	59.268	60.879	62.693	60.947	1.713
240	124.470	109.414	106.996	68.085	60.524	59.176	62.595	4.802

Table A-36

USP II dissolution data of LBF No.3 in SIFsp.

Time	Vessel Conc. (μg mL^{-1})			Cumulative % Dissoved				
(min)	No. 1	No. 2	No. 3	No. 1	No. 2	No. 3	Mean	SD
0	0.000	0.000	0.000	0.000	0.000	0.000	0.000	0.000
5	264.606	289.066	274.295	82.689	90.333	85.717	86.247	3.849
10	268.301	293.434	298.016	84.671	92.602	93.987	90.420	5.027
15	262.427	281.203	274.125	83.674	89.696	87.453	86.941	3.044
20	266.258	294.339	274.746	85.691	94.680	88.503	89.625	4.598
30	262.180	273.469	274.528	85.249	89.078	89.294	87.873	2.276
45	249.842	277.337	274.573	82.212	91.141	90.166	87.840	4.898
60	252.945	268.267	268.575	83.963	89.174	89.149	87.429	3.002
90	248.977	275.434	262.414	83.513	92.252	88.063	87.943	4.371
150	252.595	269.270	263.616	85.422	91.186	89.259	88.622	2.934
240	251.185	265.801	268.487	85.771	90.943	91.605	89.440	3.195

Table A-37

USP II dissolution data of LBF No.4 in SIFsp.

Time	Vessel Conc. (µg mL^{-1})			Cumulative % Dissoved				
(min)	No. 4	No. 5	No. 6	No. 4	No. 5	No. 6	Mean	SD
0	0.000	0.000	0.000	0.000	0.000	0.000	0.000	0.000
5	262.960	247.993	231.672	82.175	77.498	72.397	77.357	4.890
10	265.063	270.176	284.517	83.654	85.205	89.636	86.165	3.104
15	282.310	323.647	278.097	89.872	102.759	88.518	93.716	7.860
20	292.072	252.224	309.115	93.805	81.451	99.080	91.445	9.049
30	280.503	276.773	266.543	91.102	89.911	86.743	89.252	2.253
45	245.085	230.834	274.353	80.911	76.420	90.016	82.449	6.928
60	244.961	246.933	258.903	81.638	82.172	86.045	83.285	2.406
90	274.270	257.938	270.805	91.562	86.382	90.574	89.506	2.750
150	234.186	245.084	277.655	79.893	83.172	93.561	85.542	7.136
240	264.631	248.196	271.312	90.139	84.910	92.446	89.165	3.861

Table A-38

USP II dissolution data of fenofibrate pure drug in FaSSGF pH2.

Time	Vessel Conc. (µg mL^{-1})			Cumulative % Dissoved				
(min)	No. 1	No. 2	No. 3	No. 1	No. 2	No. 3	Mean	SD
0	0.000	0.000	0.000	0.000	0.000	0.000	0.000	0.000
5	0.059	0.023	0.052	0.009	0.004	0.008	0.007	0.003
10	0.035	0.043	0.054	0.006	0.007	0.009	0.007	0.001
15	0.047	0.060	0.137	0.008	0.009	0.022	0.013	0.008
20	0.071	0.074	0.111	0.011	0.012	0.018	0.014	0.004
30	0.091	0.092	0.085	0.015	0.015	0.014	0.014	0.000
45	0.132	0.095	0.119	0.021	0.015	0.019	0.019	0.003
60	0.149	0.102	0.149	0.024	0.017	0.024	0.022	0.004
90	0.168	0.120	0.137	0.027	0.020	0.023	0.023	0.004
150	0.154	0.122	0.144	0.025	0.020	0.024	0.023	0.003
240	0.130	0.093	0.139	0.022	0.016	0.024	0.020	0.004

Table A-39

USP II dissolution data of Lipidil-Ter in FaSSGF pH2.

Time	Vessel Conc. (μg mL^{-1})			Cumulative % Dissoved				
(min)	No. 4	No. 5	No. 6	No. 4	No. 5	No. 6	Mean	SD
0	0.000	0.000	0.000	0.000	0.000	0.000	0.000	0.000
5	0.087	0.203	0.186	0.014	0.032	0.029	0.025	0.010
10	0.377	0.473	0.443	0.059	0.074	0.070	0.068	0.008
15	0.608	0.567	0.589	0.096	0.090	0.093	0.093	0.003
20	0.587	0.599	0.594	0.094	0.096	0.095	0.095	0.001
30	0.452	0.601	0.602	0.074	0.097	0.097	0.089	0.014
45	0.550	0.601	0.569	0.090	0.098	0.093	0.094	0.004
60	0.500	0.555	0.691	0.083	0.092	0.114	0.096	0.016
90	0.493	0.519	0.617	0.083	0.088	0.103	0.091	0.011
150	0.527	0.518	0.466	0.089	0.089	0.081	0.086	0.005
240	0.459	0.486	0.478	0.080	0.085	0.084	0.083	0.003

Table A-40

USP II dissolution data of LBF No.1 in FaSSGF pH2.

Time	Vessel Conc. (μg mL^{-1})			Cumulative % Dissoved				
(min)	No. 1	No. 2	No. 3	No. 1	No. 2	No. 3	Mean	SD
0	0.000	0.000	0.000	0.000	0.000	0.000	0.000	0.000
5	317.635	380.617	346.226	79.409	95.154	86.556	87.040	7.884
10	328.525	395.871	360.260	82.925	99.919	90.931	91.258	8.502
15	327.557	397.427	356.548	83.505	101.298	90.903	91.902	8.939
20	324.014	333.598	356.484	83.438	86.334	91.778	87.184	4.235
30	326.818	383.040	347.095	84.949	99.529	90.323	91.600	7.373
45	314.843	378.735	341.752	82.772	99.410	89.855	90.679	8.350
60	323.628	378.281	342.543	85.755	100.244	90.907	92.302	7.344
90	311.906	352.144	343.728	83.634	94.655	92.059	90.116	5.762
150	314.783	365.164	342.817	85.133	98.790	92.691	92.205	6.842
240	307.297	374.939	341.717	84.048	102.147	93.273	93.156	9.050

Table A-41

USP II dissolution data of LBF No.2 in FaSSGF pH2.

Time	Vessel Conc. (µg mL^{-1})			Cumulative % Dissoved				
(min)	No. 4	No. 5	No. 6	No. 4	No. 5	No. 6	Mean	SD
0	0.000	0.000	0.000	0.000	0.000	0.000	0.000	0.000
5	387.056	304.417	385.615	96.764	76.104	96.404	89.757	11.825
10	358.733	272.283	384.947	90.651	68.832	97.201	85.561	14.854
15	331.907	224.572	378.341	84.841	57.585	96.512	79.646	19.977
20	280.428	230.765	322.480	72.801	59.695	83.492	71.996	11.919
30	268.451	223.863	315.917	70.508	58.546	82.658	70.571	12.056
45	248.112	208.264	262.642	66.094	55.206	70.129	63.810	7.719
60	244.435	200.982	269.059	65.795	53.906	72.390	64.030	9.367
90	248.969	206.401	249.063	67.540	55.763	68.063	63.789	6.955
150	282.029	221.691	263.759	76.428	60.102	72.360	69.630	8.498
240	236.300	206.138	284.178	65.700	56.767	78.124	66.864	10.726

Table A-42

USP II dissolution data of LBF No.3 in FaSSGF pH2.

Time	Vessel Conc. (µg mL^{-1})			Cumulative % Dissoved				
(min)	No. 1	No. 2	No. 3	No. 1	No. 2	No. 3	Mean	SD
0	0.000	0.000	0.000	0.000	0.000	0.000	0.000	0.000
5	464.854	531.382	517.203	72.633	83.028	80.813	78.825	5.475
10	470.941	543.729	533.277	74.456	85.954	84.294	81.568	6.215
15	465.598	532.964	536.632	74.504	85.291	85.818	81.871	6.386
20	459.708	534.585	550.823	74.457	86.544	89.042	83.348	7.800
30	454.845	528.641	520.338	74.559	86.618	85.311	82.163	6.617
45	456.751	525.005	515.511	75.710	87.041	85.533	82.761	6.153
60	458.027	513.625	520.259	76.766	86.247	87.241	83.418	5.783
90	452.264	530.711	538.803	76.724	89.880	91.114	85.906	7.976
150	446.437	508.632	515.818	76.661	87.425	88.533	84.206	6.558
240	439.081	505.225	517.458	76.349	87.846	89.757	84.651	7.253

Table A-43

USP II dissolution data of LBF No.4 in FaSSGF pH2.

Time	Vessel Conc. (μg mL^{-1})			Cumulative % Dissoved				
(min)	No. 4	No. 5	No. 6	No. 4	No. 5	No. 6	Mean	SD
0	0.000	0.000	0.000	0.000	0.000	0.000	0.000	0.000
5	408.535	504.554	515.801	63.834	78.837	80.594	74.421	9.211
10	438.257	546.258	545.274	69.244	86.299	86.166	80.570	9.809
15	450.464	494.088	562.273	71.973	79.171	89.845	80.330	8.992
20	449.131	534.458	552.671	72.609	86.406	89.399	82.804	8.955
30	437.242	547.669	555.495	71.593	89.472	90.876	83.981	10.751
45	425.311	532.449	540.642	70.549	88.121	89.597	82.756	10.597
60	434.640	485.443	528.674	72.804	81.774	88.741	81.106	7.989
90	376.361	509.701	511.140	64.513	86.475	86.992	79.327	12.832
150	408.132	489.995	462.142	70.183	84.352	80.295	78.276	7.297
240	449.126	484.862	480.766	77.354	84.468	84.071	81.964	3.998

Table A-44

USP II dissolution data of fenofibrate pure drug in FaSSIF-V2(PO_4).

Time	Vessel Conc. (μg mL^{-1})			Cumulative % Dissoved				
(min)	No. 1	No. 2	No. 3	No. 1	No. 2	No. 3	Mean	SD
0	0.000	0.000	0.000	0.000	0.000	0.000	0.000	0.000
5	0.188	0.232	0.798	0.059	0.072	0.249	0.127	0.106
10	0.284	0.183	0.782	0.089	0.058	0.247	0.131	0.101
15	0.382	0.269	0.904	0.121	0.085	0.288	0.165	0.108
20	0.464	0.376	0.877	0.148	0.120	0.282	0.183	0.087
30	0.653	0.483	1.108	0.208	0.154	0.357	0.240	0.105
45	0.943	0.784	1.390	0.301	0.250	0.448	0.333	0.103
60	1.184	0.951	1.540	0.379	0.304	0.499	0.394	0.098
90	1.739	1.341	1.986	0.556	0.429	0.644	0.543	0.108
150	2.308	2.137	2.634	0.739	0.682	0.852	0.758	0.087
240	2.706	2.489	3.030	0.871	0.799	0.984	0.885	0.094

Table A-45

USP II dissolution data of Lipidil-Ter in FaSSIF-V2(PO_4).

Time	Vessel Conc. (µg mL^{-1})			Cumulative % Dissoved				
(min)	No. 4	No. 5	No. 6	No. 4	No. 5	No. 6	Mean	SD
0	0.000	0.000	0.000	0.000	0.000	0.000	0.000	0.000
5	2.007	2.396	2.572	0.627	0.749	0.804	0.726	0.090
10	3.368	3.518	3.723	1.059	1.107	1.171	1.112	0.057
15	3.501	3.706	3.877	1.111	1.177	1.231	1.173	0.060
20	3.514	3.711	3.851	1.126	1.190	1.235	1.184	0.055
30	3.581	3.733	3.672	1.158	1.208	1.191	1.186	0.026
45	3.522	3.642	3.775	1.151	1.191	1.235	1.192	0.042
60	3.540	3.818	3.694	1.167	1.258	1.222	1.215	0.046
90	3.438	3.783	3.758	1.146	1.259	1.253	1.219	0.063
150	3.539	3.646	3.831	1.189	1.228	1.287	1.235	0.050
240	3.646	3.894	3.774	1.233	1.317	1.282	1.277	0.042

Table A-46

USP II dissolution data of LBF No.1 in FaSSIF-V2(PO_4).

Time	Vessel Conc. (µg mL^{-1})			Cumulative % Dissoved				
(min)	No. 1	No. 2	No. 3	No. 1	No. 2	No. 3	Mean	SD
0	0.000	0.000	0.000	0.000	0.000	0.000	0.000	0.000
5	172.076	184.616	184.139	86.038	92.308	92.069	90.139	3.553
10	188.053	200.971	200.711	94.887	101.408	101.276	99.190	3.728
15	185.386	199.735	199.665	94.494	101.796	101.757	99.349	4.205
20	186.076	199.100	195.779	95.765	102.477	100.812	99.685	3.495
30	183.494	195.249	195.085	95.405	101.546	101.444	99.465	3.517
45	176.663	189.696	189.231	92.907	99.746	99.492	97.382	3.877
60	177.697	189.856	189.116	94.307	100.775	100.381	98.488	3.626
90	177.596	185.995	187.300	95.145	99.794	100.419	98.452	2.881
150	175.443	187.529	185.892	94.957	101.491	100.651	99.033	3.555
240	174.769	186.746	187.261	95.497	102.037	102.265	99.933	3.844

Table A-47

USP II dissolution data of LBF No.2 in FaSSIF-V2(PO_4).

Time	Vessel Conc. (μg mL^{-1})			Cumulative % Dissoved				
(min)	No. 4	No. 5	No. 6	No. 4	No. 5	No. 6	Mean	SD
0	0.000	0.000	0.000	0.000	0.000	0.000	0.000	0.000
5	157.571	168.131	168.642	78.785	84.065	84.321	82.391	3.125
10	167.509	156.753	174.803	84.542	79.217	88.245	84.001	4.538
15	164.516	160.292	167.962	83.883	81.771	85.698	83.784	1.966
20	160.782	160.168	143.345	82.839	82.510	74.230	79.860	4.878
30	149.360	124.888	136.359	77.932	65.671	71.453	71.685	6.134
45	125.350	134.373	139.600	66.673	71.038	73.755	70.489	3.573
60	126.613	128.316	133.419	67.932	68.681	71.363	69.325	1.804
90	137.801	141.608	133.429	74.159	75.969	72.035	74.054	1.969
150	140.156	146.323	149.928	76.026	79.034	80.952	78.670	2.483
240	143.789	144.893	145.751	78.543	79.051	79.613	79.069	0.535

Table A-48

USP II dissolution data of LBF No.3 in FaSSIF-V2(PO_4).

Time	Vessel Conc. (μg mL^{-1})			Cumulative % Dissoved				
(min)	No. 1	No. 2	No. 3	No. 1	No. 2	No. 3	Mean	SD
0	0.000	0.000	0.000	0.000	0.000	0.000	0.000	0.000
5	264.239	211.738	226.636	82.575	66.168	70.824	73.189	8.455
10	291.036	248.152	257.521	91.775	78.209	81.184	83.722	7.130
15	305.455	258.085	262.676	97.190	82.089	83.599	87.626	8.317
20	306.581	250.394	264.039	98.496	80.492	84.846	87.945	9.394
30	302.867	253.181	257.788	98.294	82.145	83.718	88.052	8.904
45	308.092	253.411	259.151	100.873	83.008	84.949	89.610	9.802
60	302.306	245.189	257.339	100.028	81.231	85.193	88.817	9.909
90	294.470	247.810	251.465	98.524	82.816	84.161	88.500	8.706
150	292.258	248.272	249.090	98.753	83.735	84.205	88.897	8.538
240	296.062	248.103	252.169	100.855	84.458	85.946	90.419	9.068

Table A-49

USP II dissolution data of LBF No.4 in FaSSIF-V2(PO_4).

Time	Vessel Conc. (µg mL^{-1})			Cumulative % Dissoved				
(min)	No. 4	No. 5	No. 6	No. 4	No. 5	No. 6	Mean	SD
0	0.000	0.000	0.000	0.000	0.000	0.000	0.000	0.000
5	174.574	177.806	167.913	54.554	55.564	52.473	54.197	1.576
10	258.534	267.933	290.836	81.337	84.285	91.411	85.678	5.179
15	286.515	275.989	283.825	90.890	87.640	90.129	89.553	1.700
20	318.511	306.800	273.344	101.783	98.130	87.741	95.885	7.286
30	290.223	300.732	268.114	93.939	97.193	86.960	92.697	5.228
45	275.889	282.604	266.154	90.366	92.468	87.186	90.007	2.659
60	291.972	251.843	265.479	96.255	83.738	87.806	89.266	6.385
90	273.146	275.223	271.196	91.284	91.831	90.423	91.179	0.710
150	254.744	267.018	248.491	86.387	90.127	84.175	86.896	3.009
240	256.270	232.221	235.171	87.660	80.088	80.789	82.845	4.184

Table A-50

USP II dissolution data from the transfer model for prediction of intestinal precipitation of LBF No.3 in the fasted state. The donor phase is FaSSGF pH 2 and the acceptor phase is FaSSIF-V2(PO_4) with 0.2 mM lecithin. The transfer rate was kept at 2mL/min and the paddle revolution speed was 75 rpm.

Time	Vessel Conc. (µg mL^{-1})			Cumulative % Dissoved				
(min)	No. 1	No. 2	No. 3	No. 1	No. 2	No. 3	Mean	SD
0	0.00	0.00	0.00	0.00	0.00	0.00	0.00	0.00
5	2.66	2.77	2.73	0.85	0.88	0.87	0.87	0.02
10	10.17	11.49	11.79	3.28	3.71	3.80	3.60	0.28
15	21.07	21.10	21.72	6.89	6.90	7.10	6.97	0.12
20	32.46	30.44	32.41	10.76	10.10	10.75	10.53	0.38
25	42.55	41.01	43.80	14.30	13.79	14.72	14.27	0.47
30	52.19	49.76	54.66	17.79	16.97	18.63	17.80	0.83
40	71.19	67.93	73.79	24.98	23.84	25.89	24.90	1.03
50	87.63	87.33	89.52	31.67	31.54	32.37	31.86	0.44
60	104.60	103.29	110.65	38.92	38.42	41.14	39.49	1.45
75	122.80	121.57	126.27	47.76	47.27	49.12	48.05	0.96
90	141.47	146.96	158.44	57.41	59.54	64.16	60.37	3.45
105	152.51	153.66	171.07	64.58	65.04	72.30	67.31	4.33
120	180.86	181.27	191.40	79.50	79.66	84.15	81.10	2.64
135	187.43	201.15	202.62	83.44	89.30	90.15	87.63	3.66
150	179.65	171.62	199.46	80.13	76.75	88.81	81.90	6.22
180	186.15	180.44	181.26	82.87	80.47	81.13	81.49	1.24
210	172.70	176.89	192.69	77.24	78.98	85.91	80.71	4.59
240	182.86	180.21	199.82	81.46	80.37	88.87	83.57	4.63

Table A-51

USP II dissolution data of E5(80) solution in FaSSGF pH 2.

Time	Vessel Conc. (µg mL^{-1})			Cumulative % Dissoved				
(min)	No. 1	No. 2	No. 3	No. 1	No. 2	No. 3	Mean	SD
0	0.000	0.000	0.000	0.000	0.000	0.000	0.000	0.000
5	56.813	151.923	157.281	28.407	75.961	78.640	61.003	28.261
10	143.584	159.820	153.337	72.076	80.670	77.455	76.734	4.342
15	178.619	164.857	150.643	90.311	83.987	76.874	83.724	6.722
20	170.917	159.828	153.046	87.353	82.297	78.830	82.827	4.287
30	164.800	158.258	150.619	85.150	82.311	78.381	81.947	3.399
45	162.788	157.933	153.549	84.968	82.940	80.599	82.835	2.186
60	158.755	156.024	150.105	83.765	82.775	79.645	82.062	2.151
90	158.916	153.376	149.970	84.640	82.231	80.328	82.400	2.161
120	155.512	152.575	147.453	83.732	82.597	79.819	82.050	2.013
180	145.375	144.820	141.141	79.441	79.483	77.400	78.775	1.190
240	148.175	149.014	143.726	81.568	82.304	79.399	81.090	1.510

Table A-52

USP II dissolution data of E5(80) capsule in FaSSGF pH 2.

Time	Vessel Conc. (µg mL^{-1})			Cumulative % Dissoved				
(min)	No. 1	No. 2	No. 3	No. 1	No. 2	No. 3	Mean	SD
0	0.000	0.000	0.000	0.000	0.000	0.000	0.000	0.000
5	10.595	21.975	26.641	5.284	11.010	13.220	9.838	4.096
10	44.145	56.452	46.711	22.068	28.393	23.312	24.591	3.351
15	80.832	94.372	81.334	40.584	47.673	40.725	42.994	4.053
20	117.525	140.214	125.264	59.286	71.113	62.927	64.442	6.057
30	148.005	164.490	151.725	75.073	83.978	76.679	78.577	4.746
45	158.869	175.702	174.092	81.229	90.420	88.532	86.727	4.854
60	162.476	165.684	163.897	83.820	86.281	84.337	84.812	1.298
90	179.271	161.566	170.757	93.006	85.048	88.554	88.869	3.989
120	170.359	162.661	172.087	89.456	86.406	90.061	88.641	1.959
180	164.441	155.880	150.125	87.354	83.823	80.017	83.731	3.669
240	165.701	149.591	151.872	88.802	81.453	81.629	83.961	4.193

Table A-53

USP II dissolution data of E5(20) capsule in FaSSGF pH 2.

Time	Vessel Conc. (μg mL^{-1})			Cumulative % Dissoved				
(min)	No. 1	No. 2	No. 3	No. 1	No. 2	No. 3	Mean	SD
0	0.000	0.000	0.000	0.000	0.000	0.000	0.000	0.000
5	11.017	5.688	7.093	5.507	2.842	3.541	3.963	1.382
10	32.461	33.375	33.930	16.282	16.703	16.973	16.653	0.348
15	57.310	52.000	50.352	28.866	26.174	25.341	26.794	1.843
20	91.308	95.138	85.505	46.149	47.986	43.140	45.758	2.446
30	111.630	129.093	127.242	56.764	65.425	64.402	62.197	4.733
45	124.255	139.312	134.560	63.634	71.175	68.691	67.833	3.843
60	152.906	162.820	143.965	78.577	83.616	74.057	78.750	4.782
90	149.846	168.436	169.396	77.812	87.235	87.471	84.173	5.510
120	140.488	133.174	187.598	73.883	70.460	97.403	80.582	14.668
180	153.121	125.444	139.100	80.900	67.264	74.130	74.098	6.818
240	140.496	114.312	124.345	75.355	62.328	67.458	68.381	6.562

Table A-54

USP II dissolution data of MDS capsule in FaSSGF pH 2.

Time	Vessel Conc. (μg mL^{-1})			Cumulative % Dissoved				
(min)	No. 1	No. 2	No. 3	No. 1	No. 2	No. 3	Mean	SD
0	0.000	0.000	0.000	0.000	0.000	0.000	0.000	0.000
5	0.141	0.013	0.468	0.070	0.006	0.216	0.097	0.108
10	15.913	5.923	8.242	7.897	2.768	3.809	4.825	2.711
15	23.208	12.272	19.340	11.596	5.762	8.974	8.778	2.922
20	36.391	17.032	26.792	18.253	8.044	12.506	12.934	5.118
30	33.972	23.272	33.014	17.233	11.039	15.504	14.592	3.196
45	36.413	28.010	36.997	18.613	13.362	17.496	16.491	2.766
60	39.550	28.995	32.715	20.351	13.953	15.689	16.664	3.308
90	37.836	27.776	35.930	19.696	13.519	17.325	16.847	3.116
120	52.123	28.961	38.204	26.974	14.203	18.541	19.906	6.494
180	43.009	32.269	41.722	22.710	15.884	20.343	19.645	3.466
240	30.403	26.878	27.722	16.667	13.515	14.069	14.751	1.683

Table A-55

USP II dissolution data of E5(80) solution in FaSSIF-V2(PO_4).

Time	Vessel Conc. (µg mL^{-1})			Cumulative % Dissoved				
(min)	No. 1	No. 2	No. 3	No. 1	No. 2	No. 3	Mean	SD
0	0.000	0.000	0.000	0.000	0.000	0.000	0.000	0.000
5	74.781	76.545	78.882	74.781	76.545	78.882	76.736	2.057
10	75.930	80.609	83.402	76.677	81.374	84.191	80.748	3.796
15	76.455	81.161	82.459	77.962	82.733	84.081	81.592	3.215
20	76.216	80.850	83.510	78.488	83.233	85.957	82.560	3.780
30	77.720	80.937	85.896	80.754	84.128	89.178	84.687	4.240
45	73.964	78.392	82.841	77.775	82.394	86.983	82.384	4.604
60	74.175	78.210	83.205	78.726	82.995	88.175	83.299	4.732
90	74.199	77.708	81.890	79.491	83.275	87.692	83.486	4.104
120	73.413	75.329	79.770	79.447	81.673	86.391	82.504	3.545
180	71.665	71.401	78.372	78.434	78.499	85.791	80.908	4.229
240	70.446	72.923	75.927	77.931	80.734	84.130	80.932	3.104

Table A-56

USP II dissolution data of E5(80) capsule in FaSSIF-V2(PO_4).

Time	Vessel Conc. (µg mL^{-1})			Cumulative % Dissoved				
(min)	No. 1	No. 2	No. 3	No. 1	No. 2	No. 3	Mean	SD
0	0.000	0.000	0.000	0.000	0.000	0.000	0.000	0.000
5	5.837	19.621	7.319	5.806	19.539	7.329	10.891	7.528
10	16.590	13.278	15.859	16.559	13.418	15.955	15.311	1.667
15	8.771	47.757	11.823	8.947	47.885	12.072	22.968	21.635
20	18.375	45.026	18.591	18.587	45.641	18.967	27.732	15.511
30	28.669	48.952	27.019	29.008	49.999	27.594	35.533	12.547
45	42.998	58.624	42.481	43.546	60.118	43.348	49.004	9.625
60	58.034	65.722	57.075	58.928	67.770	58.388	61.696	5.268
90	62.479	68.838	63.177	63.926	71.527	65.070	66.841	4.098
120	67.394	67.945	63.874	69.437	71.323	66.400	69.053	2.484
180	66.180	68.361	67.956	68.899	72.414	71.128	70.814	1.778
240	62.444	67.473	63.236	65.842	72.211	67.081	68.378	3.377

Table A-57

USP II dissolution data of E5(20) capsule in FaSSIF-V2(PO_4).

Time	Vessel Conc. (μg mL^{-1})			Cumulative % Dissoved				
(min)	No. 1	No. 2	No. 3	No. 1	No. 2	No. 3	Mean	SD
0	0.000	0.000	0.000	0.000	0.000	0.000	0.000	0.000
5	4.126	7.294	7.711	4.131	7.291	7.717	6.380	1.959
10	14.084	12.866	16.792	14.142	12.934	16.883	14.653	2.023
15	17.418	19.538	24.946	17.622	19.732	25.211	20.855	3.917
20	23.420	25.306	29.574	23.805	25.693	30.093	26.530	3.226
30	34.940	44.764	42.979	35.573	45.396	43.804	41.591	5.272
45	46.713	56.087	63.174	47.710	57.162	64.446	56.439	8.391
60	53.792	61.451	65.035	55.265	63.084	66.941	61.763	5.949
90	62.578	54.364	64.990	64.600	56.614	67.546	62.920	5.656
120	60.382	62.557	54.742	63.028	65.348	57.941	62.106	3.789
180	55.155	56.960	52.893	58.399	60.379	56.638	58.472	1.872
240	49.664	43.980	49.208	53.454	47.973	53.479	51.636	3.172

Table A-58

USP II dissolution data of MDS capsule in FaSSIF-V2(PO_4).

Time	Vessel Conc. (μg mL^{-1})			Cumulative % Dissoved				
(min)	No. 1	No. 2	No. 3	No. 1	No. 2	No. 3	Mean	SD
0	0.000	0.000	0.000	0.000	0.000	0.000	0.000	0.000
5	-0.602	0.103	0.943	-0.577	0.096	0.927	0.149	0.753
10	0.792	3.345	4.623	0.753	3.114	4.554	2.807	1.919
15	3.393	5.887	7.068	3.251	5.511	7.003	5.255	1.889
20	5.690	7.680	8.568	5.484	7.235	8.547	7.089	1.537
30	8.728	10.699	10.794	8.449	10.116	10.820	9.795	1.218
45	11.587	12.780	11.685	11.271	12.153	11.802	11.742	0.444
60	12.236	13.516	12.629	12.004	12.957	12.845	12.602	0.521
90	12.908	14.423	13.372	12.764	13.927	13.699	13.463	0.616
120	12.762	14.100	13.317	12.748	13.760	13.777	13.428	0.589
180	12.928	14.767	12.969	13.030	14.512	13.566	13.702	0.751
240	13.188	14.612	14.387	13.402	14.505	15.088	14.332	0.856

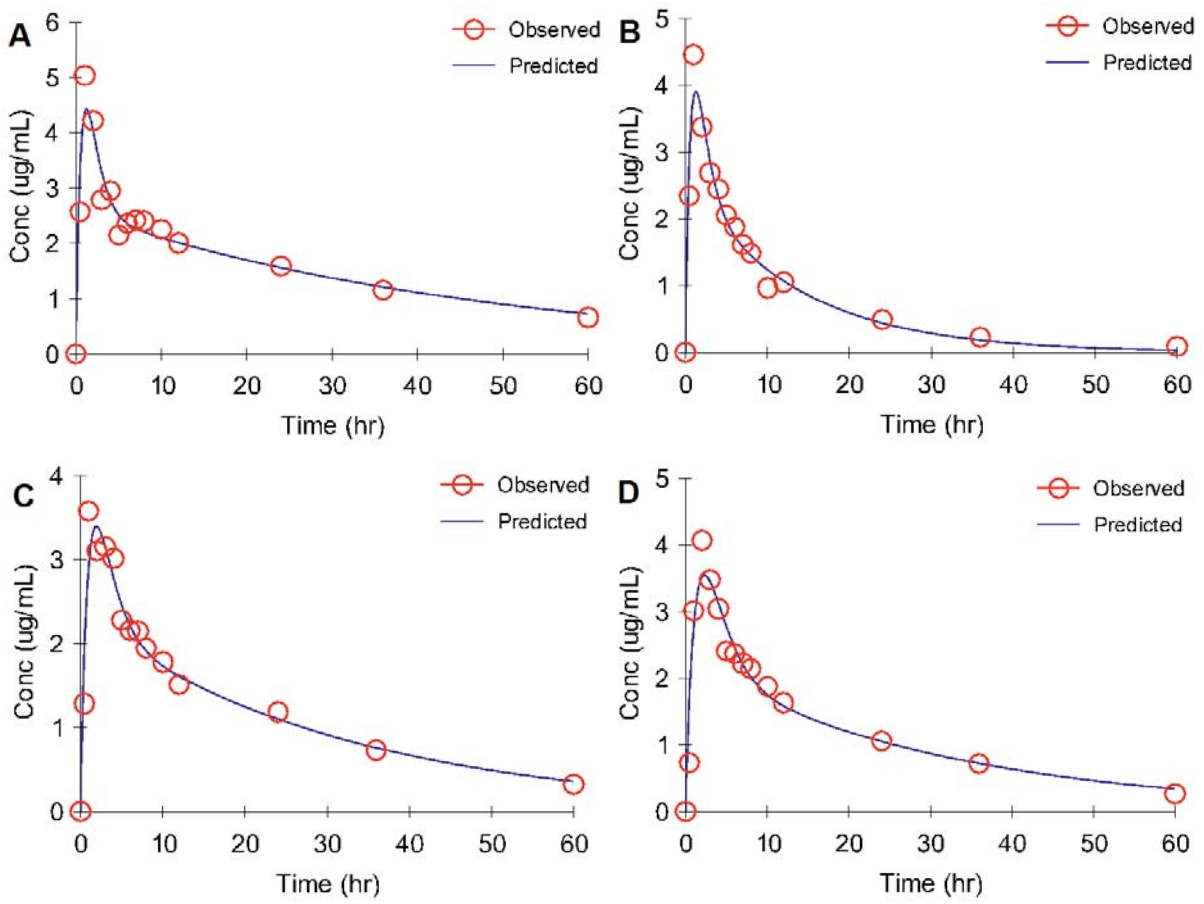

Fig. A-3. Individual *in vivo* and WinNonlin® plasma profiles of the E5(80) solution.

Table A-59

Individual PK parameters of *in vivo* profiles of the E5(80) solution using WinNonlin®.

Subject	A	B	C	D	Mean[a] ± S.D.
Model	11	11	11	11	11
V/F (mL)	4817.0	5516.7	6551.8	5978.4	5716.0 ± 733.8
k_a (h^{-1})	1.0447	1.0182	0.7049	0.5512	0.8298 ± 0.2415
AUC (μg mL^{-1} h)	126.25	38.85	78.64	77.37	80.28 ± 35.78
Cl/F (mL h^{-1})	377.9	1228.0	606.6	616.5	707.2 ± 364.3
In silico T_{max} (h)	1.27	1.30	1.98	2.37	1.73 ± 0.54
In silico C_{max} (μg mL^{-1})	4.42	3.91	3.40	3.54	3.82 ± 0.46
Correlation	0.9630	0.9795	0.9657	0.9614	–

Table A-60

Equation code of STELLA®-based simulation for LBF E5(80) solution in fasted state:

```
Dissolved_stom(t) = Dissolved_stom(t - dt) + (Dissolution_stom - Liquid_emptying) *
dt
INIT Dissolved_stom = 0
INFLOWS:
Dissolution_stom = IF(Dose)>0 AND(Dissolved_stom/vfluid)<(33.872/240)
THEN(9.4565*240*((Dose)^(2/3))*(33.872/240-Dissolved_stom/vfluid)) ELSE(0)
OUTFLOWS:
Liquid_emptying = IF(Dissolved_stom)>0 AND(vfluid)>0
THEN(Dissolved_stom)*2.8 ELSE(0)
Dose(t) = Dose(t - dt) + (- Dissolution_stom - Formulation_emptying) * dt
INIT Dose = 47.704
OUTFLOWS:
Dissolution_stom = IF(Dose)>0 AND(Dissolved_stom/vfluid)<(33.872/240)
THEN(9.4565*240*((Dose)^(2/3))*(33.872/240-Dissolved_stom/vfluid)) ELSE(0)
Formulation_emptying = IF(Dose)>0 AND(vfluid)>0    THEN(Dose)*2.8 ELSE(0)
Formulation_si(t) = Formulation_si(t - dt) + (Formulation_emptying - Dissolution_si)
* dt
INIT Formulation_si = 0
INFLOWS:
Formulation_emptying = IF(Dose)>0 AND(vfluid)>0    THEN(Dose)*2.8 ELSE(0)
OUTFLOWS:
Dissolution_si = IF(Formulation_si)>0
THEN(7.5276*((Formulation_si)^(2/3))*(31.216-GI_lumen)) ELSE(0)
GI_lumen(t) = GI_lumen(t - dt) + (Dissolution_si + Liquid_emptying - Absorption) *
dt
INIT GI_lumen = 0
INFLOWS:
Dissolution_si = IF(Formulation_si)>0
```

Table A-60 (*Continued*)

THEN(7.5276*((Formulation_si)^(2/3))*(31.216-GI_lumen)) ELSE(0)

Liquid_emptying = IF(Dissolved_stom)>0 AND(vfluid)>0

THEN(Dissolved_stom)*2.8 ELSE(0)

OUTFLOWS:

Absorption = GI_lumen

Periphery(t) = Periphery(t - dt) + (K12 - K21) * dt

INIT Periphery = 0

INFLOWS:

K12 = Plasma*0.4804

OUTFLOWS:

K21 = Periphery*0.2541

Plasma(t) = Plasma(t - dt) + (Absorption + K21 - K12 - K10) * dt

INIT Plasma = 0

INFLOWS:

Absorption = GI_lumen

K21 = Periphery*0.2541

OUTFLOWS:

K12 = Plasma*0.4804

K10 = Plasma*0.1242

vfluid(t) = vfluid(t - dt) + (- vfge) * dt

INIT vfluid = 240

OUTFLOWS:

vfge = IF(vfluid)>0 THEN(vfluid)*2.8 ELSE(0)

Plasma_con = 1000*Plasma/vcf

vcf = 5715.9932

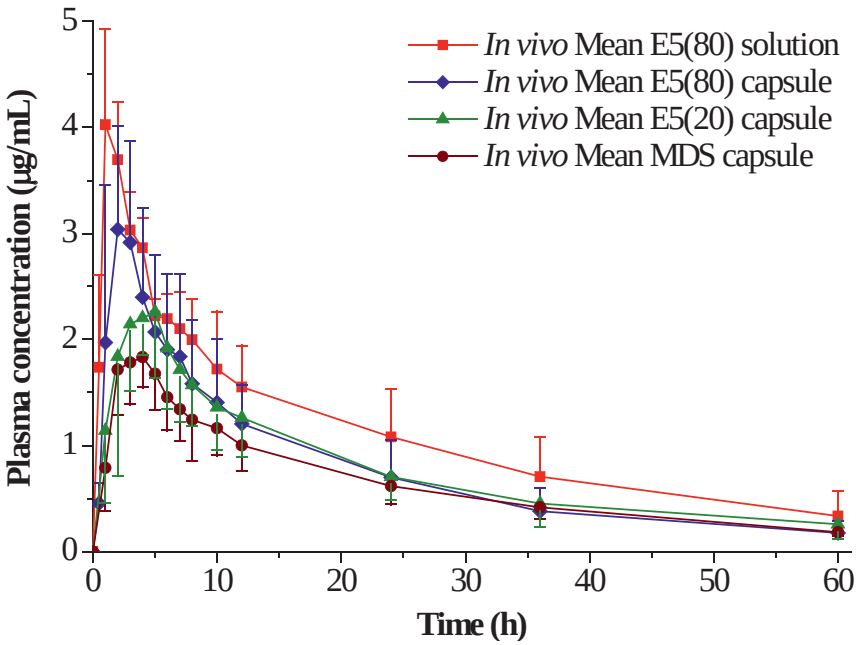

Fig. A-4. *In vivo* mean data of plasma fenofibric acid concentration profiles of three fenofibrate SMEDDS formulations and MDS in the fasted state (n = 4).

Table A-61

Deconvoluted PK parameters using mean data of Fig. A-4 and Winnonlin® software:

Formulation	E5(80) solution	E5(80) capsule	E5(20) capsule	MDS capsule
V/F (mL)	5784.29	7312.00	9518.36	11955.47
k_{01} (h^{-1})	0.8109	0.7693	0.3774	0.3659
k_{10} (h^{-1})	0.1077	0.1343	0.0939	0.0884
k_{12} (h^{-1})	0.4798	0.4083	0.1949	0.1954
k_{21} (h^{-1})	0.2472	0.2741	0.1250	0.1255
$AUC_{0\text{-inf}}$ (µg mL^{-1} h)	76.54	48.56	53.37	45.08
Cl/F (mL h^{-1})	623.1	982.2	893.7	1058.0
T_{max} (h)	1.66	2.19	3.64	3.51
C_{max} (µg mL^{-1})	3.74	3.00	2.20	1.74

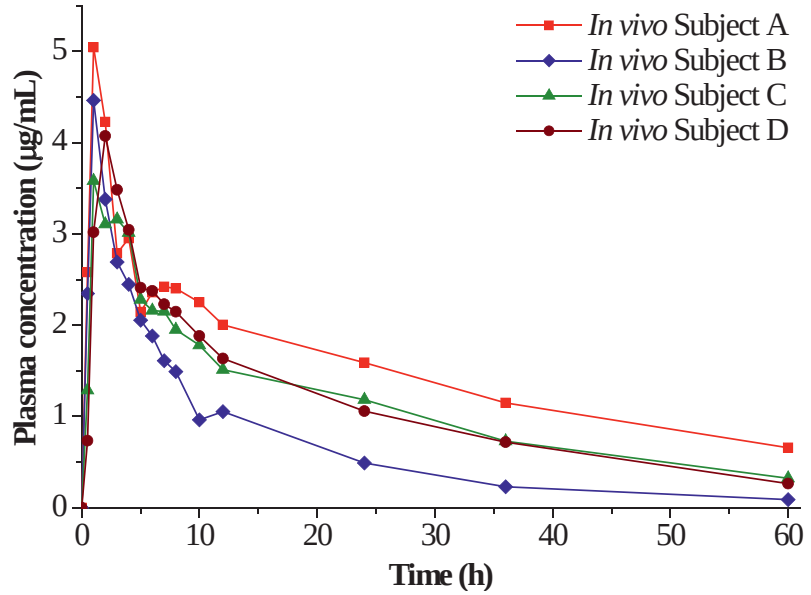

Fig. A-5. *In vivo* plasma fenofibric acid concentration profiles of E5(80) solution in four individual subjects.

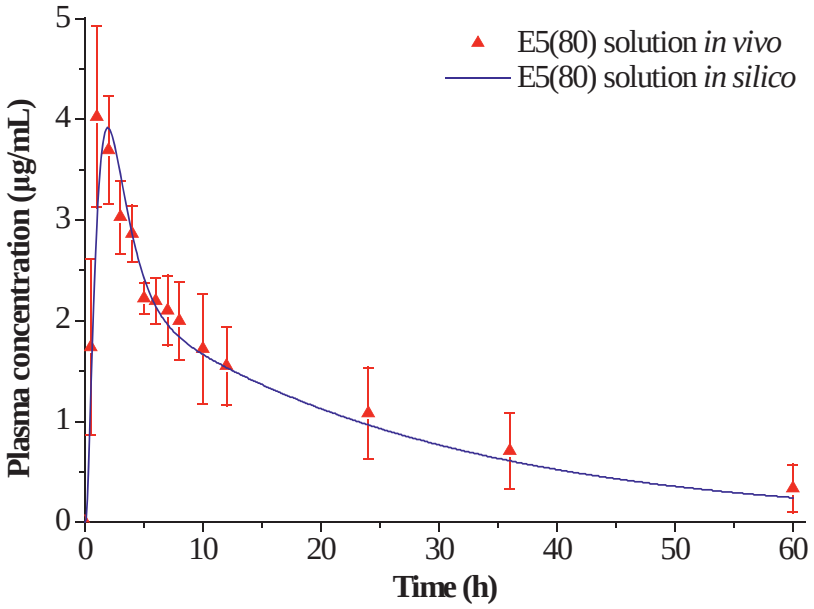

Fig. A-6. Simulated plasma fenofibric acid concentration profiles of E5(80) solution.

Table A-62

Comparison of PK parameters of E5(80) solution:

	$AUC_{0\text{-inf}}$ (µg mL^{-1} h)	Ratio	C_{max} (µg mL^{-1})	Ratio	T_{max} (h)	Ratio	f_2
in silico	70.51	0.90	3.92	0.91	1.90	1.52	52.78
in vivo	78.31	–	4.29	–	1.25	–	–

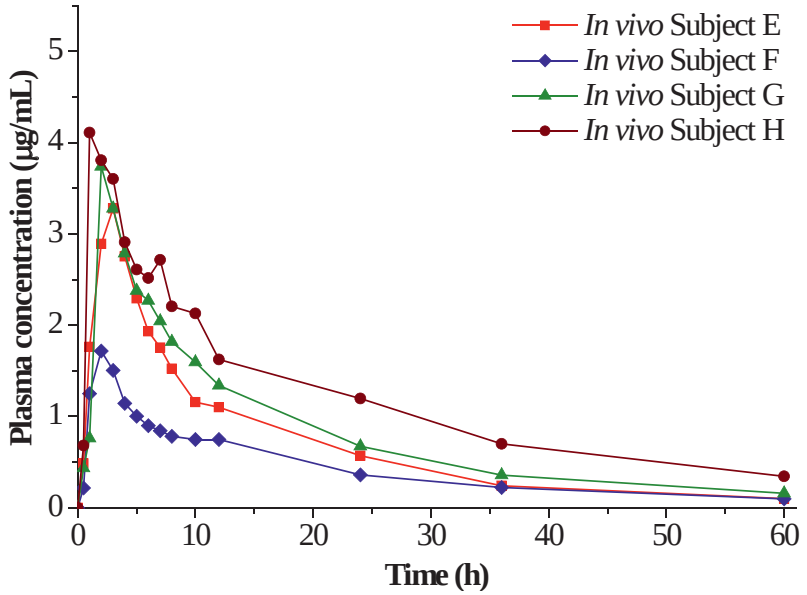

Fig. A-7. *In vivo* plasma fenofibric acid concentration profiles of E5(80) capsule in four individual subjects.

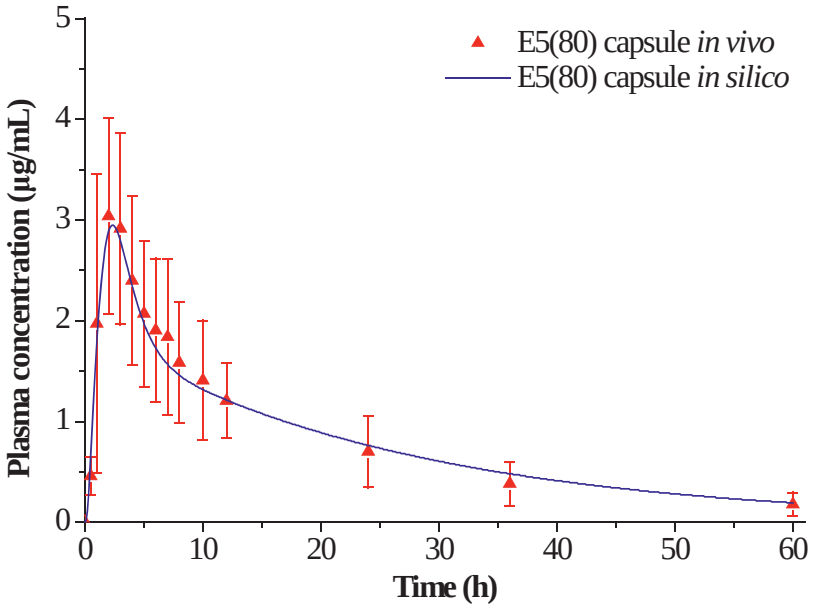

Fig. A-8. Simulated plasma fenofibric acid concentration profiles of E5(80) capsule.

Table A-63

Comparison of PK parameters of E5(80) capsule:

	$AUC_{0\text{-inf}}$ (µg mL^{-1} h)	Ratio	C_{max} (µg mL^{-1})	Ratio	T_{max} (h)	Ratio	f_2
in silico	53.66	1.04	2.95	0.92	2.35	1.18	66.28
in vivo	51.66	–	3.21	–	2.00	–	–

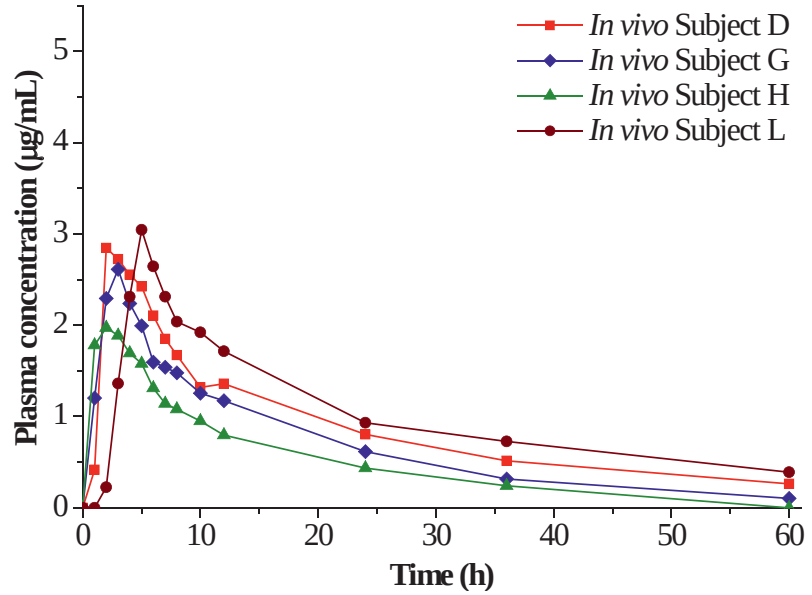

Fig. A-9. *In vivo* plasma fenofibric acid concentration profiles of E5(20) capsule in four individual subjects.

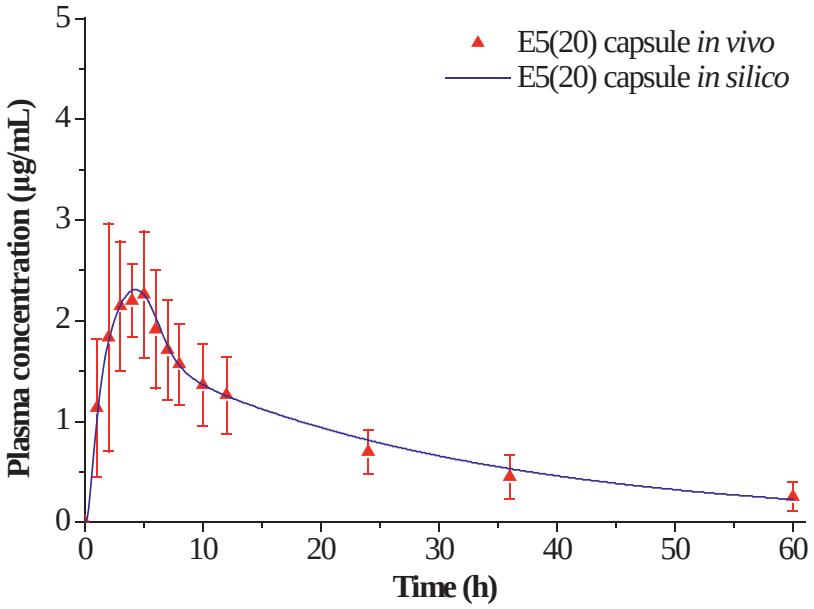

Fig. A-10. Simulated plasma fenofibric acid concentration profiles of E5(20) capsule.

Table A-64

Comparison of PK parameters of E5(20) capsule:

	$AUC_{0\text{-inf}}$ (µg mL^{-1} h)	Ratio	C_{max} (µg mL^{-1})	Ratio	T_{max} (h)	Ratio	f_2
in silico	56.75	1.08	2.31	0.88	4.25	1.42	74.40
in vivo	52.66	–	2.62	–	3.00	–	–

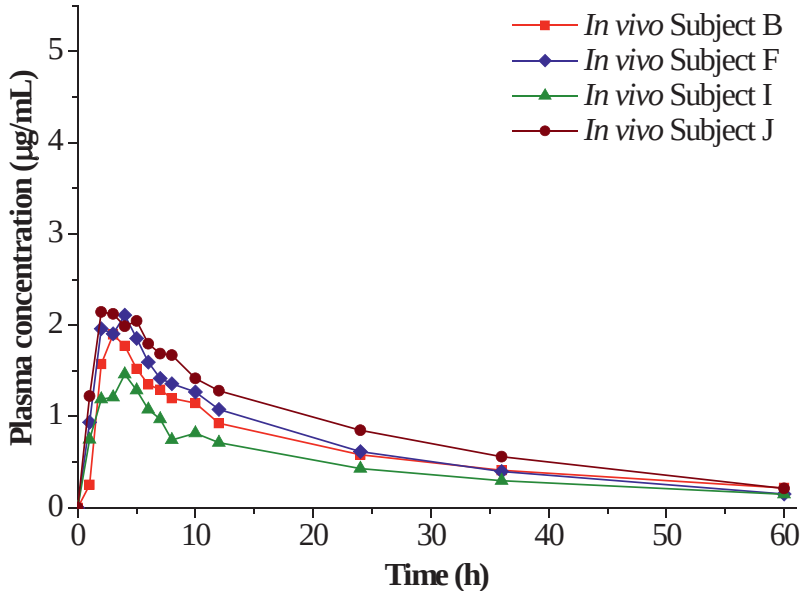

Fig. A-11. *In vivo* plasma fenofibric acid concentration profiles of MDS capsule in four individual subjects.

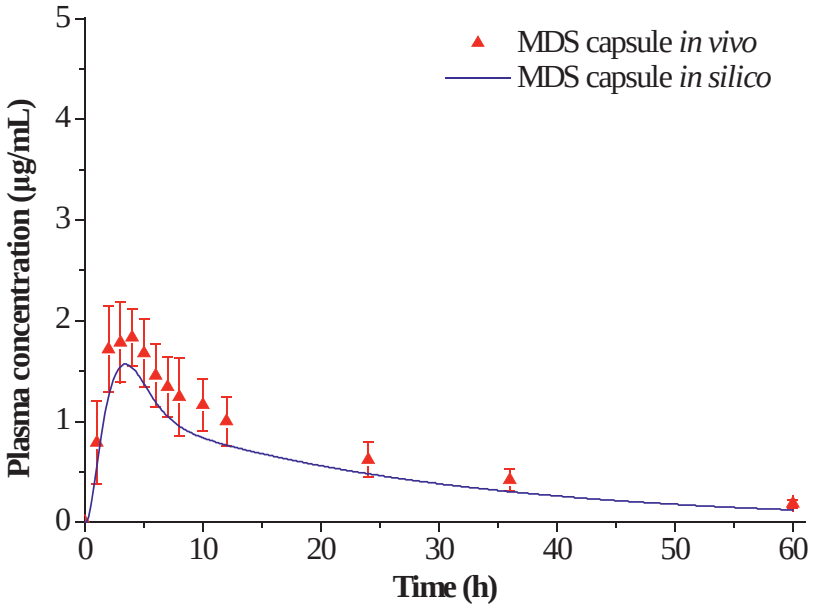

Fig. A-12. Simulated plasma fenofibric acid concentration profiles of MDS capsule.

Table A-65

Comparison of PK parameters of MDS capsule:

	$AUC_{0\text{-inf}}$ (µg mL^{-1} h)	Ratio	C_{max} (µg mL^{-1})	Ratio	T_{max} (h)	Ratio	f_2
in silico	33.31	0.75	1.57	0.83	3.40	1.05	41.37
in vivo	44.52	–	1.90	–	3.25	–	–

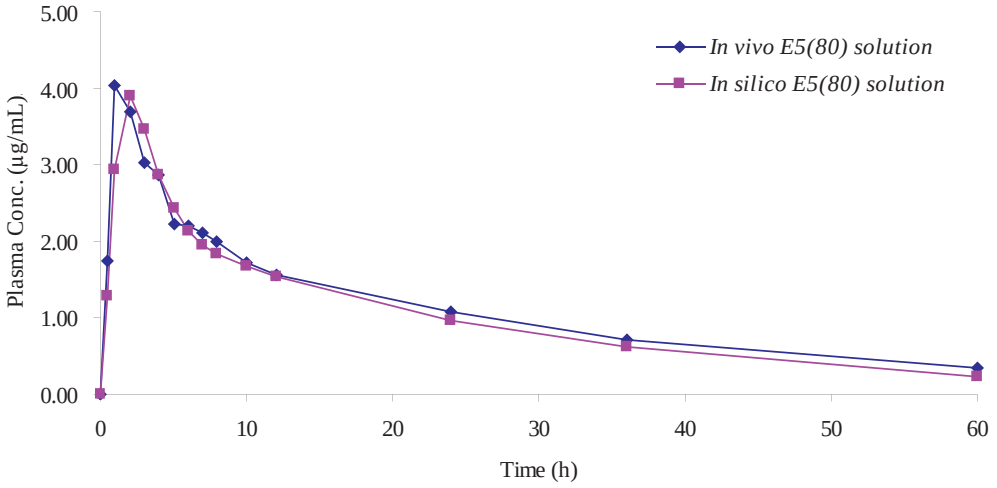

Fig. A-13. Observed & simulated plasma fenofibric acid profiles of E5(80) solution.

Table A-66

Estimation of similarity factor (f_2) between *in vivo* & *in silico* data of E5(80) solution.

Time (h)	*in vivo* R_t Plasma con. (µg mL^{-1})	*in silico* T_t Plasma con. (µg mL^{-1})	*in vivo* R_t % Fraction	*in silico* T_t % Fraction	$\|R_t-T_t\|$ % Fraction
0	0.0000	0.00	0.000	0.0	0.0
0.5	1.7370	1.29	43.148	32.0	11.1
1	4.0256	2.94	100.000	73.0	27.0
2	3.6957	3.91	91.804	97.1	5.3
3	3.0299	3.46	75.267	85.9	10.7
4	2.8647	2.86	71.162	71.0	0.1
5	2.2225	2.43	55.208	60.4	5.2
6	2.1951	2.14	54.530	53.2	1.4
7	2.1026	1.96	52.230	48.7	3.5
8	1.9972	1.84	49.612	45.7	3.9
10	1.7195	1.67	42.713	41.5	1.2
12	1.5515	1.53	38.542	38.0	0.5
24	1.0816	0.97	26.868	24.1	2.8
36	0.7073	0.61	17.571	15.2	2.4
60	0.3348	0.24	8.316	6.0	2.4
n=14					f_2=52.78

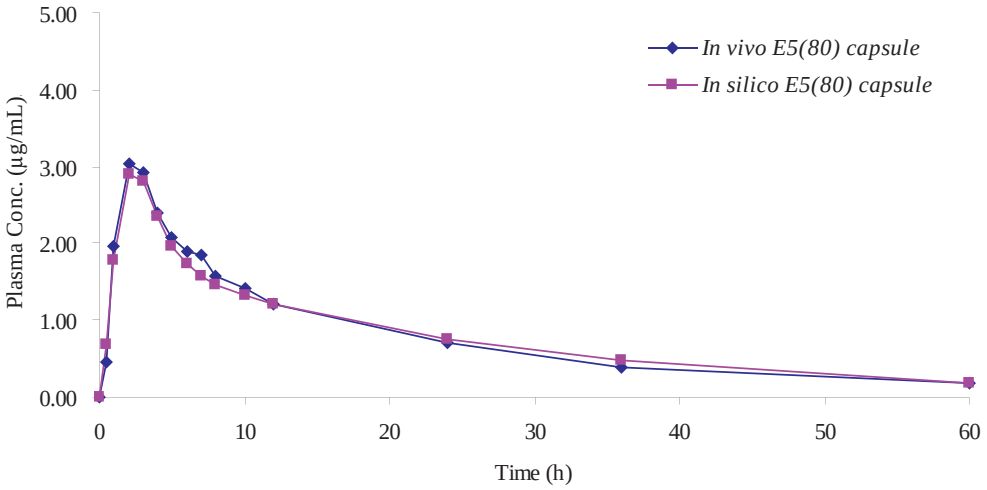

Fig. A-14. Observed & simulated plasma fenofibric acid profiles of E5(80) capsule.

Table A-67

Estimation of similarity factor (f_2) between *in vivo* & *in silico* data of E5(80) capsule.

Time (h)	*in vivo* R_t Plasma con. (µg mL^{-1})	*in silico* T_t Plasma con. (µg mL^{-1})	*in vivo* R_t % Fraction	*in silico* T_t % Fraction	$\|R_t$-$T_t\|$ % Fraction
0	0.0000	0.00	0.000	0.0	0.0
0.5	0.4555	0.69	14.997	22.7	7.7
1	1.9716	1.79	64.911	58.9	6.0
2	3.0374	2.89	100.000	95.1	4.9
3	2.9162	2.80	96.011	92.2	3.8
4	2.3990	2.35	78.981	77.4	1.6
5	2.0711	1.97	68.185	64.9	3.3
6	1.9042	1.73	62.692	57.0	5.7
7	1.8397	1.57	60.569	51.7	8.9
8	1.5833	1.46	52.126	48.1	4.1
10	1.4074	1.32	46.337	43.5	2.9
12	1.2038	1.21	39.632	39.8	0.2
24	0.7008	0.76	23.074	25.0	1.9
36	0.3803	0.48	12.522	15.8	3.3
60	0.1756	0.19	5.780	6.3	0.5
n=14					f_2=66.28

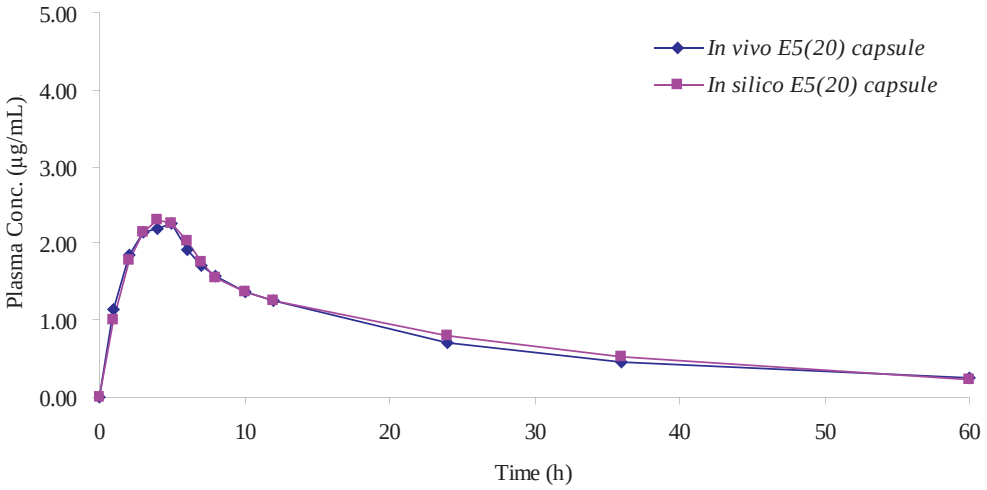

Fig. A-15. Observed & simulated plasma fenofibric acid profiles of E5(20) capsule.

Table A-68

Estimation of similarity factor (f_2) between *in vivo* & *in silico* data of E5(20) capsule.

Time (h)	*in vivo* R_t Plasma con. (µg mL^{-1})	*in silico* T_t Plasma con. (µg mL^{-1})	*in vivo* R_t % Fraction	*in silico* T_t % Fraction	$\|R_t-T_t\|$ % Fraction
0	0.0000	0.00	0.000	0.0	0.0
1	1.1417	1.00	50.538	44.3	6.3
2	1.8381	1.79	81.362	79.2	2.1
3	2.1457	2.15	94.982	95.2	0.2
4	2.2024	2.30	97.491	101.8	4.3
5	2.2591	2.26	100.000	100.0	0.0
6	1.9190	2.03	84.947	89.9	4.9
7	1.7166	1.75	75.986	77.5	1.5
8	1.5709	1.56	69.534	69.1	0.5
10	1.3603	1.36	60.215	60.2	0.0
12	1.2632	1.25	55.914	55.3	0.6
24	0.7045	0.81	31.183	35.9	4.7
36	0.4534	0.53	20.072	23.5	3.4
60	0.2591	0.23	11.470	10.2	1.3
n=13					f_2=74.40

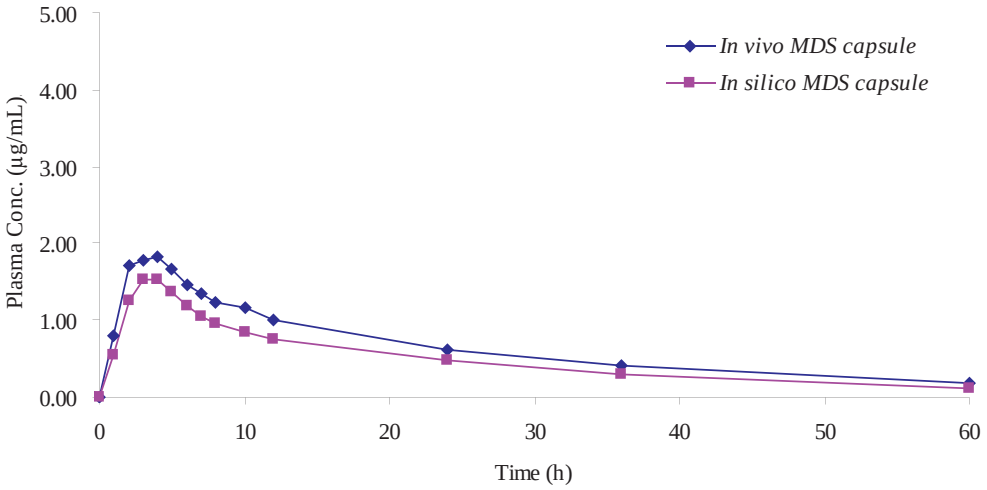

Fig. A-16. Observed & simulated plasma fenofibric acid profiles of MDS capsule.

Table A-69

Estimation of similarity factor (f_2) between *in vivo* & *in silico* data of MDS capsule.

Time (h)	*in vivo* R_t Plasma con. (µg mL^{-1})	*in silico* T_t Plasma con. (µg mL^{-1})	*in vivo* R_t % Fraction	*in silico* T_t % Fraction	$\|R_t$-$T_t\|$ % Fraction
0	0.0000	0.00	0.000	0.0	0.0
1	0.7896	0.55	43.069	30.0	13.1
2	1.7169	1.25	93.644	68.2	25.5
3	1.7845	1.54	97.330	84.0	13.3
4	1.8334	1.53	99.997	83.5	16.5
5	1.6780	1.37	91.525	74.7	16.8
6	1.4551	1.19	79.368	64.9	14.5
7	1.3416	1.05	73.173	57.3	15.9
8	1.2435	0.95	67.826	51.8	16.0
10	1.1633	0.84	63.448	45.8	17.6
12	1.0005	0.76	54.571	41.5	13.1
24	0.6188	0.48	33.749	26.2	7.6
36	0.4176	0.30	22.776	16.4	6.4
60	0.1824	0.12	9.950	6.5	3.4
n=13					f_2=41.37

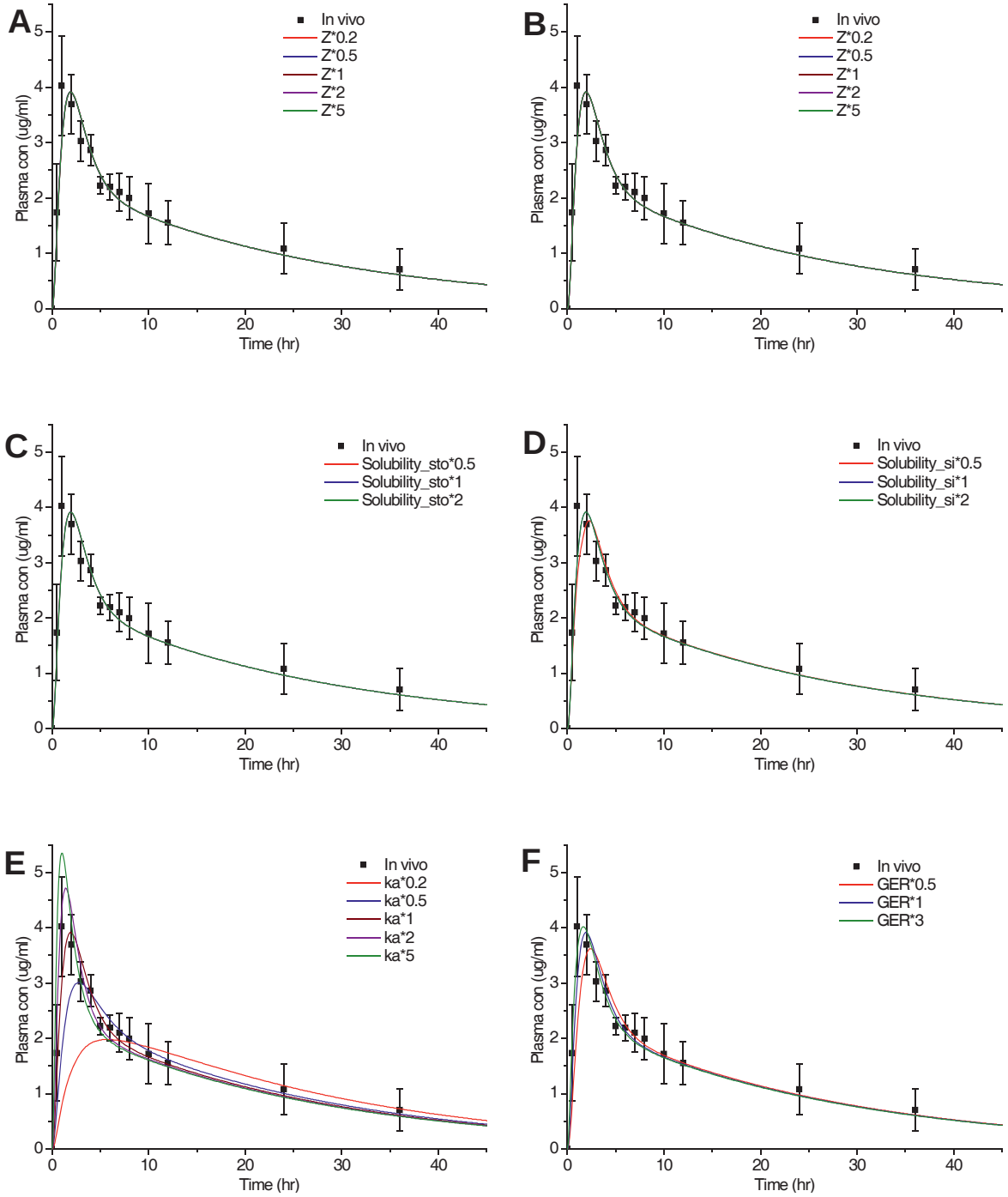

Fig. A-17. Detailed sensitivity analysis of LBF E5(80) solution in the fasted state: (A) dissolution rate in stomach (0.2–5 fold), (B) dissolution rate in small intestine (0.2–5 fold), (C) solubility in gastric fluid (0.5–2 fold), (D) solubility in intestinal fluid (0.5–2 fold), (E) absorption rate (0.2–5 fold), (F) gastric emptying rate (0.5–3 fold).

Note: Some profiles are on top of each other, so that the individual profiles cannot be seen clearly (i.e. Fig. A-17A, B, C & D).

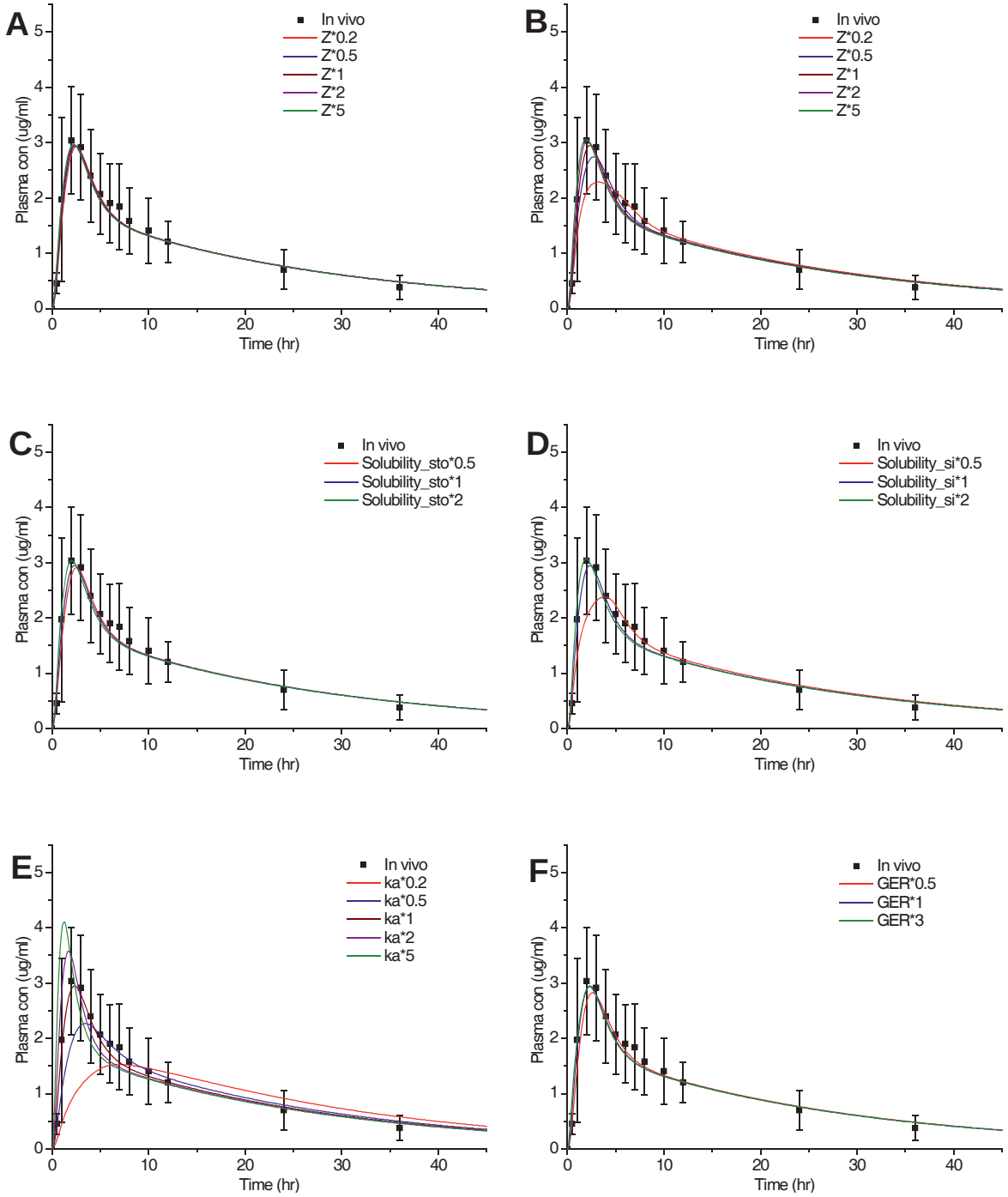

Fig. A-18. Detailed sensitivity analysis of LBF E5(80) capsule in the fasted state: (A) dissolution rate in stomach (0.2–5 fold), (B) dissolution rate in small intestine (0.2–5 fold), (C) solubility in gastric fluid (0.5–2 fold), (D) solubility in intestinal fluid (0.5–2 fold), (E) absorption rate (0.2–5 fold), (F) gastric emptying rate (0.5–3 fold).

Note: Some profiles are on top of each other, so that the individual profiles cannot be seen clearly (i.e. Fig. A-18A, C & F).

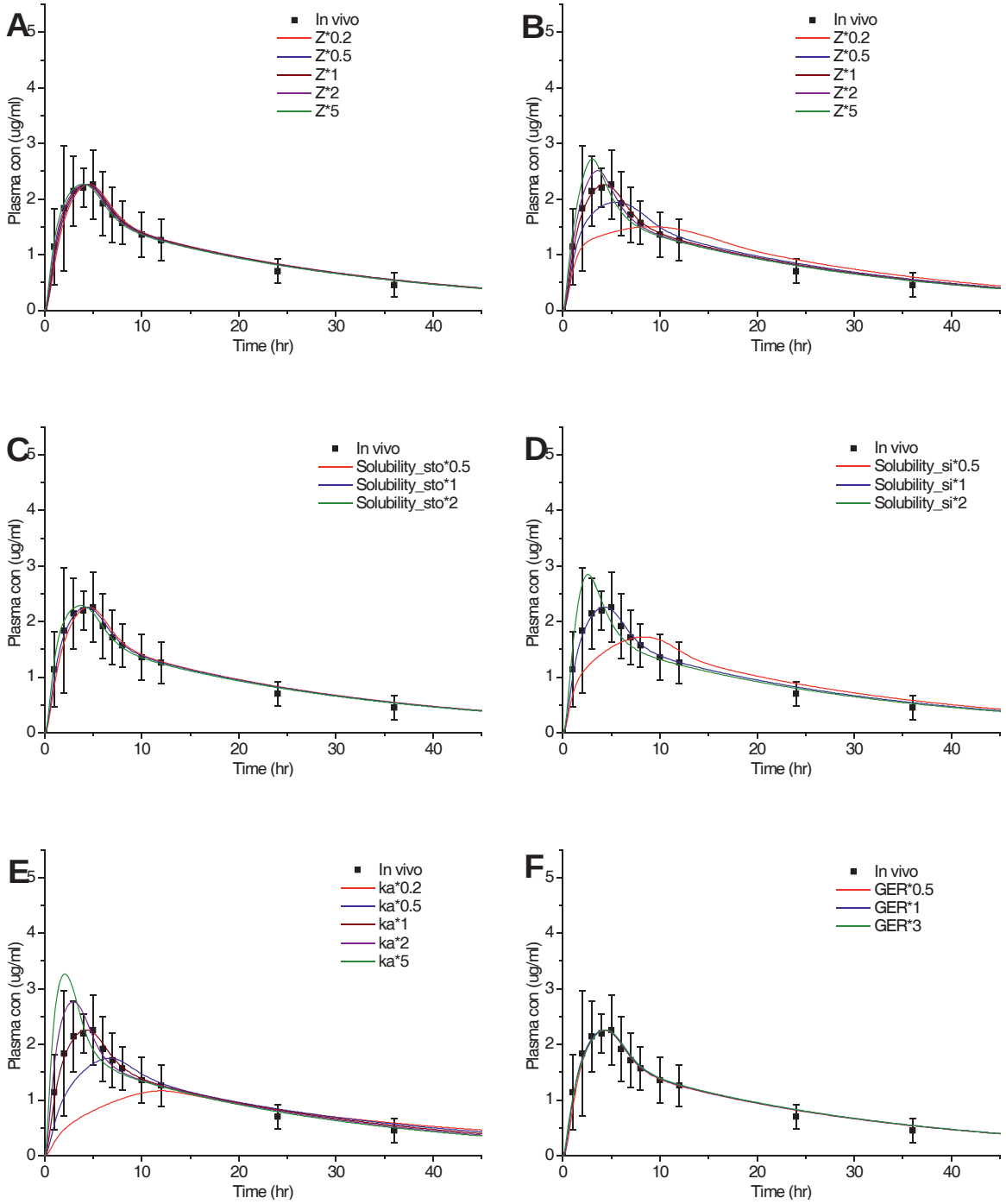

Fig. A-19. Detailed sensitivity analysis of LBF E5(20) capsule in the fasted state: (A) dissolution rate in stomach (0.2–5 fold), (B) dissolution rate in small intestine (0.2–5 fold), (C) solubility in gastric fluid (0.5–2 fold), (D) solubility in intestinal fluid (0.5–2 fold), (E) absorption rate (0.2–5 fold), (F) gastric emptying rate (0.5–3 fold).

Note: Some profiles are on top of each other, so that the individual profiles cannot be seen clearly (i.e. Fig. A-19A, C & F).

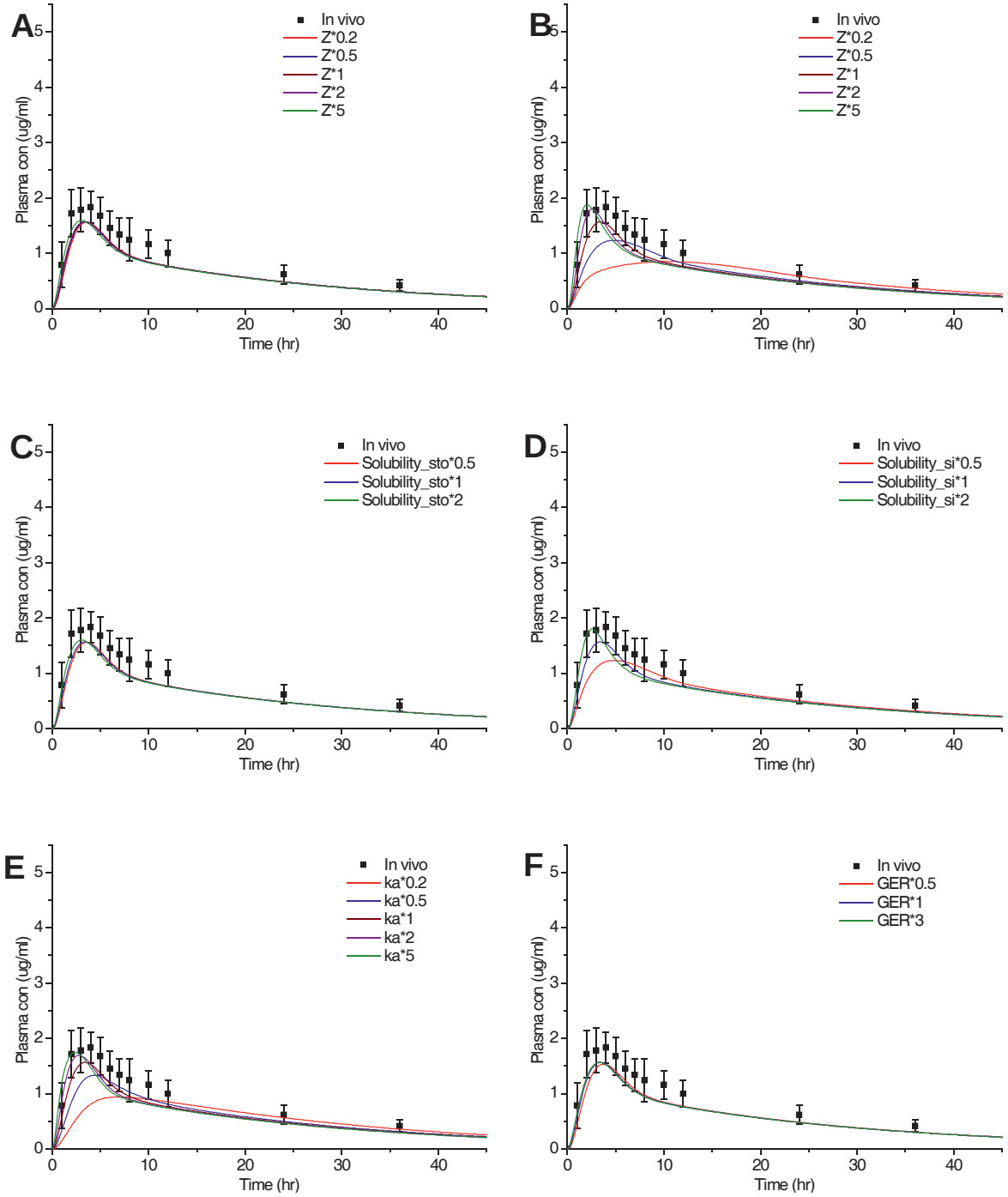

Fig. A-20. Detailed sensitivity analysis of LBF MDS capsule in the fasted state: (A) dissolution rate in stomach (0.2–5 fold), (B) dissolution rate in small intestine (0.2–5 fold), (C) solubility in gastric fluid (0.5–2 fold), (D) solubility in intestinal fluid (0.5–2 fold), (E) absorption rate (0.2–5 fold), (F) gastric emptying rate (0.5–3 fold).

Note: Some profiles are on top of each other, so that the individual profiles cannot be seen clearly (i.e. Fig. A-20A, C & F).

Table A-70

USP II dissolution data of E5(80) solution in FeSSGF.

Time	Vessel Conc. (µg mL^{-1})			Cumulative % Dissoved				
(min)	No. 1	No. 2	No. 3	No. 1	No. 2	No. 3	Mean	SD
0	0.000	0.000	0.000	0.000	0.000	0.000	0.000	0.000
5	80.269	78.045	50.860	89.188	86.716	56.511	77.472	18.194
10	90.249	90.190	74.058	101.169	101.079	82.852	95.033	10.549
15	92.590	94.382	77.731	104.772	106.738	87.756	99.755	10.438
20	91.756	94.042	77.012	104.874	107.410	87.820	100.035	10.654
30	91.557	92.428	77.075	105.673	106.660	88.746	100.360	10.070
45	90.931	92.250	77.059	105.994	107.489	89.585	101.023	9.934
60	89.643	90.693	76.577	105.574	106.785	89.905	100.755	9.415
90	89.457	89.416	74.557	106.363	106.374	88.512	100.416	10.310
120	88.941	89.290	74.802	106.783	107.227	89.613	101.208	10.044
180	88.040	89.654	74.108	106.771	108.624	89.672	101.689	10.448
240	87.668	87.837	74.093	107.336	107.601	90.479	101.805	9.810

Table A-71

USP II dissolution data of E5(80) capsule in FeSSGF.

Time	Vessel Conc. (µg mL^{-1})			Cumulative % Dissoved				
(min)	No. 1	No. 2	No. 3	No. 1	No. 2	No. 3	Mean	SD
0	0.000	0.000	0.000	0.000	0.000	0.000	0.000	0.000
5	1.845	5.689	9.010	1.804	5.660	8.921	5.462	3.563
10	7.086	14.544	14.014	6.947	14.526	13.964	11.812	4.223
15	19.654	22.875	20.724	19.307	22.958	20.747	21.004	1.839
20	28.452	33.161	28.592	28.102	33.418	28.742	30.088	2.902
30	41.667	52.944	45.867	41.304	53.429	46.129	46.954	6.104
45	68.677	74.788	91.570	68.124	75.686	91.834	78.548	12.111
60	90.329	88.315	95.894	89.969	89.888	97.022	92.293	4.096
90	94.376	91.731	94.830	94.810	94.164	96.917	95.297	1.440
120	93.222	91.724	93.957	94.605	95.070	96.992	95.556	1.265
180	92.996	90.774	92.993	95.296	95.038	96.968	95.767	1.048
240	91.932	89.989	92.623	95.164	95.159	97.522	95.948	1.363

Table A-72

USP II dissolution data of E5(20) capsule in FeSSGF.

Time	Vessel Conc. (μg mL^{-1})			Cumulative % Dissoved				
(min)	No. 1	No. 2	No. 3	No. 1	No. 2	No. 3	Mean	SD
0	0.000	0.000	0.000	0.000	0.000	0.000	0.000	0.000
5	5.845	4.509	8.154	5.842	4.499	8.086	6.142	1.812
10	26.240	26.153	22.059	26.283	26.135	21.956	24.791	2.457
15	40.951	34.207	41.799	41.247	34.431	41.750	39.143	4.088
20	48.791	36.881	60.684	49.491	37.440	60.893	49.275	11.728
30	60.476	45.968	76.125	61.658	46.873	76.806	61.779	14.967
45	86.134	77.870	83.841	87.904	79.157	85.214	84.092	4.480
60	86.407	91.736	88.240	89.038	93.767	90.407	91.071	2.433
90	87.376	93.536	86.745	90.870	96.478	89.800	92.382	3.587
120	85.849	92.307	86.853	90.217	96.185	90.767	92.389	3.298
180	86.589	92.309	85.859	91.814	97.108	90.642	93.188	3.445
240	85.223	90.967	86.266	91.315	96.690	91.897	93.301	2.950

Table A-73

USP II dissolution data of MDS capsule in FeSSGF.

Time	Vessel Conc. (μg mL^{-1})			Cumulative % Dissoved				
(min)	No. 1	No. 2	No. 3	No. 1	No. 2	No. 3	Mean	SD
0	0.000	0.000	0.000	0.000	0.000	0.000	0.000	0.000
5	1.539	1.904	0.373	1.463	1.827	0.340	1.210	0.775
10	5.471	10.213	2.341	5.215	9.820	2.133	5.723	3.868
15	9.392	15.157	4.877	8.994	14.662	4.462	9.373	5.111
20	11.702	18.343	7.374	11.280	17.865	6.778	11.974	5.576
30	15.553	21.673	10.331	15.051	21.237	9.535	15.275	5.854
45	20.591	25.479	15.426	19.989	25.098	14.264	19.783	5.420
60	25.421	30.073	20.408	24.776	29.751	18.937	24.488	5.413
90	27.803	32.453	23.491	27.281	32.324	21.927	27.177	5.199
120	27.626	32.421	25.084	27.377	32.605	23.590	27.857	4.526
180	28.369	33.028	25.331	28.346	33.499	24.043	28.629	4.734
240	29.439	33.623	26.461	29.633	34.386	25.302	29.774	4.544

Table A-74

USP II dissolution data of fenofibrate pure drug in FeSSGF.

Time	Vessel Conc. (µg mL^{-1})			Cumulative % Dissoved				
(min)	No. 1	No. 2	No. 3	No. 1	No. 2	No. 3	Mean	SD
0	0.000	0.000	0.000	0.000	0.000	0.000	0.000	0.000
5	0.348	0.327	0.099	0.346	0.328	0.097	0.257	0.139
10	0.627	0.709	0.464	0.627	0.715	0.456	0.599	0.132
15	1.030	0.930	0.714	1.033	0.944	0.706	0.894	0.169
20	1.417	1.235	1.022	1.428	1.260	1.015	1.234	0.208
30	2.224	2.062	2.166	2.245	2.102	2.146	2.165	0.073
45	3.428	3.086	3.297	3.464	3.151	3.276	3.297	0.157
60	4.659	4.190	4.569	4.721	4.291	4.556	4.522	0.217
90	6.785	6.771	6.978	6.881	6.925	6.962	6.922	0.041
120	8.550	9.132	9.524	8.703	9.362	9.526	9.197	0.436
180	10.171	13.924	13.923	10.400	14.265	13.933	12.866	2.142
240	11.740	18.447	18.377	12.060	18.946	18.436	16.481	3.837

Table A-75

USP II dissolution data of E5(80) solution in FeSSIF-V2.

Time	Vessel Conc. (µg mL^{-1})			Cumulative % Dissoved				
(min)	No. 1	No. 2	No. 3	No. 1	No. 2	No. 3	Mean	SD
0	0.000	0.000	0.000	0.000	0.000	0.000	0.000	0.000
5	98.687	88.447	82.330	109.652	98.275	91.478	99.802	9.183
10	96.447	89.134	82.506	108.260	100.020	92.588	100.290	7.840
15	96.265	87.917	81.365	109.129	99.659	92.237	100.342	8.466
20	95.548	86.565	81.219	109.403	99.133	92.979	100.505	8.297
30	94.921	87.126	79.812	109.767	100.719	92.318	100.934	8.727
45	93.044	85.696	78.481	108.736	100.098	91.726	100.187	8.505
60	92.530	85.501	79.393	109.199	100.833	93.611	101.214	7.801
90	91.700	84.505	77.714	109.304	100.677	92.628	100.870	8.340
120	91.610	82.599	76.988	110.224	99.497	92.685	100.802	8.842
180	89.341	82.139	76.088	108.720	99.905	92.540	100.388	8.101
240	87.829	80.706	75.312	108.034	99.225	92.523	99.927	7.779

Table A-76

USP II dissolution data of E5(80) capsule in FeSSIF-V2.

Time	Vessel Conc. (μg mL^{-1})			Cumulative % Dissoved				
(min)	No. 1	No. 2	No. 3	No. 1	No. 2	No. 3	Mean	SD
0	0.000	0.000	0.000	0.000	0.000	0.000	0.000	0.000
5	5.282	2.250	8.849	5.255	2.250	8.671	5.392	3.213
10	16.779	12.129	22.645	16.745	12.151	22.275	17.057	5.069
15	29.038	23.860	33.712	29.108	24.004	33.340	28.817	4.675
20	41.807	37.063	42.835	42.100	37.445	42.609	40.718	2.846
30	59.974	57.522	58.885	60.589	58.275	58.755	59.206	1.221
45	83.673	89.335	88.549	84.761	90.664	88.397	87.941	2.978
60	99.625	94.471	95.679	101.463	96.692	96.251	98.135	2.890
90	95.189	92.840	97.584	98.041	96.006	99.055	97.701	1.553
120	95.444	96.377	95.978	99.242	100.472	98.438	99.384	1.024
180	98.574	95.316	97.528	103.305	100.374	100.897	101.525	1.563
240	95.046	98.063	93.591	100.776	104.074	97.995	100.948	3.043

Table A-77

USP II dissolution data of E5(20) capsule in FeSSIF-V2.

Time	Vessel Conc. (μg mL^{-1})			Cumulative % Dissoved				
(min)	No. 1	No. 2	No. 3	No. 1	No. 2	No. 3	Mean	SD
0	0.000	0.000	0.000	0.000	0.000	0.000	0.000	0.000
5	23.154	8.774	6.317	22.776	8.632	6.204	12.537	8.950
10	24.798	29.310	33.609	24.621	28.924	33.070	28.872	4.225
15	34.178	39.148	42.952	34.092	38.891	42.576	38.520	4.254
20	40.595	48.332	48.484	40.740	48.312	48.431	45.828	4.407
30	56.093	67.737	60.097	56.384	67.879	60.313	61.525	5.843
45	69.643	76.302	67.439	70.264	76.973	68.114	71.784	4.621
60	80.296	79.311	76.586	81.429	80.684	77.760	79.958	1.939
90	81.264	85.016	73.174	83.171	87.077	75.161	81.803	6.075
120	81.540	82.641	75.906	84.242	85.577	78.562	82.794	3.725
180	84.538	86.421	75.273	87.993	90.109	78.686	85.596	6.077
240	85.911	79.077	78.660	90.175	83.734	82.752	85.554	4.032

Table A-78

USP II dissolution data of MDS capsule in FeSSIF-V2.

Time	Vessel Conc. (µg mL^{-1})			Cumulative % Dissoved				
(min)	No. 1	No. 2	No. 3	No. 1	No. 2	No. 3	Mean	SD
0	0.000	0.000	0.000	0.000	0.000	0.000	0.000	0.000
5	0.847	3.167	3.547	0.770	3.020	3.239	2.343	1.366
10	5.443	11.570	10.932	4.954	11.062	10.014	8.677	3.266
15	10.485	18.828	14.906	9.585	18.092	13.742	13.807	4.254
20	14.625	22.297	18.048	13.443	21.579	16.748	17.257	4.092
30	18.966	25.016	20.682	17.521	24.385	19.318	20.408	3.559
45	22.739	28.079	24.253	21.122	27.544	22.767	23.811	3.336
60	25.604	29.135	26.910	23.932	28.818	25.414	26.055	2.505
90	27.090	30.205	29.907	25.516	30.116	28.397	28.009	2.324
120	28.323	29.740	29.616	26.882	29.961	28.404	28.415	1.539
180	29.909	32.269	31.205	28.581	32.655	30.125	30.454	2.057
240	32.228	32.007	32.687	30.960	32.714	31.763	31.812	0.878

Table A-79

USP II dissolution data of fenofibrate pure drug in FeSSIF-V2.

Time	Vessel Conc. (µg mL^{-1})			Cumulative % Dissoved				
(min)	No. 1	No. 2	No. 3	No. 1	No. 2	No. 3	Mean	SD
0	0.000	0.000	0.000	0.000	0.000	0.000	0.000	0.000
5	0.855	1.484	1.237	0.858	1.460	1.223	1.180	0.303
10	2.545	2.770	2.453	2.563	2.741	2.437	2.580	0.153
15	3.821	3.875	3.802	3.871	3.856	3.793	3.840	0.041
20	4.978	5.740	5.257	5.070	5.729	5.268	5.356	0.338
30	7.791	8.591	8.196	7.945	8.592	8.225	8.254	0.324
45	11.067	12.158	11.684	11.312	12.188	11.753	11.751	0.438
60	14.771	15.781	15.753	15.143	15.873	15.889	15.635	0.426
90	19.762	21.196	21.034	20.301	21.358	21.263	20.974	0.585
120	24.501	25.840	25.640	25.258	26.138	26.022	25.806	0.478
180	30.557	32.800	32.128	31.584	33.243	32.686	32.504	0.844
240	35.365	37.503	37.492	36.718	38.195	38.304	37.739	0.886

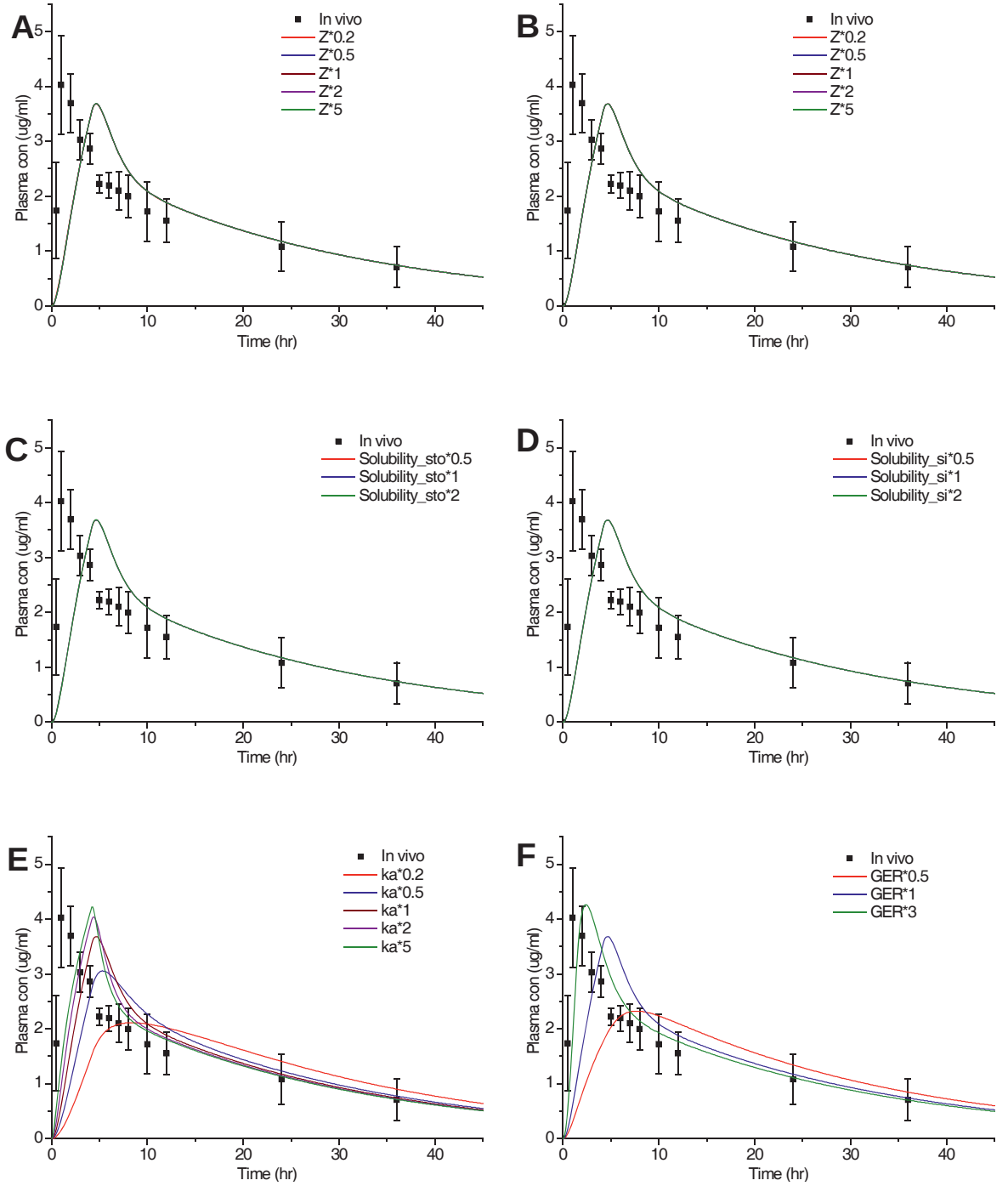

Fig. A-21. Detailed sensitivity analysis of LBF E5(80) solution in the fed state: (A) dissolution rate in stomach (0.2–5 fold), (B) dissolution rate in small intestine (0.2–5 fold), (C) solubility in gastric fluid (0.5–2 fold), (D) solubility in intestinal fluid (0.5–2 fold), (E) absorption rate (0.2–5 fold), (F) gastric emptying rate (0.5–3 fold).

Note: Some profiles are on top of each other, so that the individual profiles cannot be seen clearly (i.e. Fig. A-21A, B, C & D).

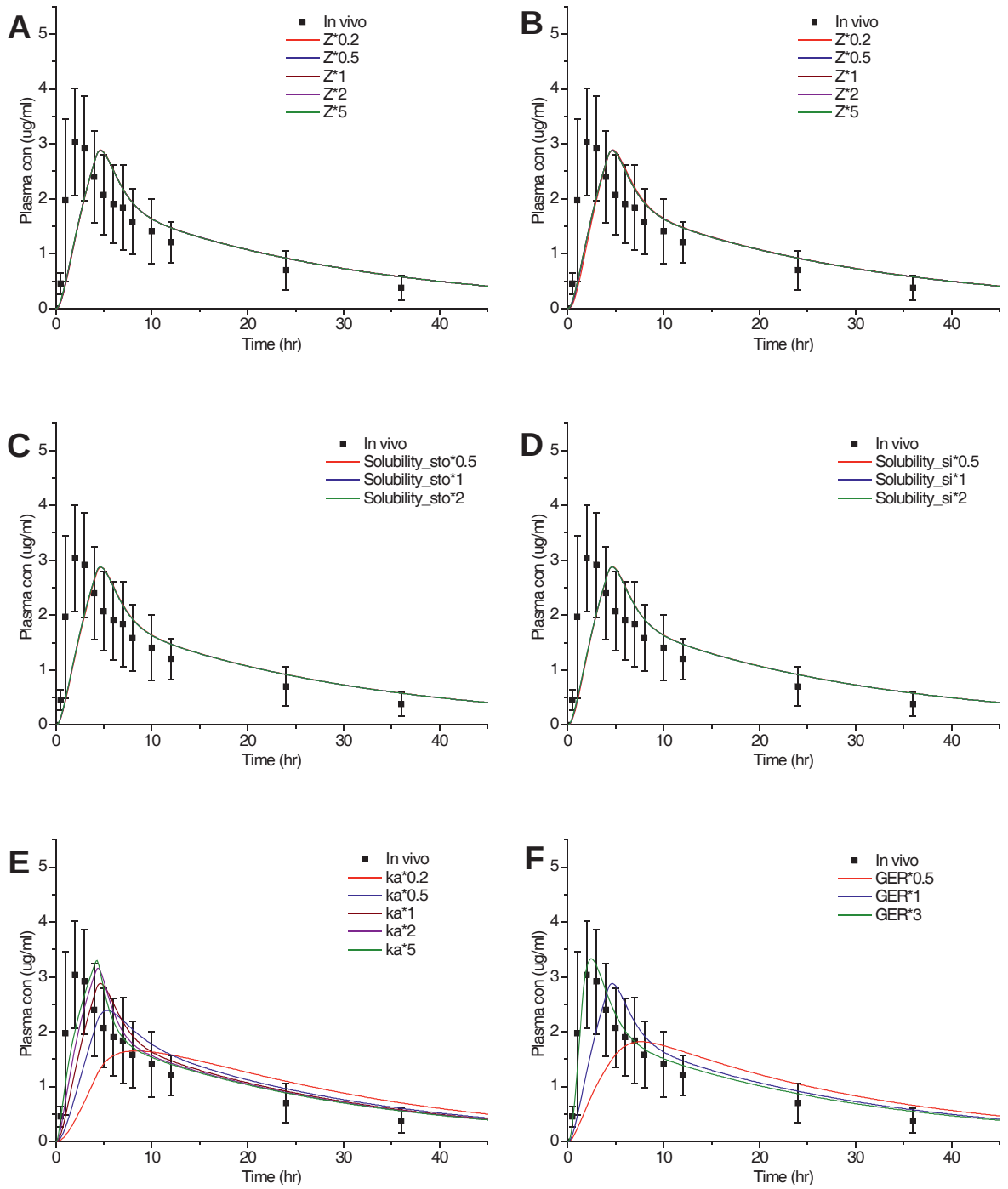

Fig. A-22. Detailed sensitivity analysis of LBF E5(80) capsule in the fed state: (A) dissolution rate in stomach (0.2–5 fold), (B) dissolution rate in small intestine (0.2–5 fold), (C) solubility in gastric fluid (0.5–2 fold), (D) solubility in intestinal fluid (0.5–2 fold), (E) absorption rate (0.2–5 fold), (F) gastric emptying rate (0.5–3 fold).

Note: Some profiles are on top of each other, so that the individual profiles cannot be seen clearly (i.e. Fig. A-22A, B, C & D).

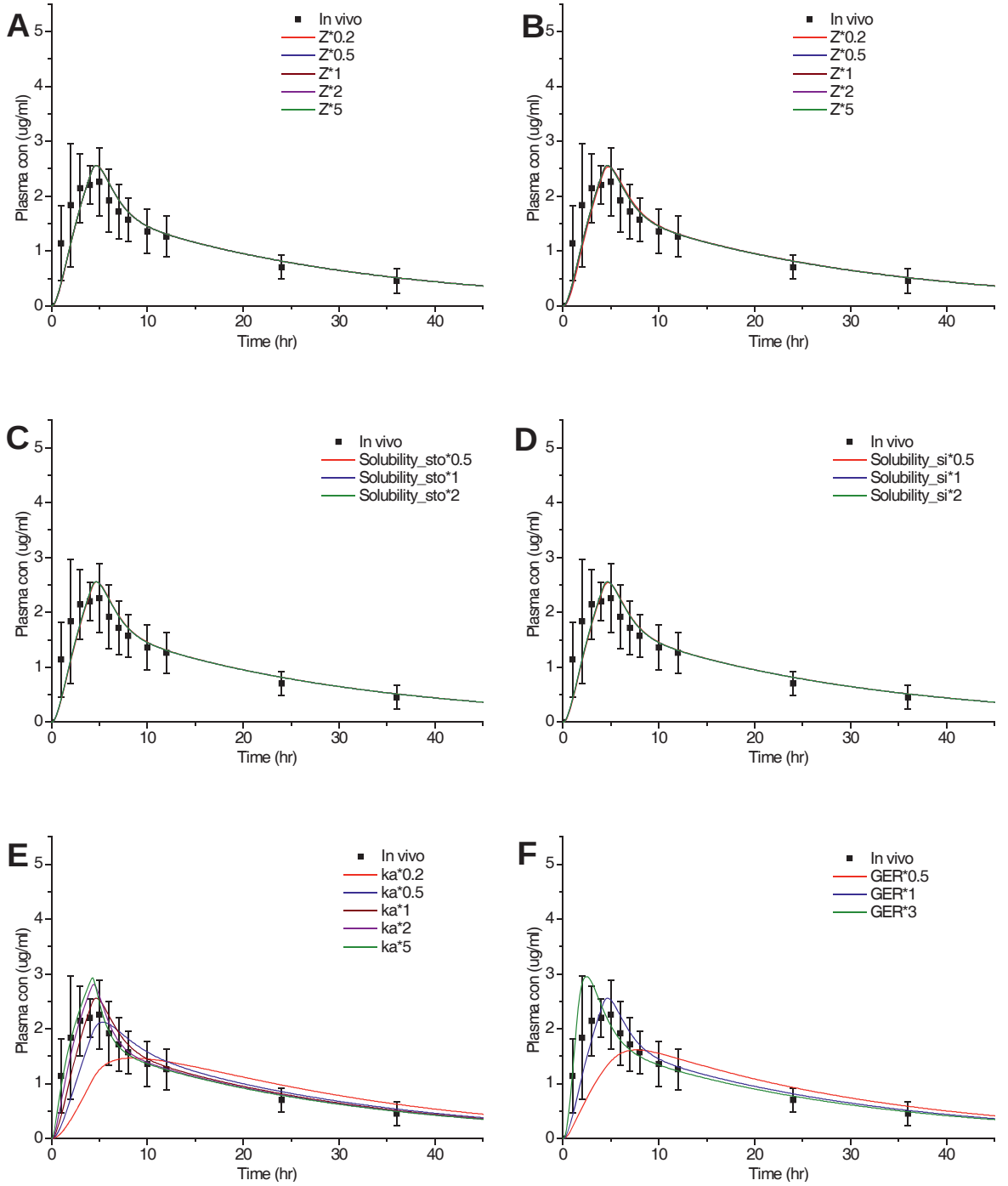

Fig. A-23. Detailed sensitivity analysis of LBF E5(20) capsule in the fed state: (A) dissolution rate in stomach (0.2–5 fold), (B) dissolution rate in small intestine (0.2–5 fold), (C) solubility in gastric fluid (0.5–2 fold), (D) solubility in intestinal fluid (0.5–2 fold), (E) absorption rate (0.2–5 fold), (F) gastric emptying rate (0.5–3 fold).

Note: Some profiles are on top of each other, so that the individual profiles cannot be seen clearly (i.e. Fig. A-23A, B, C & D).

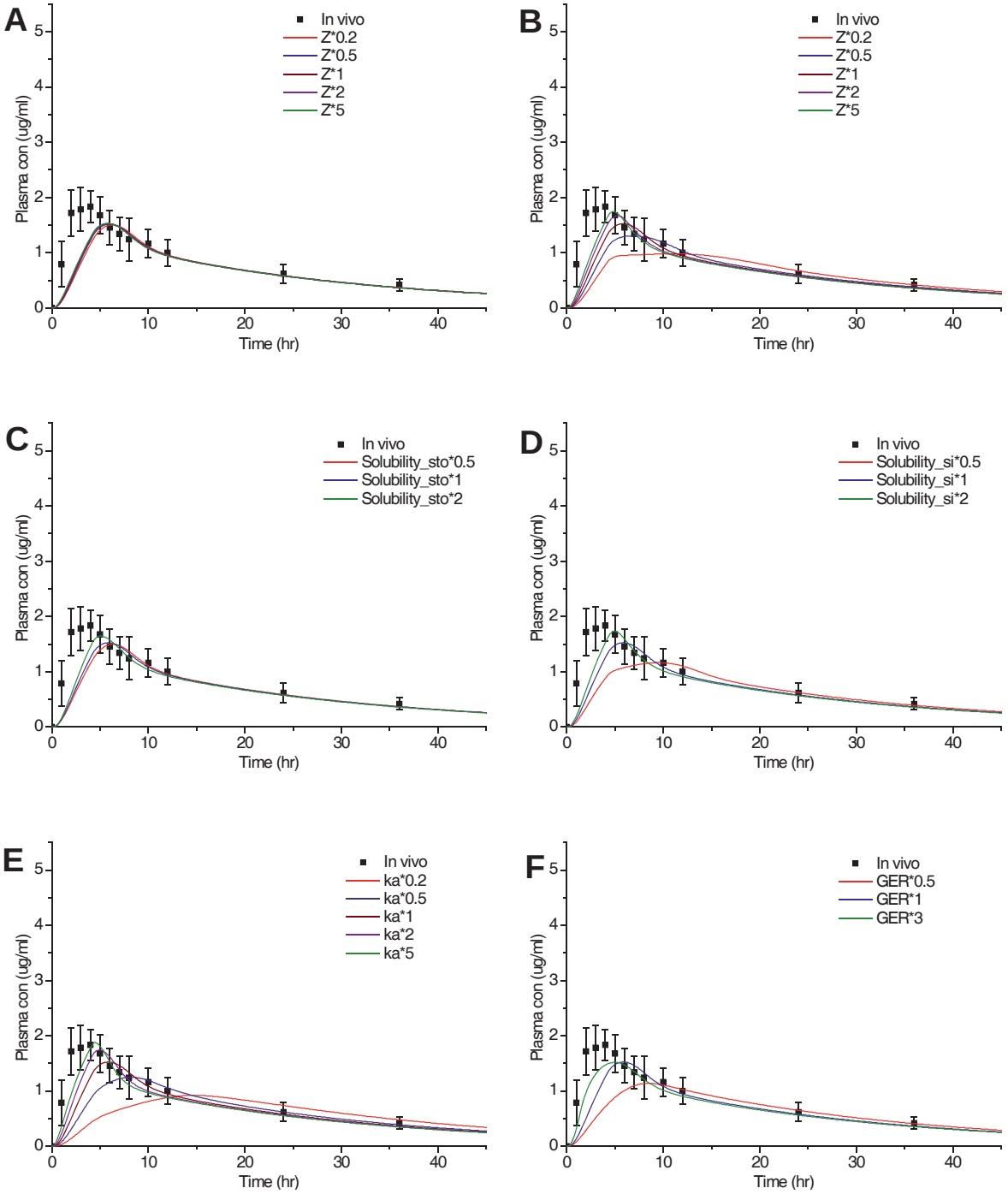

Fig. A-24. Detailed sensitivity analysis of LBF MDS capsule in the fed state: (A) dissolution rate in stomach (0.2–5 fold), (B) dissolution rate in small intestine (0.2–5 fold), (C) solubility in gastric fluid (0.5–2 fold), (D) solubility in intestinal fluid (0.5–2 fold), (E) absorption rate (0.2–5 fold), (F) gastric emptying rate (0.5–3 fold).

Note: Some profiles are on top of each other, so that the individual profiles cannot be seen clearly (i.e. Fig. A-24A & C).

References

Anby, M.U., Williams, H.D., McIntosh, M., Benameur, H., Edwards, G.A., Pouton, C.W., Porter, C.J.H., 2012. Lipid digestion as a trigger for supersaturation evaluation of the impact of supersaturation stabilization on the *in vitro* and *in vivo* performance of self-emulsifying drug delivery systems, Mol. Pharmaceutics 9, 2063–2079.

Arndt, M., Chokshi, H., Tang, K., Parrott, N.J., Reppas, C., Dressman, J.B., 2013. Dissolution media simulating the proximal canine gastrointestinal tract in the fasted state, Eur. J. Pharm. Biopharm. 84, 633–641.

Arndt, M., Kilic, M., Jünemann, D., Dressman, J.B., 2010. Comparison of various media simulating fed state gastric conditions in dissolution tests, AAPS poster, New Orleans, LA, USA.

Artursson, P., Karlsson, J., 1991. Correlation between oral drug absorption in humans and apparent drug permeability coefficients in human intestinal epithelial (Caco-2) cells, Biochem. Biophys. Res. Commun. 175, 880–885.

Berlin, M., Przyklenk, K.H., Richtberg, A., Baumann, W., Dressman, J.B., 2014. Prediction of oral absorption of cinnarizine–a highly supersaturating poorly soluble weak base with borderline permeability, Eur. J. Pharm. Biopharm. 88, 795–806.

Buch, P., 2010. Solubility and permeability as *in vitro* predictors for *in vivo* performance of fenofibrate IR solid dosage forms, Doctoral dissertation, Gutenberg University Mainz.

Buch, P., Holm, P., Thomassen, J.Q., Scherer, D., Branscheid, R., Kolb, U., Langguth, P., 2009a. IVIVC for fenofibrate immediate release tablets using solubility and permeability as *in vitro* predictors for pharmacokinetics, J. Pharm. Sci. 99, 4427–4436.

Buch, P., Languth, P., Kataoka, M., Yamashita, S., 2009b. IVIVC in oral absorption for fenofibrate immediate release tablets using a dissolution/permeation system, J. Pharm. Sci. 98, 2001–2009.

Cardot, J.M., Davit, B.M., 2012. *In vitro-in vivo* correlations: tricks and traps, AAPS J. 14, 491–499.

Chapman, M.J., 1987. Pharmacology of fenofibrate, Am. J. Med. 83, 21–25.

Devraj, R., Williams, H.D., Warren, D.B., Mohsin, K., Porter, C.J., Pouton, C.W., 2013a. *In vitro* assessment of drug-free and fenofibrate-containing lipid formulations using dispersion and digestion testing gives detailed insights into the likely fate of formulations in the intestine, Eur. J. Pharm. Sci. 49, 748–760.

Devraj, R., Williams, H.D., Warren, D.B., Müllertz, A., Porter, C.J., Pouton, C.W., 2013b. *In vitro* digestion testing of lipid-based delivery systems: Calcium ions combine with fatty acids liberated from triglyceride rich lipid solutions to form soaps and reduce the solubilization capacity of colloidal digestion products, Int. J. Pharm. 441, 323–333.

Donald, B., Van Slyke, D., 1922. On the measurement of buffer values on the relationship of buffer values to the dissociation constant of the buffer and the concentration and reaction of the buffer solution, J. Biol. Chem. 52, 525–570.

Dressman, J., Kraemer, J., 2005. Pharmaceutical Dissolution Testing, Taylor & Francis Group, Boca Raton, USA.

Dressman, J.B., Thelen, K., Jantratid, E., 2008. Towards quantitative prediction of oral drug absorption, Clin. Pharmacokinet. 47, 655–667.

EMEA, 2010. Guideline on the investigation of bioequivalence, CPMP/EWP/QWP/1401/98. Available from: <http://www.ema.europa.eu/docs/en_GB/document_library/Scientific_guideline/2010/01/WC500070039.pdf>.

Feeney, O.M., Crum, M.F., McEvoy, C.L., Trevaskis, N.L., Williams, H.D., Pouton, C.W., Charman, W.N., Bergström, C.A., Porter, C.J., 2016. 50 years of oral lipid-based formulations: Provenance, progress and future perspectives, Adv. Drug Deliv. Rev. 101, 167–194.

Fei, Y., Herbert, E., Wieber, A., Saal, C., Lubda, D., Kucera, S., Dressman, J., 2013a. *In vitro* dissolution performance of novel mesoporous fenofibrate loaded silica formulations consisting of various precipitation inhibitors, AAPS poster, San Antonio, TX, USA.

Fei, Y., Herbert, E., Wieber, A., Saal, C., Lubda, D., Kucera, S., Dressman, J., 2013b. Evaluation of the dissolution behavior of novel fenofibrate silica formulations in preprandial biorelevant media, AAPS poster, San Antonio, TX, USA.

Fei, Y., Kostewicz, E.S., Sheu, M.T., Dressman, J.B., 2013c. Analysis of the enhanced oral bioavailability of fenofibrate lipid formulations in fasted humans using an *in vitro-in silico-in vivo* approach, Eur. J. Pharm. Biopharm. 85, 1274–1284.

Galia, E., Nicolaides, E., Hörter, D., Löbenberg, R., Reppas, C., Dressman, J.B., 1998. Evaluation of various dissolution media for predicting *in vivo* performance of class I and II drugs, Pharm. Res. 15, 698–705.

Goosen, T.C., Bauman, J.N., Davis, J.A., Yu, C., Hurst, S.I., Williams, J.A., Loi, C.M., 2007. Atorvastatin glucuronidation is minimally and nonselectively inhibited by the fibrates gemfibrozil, fenofibrate, and fenofibric acid, Drug Metab. Dispos. 35, 1315–1324.

Granero, G.E., Ramachandran, C., Amidon, G.L., 2005. Dissolution and solubility behavior of fenofibrate in sodium lauryl sulfate solutions, Drug Dev. Ind. Pharm. 31, 917–922.

Grass, G.M., 1997. Simulation models to predict oral drug absorption from *in vitro* data, Adv. Drug Deliv. Rev. 23, 199–219.

Griffin, B.T., Kuentz, M., Vertzoni, M., Kostewicz, E.S., Fei, Y., Faisal, W., Stillhart, C., O'Driscoll, C., Reppas, C., Dressman, J.B., 2014. Comparison of *in vitro* tests at various levels of complexity for the prediction of *in vivo* performance of lipid-based formulations: Case studies with fenofibrate, Eur. J. Pharm. Biopharm. 86, 427–437.

Han, S.F., Yao, T.T., Zhang, X.X., Gan, L., Zhu, C., Yu, H.Z., Gan, Y., 2009. Lipid-based formulations to enhance oral bioavailability of the poorly water-soluble drug anethol trithione: effects of lipid composition and formulation, Int. J. Pharm. 379, 18–24.

Hanafy, A., Spahn-Langguth, H., Vergnault, G., Grenier, P., Grozdanis, M.T., Lenhardt, T., Langguth, P., 2007. Pharmacokinetic evaluation of oral fenofibrate nanosuspensions and SLN in comparison to conventional suspensions of micronized drug, Adv. Drug Deliv. Rev. 59, 419–426.

Hauss, D.J., 2007. Oral lipid-based formulations: enhancing the bioavailability of poorly water-soluble drugs, CRC Press.

Hu, L., Wu, H., Niu, F., Yan, C., Yang, X., Jia, Y., 2011. Design of fenofibrate microemulsion for improved bioavailability, Int. J. Pharm. 420, 251–255.

Humberstone, A.J., Charman, W.N., 1997. Lipid-based vehicles for the oral delivery of poorly water soluble drugs, Adv. Drug Deliv. Rev. 25, 103–128.

Jamei, M., Dickinson, G.L., Rostami-Hodjegan, A., 2009a. A framework for assessing inter-individual variability in pharmacokinetics using virtual human populations and integrating general knowledge of physical chemistry, biology, anatomy, physiology and genetics: a tale of 'bottom-up' vs 'top-down' recognition of covariates, Drug Metab. Pharmacokinet. 24, 53–75.

Jamei, M., Turner, D., Yang, J., Neuhoff, S., Polak, S., Rostami-Hodjegan, A., Tucker, G., 2009b. Population-based mechanistic prediction of oral drug absorption, AAPS J. 11, 225–237.

Jantratid, E., Janssen, N., Reppas, C., Dressman, J.B., 2008. Dissolution media simulating conditions in the proximal human gastrointestinal tract: an update, Pharm. Res. 25, 1663–1676.

Juenemann, D., 2012. Analytics of dissolution testing of products containing nanosized drugs with a view to predicting plasma profiles, Doctoral dissertation, Goethe University Frankfurt.

Juenemann, D., Dressman, J., 2012. Analytical methods for dissolution testing of nanosized drugs, J. Pharm. Pharmacol. 64, 931–943.

Juenemann, D., Jantratid, E., Wagner, C., Reppas, C., Vertzoni, M., Dressman, J.B., 2011. Biorelevant *in vitro* dissolution testing of products containing micronized or nanosized fenofibrate with a view to predicting plasma profiles, Eur. J. Pharm. Biopharm. 77, 257–264.

Kataoka, M., Masaoka, Y., Yamazaki, Y., Sakane, T., Sezaki, H., Yamashita, S., 2003. *In vitro* system to evaluate oral absorption of poorly water-soluble drugs: simultaneous analysis on dissolution and permeation of drugs, Pharm. Res. 20, 1674–1680.

Kilic, M., Arndt, M., Jünemann, D., Dressman, J.B., 2010. Fed state simulated gastric emulsions - biorelevant dissolution media based on the gastric snapshot approach, AAPS poster, New Orleans, LA, USA.

Klein, S., 2006. The mini paddle apparatus-a useful tool in the early developmental stage? Experiences with immediate-release dosage forms, Dissol. Technol. 13, 6–11.

Kostewicz, E.S., Aarons, L., Bergstrand, M., Bolger, M.B., Galetin, A., Hatley, O., Jamei, M., Lloyd, R., Pepin, X., Rostami, A., Sjögren, E., Tannergren, C., Turner, D.B., Wagner, C., Weitschies, W., Dressman, J.B., 2014a. PBPK models for the prediction of *in vivo* performance of oral dosage forms, Eur. J. Pharm. Sci. 57, 300–321.

Kostewicz, E.S., Abrahamsson, B., Brewster, M., Brouwers, J., Butler, J., Carlert, S., Dickinson, P.A., Dressman, J., Holm, R., Klein, S., Mann, J., 2014b. *In vitro* models for the prediction of *in vivo* performance of oral dosage forms. Eur. J. Pharm. Sci. 57, 342–366.

Kostewicz, E.S., Wunderlich, M., Brauns, U., Becker, R., Bock, T., Dressman, J.B., 2004. Predicting the precipitation of poorly soluble weak bases upon entry in the small intestine, J. Pharm. Pharmacol. 56, 43–51.

Lee, K.W.Y., Porter, C.J., Boyd, B.J., 2013. The effect of administered dose of lipid-based formulations on the *In Vitro* and *In Vivo* performance of cinnarizine as a model poorly water-soluble drug, J. Pharm. Sci. 102, 565–578.

Lin, Y.M., Wu, J.Y., Chen, Y.C., Su, Y.D., Ke, W.T., Ho, H.O., Sheu, M.T., 2011. *In situ* formation of nanocrystals from a self-microemulsifying drug delivery system to enhance oral bioavailability of fenofibrate, Int. J. Nanomedicine. 6, 2445–2457.

Miller, D.B., Spence, J.D., 1998. Clinical pharmacokinetics of fibric acid derivatives (fibrates), Clin. Pharmacokinet. 34, 155–162.

Mohsin, K., Long, M.A., Pouton, C.W., 2009. Design of lipid-based formulations for oral administration of poorly water-soluble drugs: precipitation of drug after dispersion of formulations in aqueous solution, J. Pharm. Sci. 98, 3582–3595.

Moore, J.W., Flanner, H.H., 1996. Mathematical comparison of curves with an emphasis on *in-vitro* dissolution profiles, Pharm. Technol. 20, 64–74.

Mu, H., Holm, R., Müllertz, A., 2013. Lipid-based formulations for oral administration of poorly water-soluble drugs, Int. J. Pharm. 453, 215–224.

Muria, M.D., Lamberti, G., Titomanlio, G., 2010. Physiologically based pharmacokinetics: a simple, all purpose model, Ind. Eng. Chem. Res. 49, 2969–2978.

Mutschler, E., 2001. Arzneimittelwirkungen, Wissenschaftliche Verlagsgesellschaft mbH Stuttgart, Stuttgart, Germany.

Müllertz, A., Ogbonna, A., Ren, S., Rades, T., 2010. New perspectives on lipid and surfactant based drug delivery systems for oral delivery of poorly soluble drugs, J. Pharm. Pharmacol. 62, 1622–1636.

Najib, J., 2002. Fenofibrate in the treatment of dyslipidemia: a review of the data as they relate to the new suprabioavailable tablet formulation, Clin. Ther. 24, 2022–2050.

Nicolaides, E., Symillides, M., Dressman, J.B., Reppas, C., 2001. Biorelevant dissolution testing to predict the plasma profile of lipophilic drugs after oral administration, Pharm. Res. 18, 380–388.

O'Hara, T., Dunne, A., Butler, J., Devane, J., 1998. A review of methods used to compare dissolution profile data, Pharm. Sci. Technol. Today 1, 214–223.

Porter, C.J.H., Pouton, C.W., Cuine, J.F., Charman, W.N., 2008. Enhancing intestinal drug solubilisation using lipid-based delivery systems, Adv. Drug Deliv. Rev. 60, 673–691.

Pouton, C.W., 2000. Lipid formulation for oral administration of drugs: non-emulsifying, self-emulsifying and 'self-microemulsifying' drug delivery systems, Eur. J. Pharm. Sci. 11, 93–98.

Pouton, C.W., 2006. Formulation of poorly water-soluble drugs for oral administration: physicochemical and physiological issues and the lipid formulation classification system, Eur. J. Pharm. Sci. 29, 278–287.

Ratanabanangkoon, P., Guzman, H., Almarsson, O., Berkovitz, D., Tokarcyzk, S., Straughn, A.B., Chen, H., 2008. A high-throughput approach towards a novel formulation of fenofibrate in omega-3 oil, Eur. J. Pharm. Sci. 33, 351–360.

Ruff, A., Fiolka, T., Kostewicz, E.S., 2017. Prediction of Ketoconazole absorption using an updated *in vitro* transfer model coupled to physiologically based pharmacokinetic modeling, Eur. J. Pharm. Sci. 100, 42–55.

Sauron, R., Wilkins, M., Jessent, V., Dubois, A., Maillot, C., Weil, A., 2006. Absence of a food effect with a 145 mg nanoparticle fenofibrate tablet formulation, Int. J. Clin. Pharmacol. Ther. 44, 64–70.

Schiller, C., Frohlich, C.P., Giessmann, T., Siegmund, W., Monnikes, H., Hosten, N., Weitschies, W., 2005. Intestinal fluid volumes and transit of dosage forms as assessed by magnetic resonance imaging, Aliment. Pharmacol. Ther. 22, 971–979.

Sek, L., Porter, C. J., Kaukonen, A. M., Charman, W. N., 2002. Evaluation of the *in-vitro* digestion profiles of long and medium chain glycerides and the phase behaviour of their lipolytic products, J. Pharm. Pharmacol. 54, 29–41.

Serajuddin, A., Sheen, P.C., Mufson, D., Bernstein, D.F., Augustine, M.A., 1988. Effect of vehicle amphiphilicity on the dissolution and bioavailability of a poorly water-soluble drug from solid dispersions, J. Pharm. Sci. 77, 414–417.

Shah, N.H., Carvajal, M.T., Patel, C.I., Infeld, M.H., Malick, A.W., 1994. Self-emulsifying drug delivery systems (SEDDS) with polyglycolyzed glycerides for improving *in vitro* dissolution and oral absorption of lipophilic drugs, Int. J. Pharm. 106, 15–23.

Shono, Y., Jantratid, E., Dressman, J.B., 2011. Precipitation in the small intestine may play a more important role in the *in vivo* performance of poorly soluble weak bases in the fasted state: Case example nelfinavir, Eur. J. Pharm. Biopharm. 79, 349–356.

Shono, Y., Jantratid, E., Janssen, N., Kesisoglou, F., Mao, Y., Vertzoni, M., Reppas, C., Dressman, J.B., 2009. Prediction of food effects on the absorption of celecoxib based on biorelevant dissolution testing coupled with physiologically based pharmacokinetic modeling, Eur. J. Pharm. Biopharm. 73, 107–114.

Sunesen, V.H., Vedelsdal, R., Kristensen, H.G., Christrup, L., Mullertz, A., 2005. Effect of liquid volume and food intake on the absolute bioavailability of danazol, a poorly soluble drug, Eur. J. Pharm. Sci. 24, 297–303.

Takano, R., Sugano, K., Higashida, A., Hayashi, Y., Machida, M., Aso, Y., Yamashita, S., 2006. Oral absorption of poorly water-soluble drugs: Computer simulation of

fraction absorbed in humans from a miniscale dissolution test, Pharm. Res. 23, 1144–1156.

Trevaskis, N.L., Shackleford, D.M., Charman, W.N., Edwards, G.A., Gardin, A., Dingemanse, S.A., Kretz, O., Galli, B., Porter, C.J.H., 2008. Lipid-based delivery systems and intestinal lymphatic drug transport: A mechanistic update, Adv. Drug Deliv. Rev. 60, 702–716.

Vertzoni, M., Dressman, J., Butler, J., Hempenstall, J., Reppas, C., 2005. Simulation of fasting gastric conditions and its importance for the *in vivo* dissolution of lipophilic compounds, Eur. J. Pharm. Biopharm. 60, 413–417.

Vertzoni, M., Fotaki, N., Kostewicz, E., Stippler, E., C., Leuner, Nicolaides, E., Dressman, J., Reppas, C., 2004. Dissolution media simulating the intralumenal composition of the small intestine: physiological issues and practical aspects, J. Pharm. Pharmacol. 56, 453–462.

Vogt, M., Kunath, K., Dressman, J.B., 2008. Dissolution enhancement of fenofibrate by micronization, cogrinding and spray-drying: comparison with commercial preparations, Eur. J. Pharm. Biopharm. 68, 283–288.

Wagner, C., Jantratid, E., Kesisoglou, F., Vertzoni, M., Reppas, C., Dressman, J.B., 2012. Predicting the oral absorption of a poorly soluble, poorly permeable weak base using biorelevant dissolution and transfer model tests coupled with a physiologically based pharmacokinetic model, Eur. J. Pharm. Biopharm. 82, 127–138.

Wagner, C., Thelen, K., Willmann, S., Selen, A., Dressman, J.B., 2013. Utilizing *in vitro* and PBPK tools to link ADME characteristics to plasma profiles: Case example nifedipine immediate release formulation, J. Pharm. Sci. 102, 3205–3219.

Wei, J.D., Ho, H.O., Chen, C.H., Ke, W.T., Chen, E.T.H., Sheu, M.T., 2010. Characterisation of fenofibrate dissolution delivered by a self-microemulsifying drug-delivery system, J. Pharm. Pharmacol. 62, 1685–1696.

Williams, H.D., Sassene, P., Kleberg, K., Bakala-N'Goma, J.C., Calderone, M., Jannin, V., Igonin, A., Partheil, A., Marchaud, D., Jule, E., Vertommen, J., Maio, M., Blundell, R., Benameur, H., Carriere, F., Mullertz, A., Porter, C.J.H., Pouton,

C.W., 2012. Toward the establishment of standardized *in vitro* tests for lipid-based formulations, part 1: Method parameterization and comparison of *in vitro* digestion profiles across a range of representative formulations, J. Pharm. Sci. 101, 3360–3380.

Williams, H.D., Sassene, P., Kleberg, K., Calderone, M., Igonin, A., Jule, E., Vertommen, J., Blundell, R., Benameur, H., Müllertz, A., Pouton, C.W., Porter, C.J., 2013a. Toward the establishment of standardized *in vitro* tests for lipid-based formulations, part 3: understanding supersaturation versus precipitation potential during the *in vitro* digestion of Type I, II, IIIA, IIIB and IV lipid-based formulations, Pharm. Res. 30, 3059–3076.

Williams, H.D., Trevaskis, N.L., Yeap, Y.Y., Anby, M.U., Pouton, C.W., Porter, C.J., 2013b. Lipid-based formulations and drug supersaturation: Harnessing the unique benefits of the lipid digestion/absorption pathway, Pharm. Res. 30, 2976–2992.

Yu, L.X., 1999. An integrated model for determining causes of poor oral drug absorption, Pharm. Res. 16, 1883–1887.

Curriculum vitae

Personal information.

Given & surname:	Yang Fei
Birth:	18.08.1984, Hohhot, China
Marital status:	Married

Education.

08.2010 – 03.2014	Ph.D. study in pharmaceutical technology Institute of Pharmaceutical Technology, Johann Wolfgang Goethe University, 60438 Frankfurt am Main, Germany
09.2007 – 07.2010	Master of pharmacy engineering (APS certificate, grade 2.5) Department of Pharmacy Engineering, School of Chemistry and Chemical Engineering, South China University of Technology, 510640 Guangzhou, China
09.2003 – 07.2007	Bachelor of pharmaceutical engineering (APS certificate, grade 2.5) Department of Pharmaceutical Engineering, School of Chemistry and Chemical Engineering, Central South University, 410083 Changsha, China
09.1997 – 06.2003	Junior high- and high school education Hohhot No.2 Middle School, 010000 Hohhot, China
09.1995 – 07.1997	Elementary school education Beiyuan Street Elementary School, 010000 Hohhot, China
09.1991 – 07.1995	Elementary school education Suhujie Elementary School, 010010 Hohhot, China

Note: My academic tutors (professors, researchers, associate professors, associate research fellows, senior engineers, senior scientists and lecturers) in pharmacy, biochemistry and chemistry were: J.B. Dressman, E.S. Kostewicz, L. Zhang, B. Zhu, D.S. Zhu, J. Li, Y. Ye, H.H. Wang, Y.B. Jiang, P.L. Yue, X.M. Lang, Q. Li, X.Y. Zheng, X.R. Li, Y. Wang, Y.M. Luo, Z.P. Wu, D. Lin, M.L. Hou, J.J. Liu, Y.R. Jiang, X.Q. Liu, D.L. Yang, F.L. Liu, G.P. Zhan, C.H. Li, Y.Z. Liang, X.N. Li and H. Ye.

Publications and presentations

Publications and presentations during Ph.D. study in Goethe University Frankfurt.

03.2014	A. Wieber, Y. Fei, E. Herbert, C. Saal, D. Lubda, S. Kucera, J.B. Dressman, Dissolution performance of mesoporous fenofibrate loaded silica formulations in a transfer model which predicts "worst case" intestinal performance, *The 9th world meeting of Pharmaceutics, Biopharmaceutics and Pharmaceutical technology*, (Lisbon, Portugal), (2014). (Poster Presentation) (Not included in the thesis)
11.2013	Y. Fei, E. Herbert, A. Wieber, C. Saal, D. Lubda, S. Kucera, J.B. Dressman, Evaluation of the dissolution behavior of novel fenofibrate silica formulations in preprandial biorelevant media, *AAPS Annual Meeting and Exposition*, (San Antonio, USA), (2013). (Poster Presentation) (Not included in the thesis)
11.2013	Y. Fei, E. Herbert, A. Wieber, C. Saal, D. Lubda, S. Kucera, J.B. Dressman, *In vitro* dissolution performance of novel mesoporous fenofibrate loaded silica formulations consisting of various precipitation inhibitors, *AAPS Annual Meeting and Exposition*, (San Antonio, USA), (2013). (Poster Presentation) (Not included in the thesis)
10.2013	B.T. Griffin, M. Kuentz, M. Vertzoni, E.S. Kostewicz, Y. Fei, W. Faisal, C. Stillhart, C. O'Driscoll, C. Reppas, J.B. Dressman, Comparison of *in vitro* tests at various levels of complexity for the prediction of *in vivo* performance of lipid-based formulations: Case studies with fenofibrate, *Eur. J. Pharm. Biopharm*. 86 (2014) 427-437. (SCI Journal Paper) (Chapter 4)
03.2013	Y. Fei, E.S. Kostewicz, J.B. Dressman, *IVISIVC* for lipid-based formulations of fenofibrate, *European Drug Absorption Network Meeting*, (Leuven, Belgium), (2013). (Invited Podium Presentation) (Chapter 5)
03.2013	Y. Fei, E.S. Kostewicz, M.T. Sheu, J.B. Dressman, Analysis of the enhanced oral bioavailability of fenofibrate lipid formulations in fasted humans using an *in vitro-in silico-in vivo* approach, *Eur. J. Pharm. Biopharm*. 85 (2013) 1274-1284. (SCI Journal Paper) (Chapter 5)
03.2012	Y. Fei, E.S. Kostewicz, J.B. Dressman, Solubility and dissolution study of lipid-based formulation of fenofibrate in fasted state media, *The 8th world meeting of Pharmaceutics, Biopharmaceutics and Pharmaceutical technology*, (Istanbul, Turkey), (2012). (Poster Presentation) (Chapter 4)